DEVELOPMENT STUDIES OF LUBRICATING FLUIDS TO ACCELERATE REMOVAL OF MATERIAL FROM SILICON NITRIDE

A Thesis Submitted for Degree of Doctor of Philosophy

by

Gulsharan Rita Kaur
BSc/BSc (Hons), MSc

Department of Mechanical Engineering, Brunel University

March 1998

CONTENTS

Abstract

The superior qualities of ceramics such as high hardness, chemical stability and wear resistance make them promising tribological materials for machine elements, for example, pumps, bearings and heat engines. Ceramics are hard and brittle, therefore, machining such materials is time-consuming, difficult and expensive. A low cost machining process that can remove material rapidly while maintaining a good surface finish is required.

The general aim of the studies presented is to find a correlation between the wear mechanisms and surface modifications induced by interactions of tribochemical nature and to identify the most effective combination of parameters involved in producing high material removal rates of ceramics. This study concentrates on silicon nitride, as this material has most potential for use in industry.

The influence of lubricant chemistry on the friction and wear of silicon nitride is investigated using a ball-on -plate tribotester and a modified four-ball machine. A wide variety of liquid lubricants and additives supplied by Castrol International are tested to evaluate the role of the chemical characteristics of the lubricant on the friction and wear of silicon nitride. Surface and chemical analysis results reveal that by using different chemistries of liquids, the material removal rate and the surface finish of the silicon nitride can be significantly altered. The highest material removal rate is obtained when using the ester base fluid T80884 + 0.3% triethanol amine. This gives an increase by four fold when compared to the material removal rate obtained with the industrial reference slurry Kemet. The topography of the silicon nitride ball after the grinding test is found to be very smooth indicating that the predominant mechanism of material removal rate could be due to a tribochemical reaction occurring at the contact interface.

Acknowledgements

I would like to thank Prof. T. A. Stolarski for his encouragement and inspiration. I am grateful for his fine introduction to academic life, giving me many opportunities to exchange ideas and to increase to my knowledge.

I would also like to show my gratitude to Castrol International Ltd., for their financial support and in particular to Dr D. A Coates and Dr A. Gelder whose industrial support and guidance provided the structure and framework for my research.

Many thanks to Prof S. Tobe from the Institute of Technology in Ashikaga, Japan, Prof L. Henshall of Brunel University and Dr E. Jisheng from GKN Technology, Wolverhampton, for their useful discussions and much expert advice. I would like to acknowledge the technical assistance provided by Keith Withers, Bob Webb, John Langdon and all the technicians in the department mechanical engineering.

Many special thanks to my friends Andy, Michael, Justin, David, Darron, Shahram, Rehan, Mohammad, Reza, Robin, Faustin, Mamadou, the Famous Five, Sara (my daughter!) and Yoong (my godson!) but in particular to Debra for her words of wisdom.

Many thanks to all my family but especially my Dad (Mr Shane Singh), Mum (Mrs Ranbir Kaur) and last but not least, Harv, without whose support I would not have embarked on a PhD.

List of Figures

List of Tables

Nomenclature

A	Real contact area (m^2)
F	Friction force (N)
f_{adh}	Coefficient of friction due to adhesion
f_{def}	Coefficient of friction due to deformation
H_o	Surface hardness (MN/m^2)
K_{ic}	Fracture toughness ($MN/m^{3/2}$)
L	length of groove (m)
P	Applied load (N)
R_a	Surface roughness (μm)
S	Sliding distance (m)
μ	Friction coefficient
V_w	Wear volume (mm^3)
W	Normal load (N)

Abbreviations

AES	Auger Electron Spectroscopy
AFM	Atomic Force Microscope
DSP	Digital Signal Processor
EDM	Electrical Discharge Machining
EDX	Energy Dispersive X-Ray
FTIR	Fourier Transform Infrared Spectroscopy
HIP	Hot Isostatically Pressed
SEM	Scanning Electron Microscope
WDX	Wavelength Dispersive X-Ray
XPS	X-Ray Photoelectron Spectroscopy

Chapter 1
INTRODUCTION

1.1 Introduction to Ceramics

Ceramics are materials based on inorganic non-metallic compounds, such as oxygen, nitrogen or carbon. They range from traditional ceramics such as refractories (bricks and blocks) and domestic claywares (fine pottery, porcelain) to glasses and advanced high performance ceramics (engineering ceramics) which are used for engineering components (Morrell, 1995), such as aluminium oxide, silicon nitride, silicon carbide and zirconia.

Ceramic materials have a number of interesting properties which are becoming increasingly important in many areas of industry. Their high hardness, good wear and corrosion resistance, low densities, high chemical and thermal stability, mechanical, insulating and electromagnetic properties make them eminently suitable for many diverse applications. Some general material properties of the following ceramics :silicon nitride (Si_3N_4), zirconia (ZrO_2) and aluminium oxide (Al_2O_3) are presented in Table 1.1 .

Table 1.1: Material Properties of Engineering Ceramics (Tenmat Ltd., 1996)

Property	Si_3N_4	ZrO_2	Al_2O_3
Density r(kg/m^3)	3250	6000	3950
Coeff. of linear exp. a(10^{-6}/K)	3.2	10.5	8.5
Modulus of Elasticity E (GPa)	320	210	380
Poisson's ratio	0.26	0.3	0.22
Hardness HV10	1500	1250	1800
Bending Strength dB(MN/m^2)	600	950	300
Fracture Toughness K_{ic} ($MN/m^{3/2}$)	6	10.5	5.5
Thermal Conductivity l (W/m K)	35	2.5	30
Specific electrical resistance (Ωm)	10^{12}	10^{9}	10^{12}

1.2 Application of Advanced Ceramics

Some of the new advanced ceramics are being used in armour systems to protect military personnel and vehicles from ballistic projectiles. The chief consideration in these applications is the weight of the protective material required to withstand projectile impact. Advanced ceramics are also being considered utilised in jet aircraft engines, for example, for turbine blades which are much lighter than their superalloy counterparts.

Advanced ceramic materials are increasingly being used for components in automobile internal combustion engines. The principal advantages of these new materials over the conventional metal alloys include: the ability to withstand higher operating temperatures, thereby increasing the fuel efficiency; excellent wear and corrosion resistance; lower frictional losses; the ability to operate without a cooling system; and lower densities, which result in lighter engines (Callister, 1994) . Such engines are still in the development stage; however, ceramic engine blocks as well as valves, cylinder liners, pistons, bearings and other components have been well demonstrated. Materials presently under consideration for use in ceramic heat engines include silicon nitride (Si_3N_4), silicon carbide (SiC), and zirconia (ZrO_2).

1.3 Materials for Rolling Elements

A primary requirement for the operation of a rolling element bearing is that the deformation of its component parts should at all times be elastic: in view of the high stresses which result from contact between the balls or rollers and the tracks, the material must have a high yield stress. A high resistance to fatigue failure is also desirable. For the selection of materials for a high temperature rolling bearing the following properties are important (Bushan & Sibley, 1981); hardness, tensile strength, thermal conductivity, resistance to thermal shock and corrosion. For high speed bearing applications, the bearing material should also have low density to reduce centrifugal forces and skidding. Additional desired properties are; low elastic modulus, low friction and wear, adequate fracture toughness, long spalling fatigue life, and to be able to be manufactured to desired tolerances.

In most applications high-carbon chromium steel (AISI 52100) is used for both balls and rollers. For high temperature applications, as in gas turbine engines, high speed tool steels are adopted. Bearings required to operate in corrosive environments are often made from stainless steels. However, ceramic rolling bearings have excellent corrosion resistance in many environments, a high-load carrying capacity and can also be used for operation at very high temperatures. Among the ceramic materials, sintered silicon nitride has been known as the most promising material for bearing manufacture. Though it is neither the hardest nor the toughest of the engineering ceramics, it is considered to have the best combination of mechanical and physical properties for use in high performance bearing applications (Burrier, 1996).

1.3.1 Silicon Nitride Bearings

The properties of silicon nitride bearings in comparison with steel bearings are presented below (Cundill, 1991).

Table 1.2 Properties of Steel Bearings and Silicon Nitride Bearings

Property	Steel Bearings	Silicon Nitride Bearings
Density r(kg/m^3)	7850	3250
Coeff. Of linear exp. a($10^{-6}/K$)	11	3.2
Modulus of Elasticity E (GPa)	208	320
Poisson's ratio	0.30	0.26
Hardness HV10	700	1500
Bending Strength dB(MN/m^2)	2400	600
Fracture Toughness K_{ic} ($MN/m^{3/2}$)	25	6
Thermal Conductivity l (W/m K)	30....40	35
Specific electrical resistance (Ωm)	0.1....1	10^{12}

From the table it can be noted that:

- The density of silicon nitride is about 40 % that of steels which reduces centrifugal effects especially at high operating speeds and so will minimise the skidding of the balls on the inner races.

- The thermal expansion of silicon nitride is about 30% that of steels which is good in preventing seizure.
- The modulus of silicon nitride is 50% larger than steel. This increases the stiffness of bearings which is ideal for machine tool spindle bearings which require high stiffness.

Some further properties of silicon nitride are that they are corrosion resistant; they have a high loading capacity; they can operate at very high temperatures (1000°C); they have a low friction coefficient which minimises heat generation and can operate under conditions of marginal lubrication; they have an excellent fatigue life and they fail by the least harmful mode of failure which is spalling. The disadvantage of using silicon nitride bearings are their sensitivity to tensile and impact stresses which can result in catastrophic brittle fracture and also their very high manufacturing costs in comparison to steel bearings.

1.4 Machining Ceramics

The two critical issues which prevent the wide use of ceramics are first of all they are very difficult to mass produce because of their physical properties and secondly, the machining process is very time consuming and expensive. The machining cost often accounts for 50-80 percent of the final ceramic component cost whereas for steels this is only 5-15 percent of the total component cost (Wang & Hsu, 1994). Depending on the purpose of the machined component, the surface properties of the ceramic must be optimised by grinding without any effect on the volume properties. Hence it is important to control the machining process in such a way that a favourable surface topography can be achieved. In addition, it should be ensured that any sub-surface changes caused by machining do not extend into the bulk material, since these will be responsible for reducing the strength of the ceramic. Therefore, it is important to find a low cost machining process that can remove material rapidly whilst maintaining a good surface finish free from defects.

Current machining technology relies on: near-net-shape forming to minimise the amount of material to be removed; repeated incremental grinding and polishing steps to achieve good surface quality; slow grinding and cutting speeds to avoid severe tool wear and the formation of cracks. There are many methods of machining ceramics either by abrasive machining processes or non abrasive machining processes, however, the most effective commercial current practice is conventional grinding using diamond slurries (Stinton, 1988).

1.5 Abrasive Machining Processes

1.5.1 Conventional Grinding

Conventional grinding is carried out by machining with diamond abrasive particles by lapping, honing and polishing. The lapping process uses loose rather than bonded abrasives as the cutting tool. The loose abrasive may roll, slide or be restricted in its movement. However, it is not bonded to a substrate as in grinding wheels, honing tools, or coated abrasives. Diamond wheels have become indispensable to achieve high precision and high efficiency grinding and the optimum composition of a diamond wheel for grinding ceramics is governed by many factors (Stinton, 1988). There are a variety of grinding methods to choose from, such as creep feed grinding, form grinding and centreless grinding the use of which depends on the following factors:

- The properties of the ceramic material
- The shape, surface specification and dimensional tolerances of the component
- The machine design and grinding parameters
- The coolant

1.5.2 Ultrasonic Abrasive Machining

Ultrasonic abrasive machining is a non-traditional method of machining used in the machining of hard, brittle materials. In ultrasonic machining, electrical energy is converted into mechanical motion. A low amplitude vibration is acoustically transmitted to a tool holder and specially designed tool. When combined with abrasive slurry, the workpiece material is microscopically ground away and the machined area becomes a mirror or counterpart of the vibrating tool (Mooreland & Moore, 1988).

1.5.3 Abrasive Fluid Jet Machining

Abrasive jet machining refers to the use of abrasive-water jets to propel particles against a surface and to removal the material from that surface via particle impact and shear. In abrasive slurry jets, a thin mixture of abrasive and water is directly pumped to a high pressure and then passed through a nossle to form a jet. Although abrasive water jets can be confined to a small diameter without spreading and can accelerate particles to desired velocities in a relatively short distance, other problems easily outweigh these advantages. Pump and component life is greatly reduced and the uniform mixing of slurry is a problem (Singh, 1997).

1.5.4 Magnetic Fluid Grinding

Recently a new process known as magnetic fluid grinding has been developed in Japan to remove material in the finishing of ceramic balls. The ceramic balls are placed in a non-ferromagnetic cylindrical container filled with a ferromagnetic fluid (a water or oil based liquid with a colloidal suspension of ferrite particles in it) and the container is placed above a bed of permanent magnets. The magnets and fluid create buoyancy forces that levitate the grinding grits in the fluid and also provide the loads for the process. The material is removed from the balls by skidding action of the balls and drive shaft (Childs & Mahmood, 1994) .

1.6 Non-Abrasive Machining Processes

1.6.1 Laser Beam machining

The laser machining of ceramics requires a laser beam with a gaussian or transverse electromagnetic mode ($TEM_{0.0}$). This mode causes rapid vaporisation of the ceramic at the centre of the focal point. However, there are secondary hot spots located around the periphery of the centre hot spot that cause excessive heating of the bulk material and inefficient vaporisation. Ideally when using this technique the focused spot size should be as small as possible but this will be limited by the optics of the laser system. The advantages of laser beam machining include high processing speed and flexibility but the disadvantages are that the high temperature gradients created may cause fracture failure (Capp & Luther, 1985).

1.6.2 Electrical Discharge Machining (EDM)

Electrical discharge machining (EDM) removes material by melting, evaporating, or fracturing the surface depending on the melting point of the material. Because the tool and the workpiece are separated by a dielectric field, extremely hard and brittle materials can be cut. Relatively smooth machined surfaces can be obtained because there is no direct mechanical contact (Petrofes, 1988). However, the materials which can be machined this way are restricted to materials having a large electrical resistivity, and the material removal rate is low. Spalling may also occur for materials of high melting point, high thermal expansion, and low thermal conductivity.

1.6.3 Chemical Milling

Chemical milling refers to a process that uses strong acids to etch away a small quantity of the surface material. The process relies on the proper selection of etchant and the interaction between the material and etchant (Wang & Hsu, 1994).

1.7 Manufacture of Silicon Nitride Bearings

1.7.1 Preparation of Silicon Nitride Powder

Although silicon and nitrogen are both very abundant elements, silicon nitride (Si_3N_4) does not occur in nature. Each silicon atom is covalently bonded to four nitrogen atoms, forming a Si_3N_4 tetrahedron which is the building block for the Si_3N_4 structure. It is a white, high melting point crystalline solid which exists in α and β forms, both of which have 3D lattice structures similar to diamond. The β form is slightly denser than the α form and is also more stable at higher temperatures.

Commercial powders with a high α content are preferred as raw material, because, during sintering, the transformation to β favours the development of an elongated microstructure. Silicon nitride powders can be made by three processes; direct nitridation of silicon powder, carbothermal reduction of silicon oxide (SiO_2) in nitrogen and silicon imide reduction (Pearce, 1972). The processes are described as follows:

1. Direct nitridation of silicon powder of 100μm fineness can form coarse β-Si_3N_4. If nitrogen, nitrogen/hydrogen, or ammonia gases are used as a source of nitrogen

This process can produce high purity silicon nitride with less than 100ppm impurities (Komeya & Inone, 1975)

$$Si(s) + N_2(g) \rightarrow Si_3N_4(s)$$

2. In the carbothermal reduction of silicon oxide (SiO_2) in nitrogen. In this process silica and carbon are heated in a nitrogen atmosphere.

$$SiO_2 + C \rightarrow Si_3N_4 + CO_2$$

3. In the silicon imide reduction process (Pearce, 1972), silicon nitride can be prepared by heating polymeric silazane which is formed by the reaction of silicon tetrachloride with ammonia.

$$nSiCl_4(l) + 6nNH_3 \rightarrow [Si(NH)_2]_n + 4nNH_4Cl(s)$$

$$3[Si(NH)_2]_n(s) \xrightarrow{1670K} [Si_3N_4]_n(s) + 2nNH_3(g)$$

The silicon nitride powder characteristics depend on the production method used. The direct nitridation of silicon generally results in an agglomerated product that requires milling to reach high surface area values. Purity of these powders is achieved by using high purity silicon or by post treatment of the powders. The carbothermal reduction and silicon imide reduction processes are capable of directly producing high surface area powders. The carbothermal reduction of SiO_2 requires excess carbon. Most of the carbon can be eliminated by air firing. The silicon imide thermal decomposition process yields some of the highest purity powders commercially available.

1.7.2 Hot Isostatic Pressing

The starting material for this material is usually high purity silicon nitride powder with a mean particle size of less than 1 micron. Mixing/milling of the powder with additives such as yttrium oxide is an important stage which promotes densification by liquid phase sintering and influences the final product quality (Cundill, 1991). The balls are primarily processed by sintering and hot isostatic pressing (HIP) of ceramic powders. For hot isostatic pressing the powdered material is contained in a graphite die and pressures of 100MPa are applied by a fluid isostatically at temperatures in the region of 1000°C. The sintering process is a firing process used to reduce the porosity and improve the mechanical integrity and the sintering is normally carried out at temperatures above 1700°C.

1.7.3 Finishing Process

The sintering results in shrinkage, affecting the roundness of the balls, which has to be corrected by grinding which is the first stage of the finishing process. The three finishing processes cover subsequent grinding, lapping and polishing operations which are carried out by diamond abrasive lapping. Each stage is distinguished only by the coarseness of the abrasive particles. A typical finishing process uses two circular cast iron plates placed face to face with concentric matching grooves cut in them. Balls are fed into the grooves and are forced to roll by the rotation of the plates. In order to secure uniform material removal, the motion of the balls is interrupted by returning them to a hopper. When the ball enters the process again it's orientation is random with respect to its previous pass. A typical batch size of balls in the 6-15mm diameter size range may be in the high hundreds. Total processing time may be several days which can make the cost of the ceramic ball very high, therefore a low cost rapid machining process which can produce a ball surface free from defects and with a good finish is required (Stolarski et al., 1995).

1.8 The Objectives of Research Work

The research work presented in this thesis focusses on the process of rapid material removal from silicon nitride balls and the development of the process to a stage that is industrially acceptable as an effective and reproducible manufacturing method. Some of the important concepts of silicon nitride ceramics as rolling bearing material and the machining methods used have already been described in this chapter.

The main objectives of the study were:

- To identify the most effective combination of parameters involved in producing, in a safe way, high removal rates of material from silicon nitride samples.
- To establish and explain the correlation between the material removal rate and surface modifications of silicon nitride induced by interactions of tribochemical nature.

These objectives were achieved by:

- Experimental studies of the friction and wear behaviour of silicon nitride ceramics using a range of lubricating liquids.
- Post-test inspections of the surfaces of silicon nitride samples using microscopy, surface and chemical analysis techniques.

The work was sponsored by Brunel University and Castrol International, located at Reading, UK. Close collaboration regarding academic and technical guidance took place with Castrol International and this resulted in an outline for the testing programme. Castrol International was also responsible for supplying the lubricating liquids and additives and grinding work was also carried out on Castrol premises.

1.9 Outline of Thesis

This thesis is organised in seven chapters. Chapter One presents the general background to the area of study. Chapter Two presents a broad literature survey on the subject, with particular reference to the friction, wear and lubrication of ceramics.

Chapter Three describes the experimental design and instrumentation of the test facilities for the friction and grinding experiments. It also describes the experimental procedures and methods of analysis of material properties.

Chapter Four presents the experimental results and discussion from the model friction tests. It compares the performance of the test samples using various types of lubricating liquids and identifies the surface analysis observations.

Chapter Five presents the experimental results and discussion from the model grinding tests. It compares the performance of the test samples using various types of lubricating liquids with abrasive particles and also identifies the surface analysis observations.

Chapter Six is concerned with the analysis and interpretation of the results from the surface and chemical analyses. Finally, the major conclusions and recommendations for future work are presented in Chapter Seven.

REFERENCES

Bushan, B. & Sibley, L. B., 1981, **"Silicon Nitride Rolling Bearings for Extreme Operating Conditions",** ASLE Transactions, Vol. 25, No.4, pp.417-428.

Burrier, I. H., 1996 **"Optimizing the Structure and Properties of Silicon Nitride for Rolling Contact Bearing Performance",** Tribology Transactions, Vol.39, No.2, pp.276-285.

Callister, W. D., 1994, **"Materials Science and Engineering",** pp.377-438.

Capp, M. L. & Luther, R.R., 1985, **"Analysis of the Effect of Laser Machining on 96% Alumina Ceramic Substrates and the Advantages of New Latite Finish",** Proceedings of the 1985 International Symposium on Microelectronics.

Childs, T. H. C. & Mahmood, S., 1994, **"The material removal mechanism in magnetic fluid grinding of ceramic ball bearings",** Proc. Mech. Eng., Vol.208, pp. 47-59.

Croft, W. J., 1973, **" Review of Silicon Nitride, Summary Report, E. R. O.",** NO. 2-73, ONR No. R-16-73.

Cundill, R. T., 1991,**"High Precision Silicon Nitride Balls for Bearings",** SPIE Proceedings, Vol.1573, pp.75-86.

Komeya, K. & Inone, H., 1975, J. Mat. Sci., Vol.10, pp.1244.

Moreland, M. A. & Moore, D., 1988, **"Versatile Performance of Ultrasonic Machining",** Ceram. Bull., Vol.67, No. 6, pp.1045-1047.

Morrell, R., 1985, **"Handbook of properties of Technical and Engineering Ceramics - Part 1: An Introduction for the Engineer and Designer",** National Physics Laboratory, London: Her Majesty's Stationary Office, pp.39-54.

Singh, P., 1997, Abrasive Fluid Jet Mchining, Ingersoll-Rand Waterjet Cutting Systems, Germany.

Stinton, D.P., 1988, **"Assessment of the State of the Art Machining and Surface Preparation of Ceramics",** ORNL Report to DOE ECUT Program DEACO5-84OR21400.

Stolarski, T. A., Jisheng, E., Gawne, D. T. & Panesar, S., 1995, **"The effect of Load and Abrasive Particle Size on the Material Removal Rate of Silicon Nitride Artefacts",** Ceramics International, Vol.21, pp.355-366.

Wang, J. C. & Hsu, S. M., 1994, **"Chemically Assisted Machining of Ceramics",** Transactions of the ASME, Vol.116, pp.423-429.

Tenmat Ltd., 1997, Engineering Ceramics Division, **"Technical Data Sheets",** Manchester.

Chapter 2

LITERATURE SURVEY

2.1 Introduction

Chapter one has presented a review of the microstructure, properties and preparation of silicon nitride; the material selection criteria for rolling bearings and the significance of using ceramics for rolling bearings especially silicon nitride and the machining methods for these ceramics. Silicon nitride is the most difficult ceramic to machine due to its toughness and wear resistance.

Successful machining of silicon nitride ceramics in many tribological applications requires an understanding of the physical, chemical and mechanical properties of the material.
In this chapter the basic concepts associated with the friction and wear of materials are discussed as they relate to ceramics. The friction and wear of ceramics are examined when in contact with themselves and when in contact with metals. The influences of environmental constituents such as water and hydrocarbons on the friction and wear properties are also reviewed.

2.2 Friction and Wear of Materials

2.2.1 Friction

When two materials are placed in contact, any attempt to cause one of the materials to slide or roll over the other is resisted by a friction force.

The friction coefficient (Halling, 1978) is defined as

$$\mu = \frac{F}{W}$$

where F is the value of the resisting force and W is the normal force acting between the surfaces.

Leonardo da Vinci (1452-1519) was the first to develop the basic concepts of friction, and his sketches inspired the French scientist Amontons in 1699 to conduct experiments and later formulate his laws of friction. Coulomb in 1785 also conducted careful experiments, and expanded on Amontons work. Coulomb thought that roughness was a major factor for the cause of friction. Later Bowden and Tabor (1964), formed the

'adhesion' concept of friction, arguing that the main resistance to sliding is imparted by the need to shear the strongly adhering surface atoms of the contacting asperities. The Bowden and Tabor model for sliding friction, in its simplest form, assumes that the frictional force arises from two sources, an adhesion force developed in the areas of real contact between the surfaces (the asperity), and a deformation force needed to plough the asperities of the harder surface through the softer surface. Ultimately, the resultant frictional force F is assumed to be the sum of the two contributing terms, F_{adh} due to adhesion and F_{def} due to deformation.

The classic Laws of Friction as they evolved from these early studies may be summarised as follows:

1) ***The coefficient of friction is proportional to load***
2) ***The coefficient of friction is independent of apparent contact area***
3) ***The static coefficient is greater than the kinetic coefficient***
4) ***The coefficient is independent of sliding speed***

These laws have deviations in practical cases for statements 1 and 2. For example, very rough surfaces cause more direct resistance, for to cause motion one asperity has to be lifted over the other.

It is now recognised that there are three basic elements involved in the dry friction of solids (Tabor, 1981):

1) ***The area of true contact***
2) ***The strength of the bond that is formed at the interface***
3) ***The way material is sheared in and around the contacting regions and ruptured during sliding.***

The true or real area of contact is proportional to the load. If all asperities were of the same height assuming homogeneous properties of the contacting materials, and such that elastic deformation is produced, then $A \propto W^{2/3}$ where A is the real area and W is the applied load. When the contact is wholly plastic, $A \propto W$. The strength of the bonds at contact are generally dependent on the mutual solubility and cleanliness of the surfaces.

Friction is the result of extremely complex interactions between surface and near-surface regions of the two materials. These regions differ from the bulk of the materials in their physical, chemical and mechanical properties. Furthermore, these properties themselves can change radically as a result of interactions of the surface atoms with their environment and with each other. For example friction values are generally found to be higher in vacuum than in air for metallic materials. The friction coefficient for a given pair of sliding materials is not constant, but varies with different conditions. The chemical state of the surfaces is also very important; oxidation of the surface can give a low friction coefficient value. The value for a tribo-system will therefore depend on the following:

1) ***Surface conditions- surface topography, hardness***
2) ***Environmental conditions- vacuum or atmospheric conditions***
3) ***Surface contamination and adsorbed layers- oxides, grease, moisture***
4) ***Material condition due to its preparation treatment.***

2.2.2 Friction Heating and Surface Temperature

The work required to overcome friction will be converted into heat energy and the consequent increase in temperature in the surface layers of the materials in contact may cause changes in the properties and microstructure of materials (Department of Trade & Industry, 1986). The heat generated will be distributed between the two materials in contact and some will be lost to the surroundings. The distribution of heat will depend on the thermal properties of the materials and the area of contact.

Surface films can increase resistance to heat flow between contacting surfaces and consequently affect surface temperatures. Since the contact is at the asperities, these receive a considerable amount of thermal energy and there temperatures may reach a very high value for a short time. This is known as the 'flash temperature'. The bulk temperature also rises but the 'flash temperature' can approach the melting temperature of the lower melting point material. The pioneering work on the calculation of surface temperatures at sliding contacts due to frictional heat was done by Block (1937). He found that high temperatures at real contact areas could be attainable even under conditions of lubrication. He also analysed the flash temperature, which causes the lubricant breakdown and the change in the microstructure of the contacting surfaces.

A full analysis of flash temperatures was also made by Jaeger (1942). He solved cases of moving sources of heat using mathematics. By equating the average temperature of each body at a single contact area, he solved for the heat partition factors according to the moving speed ranges. Archard (1959) summarised Jaeger's solutions for the flash temperature theory. He pointed out that the flash temperature can be calculated on the assumptions that the heat generated in the area of true contact (i.e. a single area of contact is regarded as a plane source of heat) is conducted away into the bulk of the sliding members.

2.2.3 Wear

Wear, producing progressive material loss from the surface (Kragelskii, 1965) can be caused by similar processes to those which cause friction, but the underlying mechanisms are much more complicated and diverse. Wear can be classified by surface appearance, e.g., (abrasive, pitting and seizure wear), by its engineering consequences, mild or severe, and more fundamentally by the underlying mechanisms identified by Burwell (1957), adhesive, abrasive, corrosive and surface fatigue. In practice the modes of wear compete with each other, and may interact. However, one mode generally dominates under given conditions, but this changes as the conditions vary.

The origins of these wear mechanism transitions are numerous; increasing sliding velocity, thus the friction-generated temperature rise at the surface, is one example. At low temperatures, the "cold" mechanical behaviour of the material (elastic and plastic deformation or brittle fracture) determines the underlying mechanisms of the wear and friction; whereas at high temperatures, oxidation and other thermally-induced changes may dominate. At yet higher temperatures, surface melting may occur, influencing friction and wear.

2.2.3.1 Adhesive Wear

In its pure form this type of wear is brought about when the contacting asperities tend to adhere and bond due to the attractive forces which exist between the surface atoms of the two solids (Tabor, 1975). When sliding is attempted the attractive forces act in a way to pull material from one surface and may transfer it to the other. The removed material, in a single contact, is a wear fragment. The particles may transfer or come off as loose

debris. If the force required to break through the interface is greater than that required for the fracture path, then the break occurs along the path and wear particle is produced.

The wear particle formation described suggests that if fracture does not occur at the interface it should occur inside the softer material. This is not always the case in practice, as fragments of the harder material are also formed. This means that within the harder material there are regions of low strength. A weak spot in the hard surface leads to fragment formation. The fragments of the harder material are smaller than the junction.

In the formation of loose particles a general mechanism involves the residual elastic energy of adherents (Rabinowicz, 1958/59). A fragment, as it is formed on a surface, is in a state of severe stress and elastic strain. Once the surface has moved on there remain residual stresses and elastic strains. These arise from the need of the fragment and its substrate to continue to conform geometrically at the interface. For a particle to become loose the elastic energy stored in the particle must equal, or better, exceed the energy of adhesion. This is observed in experiments where powdery debris is generated and is found to cling well to one surface. The smaller the particles the less energy is available for detachment. The powder can only be removed by supplying extra energy, for example by tapping, scraping or blowing.

Quantitatively, Archard (1953) formulated the adhesive wear law as follows:

$$V_w = \frac{KSP}{H_o}$$

Where, V_w = wear volume (mm^3)

K = dimensionless wear constant representing the probability that a junction leads to formation of a particle

S = sliding distance (m)

P = applied load (N)

H_o = surface hardness (MN/m^2)

Since K is a probability its value cannot exceed 1 and in practice it remains below 0.5. For the clean surfaces of most metallic materials K falls between 0.1 and 0.01. For well lubricated surfaces it reduces to very low values in the region of 10^{-6} or 10^{-7}. This is to be expected as there should be hardly any surface contact between well lubricated surfaces, especially under hydrodynamic conditions.

In the calculation of factor K, values of V_W, S and P may be determined reasonably accurately but the actual 'dynamic' flow stress, P_m, can only be estimated from static hardness tests and other data. The relationship between V_W and sliding distance S is not always linear of any amenable form. This leads to difficulties in first quoting K values and then its interpretation for estimates for real situations.

2.2.3.2 Abrasive wear

The term abrasive wear covers two types of situations, that is, a 2-body and a 3-body situation. The 2-body wear arises when a hard particle slides against a soft surface, digging into it and ploughing out a groove .

The 3-body situation is the most common and severe mechanism, whereby, hard loose particle are introduced between the rubbing surfaces. The particles are then under high load and cannot roll to a great extent and often getting buried in the softer surface and cause micro-machining. Plastic cutting occurs at low loads and lateral fracture at high loads (Williams, 1994). The damage resulting is described as scratching, scoring or gouging. Microscopic examination shows regular directional grooves and scratch marks from which material has been removed. The degree of penetration by the abrasive is controlled by the ratio of P to H where P is the load on particle and H is the hardness of indented surface. If A is the cross-sectional area of the groove and L is the length of the groove, then

$$\text{wear volume} = \frac{PAL}{H}$$

In practice the situation is not as simple as this as the grooves obtained do not conform to standard geometrical shapes. In practice there is plastic deformation, fracture and other processes which should really be accounted for. Another important factor is that

surfaces can be deformed badly due to plastic deformation thus changing topography and dimensions without any material being removed.

Surface hardness is important for wear resistance and Richardson (1968) has shown that for adequate resistance the ratio H surface/ H abrasive must be greater than 0.5. However, beyond the value of 1.3 no significant improvement is achieved in wear resistance.

2.3 Lubrication

The concept of the lubrication of materials is dependent on the severity of the conditions. Under light loads and high speeds, lubrication may exist through separation of components by a hydrodynamic fluid film. This type of lubrication is dominated by the fluid properties, especially viscosity. Under more severe conditions, the mechanical properties of the solid surfaces become more important (elstohydrodynamic lubrication). Under still higher severity, boundary lubrication is encountered, and the chemistry taking place at the surface becomes more important.

Lubricating oils are mixtures of a base material usually derived from petroleum and additives. When the lubricant is required to provide boundary lubrication, it is these additives which are critical to the performance of the oil. Parameters to consider include its lubricity, dynamic friction coefficients, how it performs under pressure, whether its acidity affects mechanical components and how its flow properties are affected by temperature. For boundary lubrication, one of the most important parameters in determining the lubricants performance is its friction coefficient. In general the lower the friction coefficient, the better the oil will lubricate and a lower amount of energy will be lost within a machine using the oil.

Many of the concepts for boundary lubrication on metal surfaces rely on chemical reactions with the metal surface and or catalysis by the metal, since metals are chemically reactive. However, ceramics are considered to be chemically inert and can be used in high temperatures and corrosive environments.

2.4 Friction and Wear of Silicon Nitride Ceramics

Several studies have been carried out to investigate the friction and wear properties of silicon nitride ceramics sliding against themselves or a metal in under various lubricated and dry conditions (Fisher & Tomizawa, 1985; Adewoye & Page, 1981; Horton et al., 1985; Cranmer, 1985; Ishiagaki et al., 1985; Kimura,1989; Habig & Woydt, 1989).

Friction and wear properties have been shown to be affected by grinding and oxidation which induce geometrical, physical and chemical changes of the debris. In a ceramic-steel sliding contact, wear is initially caused by the steel debris predominantly oxidised as Fe_2O_3 with small amounts of Fe_3O_4. The debris forms quite hard submicronic particles that are then responsible for abrasive wear of the steel (Denape at al., 1992). However, such debris behaviour is greatly affected even by a shallow film of lubricating fluid. In a ceramic-steel sliding contact under boundary lubrication, where ceramic asperities are in direct contact with the steel, the coefficient of friction is generally quite low, but the steel wear can be higher than under dry conditions because the ceramic surface is now in close contact with unoxidised steel. Specific additives in oil lubricants react with the steel surface and can generate a reactional film. A protective effect caused by reducing bonding between the two solids, preserves the steel surfaces from severe adhesion and reduces friction forces (Denape at al., 1992).

It has been reported that ceramic/metal pairs have lower coefficients of friction than ceramic/ceramic sliding pairs (Aronow & Meseyet, 1986). Generally the friction coefficients of ceramic/ceramic rubbing pairs under dry conditions are in the range of 0.4 to 1.0, under varying the test conditions such as speed, load, specimen contact models and environmental conditions (Kato, 1989 and Usami et al., 1989). Habig and Woydt (1989) and Ishigaki et al., (1985) found that wear rates for Si_3N_4/Si_3N_4 sliding pairs, Al_2O_3/Al_2O_3 and ZrO_2/ZrO_2 sliding pairs with varying speeds were:

Ceramic Couples	Wear Rate (m^3/N.m)
Si_3N_4/Si_3N_4	1×10^{-14} to 6×10^{-14}
Al_2O_3/Al_2O_3	5×10^{-18} to 1×10^{-15}
ZrO_2/ZrO_2	5×10^{-17} to 1×10^{-13}

The wear rate of Si_3N_4/Si_3N_4 pairs varied over a small range when compared to Al_2O_3/Al_2O_3 and ZrO_2/ZrO_2.

Wear mechanism of Ceramics

The process of material removal consists of two actions, mechanical wear and tribochemical wear.

2.4.1 Mechanical Wear

At room temperature both crystalline and non-crystalline ceramics almost always fracture before any plastic deformation in response to an applied tensile load. The brittle fracture process consists of the formation and propagation of cracks. Crack growth in crystalline ceramics is usually through grains (that is, transgranular) and along specific crystallographic planes.

In contrast the types of cracks which are induced by abrasive wear are lateral or radial cracks. Lateral cracks are parallel to the surface but relatively deep in the material. They originate within the plastically deformed material beneath the surface. Under a severe contact load these cracks can run up to the surface to cause material removal and this kind of wear generates flake-like debris. Evans and Marshall, (1980) proposed a lateral crack model to describe wear of ceramics under grinding conditions using the normal force and fracture toughness K_{IC}. Radial cracks are normal to the surface and extend from the region of contact, these cracks are responsible for the microfracture of the surface and this kind of wear generates small powder-like debris.

2.4.2 Tribochemical Wear

Despite their reputation for chemical inertness, the surfaces of most ceramics are susceptible to tribochemical reactions which lead to the formation of surface films and thus modify their frictional behaviour, (Rehbinder & Shchukin, 1973).

A number of factors, particularly speed, coefficient of friction, the proportion of load carried by hydrodynamic action in the mixed lubrication regime and contact geometry contribute to the mean interfacial temperature and hence to the level of tribochemical activity.

Tribochemical Reaction

The oxidation of silicon nitride under normal sliding condition was found as a result of tribochemical reaction with water (Tomizawa & Fisher, 1987). It was thought that the dissolution occurred by oxidation of the material (through oxynitride intermediates) to form water soluble silic acid:

$$Si_3N_4 + 6H_2O \rightarrow 3SiO_2 + 4NH_3$$

$$\rightarrow 3SiO_2 + 2N_2 + 4NH_3$$

$$3SiO_2 + 6H_2O \rightarrow 3Si(OH)_4$$

The formation of a protective surface layer was reported with silicon nitride rubbed at a low temperature and in an atmosphere of high humidity (Akazawa & Kato, 1988). Enomoto and Kimura (1987) and Sugita and Ueda (1984) have studied a tribochemical reaction on silicon nitride using Fourier transform infra-red spectroscopy and suggested that silicon oxide or some silicon hydroxides are produced during friction. In general, hydroxides generated tribochemically on the surface of ceramics, are known to lead to decreased wear and friction, suggesting that these products are softer than the original material.

In a recent review, Malghan (1992) proposed that the reaction between silicon nitride and wear consists of three types of interactions: (1) formation of a molecular layer of hydrated silica or silanol, (2) release of ammonia and/or amine and the re-adsorption on the surface, (3) dissolution and readsorption of impurity ions (i.e. Na, Al, Ca etc). Following these surface reactions, bulk phase reactions can take place as a result of ionisation of the surface hydroxyl and amine groups. The net result is the formation of a solid silic acid (H_4SiO_4) film on the surface of the silicon nitride.

In grinding the actual removal of material could be due to abrasion of the tribochemically modified surface layer by hard particles present in the slurry. A fine surface can be achieved as a result of attack of chemical additives on the crystalline structure of the ceramics, however, a rough surface can be obtained by attack on the grain boundaries.

2.4.3 Lubrication of Silicon Nitride

The chemistry for effective lubrication of silicon nitride under boundary lubrication has only very recently been identified. Alcohols have been explored by researchers for their potential lubricating ability on silicon nitride under very limited conditions. Tsunai and Enomoto (1988, 1989) and Hibi and Enomoto (1990), reported wear test results of primary n-alcohols (C_1 to C_{10}) on a hot-pressed silicon nitride under very low sliding speeds of 0.002m/s with mean pressures of 1.8GPa using reciprocating ball-on-block apparatus. They speculated that boundary lubrication might have been provided through esterification reactions with the oxide surface of silicon nitride. Hibi and Enomoto also noted that a tribochemical film was formed on the surface of the ceramic but did not present any details of the nature of the film. Habeeb et al., (1987) found that the addition of 0.4% lauric acid (C_{12}) to a 150 neutral base oil resulted in increased wear of silicon nitride when measured with a four-ball machine at a speed of 0.15m/s and a mean pressure of 2.7GPa.

Earlier research by Gates and Hsu (1991) determined the effect of selected chemical compounds on the friction and wear behaviour of boundary lubricated silicon nitride. A ball-on-flat configuration was used to evaluate the tribological characteristics of a hot pressed silicon nitride lubricated with a paraffinic base oil containing 1 percent by weight additives. Friction, wear and film formation tendencies were observed for a wide range of oil soluble chemical compounds containing oxygen, sulphur, nitrogen, chlorine and phosphorous. Wear reduction was obtained by the addition of sulphonates, imidazoline, phenate, all phosphorus containing compounds and some oxygen containing compounds including several glycol compounds, oleic acid, salicylate, and, this was associated to be due to the formation of a film in the contact region. Some oxygen containing compounds such as esters and acids were found to increase wear which was considered to be the result of the structure and molecular weight of the compound and also the number and location of hydroxyl groups. Chlorine containing compounds were also found to increase wear; the wear scars were very large and very smooth, suggesting a chemical polishing action by the additives.

Klaus and co-workers (1991) also found that polyesters gave a higher wear rate for silicon nitride. With respect to oxygen containing compounds, Jahanmir and Fisher

(1986) found that 0.5% stearic acid (C_{18}) added to hexadecane reduced the friction and wear of silicon nitride in a pin-on-disc apparatus at 0.001m/s and 1.2 GPa initial mean pressure. They speculated that the stearate molecules adsorbed onto the silicon nitride surface.

Gates & Hsu (1994) have verified that a wide variety of hydroxyl-containing organic compounds such as acids and alcohols are capable of lubricating silicon nitride under boundary lubrication conditions. The very low friction coefficient of 0.05, unique wear scar morphology, and very smooth worn surface all suggest a direct chemical reaction between alcohols and silicon nitride. Their further investigations (Gates & Hsu,1995) led to direct evidence of a chemical reaction between silicon nitride and alcohols. Silicon alkoxides have been identified as being the reaction products from the wear tests. The proposed chemical reaction sequence is adsorption and reaction of the alcohol group on the oxide/hydroxide surface of the silicon nitride, followed by subsequent tribochemical reaction in the contact area to from free (poly)alkoxides.

2.4.4 Effect of Humidity

The humidity of the atmosphere is known to have a considerable effect on wear and friction. This occurs because the water vapour can interact in tribochemical reactions at the wear interface, (Gee & Butterfield, 1993). If this leads to the formation of stable coherent interfacial films which protect the wear surfaces, then reduced wear may result. The film can also act to reduce friction. Conversely, the tribochemical reactions may result in a soft reaction product which is easily removed from the wear interface resulting in high wear rates.

Tomizawa and Fischer (1986), studied the effect of temperature and humidity on the friction coefficient and wear rate of hot-pressed silicon nitride. They found that the friction coefficient for the tests conducted in dry air atmosphere and in a temperature range of 150-800°C was approximately equal to 0.80. Under these conditions, wear was primarily controlled by intergranular micro-fracture. However, in the tests that were carried out in humid environments (that is, relative humidity > 40%) wear was controlled by tribochemical reactions between the silicon nitride and water vapour in the environment. In these tests, the friction coefficient was approximately 0.20. The

transition from tribochemical reaction to micro-fracture occurred at a critical temperature, the magnitude of which was related to the contact load, sliding speed and the humidity level. This transition temperature when reduced as either the load or the sliding speed was increased, or when the relative humidity was decreased.

Park and co-workers (1989), also investigated the effect of humidity and temperature on the tribological performance of hot-pressed silicon nitride. The results were similar to those reported by Tomizawa and Fischer (1986). Park and co-workers also found that the effect of temperature on wear rate was controlled by humidity. In dry atmospheres (air and nitrogen), wear rate always increased with temperature. At temperatures above 800°C, the effect of temperature on wear was very pronounced, and wear increased rapidly with increasing temperature. However, in humid environments, the wear rate increased with temperature from 20-300°C, then decreased as the temperature was raised to 700°C. At temperatures higher than 700°C, wear rates increased rapidly with temperature, in a similar manner to the results obtained in dry atmospheres. Their study also showed that as the relative humidity increased, both the wear rate and the transition temperature increased.

2.4.5 Effect of Sliding Speed

The sliding speed can influence the tribological behaviour of ceramic samples in two major ways. As the speed increases, the temperature at the interface will increase due to flash temperature effects, while the severity of the contact conditions might be reduced if the lubricant entraining action leads to partial hydrodynamic load carrying between the very smooth surfaces of the test specimens. Win and co-workers (1995), investigated the effect of wear characteristics of lubricated silicon nitride and steel couples by varying the speed using a tri-pin-on-disc machine. The resulting wear behaviour of silicon nitride pins was indicative of a tribochemical polishing action. The wear factor for the silicon nitride pins at high speeds of 1m/s remained fairly constant, with a value of 10^{-11}mm^3/Nm with decreasing values as sliding progressed. At lower speeds, the wear factor started lower but increased steadily with sliding distance. At 0.25m/s the wear factor increased from 1.2×10^{-10} mm^3/Nm to 4.4×10^{-10} mm^3/Nm while the increase at 0.06m/s sliding speed was from 5.6×10^{-11} mm^3/Nm to 2.7×10^{-10} mm^3/Nm. The different wear characteristics and the much lower wear factors at the higher sliding speeds of 1m/s were indicative of

some partial load relief from hydrodynamic lift and a reduce severity of contact in the mixed lubrication regime.

2.4.6 Effect of Surface Topography

The successful application of ceramics as engine components depend on their surface roughness. Denape and co-workers (1992), studied the effect of the initial surface roughness of silicon nitride on hard steel in a pin-on-plate tribometer under lubricated conditions. The toughness of the sintered silicon nitride showed two distinct effects when sliding against steel:

- an aggressive effect essentially relevant to the asperity geometry of the ceramic;
- a reduction in wear effect related to the improvement of the friction surfaces by effective polishing by submicronic ceramic debris running through the contact zone.

2.4.7 Transfer Film Formation

Andersson & Holmberg (1994), studied the formation of transfer films and their consequent effects on the friction and wear behaviour of ceramic/metal pairs using a pin-on-disc apparatus in an unlubricated environment. Strong formation of tribological transfer layers occurred for most of the material combinations and the direction of the materials transfer was governed by the thermal, chemical and mechanical conditions in the sliding interface. It was found that the strongest transfer of material took place from steel to the oxide ceramics, from the silicon based ceramics to steel, and in the all-silicon-nitride contact.

For the silicon nitride against silicon nitride contact, it was found that the wear mechanism at the interface was chemically accelerated abrasion. The high local temperature at the asperity contacts caused oxidation of the surfaces and easily detachable reaction products. The wear on the pin was less than that of the disc, and this was due to the protective transfer layer on the pin wear scar and also because of the exposure of the sliding disc to ambient air which was responsible for oxidation immediately after contact. However, both the wear and the friction of the silicon nitride tribo-couple exceeded what could be allowed in a constantly operating sliding application.

Ajai and Ludema (1990), found that the presence of liquids and surface -active agents could interfere with and prevent the formation of a transfer film during sliding wear. This was thought to occur through a reduction in the driving forces holding the film onto the surface and also by physical transport of the loose particles away from the interface.

2.5 Factors affecting Material Removal In Advanced Ceramics

In the finishing of advanced ceramics, the material response to the process is an important factor that affects the quality of the surface generated. The material response in turn depends on the magnitude and size of the stress field as well as the response of the ceramic material to the abrasive environment. Alternatively, the material removal rate can be increased to some extent by combining mechanical action with chemical action. Such a process is called tribo-chemical polishing (Heinicke, 1984). It is also termed chemo-mechanical polishing or mechano-chemical polishing (Fischer, 1988).

Material removal by this process is believed to be at the molecular level thereby yielding a smooth surface in contrast to the classical removal process (by mechanical action) of entire particles by brittle fracture resulting in pitting of the surface of most ceramics. The formation of a reaction layer and its removal controls the process. In addition the dissolution of the reaction products in the carrier fluid plays a role. Chemo-mechanical action is also dependent on the contact zone the interaction of the abrasive particles, the ceramic material and the environment, (Yasunga et al., 1978).

The mechanical removal rate of ceramics in grinding and polishing is dependent on the type and hardness of the abrasive, its grain size and also on the force per abrasive on the work material. Thus, rough grinding with a hard abrasive can yield high removal rates by extensive brittle fracture, however, the surface quality will be poor. Gentle grinding or polishing with a sub-micron abrasive may yield excellent surface quality but a low material removal rate. The removal rate when polishing silicon nitride ceramics will be lower with conventional abrasives (such as aluminium oxide, silicon carbide) which are much softer than super-abrasives for example, diamond, but considerably less expensive

Model grinding tests carried out by Stolarski and co-workers (1995), using the four ball machine have also shown that the material removal rates of silicon nitride balls depend

on the mechanism of interaction between ball surface and oil-based diamond slurry. It was found that the abrasive particle size and load influence the rate of material removal and a specific combination of these two factors lead to an optimum removal rate. The highest rate of material removal occurred with the use of 15 micron abrasive particles where the predominant mechanism was apparently abrasive wear. The quality of the surface finish of the ceramic balls was affected by the rate of material removal, surface roughness increasing with increasing material removal rate. Material removal using slurries containing large abrasive particles in the range of 45 microns and under high loads (4000N) appeared to have been caused by brittle fracture and resulted in subsurface cracking in the ceramic ball.

2.6 Residual Stresses

Grinding produces subsurface cracks and residual stresses in the surface and subsurface regions. The cutting, ploughing and rubbing of diamond grits effect mechanical as well as temperature influences on the workpiece which generates the surface integrity.

Residual stresses are known to influence the wear resistance and fracture stresses of ceramic materials. Inorder to design high quality materials it is necessary to know and control the residual stress state of a material.

During production and machining of a material there are many stages in which residual stresses can be induced. For ceramic materials, an important parameter is the particle size distribution of the initial powder mix. If this distribution is not homogeneous, differences in relative shrinkage during the sintering of the product are expected and due to this residual stresses will occur.

Residual stresses are also induced during the machining of ceramics. When ceramic materials are processed, ground or polished, residual stresses ranging up to several GPa are found in the thin top layer of the machined material. Several investigations have demonstrated the existence of residual stresses at static indentations and the effect of these stresses on subsequent crack propagation. The residual stresses induced at static indentations are the result of the relaxation of the elastically deformed material against the irreversible deformed material directly under the contact, as the load is removed.

Petrovic and co-workers (1974 & 1975), indented hot pressed silicon nitride and found that the apparent critical stress intensity factors (K^*_{IC}), determined from the fracture stresses and flaw sizes, were lower than the critical stress intensity factors (K_{IC}) measured by other methods using large cracks. The difference between K^*_{IC} and K_{IC} was attributed to the residual compressive stresses at the flaw tips. However, both annealing and removal of material was effective in eliminating the stresses, restoring the expected K_{IC} values. The strength of ceramics, with residual stresses acting at the critical flaws, depend in each case on the flaw size, flaw shape and magnitude of the residual load.

REFERENCES

Adewoye, O. O. & Page, T. F., 1981, **"Frictional deformation and fracture in polycrystalline silicon nitride and silicon carbide"**, Wear, Vol.70, pp.37-51.

Akazawa, M. & Kato, K., 1988, **"Wear properties of silicon nitride in rolling sliding contact"**, Wear, Vol.124, pp.123-132.

Andersson, P. & Holmberg, K., 1994, **"Limitations on the use of ceramics in unlubricated sliding applications due to transfer layer formation"**, Wear, Vol. 175, pp.1-8.

Archard, J. F., 1953, Journal of Applied Physics, Vol.24, pp.981-988.

Archard, J. F., 1959, **"The Temperature of Rubbing Surfaces"**, Wear, Vol.2, pp.438-455.

Aronow, V. & Mesyet, T., 1986, **"Wear in Ceramic/Ceramic and ceramic/Metal reciprocating sliding contact"**, Part 1, J. Tribology, Vol. 108, pp.16-21.

Ayai, O.O. & Ludema, K. C, 1990, **"Mechanism of transfer film formation during repeat pass sliding of ceramic materials"**, Wear, Vol.140, pp.191-206.

Blok, H., 1937, Second World Petroleum Congress, Paris.

Bowden, T. P. & Tabor, D., 1964, **"The Friction and Lubrication of Solids"**, Part II, Oxford University Press.

Burwell, J. T., 1957, **"Survey of Possible Wear Mechanisms"**, Wear, No.1, pp.119-141.

Cranmer, D. C., 1985, **"Friction and wear properties of monolithic silicon-based ceramics"**, Journal of Materials Science., Vol.20, pp. 2029-2037.

Denape, J., Marinotto, A & Petit, J. A., 1992, **"Roughness effect of silicon nitride on steel under boundary lubrication"**, Wear, Vol.159, pp.173-184.

Department of Trade and Industry, 1986, **"Wear resistant surfaces in engineering"**, Her Majesty's Stationary Office, London, pp22.

Enomoto, Y. & Kimura, Y., 1987, **"Wearing behaviour of silicon nitride in plane contact"**, I. Mech. E., C123, pp.173-177.

Evans, A. G. & Marshall, D. B., 1980, **"Wear mechanisms in Ceramics"**, Fundamentals of friction and wear of materials, ASM, pp.439-452.

Fischer, T. E.& Tomizawa, H.,1985, **"Interaction of Tribochemistry and Microfracture in the Friction and Wear of Silicon Nitride"**, Wear, Vol.105, pp.29-45.

Fischer, T. E. & Tomizawa, H., 1988, **"Tribochemistry"**, Ann. Rev. Mater. Sci., Vol. 18, pp.303-323.

Gee, M. G. & Butterfield, D., 1993, **"The combined effect of speed and humidity on the wear and friction of silicon nitride"**, Wear, Vol.162-164, pp234-245.

Gates, R. S. & Hsu, S. M., 1991, **"Effect of Selected Chemical Compounds on the Lubrication of Silicon Nitride"**, Tribology Transactions, Vol. 34, No. 3, pp.417-425.

Gates, R. S. & Hsu, S. M., 1994, **"Silicon Nitride Boundary Lubrication: Effect of Oxygenates"**, ASME/STLE Tribology Conference STLE Preprint No.94-CC-43-3.

Gates, R. S. & Hsu, S. M., 1995, **"Silicon nitride boundary lubrication: Lubrication Mechanism of Alcohols"**, Tribology Transactions, Vol.38, No. 3, pp.645-653.

Habeeb, J. J., Blahey, A. G. & Rogers, W. N., 1987, **"Wear and Lubrication of Ceramics"**, I. Mech. E., pp.554-564.

Habig, K. H. & Woydt, M., 1989, **"Sliding Friction and wear of alumina, zirconia, silicon carbide and silicon nitride"**, in K. Holmberg (ed.), Proc. 5th Int. Congr. Tribology (Eurotrib 89), Finland, Vol.3, The Finnish Society for Tribology, Espoo, pp.106-113.

Halling, J., 1978, **"Principles of Tribology"**, The Macmillan Press Ltd., Chpt. 4, pp.72.

Heinicke, G., 1984, **"Tribochemistry"**, Carl Hanswe Verlag, Munich.

Hibi, Y & Enomoto, Y., 1990, **"Friction and Wear of Silicon Nitride in Water, n-Alcohols, Water-Methanol and Water-Glycol"**, Bull. of Mech. Eng. Lab.,Vol. 53.

Horton, S. A., Dawson, D., Riley, F. L. & Wallbridge, N.C., 1985, **"Wear behaviour of sintered β-Sialon ceramic under sliding conditions"**, Rev. chim. Miner., pp.564-576.

Ishiagaki, H., Kawaguchi, I., Iwasa, M. & Toibana, Y., 1985, **"Friction and wear of hot pressed silicon nitride and other ceramics in K. C. Ludema (ed)"**, Wear of Materials, 85, ASME, New York, pp.13-18.

Jaeger, J. C., 1942, **"Moving Sources of Heat and the Temperature at Sliding Contacts"**, Proc. Roy. Soc., pp.203-224.

Jahanmir, S. & Fischer, T. E., 1986, **Friction and Wear of Silicon Nitride lubricated by Humid Air, Water, Hexadecane and Hexadecane + 0.5 Percent Stearic Acid"**, ASLE Trans., Vol.31, No.1, pp.32-43.

Kato, K., 1989, **"Tribology of Ceramics"**, Proc. 5th Inter. Conf. On Tribol., Vol.1, pp.75-93.

Kimura, Y., 1989, **"Effect of water on friction and wear of silicon nitride in lubricated sliding"**, in K. Holmberg (ed.), Proc. 5th Int. Congr. Tribology (Eurotrib 89), Finland, Vol.3, The Finnish Society for Tribology, Espoo, pp.120-125.

Klaus, E. E., Duda, J. L. & Hsu, S. M., 1991, **"Lubricated Wear of Silicon Nitride"**, Lubri. Eng., Vol.47, No.8, pp.679-684.

Kragelskii, I. V., 1965, **"Friction and Wear"**, Butterworths , London.

Malghan, S. G., 1992, **"Dispersion of Si_3N_4 powders: surface chemical interactions in aqueous media"**, Colloid Surf., Vol. 62, pp.87-99.

Park, D. S., Danyluk, S. & McNallan, M., 1989, **"Friction and wear measurements of Si_3N_4 at elevated temperatures in air, Ar, and humid environments"**, Proc. Int. Conf. On Corrosion and Degradation of Ceramics, Am. Ceram. Soc., pp.159-180.

Petrovic, J. J. & Jacobson, L. A., 1974, **"The Strength of Silicon Nitride after Exposure to Different Environments"**, Ceramics for High Performance Applications, Edited by Burke, J. J., Gorum, A. E. & Katz, R. N., Brook Hill, Chestnut Hills, Mass., pp.397-414.

Petrovic, J. J., Jacobson, L. A., Talty, P. K. & Vasudevan, A. K., 1975, **"Controlled Surface Flaws in Hot Pressed Si_3N_4"**, J. Am. Ceram. Soc., Vol.58, pp.113-116.

Rabinowicz, E., 1958/59, **"The effect of size on the looseness of wear fragments"**, Wear, Vol.2, pp.4-8.

Rehbinder, P. A. & Shchukin, E. D., 1973, **"Surface deformations in solids during deformation and fracture process"**, Pergamon Press.

Richardson, R. C., 1968, Wear, Vol.2, p.245.

Sugita, T. & Ueda, K., 1984, **"Material Removal Mechanism of silicon nitride during rubbing in water"**, Wear, Vol. 97, pp.1-8.

Tabor, D., 1975, **"Interaction between Surfaces: adhesion and friction"**, ed. J.M. Blakely, "Surface Physics of Materials," Vol. 2, Academic Press, London.

Tabor, D., 1981, **"Friction-The present state of our understanding"**, J. Lub. Tech., Vol.103, pp.169-179.

Tomizawa, H. & Fisher, T.E., 1986, **"Friction and Wear of Silicon Nitride at 150-800°C"**, ASLE Trans., Vol.29, pp.481-488.

Tomizawa, H. & Fisher, T. E., 1987, **"Friction and wear of silicon nitride and silicon carbide in water: Hydrodynamic lubrication at low sliding speed obtained by tribochemical wear"**, Trans. ASME, Vol. 30, pp.41-46.

Tsunai, Y. & Enomoto,Y., 1988, **"Tribochemistry of Silicon-Based Ceramics in Alcohols"**, Proc. of the 8th Int'l Symp. of Alcohol Fuels, pp.715-720.

Tsunai, Y. & Enomoto,Y., 1989, **"Tribochemical Wear of Silicon Nitride in Water, n-Alcohols and Their Mixtures"**, Wear of Materials, pp.369-374.

Usami, H., Funabashi, K. & Nakamura, T., 1989, **"Frictional properties of several kinds of ceramics against hardened carbon steel",** Proc. 5th Inter. Conf. On Tribology., Vol. 3, pp.94-99.

Winn, A. J., Dowson, D. & Bell, J. C., 1995, **"The lubricated wear of ceramics: Part 1: The wear and friction of silicon nitride, alumina and steel in presence of a mineral oil based lubricant",** Tribology International, Vol. 28, No. 6, pp. 383-393.

Williams, J. A., 1994, **"Engineering Tribology",** Oxford University Press, pp. 179.

Yasunaga, N., Obara, A., & Imanaka, O., 1979, **"Study of Mechanochemical Effect on Wear and its Application to Surface Finishing",** J. Of JSPE, Vol. 44, pp.77-83.

Chapter 3

Experimental Techniques

3.1 Introduction

Liquid lubricants supplied by Castrol International were used to evaluate the influence of the chemical characteristics of the lubricants on the friction and wear of silicon nitride. Two types of tests are run for these evaluations:

- Friction tests using a ball on plate tribotester were carried out to select the most promising lubricants. The criteria for selection included: the friction coefficient as a function of temperature, visual observation of the lubricants to detect degradation of the oil and post-test examination of the surfaces within the contact region.
- Grinding tests using a modified four ball apparatus to simulate the grinding process.

The above testing was used to find a lubricant, which gives the best combination of low friction coefficient and a high material removal rate. Low friction, which is synonymous with low tangential force within the contact zone, is considered to be vital for safe material removal, i.e. free of secondary damage.

After the friction and grinding experiments the surface of the test samples were further analysed using surface and chemical analysis techniques.

3.2 Material Characterisation

3.2.1 Ceramic Ball

Noralide NBD-200 Silicon Nitride 6mm diameter ball blanks are used for the friction and grinding tests. The balls were of hot isotactically pressed silicon nitride (HIPSN) with 2-3 vol.% of the sintering additive MgO. The mechanical and thermal properties of the silicon nitride ball blanks are shown in Table 3.1 (Cerbec Technical Data Sheet #1A, 1994).

3.2.2 Ceramic Plate

The ceramic plate used for the friction experiments was a dense sintered silicon nitride plate from the β Sialon family, silicon oxynitride with some substituted aluminium oxide in the intergranular phase, this avoids the formation of a glassy phase grain boundaries usually found with yttrium as a sintering additive. The chemical composition of the sialon

plate is Si (49.9%), Al (4.2%), Y (7.25%), O (4%) and N (35%). The mechanical and thermal properties of these plates are shown in Table 3.1 (Morgan Matroc Ltd., Technical Data Sheet).

3.2.3 Steel Plate

BS469 (1971)- BO1 Cold Worked Tool Steel plates were used for the friction tests. The equivalent US standard is AISI-01. The chemical composition is - C (0.85-1.00%), Si (0.4%), Mn (1.10-1.35%), Cr (0.40-0.60%), W (0.4.-0.60%) and V (0.25%). The physical and thermal properties of the BO1 tool steel plates are shown in Table 3.1 (TE70 Material Specification 1994).

3.2.4 Steel Ball

DIN 5401 Carbon/Chrome steel balls were used for the friction testing. The chemical composition is C (1.04%), Si (0.25%), Mn (0.35%), Cr (1.45%) and Mo (0.35%). The physical and thermal properties of the steel balls are shown in Table 3.1 (Bearing Traders Ltd., Bearing Specification, 1994).

Table 3.1 Test Material Properties

Material	Silicon Nitride Balls	Sialon Plates	Tool Steel Plates	Steel balls
Density (Kg/m^3)	3160	3200	7840	7800
Modulus of Elasticity (GPa)	320	231	207	207
Yield Strength (MPa)	-		380	345
Tensile Strength (MPa)	400		615	635
Ductility (%EL in 2in.)	-		25	
Poissons Ratio	0.26	0.28	0.30	
Electrical conductivity [$(\Omega\text{-m})^{-1} \times 10^6$]	-		5.6	
Thermal Conductivity (W/m-K)	29.3	21.3	48	60
Coeff. of Expansion [$(°C)^{-1} \times 10^6$]	2.9	3.04	11.0	11.0
Hardness, Rockwell C	>70		20	60
Surface Roughness, R_a,, μm	0.005-polished 250 -ball blanks as sintered	0.1	0.35-0.45	
Porosity	0.1% volume	0.1% volume		

3.3 Test Lubricants

Lubrication is extremely important to ceramic materials in tribological systems. Not only the level of friction lowered by the presence of lubricants but also the probability of brittle fracture during sliding.

The properties of lubricants required for grinding differ considerably from those required in bearings and gear teeth applications. In grinding the surfaces, which have to be lubricated, are the contacting surfaces of the tool and the samples. Quite often, it is not possible to separate the two surfaces in contact, however, the lubricant must prevent scuffing, and the tool must not wear out too quickly.

In conventional high speed machining the role of the grinding fluid is also to act as a coolant. A coolant reduces the temperature of the material being cut and also increases its resistance to shear and so this tends to increase the cutting forces. There is a large variety of grinding fluids which include, fatty-acid-based soaps, formulated hydrocarbons, emulsified oils, and aqueous solutions. The synthetic lubricants currently being used in various cutting operations are polyalkylene glycols, esters and synthetic hydrocarbons.

The lubricants used in this work are specified in Table 3.2. The main reasons that these lubricants were chosen in the first place was because of their low volatility, high flash points and good thermal stabilitys.

Table 3.2 Properties of Test Lubricants

Product Name	Composition	Relative Density at 20°C (Kg/m^3)	Flash Point (°C)	Pour Point (°C)	Kinematic Viscosity (cSt)	
					40° C	100°C
Talpa 20	mineral oil	899	216.0	-33.0	94.6	8.8
T80853	mineral oil	<1000	190.0	-18.0	22.0	4.0
T80854	mineral oil	<1000	200.0	-9.0	32.0	5.2
T80855	ester base fluid	<1000	280.0	-20.0	30.0	5.5
T80884	ester base fluid	<1000	220.0	-27.0	8.5	2.5
T80856	poly alpha olefin	<1000	135.0	-60.0	5.0	1.7
T80857	poly alpha olefin	<1000	200.0	-68.0	30.0	6
T81497	polyglycol	1060	>180	-6.0	14.0	4.0

Table 3.2 Continued

Product Name	Composition	Relative Density at 20°C (Kg/m^3)	Flash Point (°C)	Pour Point (°C)	Kinematic Viscosity (cSt)	
					40°C	100° C
T81498	polyglycol	1080	>180	+12.0	27.0	6.0
T81499	polyglycol	1110	>180	-50.0	29.0	5.0
T81500	polyglycol	1110	>180	-25.0	42.0	8.0
T81501	polyglycol	1120	>180	-5.0	55.0	10.0
T81502	polyglycol	980	>180	-50.0	30.0	6.0
Kemet (reference lubricant used in industry for grinding)	Oil based +15 micron diamond particles	790	>75	<-20	3.0 at 25 °C	

3.3.1 Mineral Oil

Mineral oils are the most commonly used lubricants because of their low cost. They are petroleum based and are used in applications where the temperature requirements are moderate. The major part of mineral oils consists of hydrocarbons with approximately 30 carbon atoms in each molecule. The structure of each molecule is composed of several aliphatic (straight) chains and cyclic carbon chains bonded together as shown below

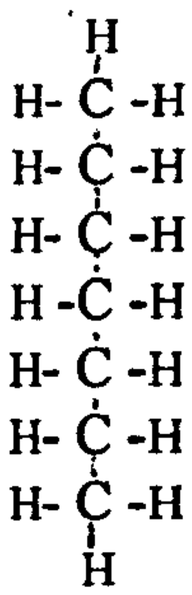

Straight Paraffin Chain

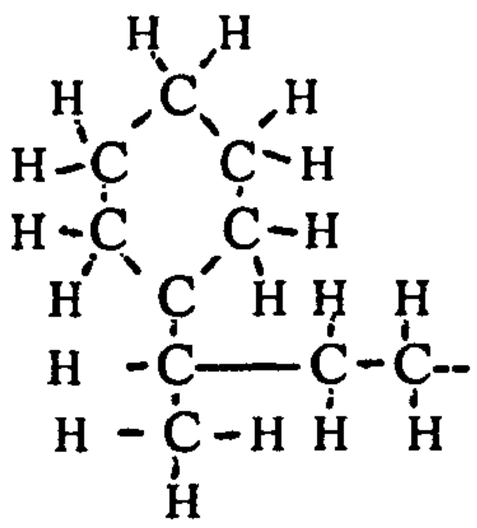

Cyclic Carbon Bonds

3.3.2 Esters

Esters are a very important group of synthetic hydrocarbons. They are produced by reacting alcohol with organic or inorganic acids. The linkage of esters is much more stable than hydrocarbons with their C-C bonds. The ester linkages have much higher bond energy, thus they are more resistant to heat. Esters also have good oxidation stability and excellent viscosity-temperature and volatility characteristics. The structure of esters is, for example, for diesters C_8H_{17}-O-CO-C_8H_{16}-CO-O-C_8H_{17}.

3.3.3 Polyalphaolefins

The physical and chemical properties of polyalphaolefin fluids make them attractive for a variety of applications requiring a wider operating temperature range than can normally be achieved by petroleum-based products (mineral oils). They are among the most promising general purpose synthetic lubricants. Olefins are unsaturated hydrocarbons with the general formula ($-CH_2-$), they consist of a straight carbon chain with an unsaturated carbon at one end of the chain, for example,

$(-CH_2-CH_2-CH_2-CH_2-)_n$ ----$CH_2-CH_2-CH=CH_2$

3.3.4 Polyglycols

Polyglycols are often used as the lubricity base for water-based cutting and grinding fluids. In addition, they have been used in drawing, stamping and rolling applications. They are often used in combination with extreme pressure additives like fatty acids and phosphate esters, where they give synergistic performance. Compared to petroleum lubricants, polygylcols have increased solvency and a higher flash point. The structure of polyglycols consists of at least one hydroxyl group on the end of the molecule, for example,

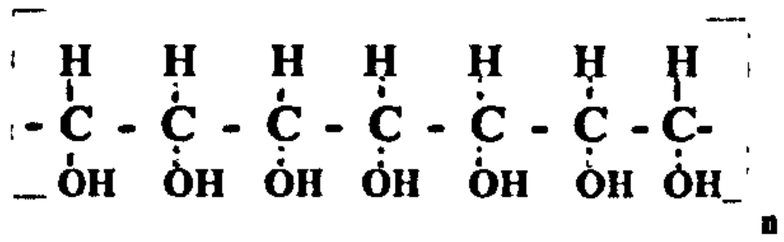

3.4 Lubricant Additives

Lubricant additives are chemicals that are added to the oils in quantities of a few percent by weight to improve the lubricating capacity and durability of the oil. The specific purpose of the chosen lubricant additives are to improve the wear and friction characteristics; to control corrosion and to control the contamination of the lubricant by the reaction products, wear particles and other debris.

The properties of the additives mixed into the most effective lubricants for further grinding and friction testing are shown in Table 3.3.

Table 3.3 Properties of Test Additives

Additives	Relative Density at 20°C (Kg/cm^3)	Flash Point (°C)	Pour Point (°C)	Kinematic Viscosity (cSt)	
				40°C	100°C
Phosphate Ester	1050	100	-48	91.98	14.04
Triethanol Amine	1120	190	MPt=22	280	~20
Alkyl Amine Phosphate	961	92	<-5	~1300	48

3.4.1 Phosphate Ester

Phosphate esters have good stability and also high surface tension. They have excellent fire resistant properties and some phosphate esters have good antiwear properties but some have been known to cause corrosive wear. The general structure of phosphate esters is

$$(CH_3\text{-}C_6H_4\text{-}O)_3P{=}O$$

3.4.2 Triethanol Amine

Triethanol amine is used as an ingredient in the production of emulsifiers, thickeners, wetting agents and also as a corrosion inhibitor. It reacts vigorously with strong oxidising agents and exothermically with mineral acids.

The structure for triethanol amine is

$$\begin{array}{c} H_2C\text{-}\ CH_2\ \text{-}OH \\ OH\text{-}CH_2\text{-}CH_2\text{-}N\text{-}CH_2\text{-}CH_2\text{-}OH \end{array}$$

3.4.3 Alkyl Amine Phosphate

Alkyl amine phosphate is a viscous liquid, insoluble in water and involatile.

The structure for alkyl amine phosphate is

$$R\text{-}\overset{\overset{O}{\|}}{\underset{\underset{O^-}{|}}{P}}\text{-}O\text{-}N\begin{array}{l}\diagup H \\ \diagdown\end{array}$$

3.5 TE70 Micro Friction Machine

The TE70 Micro Friction Machine, fig.3.1 offers friction evaluation using a reciprocating ball-on-plate contact configuration. The unit includes an electro-magnetic drive, temperature control, friction measurement system and a variable frequency and amplitude drive.

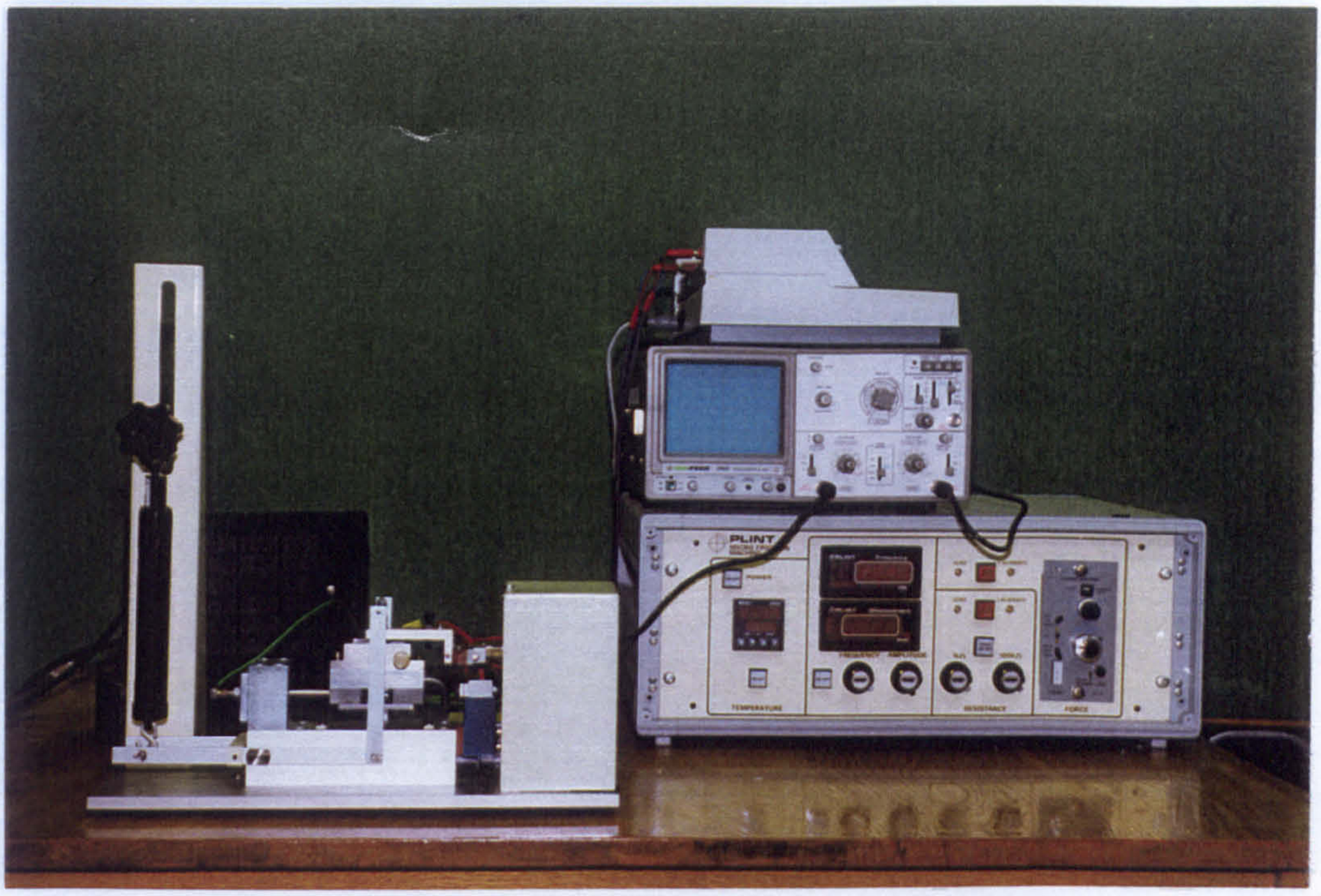

Fig. 3.1 The TE70 Micro Friction Machine

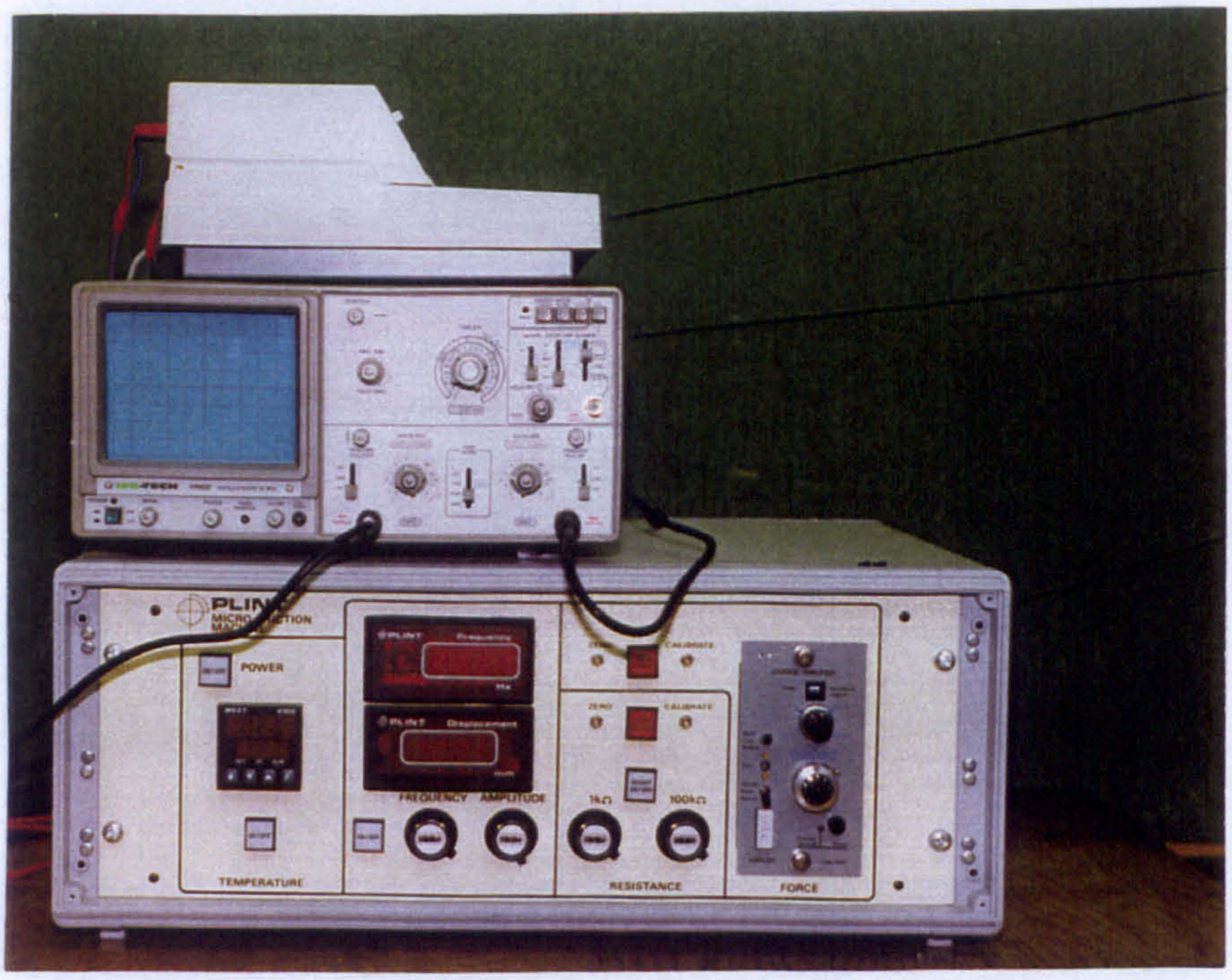

Fig. 3.2 The Chart Recorder, Oscilloscope and Micro Friction Machine

The experimental values that were be measured and used for evaluating the materials under test were as follows:

(a) Friction Force

The signal from the friction force transducer was displayed on an oscilloscope for direct visual examination, fig. 3.2. It was also output to a chart recorder as a r.m.s. signal, giving the mean friction force in oscillating sliding.

(b) Temperature

This was measured with a thermocouple located in the proximity of the specimen. This was a measurement of the bulk contact temperature as flash temperatures due to the nature of contact are highly localised.

3.5.1 Installation and Use

The TE70 Micro Friction unit is a bench-top unit. The moving sample is mounted on the carrier head, fig.3.3. The sample holder is provided for a 6mm diameter test ball. The holder is removed by lifting the oscillating arm on its hinge and unscrewing the large nut on the top. The ball can then be pushed out of the holder.

An electro-magnetic oscillator drives the ball carrier with a frequency range of 5 to 100Hz and the stroke range is 0.05 to 1.0mm. The power of the unit is 5 Watts and this means that the full load may be accommodated at all frequency and stroke settings. There is a limiter in the circuit and the stroke will not adjust higher than that limit.

Both the frequency and the stroke are displayed on the control unit. The stroke is measured from the forces exerted on the strain gauge transducer connected to the shaft by a leaf spring. This also provides a small horizontal pre-load to the drive. For short strokes (under 0.25mm) an additional horizontal pre-load is required for the oscillator to function correctly. This is mounted out-board from the oscillator arm and consists of a split clamp and rubber damping material.

Both the frequency and stroke settings are adjusted by manual potentiometers. The stroke feedback system minimises changes in stroke due to changes in friction force. However, some alteration in stroke will occur as the frequency is increased or decreased.

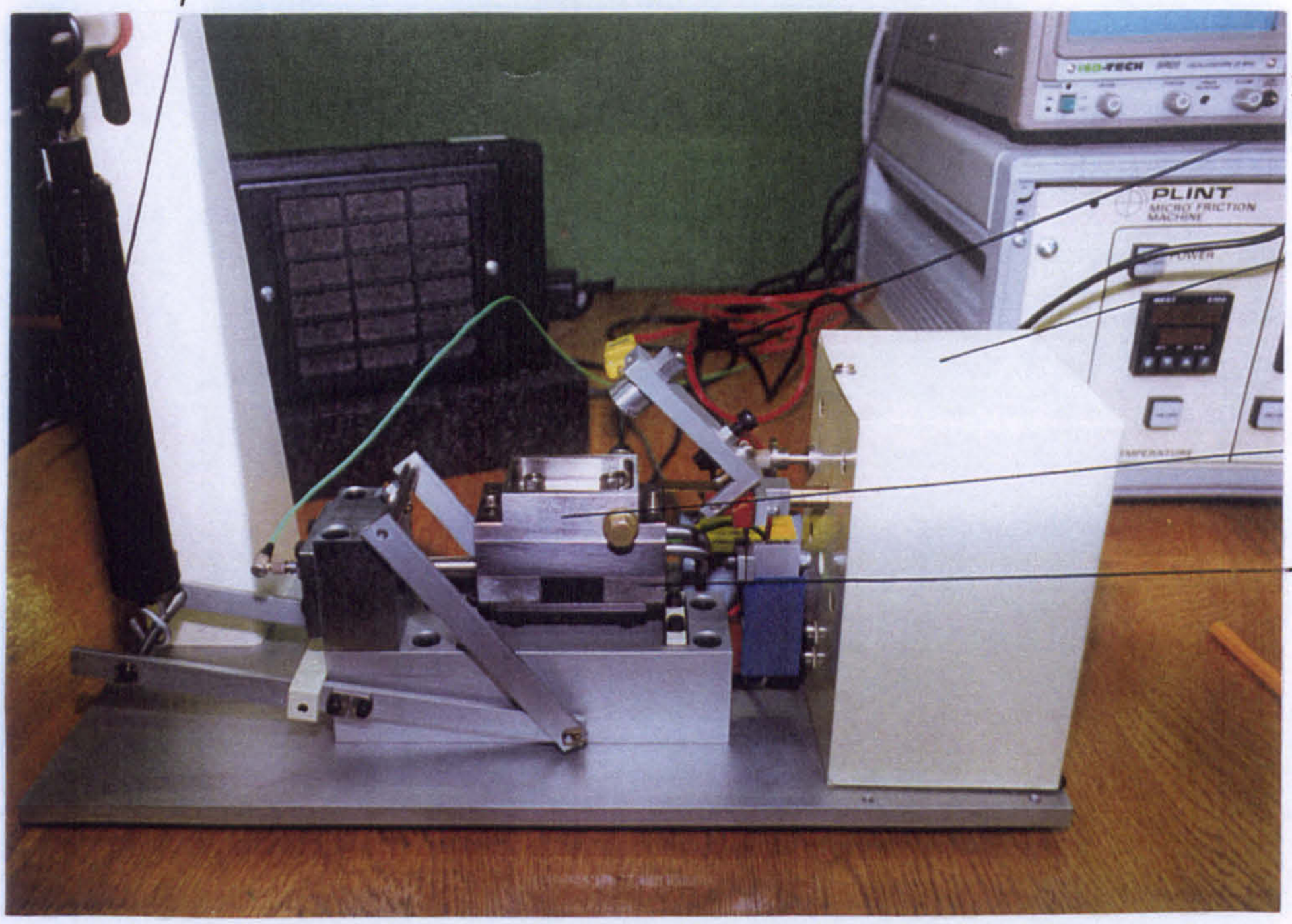

Fig. 3.3 The Friction Test Rig

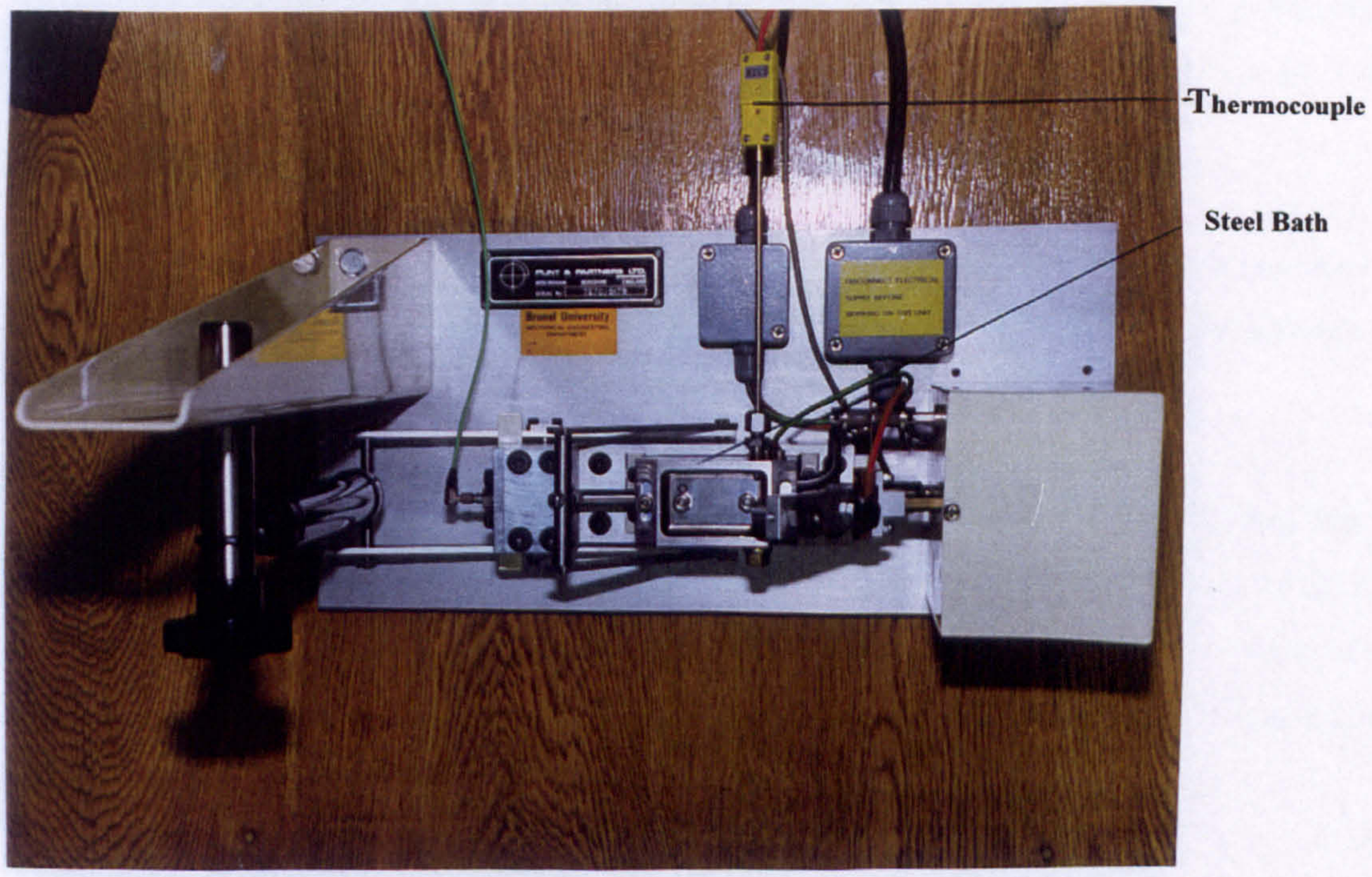

Fig. 3.4 Fixed Specimen in Stainless Steel Bath

The fixed specimen is carried in the stainless steel bath and secured to the studs by two special nuts, fig. 3.4. The bath is in turn clamped to the heater block. This assembly is mounted on two thin section flexible supports, which allow free movement in the horizontal direction. The assembly is prevented from moving by means of a stiff piezo-electric force transducer. This measures the tangential forces on the fixed specimen for both directions of motion. The moving specimen is loaded against the fixed specimen by a spring balance through a lever and stirrup mechanism.

A counterbalance weight is provided so that the lever/stirrup can be set in neutral position and the load supplied by the spring. The stirrup is swung up out of the way to gain access to change the specimens.

3.5.2 Friction Force Measurement

The piezo-electric transducer used to measure the friction force has a sensitivity of typically 43.5pC/N and the amplifier gives a resolution of 0.001N. The charge amplifier type 5007 converts the charge yielded by the piezo-electric transducer into proportional electrical signals. The amplifier is matched to the sensitivity of the connected transducer and then operates with fixed scales graded 1, 2, and 5 x 10^n mechanical units (in this case Newtons) per volt. This operating set-up means that no conversion from pc to V is necessary.

For example, when the dial is set to 10N/V then a chart output of 1V rms corresponds to 10 Newtons Friction Force. Friction coefficients are obtained by dividing the calculated force on the chart record by the normal load between the specimens.

The charge applied to the 5007 is converted by a first stage amplifier into a proportional voltage. This is followed by a low-pass filter, which fixes the upper cut off frequency of the measuring system (330Hz). This serves to suppress the transducer resonances and spurious mechanical oscillations. Final scaling of the signal for voltage output takes place in the following amplifier.

For all experimental work the charge amplifier is operated in the a.c. coupled mode, that is, with a "short" time constant. The charge amplifier output may be connected directly

to an oscilloscope in order to display the instantaneous friction force. It is also taken to the input of a true r.m.s. to d.c. converter amplifier. This amplifier gives a d.c. voltage output equivalent to the true r.m.s. value of any input signal. This output may then be taken to a Y-t recorder to obtain a continuous recording of the friction force.

3.5.3 Calibration of Charge Amplifier and Force Transducer

The machine calibration is checked periodically and this is done by resetting the RMS/DC force amplifier

1. With the force amplifier switched off, the DVM is connected to the DIN force output socket. Alternatively the calibration can be carried out using the chart recorder output.
2. The 'set zero' potentiometer is adjusted to give zero output.
3. When the force amplifier 'Calibrate' button is pressed the DVM should read 10.00V, however, if this is not the case the 'Calibrate ' potentiometer can be adjusted.

3.5.4 Temperature Control and Measurement

Tests at elevated temperatures are achieved by powering the electrical heater elements. The specimen is electrically heated and its temperature is measured by a Chromel Alumel (Type K) thermocouple pressed into contact against one edge. Power to the heater is switched by the programmable controller. The West 6100 instrument is a three-term PID controller with setpoint and ramp facilities. It may also be tuned automatically and the auto-tune has already been carried out for a temperature of 100^{0}C. When the power is switched on at the machine, the controller is in normal display mode. The machine display reads the temperature measured by the thermocouple and the lower display gives the current setpoint.

3.6 Friction Test Procedures

The sliding friction coefficients of tool steel in contact with silicon nitride were measured under boundary lubrication conditions at temperatures ranging from 30-150°C using the TE70 Micro Friction Machine. Before each test, the balls and plate were cleaned ultrasonically in an acetone bath. Figure 3.5 shows schematically the arrangement of the friction machine. The fixed specimen is secured to the base of the oil bath by means of

two hexagonal nuts. The moving specimen, in this case, the 6mm silicon nitride ball is push fitted into the holder. The holder is then fixed in the oscillating arm by means of a nut. Figure 3.6 and 3.7 show the design and dimensions of the ball holder and the steel plate in mm.

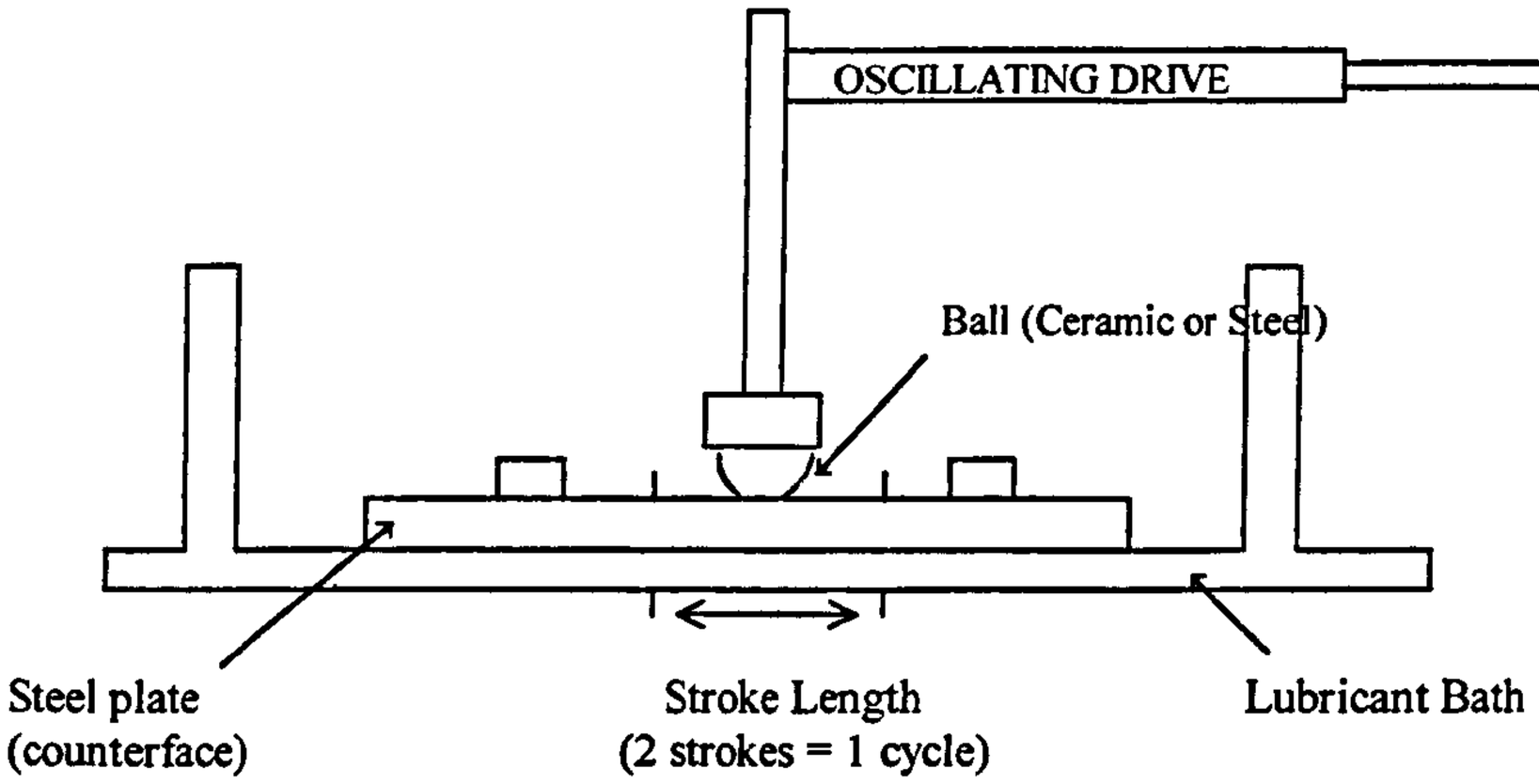

Fig. 3.5 Diagram of reciprocating testing arrangement

The friction force was monitored with both an oscilloscope and a chart recorder. The force transducer output was rectified and filtered to provide a root mean square value for friction force on the chart recorder. The load applied, amplitude and frequency of oscillation and choice of temperature ranges were the main variables. These variables and the lubricant properties determined the lubrication regime.

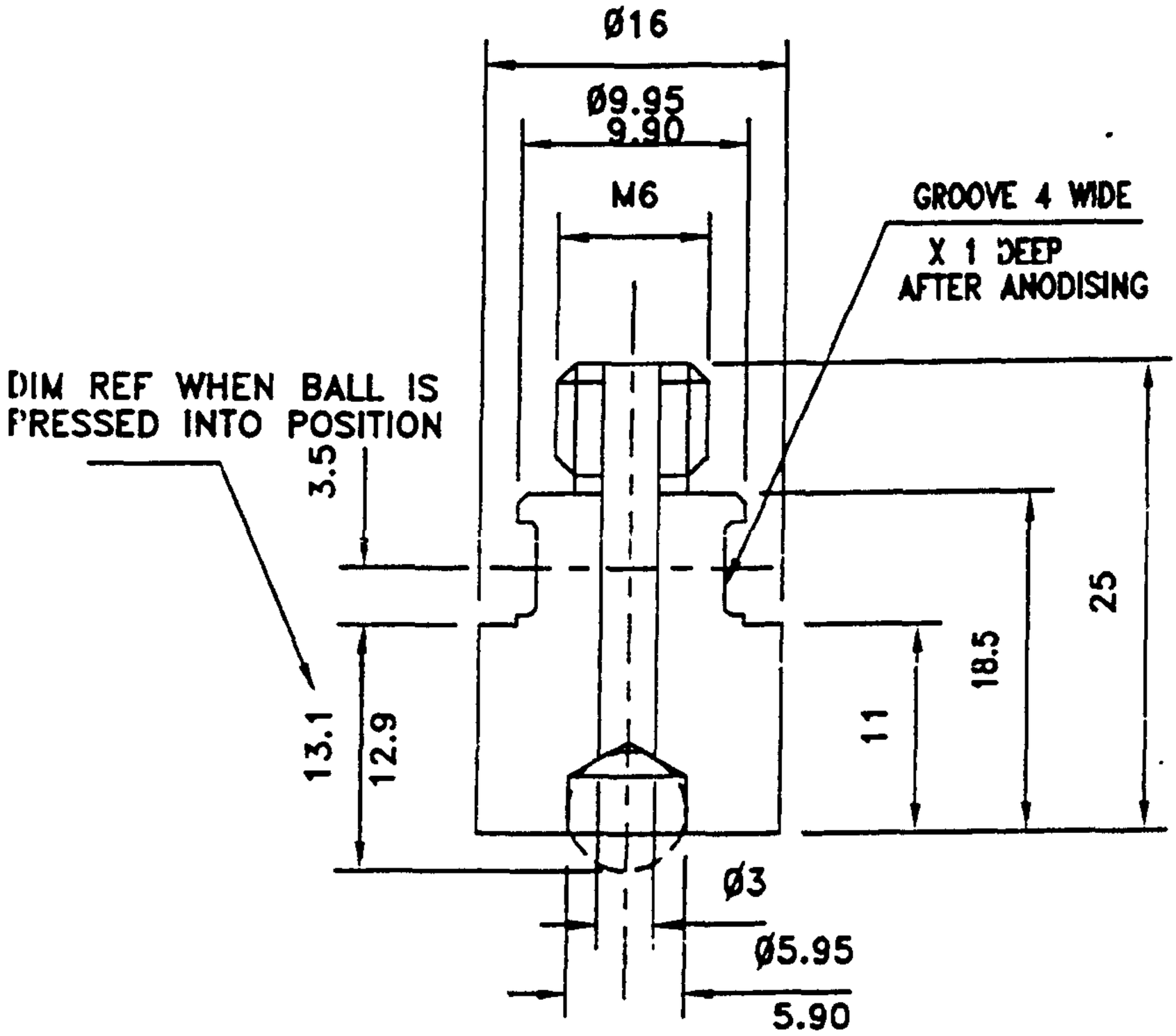

HOLDER FOR 6MM DIA BALL

Fig. 3.6 Ball Holder

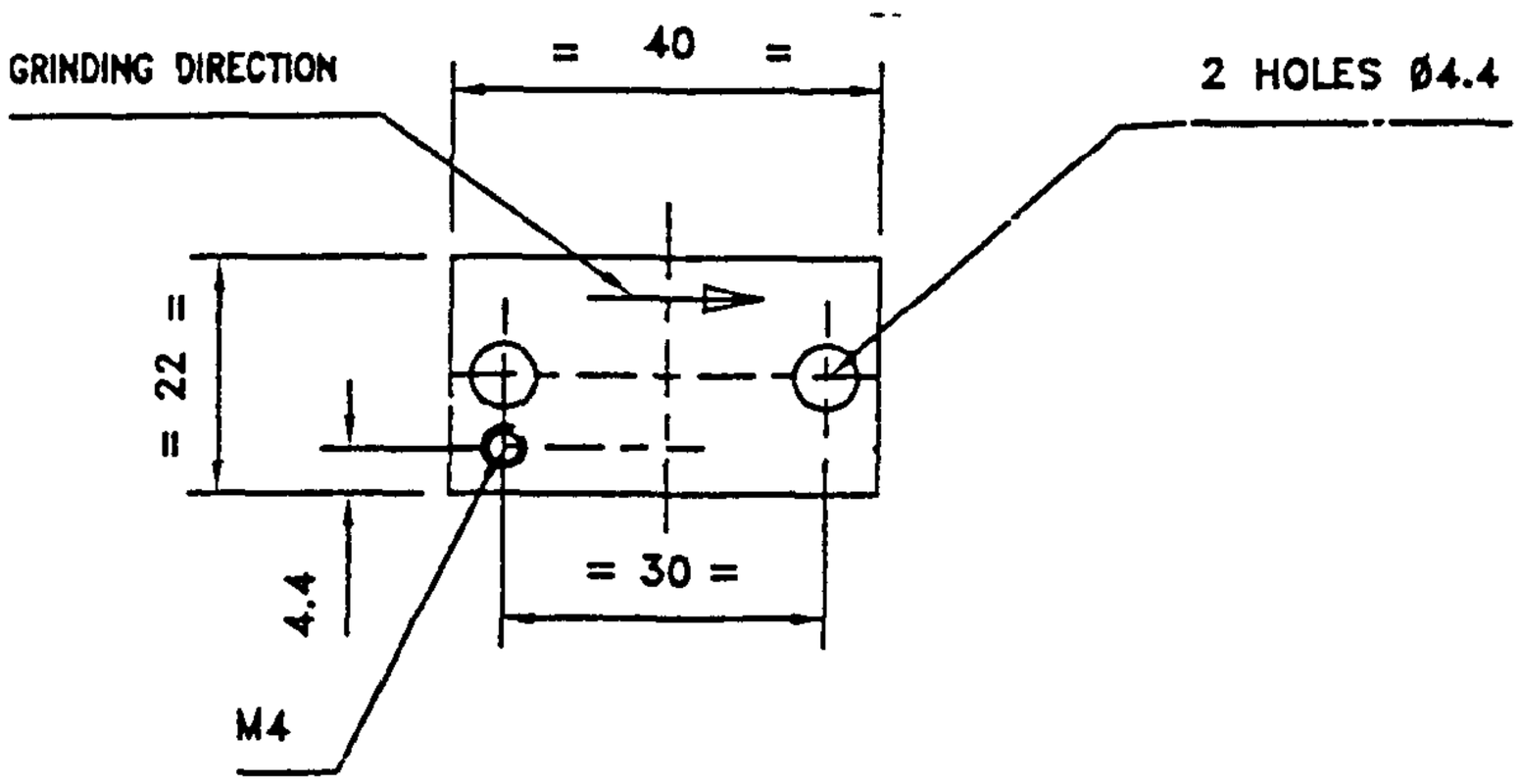

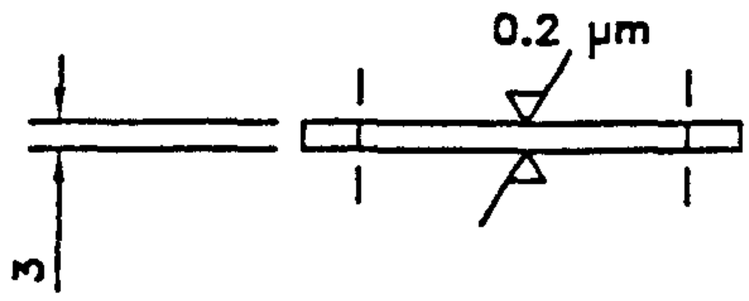

Fig. 3.7 Steel Plate (counterface)

3.6.1 Preliminary Friction Tests

Preliminary tests were carried out in order to compare the influence of the lubricant characteristics on the friction of ceramic/metal contact with that of ceramic/ceramic and metal/metal contacts, under boundary lubrication conditions. The load, frequency, stroke length and temperature were also varied, in order, to establish the most suitable test parameters. Each test was repeated four to five times in order to determine the error involved. This procedure was used for all the tests on the friction machine.

3.6.2 Friction Testing Programme

The test conditions used :

Test Sample	Ceramic ball sliding on steel plate
Lubricant	Reference: Talpa 20 Test lubricants: mineral oils - T808853, T80854, ester base fluids- T80855, T80884, poly alpha olefins - T80856, T80857, polyglycols- T81497, T81498, T81499, T81500,T81501, T81502
Additives	Phosphate Ester, Triethanol Amine and Amine Phosphate used with the most effective lubricants at concentrations of 0.1%, 0.2% and 0.3% by weight
Load	5N
Contact Stress	304 MNm^{-2}
Stroke Length	0.3 mm
Frequency	45 Hz
Mean Velocity	0.027 ms^{-1}
Temperature Range	30-150°C

The contact surfaces of the ball and plate were examined before and after friction testing by surface and chemical analysis techniques using scanning electron microscope, atomic force microscope and light element x-ray analysis.

3.7 Introduction to the Four Ball Machine

The Four Ball Machine is a stand mounting unit, fig.3.8, offering wear testing of ceramic balls using various types of oils under sliding conditions and moderate loads. The upper part of the machine carries the drive spindle, which in turn carries the test cone collet

chuck, fig.3.9. The chuck is removed by inserting an extractor into the top of the drive spindle and by screwing down to contact the chuck.

The lower part of the machine carries the loading piston, which carries the lower test assembly mounted on a thrust race. This assembly incorporates an electrical heater. Access to the test chamber is through the window in the side of the casing. The lower test assembly is inserted and removed using the detachable handles provided. Lower races are removed by removing the grub screws from the base of the housing and knocking them out with the three pinned extractor provided. The end load is applied to the loading piston by means of a load arm with a ratio of either 20:1 or 10:1. The piston may be lowered to insert or remove the lower test assembly by raising the load arm and engaging the locking lever.

Instrumentation includes:-

1. Two proximity sensors, mounted in various alternate positions close to the drive spindle.
2. A thermocouple embedded in the lower test assembly.
3. A torque transducer for low speed sliding tests which indicates friction and shuts down the machine at seizure.
4. A vibration sensor for high speed rolling which shuts down the machine at the onset of pitting.

A separate cabinet houses controls and instruments.

3.7.1 Control Cabinet

The control cabinet is in two parts. The lower part of the stand carries the motor thyristor drive, the mains contactor and the clutch starter unit. The upper panel of the cabinet carries instrumentation and the operator controls. These include a seconds timer, a programmable batch controller, a three term temperature controller tachometer.

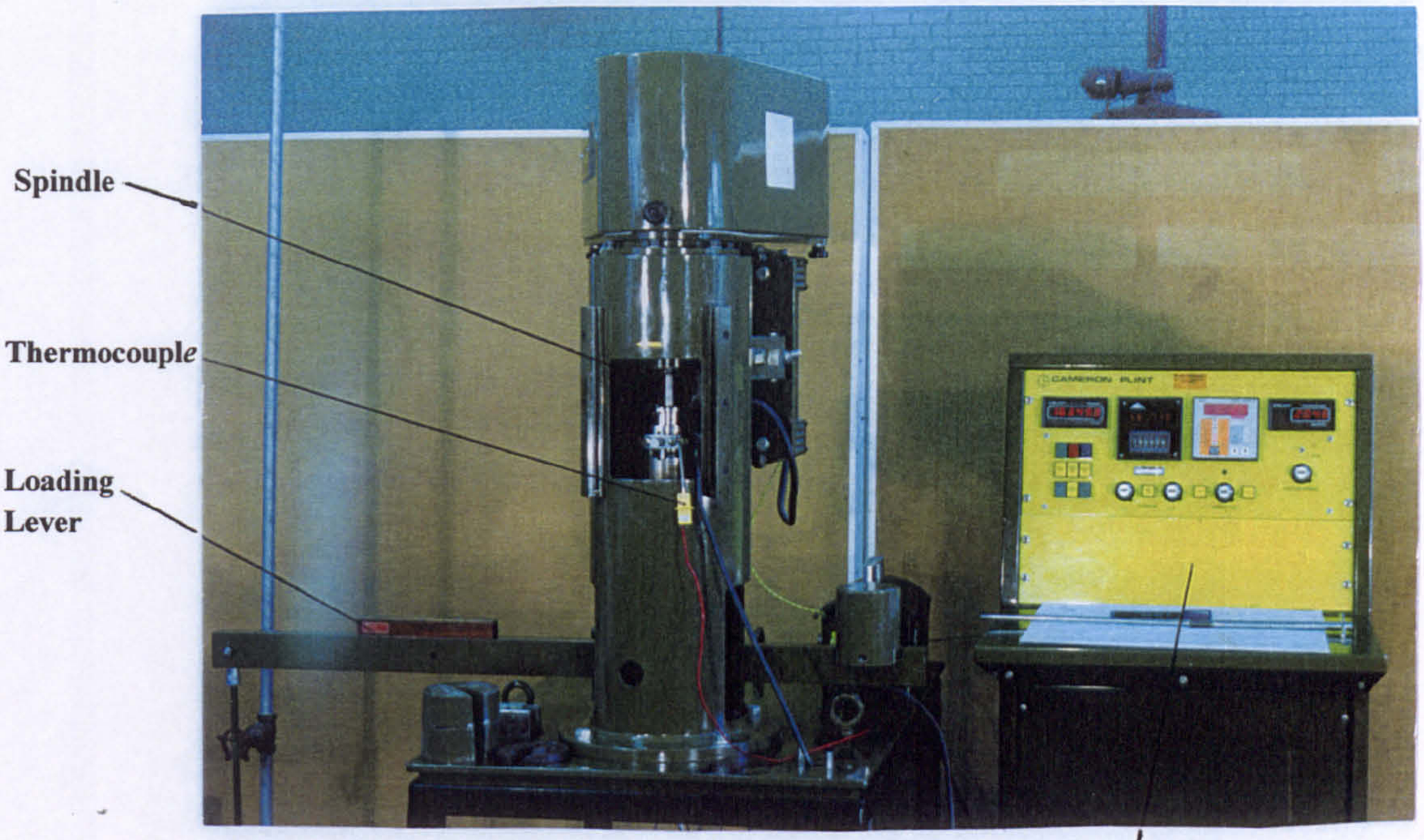

Fig. 3.8 The Four Ball Machine

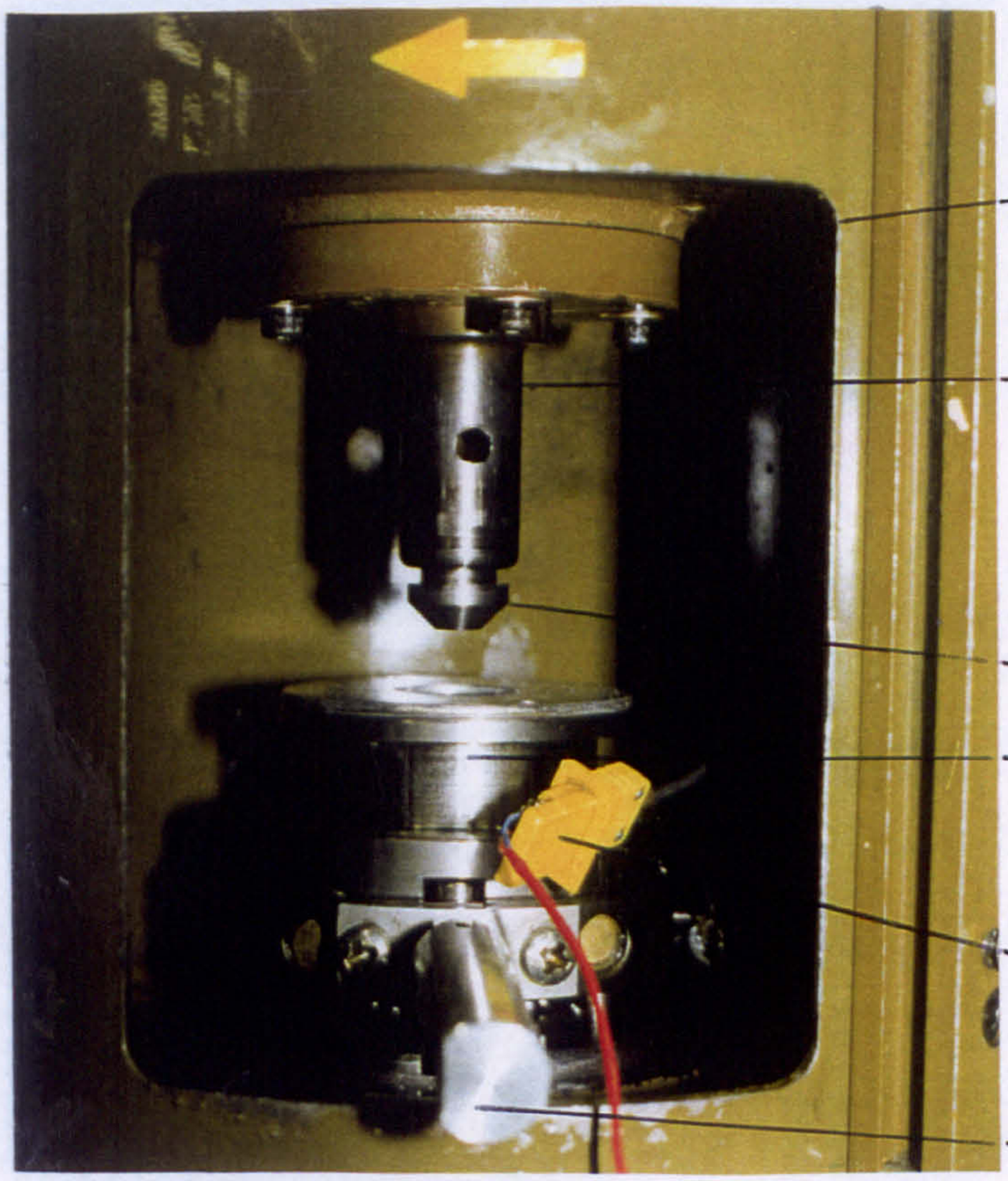

Fig. 3.9 The test assembly inside chamber

3.8 Grinding Test Procedures

Before each test run, the cup, the balls and upper test piece (cone), fig. 3.10, are thoroughly cleaned ultrasonically in an acetone bath. The diameters of the balls are noted before placing them in the cup. The assembly is loaded via a piston below the cup from a lever arm load, figure 3.11 shows the schematic diagram of the four ball machine. The cone is assembled via a collet and the cone contacts with the lower balls after a load is applied. The lower balls are free to rotate and each ball is in contact with the cup at two points, fig. 3.12; the third contact point is between the ball and cone attached to the spindle. Figures 3.13 and 3.14 show the design of the cup and the cone used in all the testing. The contacting surfaces between the cone and lower balls are immersed in a lubricating oil containing abrasive particles.

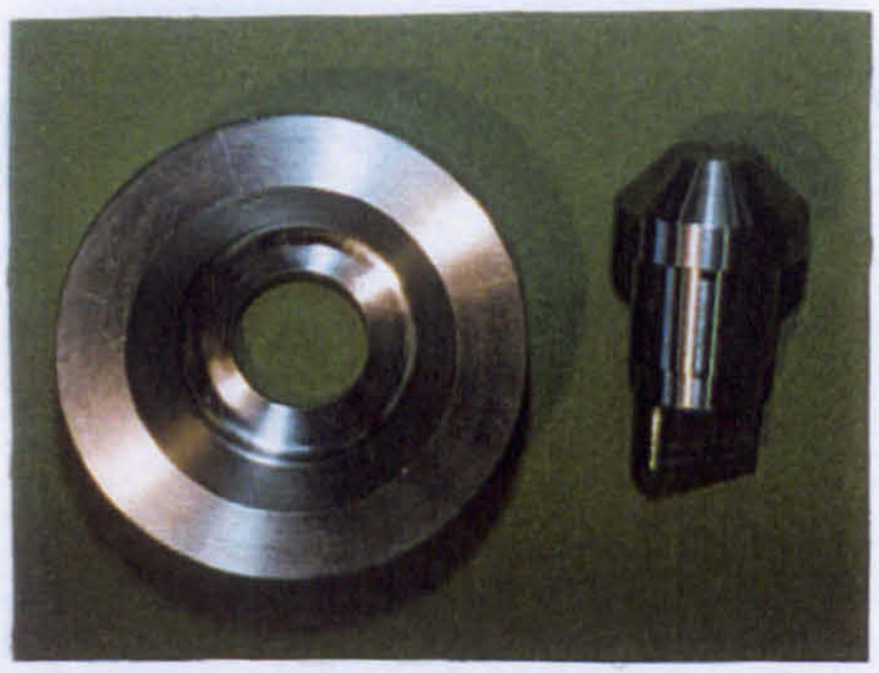

Fig.3.10 The Cup and Cone

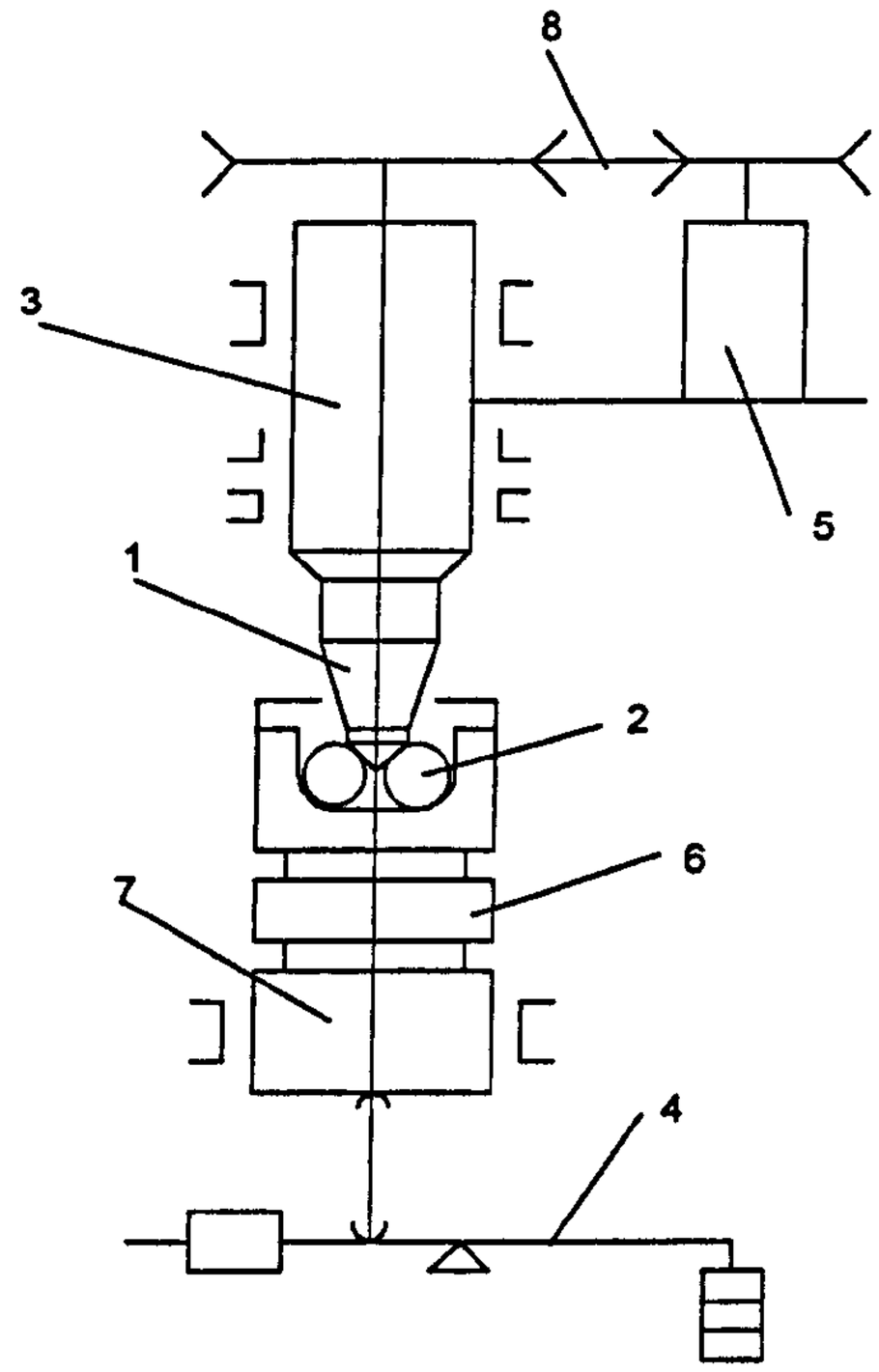

Fig. 3.11 The Modified Four Ball

1 -Cone and collet; 2 -lower balls; 3-spindle; 4 -loading lever;
5 -driving motor; 6 -heated plate;7 -loading piston; 8-belt drive

Spindle speed may be varied electronically up to 20,000rpm and a timer and tachometer record test time and spindle a revolution. The machine may be set to stop either at revolution number or maximum vibration amplitude. After each test the balls are thoroughly cleaned and the diameter is measured again.

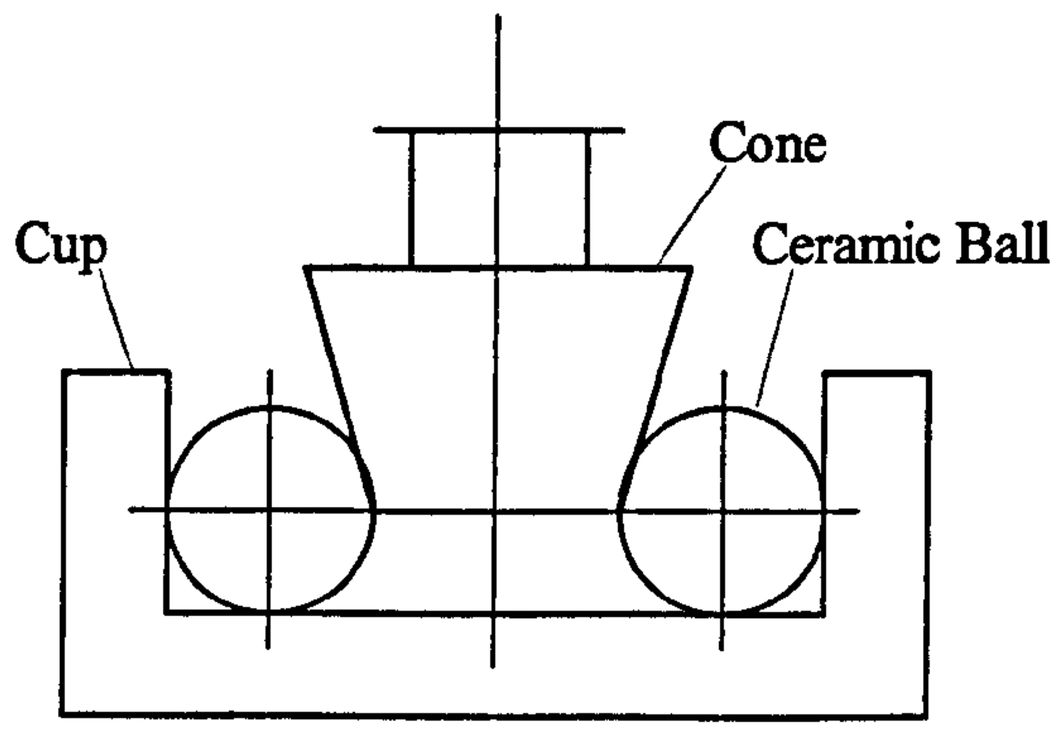

Fig. 3.12 Contact configuration used during grinding experiments

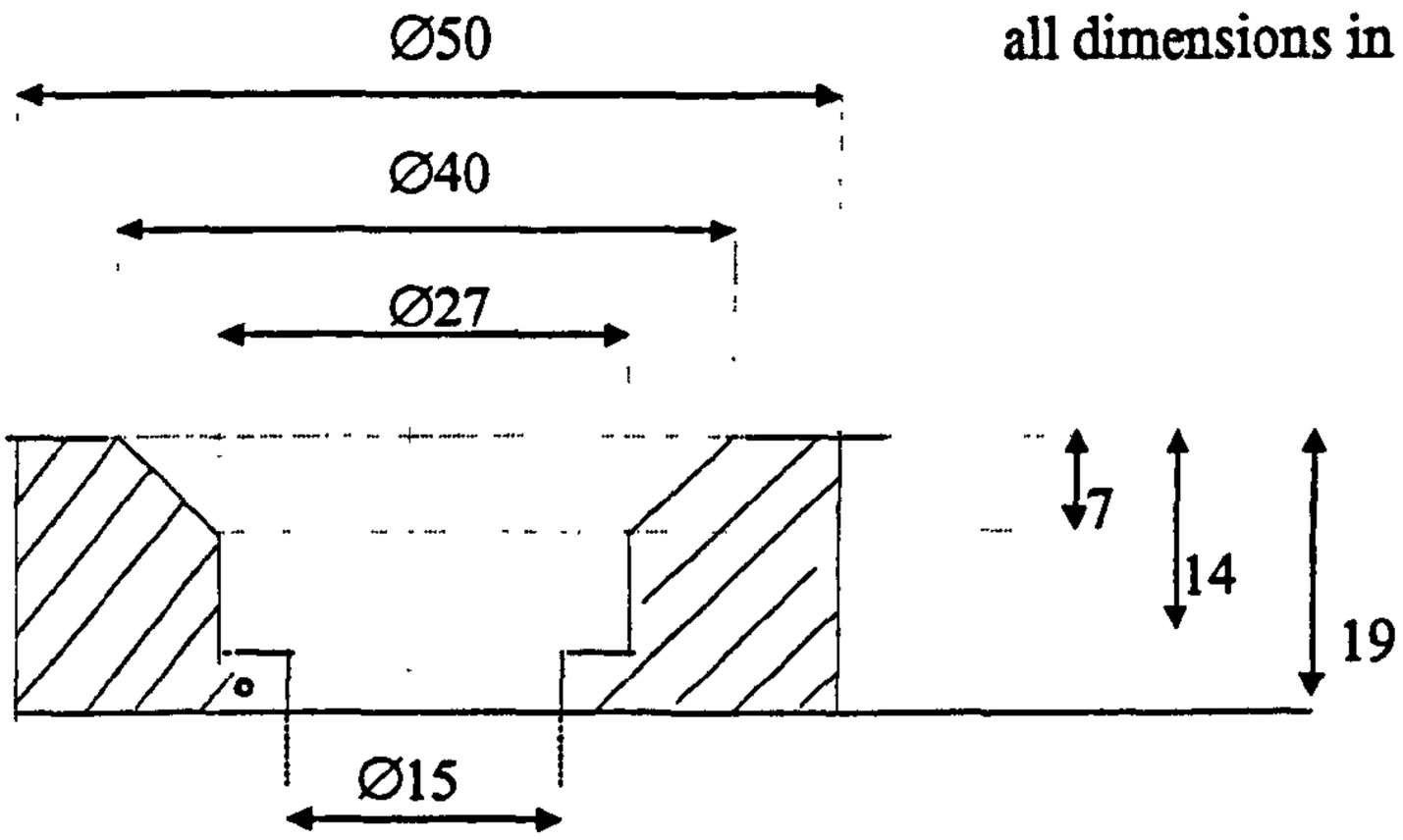

Fig.3.13 The design of the cup

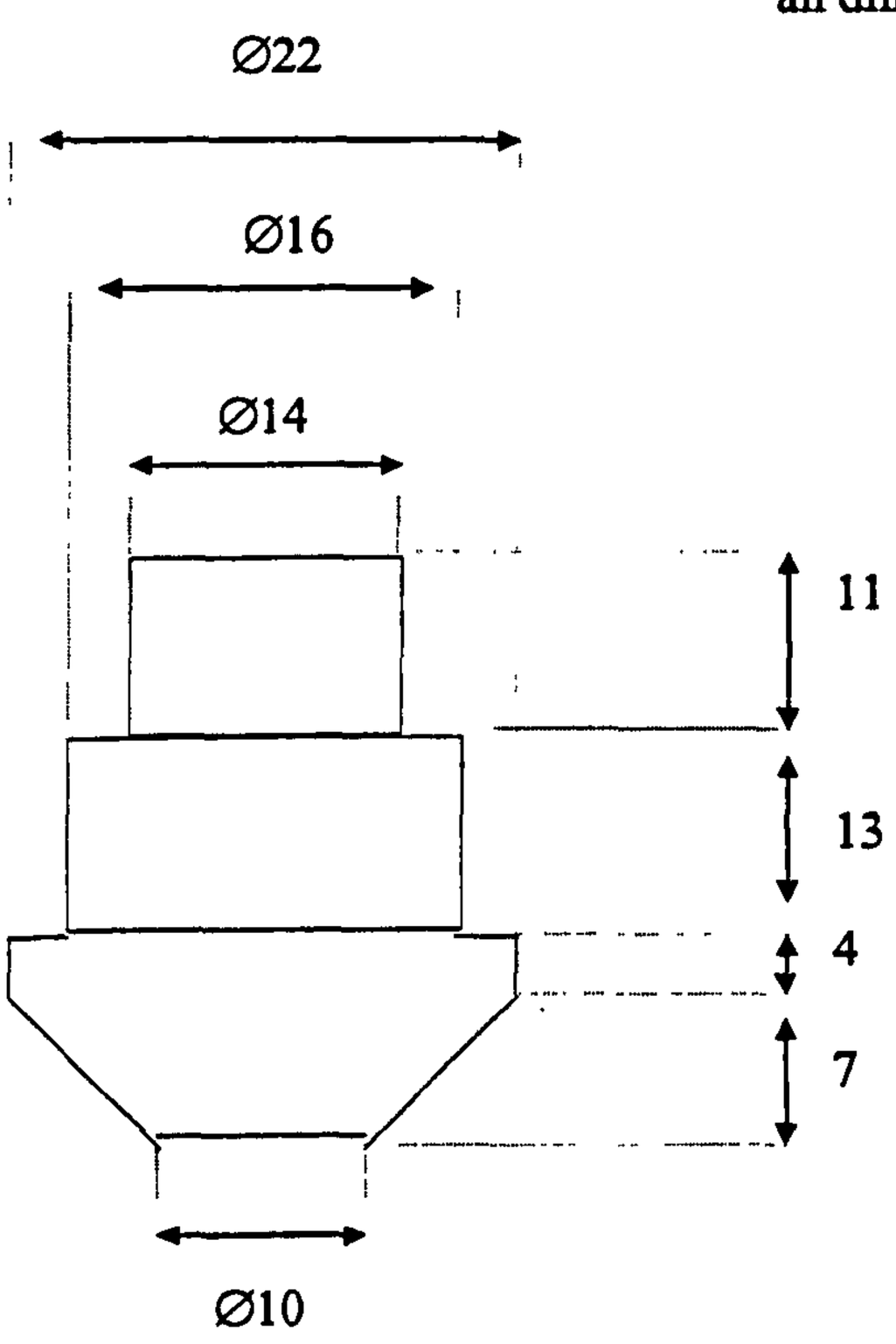

Fig.3.14 The design of the cone

3.8.1 Grinding Slurries

Two types of grinding slurries were used, a commercial slurry and developed slurries which were formulated with a mineral oil base and a synthetic oil base:

- The commercial grinding slurry Kemet was used as a reference for all the grinding tests. This is an oil-based slurry with a suspension of diamond particles. The slurries used were available with various size diamond particles ranging from 1 to 45μm and of concentration of 2 percent by weight.
- The developed grinding slurries were formulated with a mineral oil base and synthetic oil base lubricants, as described in Table 3.2, with the same concentration of diamond particles as the commercial slurries.

3.8.2 Wear Measurements

A micrometer was used to measure the diameter of the balls before each test run. After each test the balls were thoroughly cleaned and the diameter resulting from the test were measured. The average change in diameter of nine ceramic balls used during a test was recorded and the rate of material removed per unit time was calculated. The units of wear rate are μm/min.

3.8.3 Preliminary Grinding Tests

Preliminary tests were carried out on the four ball machine, in order, to identify the optimum parameters for safe material removal from the silicon nitride balls. This was done on the basis of information presented by Stolarski, 1992. The following parameters were identified as having an influence on the rate of material removal:

- cup configuration
- abrasive/fluid concentration
- abrasive and carrier fluid replenishment rate
- tribochemical effects

Further testing by Stolarski and co-workers, 1995, was done in order to investigate the effect of abrasive particles, speed and load applied during the grinding process. Experiments were carried out at a rotational velocity of the spindle ranging from 1500 to 7500rpm. The normal load on the set of nine balls ranged from 200 to 4000N and the abrasive particle size was varied from 1 to 45μm. The results from this study concluded

that the optimum parameters for material removal were achieved by using 15μm diamond abrasive particles, under a load of 400N with a rotational velocity of 3000rpm for 1 hour.

3.8.4 Grinding Test Programme

For all the tests 9 ceramic balls , each of 6.8mm in diameter, were held in cup made from EN58J steel, fig.3.15. The commercial grinding slurries supplied by Kemet are normally used in industry and were therefore used as a reference for the tests.

Kemet slurry of 15μm diamond particles was used for all the tests with 2% by weight concentration. The same concentration of abrasive particles (size 15μm) was used when preparing test grinding slurries. The silicon nitride ball blanks, in the as sintered condition, had very rough surfaces, of order 100-200μm Ra and contained many surface imperfections. Therefore, each ball before testing was subjected to a running- in process before the grinding test. Running-in was carried out in two steps. Firstly, 0.5g of 15μm diamond paste was smeared on the set of blank silicon nitride balls and 4ml of the 15μm oil based diamond slurry by Kemet was added to the stainless steel cup. The set of nine balls were pre-run at 100N and 700rev min^{-1} speed for 1 hour. The load was then increased to 200N and speed increased to 3000 rev min^{-1} for another hour. During this process, approximately 300μm of material was removed from each ball, which resulted in the average reduction of their diameters from the initial 6.8mm to 6.5mm.

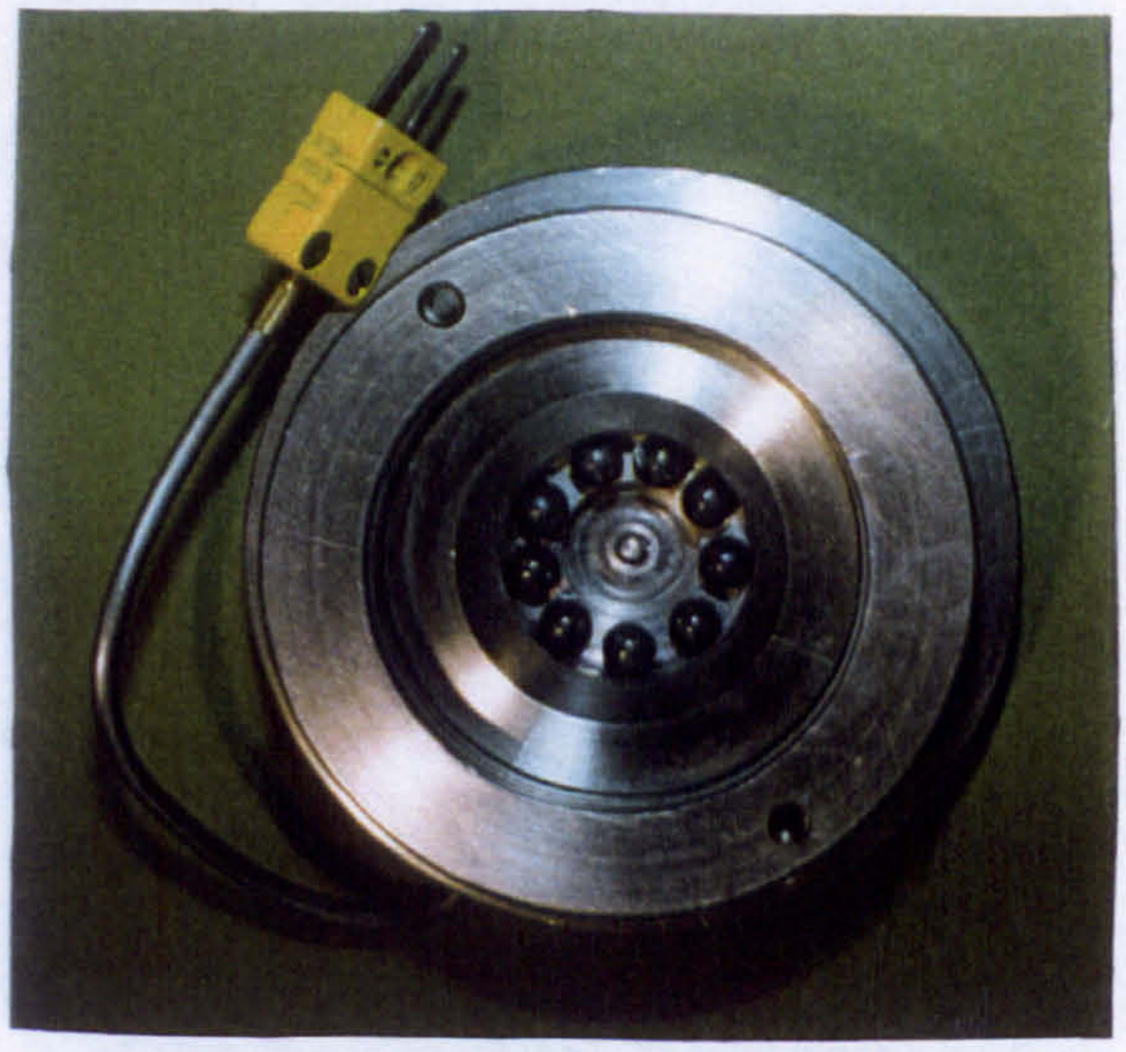

Fig. 3.15 Ceramics balls in cup

The following test parameters were used and each test was repeated four to five times.

Test Samples	9 Ceramic balls -6.5mm diameter held in a cup made of EN58J stainless steel and EN58J stainless steel cone
Lubricant	Reference: Commercial grinding slurry Kemet with 15µm diamond particles Test grinding slurries with 15µm diamond particles: mineral oils - T808853, T80854, ester base fluids- T80855, T80884, poly alpha olefins - T80856, T80857, polyglycols- T81497, T81498, T81499, T81500,T81501, T81502
Load	400 N
Rotational Velocity	3000 rpm
Test Duration	1 hr
Bulk Temperature	40°C

Before and after the tests, all silicon nitride balls and the stainless steel cup and cone were ultrasonically cleaned in acetone. The effectiveness of the lubricants in removing material from the silicon nitride balls was assessed by measuring the change in ball diameter after each test and the material removal per unit time was calculated.

Further surface and chemical analyses was carried out using the scanning electron microscope to obtain micrographs of ball surface, talysurf to measure surface roughness, x-ray diffraction to measure residual stresses and light element x-ray analysis, x-ray photoelectron analysis and infrared spectroscopy for characterising chemical data before and after the grinding tests

3.9 Surface and Chemical Analyses

3.9.1 Scanning Electron Microscope

The Scanning Electron Microscopes (SEM) used for surface analysis were Cambridge S250 and Joel 840A. The SEM has five distinct systems, that is, the electron gun source, the condenser system, the scanning system, the detection facility and the display system. The electron beam is focused into a fine probe and subsequently raster scanned over a small rectangular area. As the beam interacts with the sample it creates various signals (secondary electrons, internal currents, photon emission,etc.). These signals are highly

localised to the area directly under the beam. By using these signals to modulate the brightness of a cathode ray tube, which is raster scanned in synchronism with the electron beam, an image is formed on the screen. The image can be magnified in the range of X10 to X100,000.

Silicon nitride ceramics are non-conducting and so require the application of a conducting coating before they can be examined in the SEM. This is achieved by sputter coating the SEM specimens with gold. Argon gas bled into a vacuum chamber, is ionised in the high vacuum and accelerated towards the gold target. A uniform coating is produced and the thickness can be controlled to the nm level.

3.9.2 Atomic Force Microscope

The Atomic Force Microscope (AFM) was used to analyse the surface profile of the ceramic balls after the friction tests. This was recorded using the SPA 350 machine by SEIKO Instruments Ltd., at the Institute of Ashikaga, Japan. The AFM is a mechano-optical instrument, which detects atomic level forces (~nN) through optical measurements using a very sensitive cantilever tipped with a hard, pyramid-shaped crystal moving along the surfaces. The AFM can produce a high resolution, two- and a three-dimensional image of the sample surfaces. The vertical resolution is below 0.1nm range, whereas lateral resolution is much lower. The tip is very sharp and protrudes from a small cantilever. The laser reflects off the top side of the tip and is directed to a split photodiode.

The height of the surface of the sample deflects the cantilever causing the position of the laser on the photodiode to change. The difference in voltage from the photodiode elements provides a 'picture' of the surface . AFM scans are done in a raster pattern. As it scans it sends the cantilever deflection-error signal to the control station. The digital signal processor (DSP) in the workstation controls the Z position of the cantilever-deflection error signal. The AFM can operate in either a 'constant mode' or a 'constant height mode'. In the constant force mode, the DSP adjusts the height of the sample under the tip based on the deflection error signal, thus keeping the force constant. The constant height mode keeps the sample at a set height then measures the deflection of the laser on the photodiode.

3.9.3 Talysurf

The Rank Taylor Hobson Talysurf 120 Stylus profilometer is a precision metrology instrument used for measuring surface texture. This was used before and after the grinding tests of the silicon nitride balls. A fine stylus is dragged smoothly and steadily across the surface under examination and as the stylus travels over the surface it rises and falls. Its vertical displacement is converted by a transducer into an electrical signal, which is amplified and recorded on the chart recorder. The graph drawn on a chart recorder represents the vertical displacement of the stylus as a function of the distance travelled along the surface. The stylus tip radius is in the range of 1.5-2.5 microns.

3.9.4 Light Element X-ray Analysis (EDX and WDX)

Chemical analysis was performed on the ceramic samples using the Cambridge S250 microscope with an Energy Dispersive X-Ray system (EDX). The Jeol 840A machine was used to perform a chemical analysis by a Wavelength Dispersive X-Ray system (WDX). The basic principle of both systems is the detection of X-rays, which are generated by the interaction of the electron beam with the specimen.

The sample is usually coated with carbon when the WDX method is used, as gold interferes with accurate quantitative chemical analysis. The EDX method is quicker at qualitative analysis than the WDX method, but if quantitative is required then the WDX system must be used.

3.9.5 X-Ray Photoelectron Spectroscopy(XPS) and Auger Electron Spectroscopy(AES)

Chemical analysis information was obtained using the Fison Surface Science/V.G. Escalab 210 instrument. All elements from Lithium to Uranium can be detected using either XPS and/or AES. Surface analysis is sensitive to surface layers of less than 10nm in depth. Information on the nature of the chemical bonding of elements at the surface can be seen in XPS and Auger Spectra. Quantitative analysis of the sample surface can be obtained using advanced spectrum processing software.

XPS and Auger Depth Profiling can be performed, with computer control of both the analysis and ion beam etching gun. This allows successive layers of material to be removed from the surface.

Analytical information is then obtained at each step, to give a profile of the sample composition through the surface layers. XPS can allow analysis of regions less than 100μm in diameter. The scanning Auger analysis can provide surface chemical analysis information with a resolution of 100nm.

3.9.6 Infrared Spectroscopy

The Nicolet Fourier Transform Infrared (FTIR) 400 Laser Spectrometer was used for chemical analysis of the grinding slurries. FTIR is a powerful analytical tool for characterising and identifying organic molecules. The IR spectrum of an organic compound provides specific information about chemical bonding and molecular structure. It is based on the principles that molecular vibrations occur in the infrared region of the electromagnetic spectrum and functional groups have characteristic absorption frequencies. In an IR spectrometer there is a source of IR light, covering the whole frequency range of the instrument, which is split into two beams of equal intensity. One beam is passed through the sample and the other is used as a reference against which it is compared. The spectrum is obtained as a chart showing absorption peaks, plotted against wavelength or frequency.

3.9.7 Residual Stress Measurements

Residual Stresses induced during grinding of ceramics may have an important influence on the performance of the ceramic components. In order to design a high quality component it is necessary to know and control the residual stress state of a material.

The X-ray stress measurement method is the only non-destructive means of finding residual stress. The stress in the material can be directly measured in a non-contact manner. Residual stress is measured on the ceramic ball after the grinding tests in order to investigate the influence of grinding using the most effective lubricant on the residual stresses within the ceramic ball.

The measurement of residual stress was performed on the 'Rigaku Strainflex MSF-2M' machine at the Institute of Ashikaga in Japan. These stresses are measured using X-ray diffraction. The procedure used is known as the $\sin^2 y$-method. In X-ray diffraction a collimated beam of X-rays, with wavelength λ=~0.5 is incident on the specimen according to Braggs Law ($\lambda = 2d\sin\theta$, where d is the spacing between atomic planes in the crystalline phase). The intensity of the diffracted X-rays is measured as a function of the diffraction angle 2θ and the specimen orientation. This diffraction pattern is used to identify the specimens crystalline phases and to measure its structural properties, including strain, and the size and orientation of crystallites.

The X-ray tube is typically copper or chromium, with maximum load of 30kV and 8mA, and incident and receiving parallel slits direct the beam. A goniometer enables a detector scanning range of 120 to 170 degrees and, with standard stepper motor control, accuracy is within standard tolerances. The detector is a scintillation counter probe type, in which the rate meter transforms the count rate to direct current voltage which is fed into the recorder.

REFERENCES

Bearing Traders Ltd., 1994, Bearing Specification, Uxbridge Middlesex.

Cerbec Bearing Company, 1994, **'Technical data sheet #1A'**, East Granby, Connecticut, USA.

Morgan Matroc Ltd., 1994, Sialon Plate Technical Data, Stourport-on-Severn, Worcestershire.

Stolarski, T. A., 1992, **"Accelerated wear of ceramic balls"**, Ceramics International, Vol.18, pp.379-384.

Stolarski, T. A., Jisheng, E., Gawne, D. T. & Panesar, S., 1995, **"The effect of load and abrasive particle size on the material removal rate of silicon nitride artefacts"**, Ceramics International, Vol. 21, pp.355-366.

TE70 Material Specification, 1994, Plint & Partners Ltd., Wokingham, Berkshire, UK.

Chapter 4

RESULTS AND DISCUSSION OF MODEL FRICTION EXPERIMENTS

4.1 Introduction

The fundamental friction properties of silicon nitride ceramics are analysed and discussed, with the aim of understanding the tribological properties of these ceramics under various conditions and how they could help explain and interpret the results of model grinding experiments.

Preliminary testing was performed to investigate the effects of varying the frequency, amplitude, load, temperature and sliding material of a ceramic ball sliding on steel plate. Further work was undertaken to investigate the effect of the various lubricants used during grinding experiments on the friction characteristics of the silicon nitride ceramics.

4.2 Preliminary Friction Measurements using Lubricant Talpa 20

4.2.1 Effect of varying stroke frequency

The effect of varying frequency on the coefficient of friction of the ceramic ball sliding on the steel plate under a constant contact pressure of 304MNm^{-2} and an stroke amplitude of 0.3mm under lubricated conditions is shown in fig.4.1. The results show an initial decrease in coefficient of friction from 0.095 to 0.075 as the frequency is increased from 10 Hz to 20Hz. As the frequency is further increased the coefficient of friction values remain fairly constant within a range of 0.075 to 0.08. The decrease in coefficient of friction coefficient could be due to the possible creation of a lubricant film separating the contact surfaces as the frequency increased.

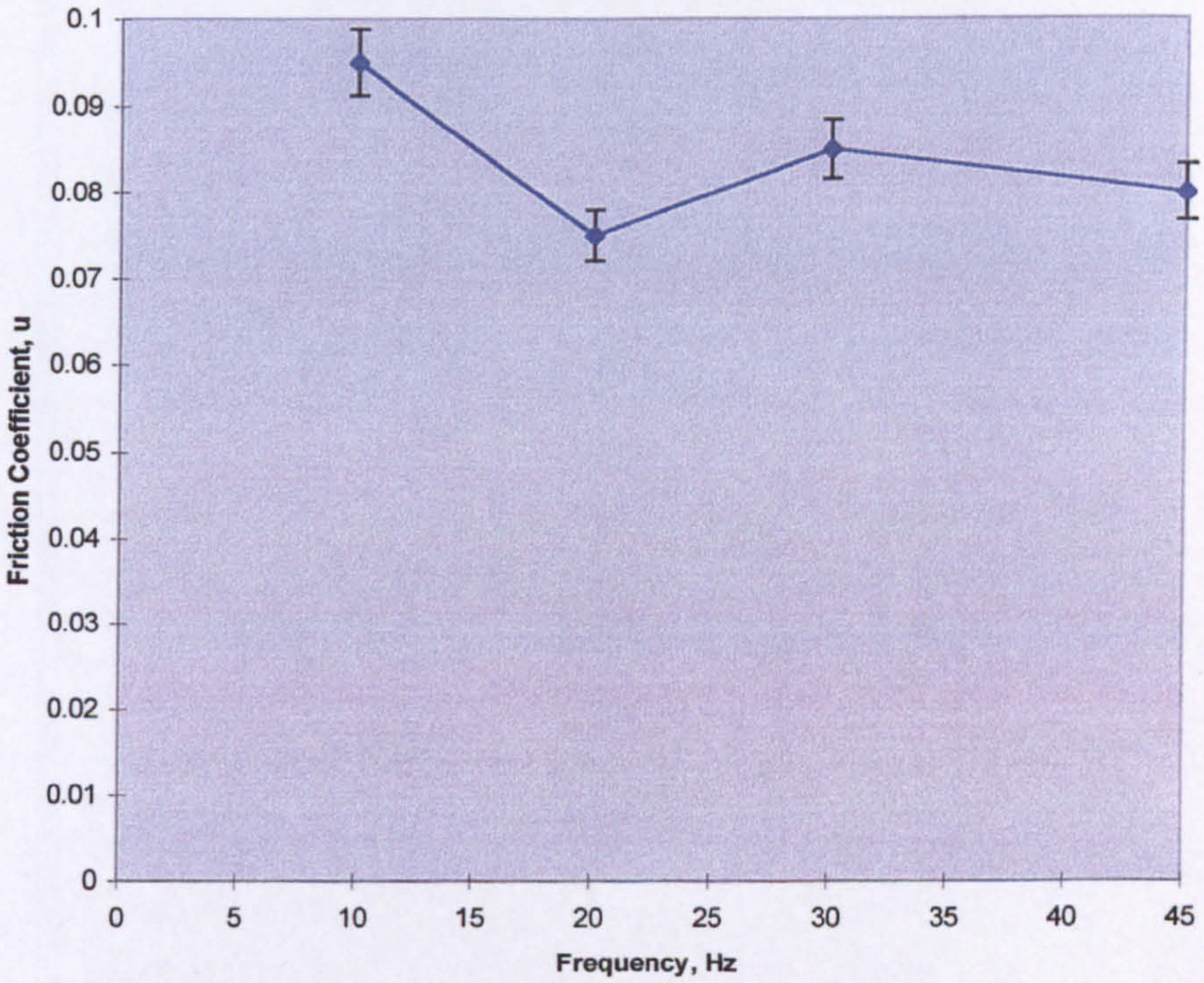

Fig. 4.1 The variation of friction coefficient with a stroke frequency for a ceramic ball sliding on a steel plate lubricated with Talpa 20 (Load 5N, amplitude 0.3mm)

4.2.2 Effect of varying amplitude

The effect of varying amplitude on the coefficient of friction of a ceramic ball sliding on a steel plate under a constant contact pressure 304MNm^{-2} (load 5N) and a frequency of 30Hz, under lubricated conditions is shown in fig. 4.2. There is a very gradual and small increase in the coefficient of friction from 0.07 to 0.095 as the amplitude is increased from 0.2mm to 1mm. By increasing the amplitude the sliding speed is also increased since the frequency is kept constant at 30Hz. As the sliding speed is increased the interface temperature increases causing degradation of the lubricant, hence an increase in the coefficient of friction.

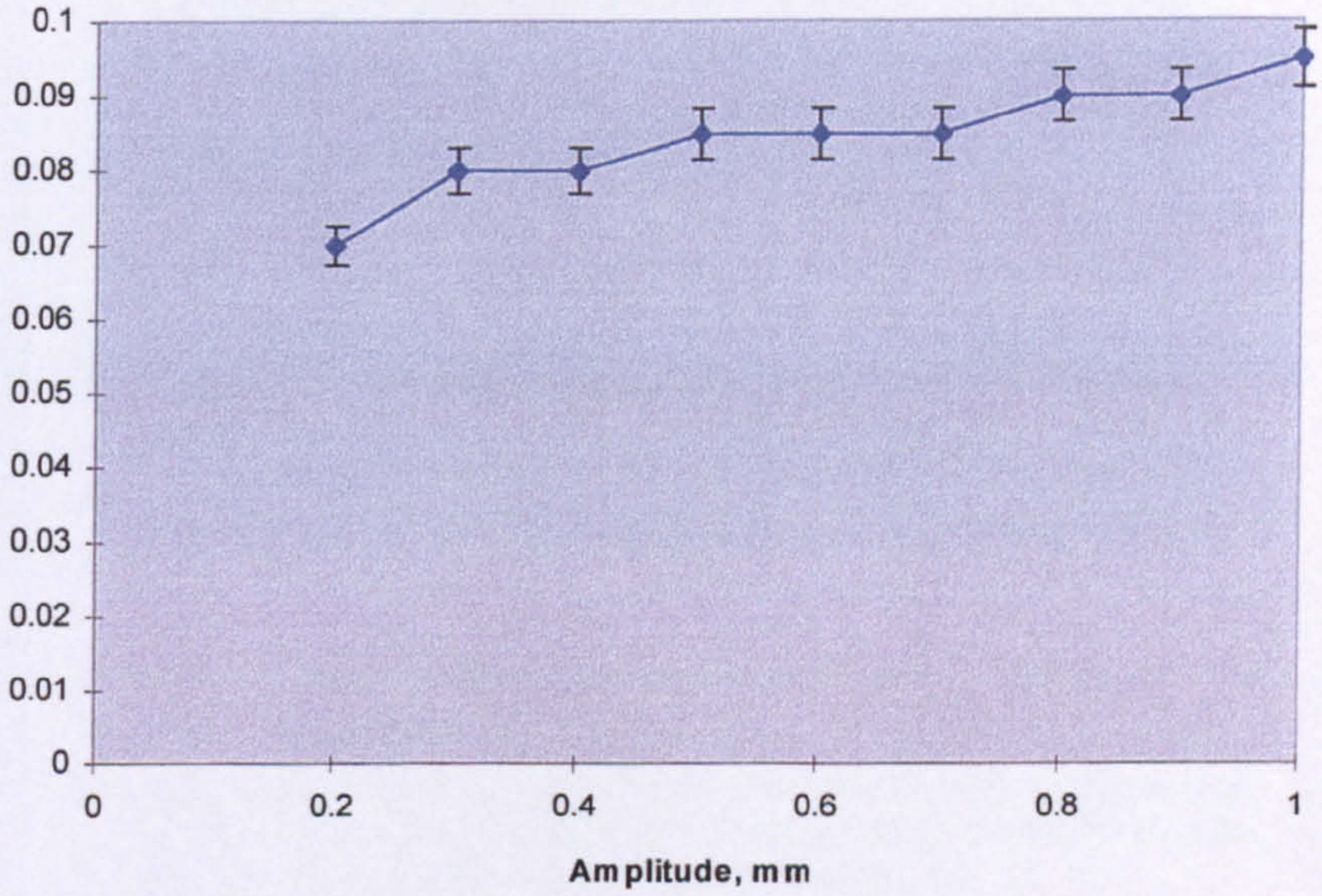

Fig. 4.2 The variation of friction coefficient with amplitude for a ceramic ball sliding on a steel plate lubricated with Talpa 20 (Load 5N, frequency 30Hz)

4.2.3 Effect of varying normal load

The relationship between the coefficient of friction and load for a ceramic ball sliding on a steel plate at a constant frequency of 45Hz and an amplitude of 0.3mm under lubricated conditions is shown in fig. 4.3. The results show no significant effect on the coefficient of friction by varying the load from 5N to 25N (corresponding contact pressure is from 304 to 521MNm^{-2}. The values show very little scatter and the coefficient of friction increases gradually from 0.09 to 0.098.

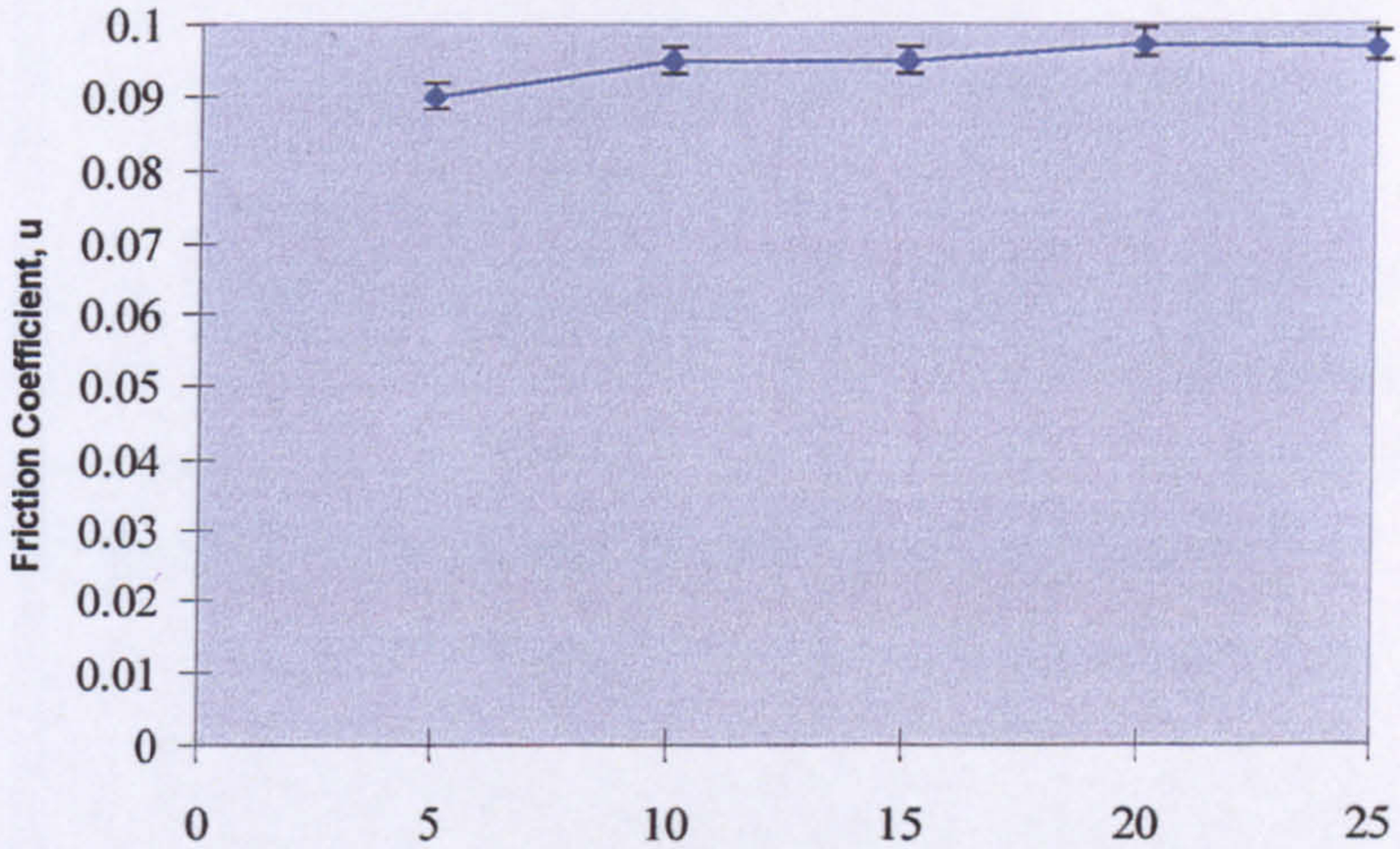

Fig. 4.3 The variation of friction coefficient with normal load for a ceramic ball sliding on a steel plate lubricated with Talpa 20 (frequency 45Hz, amplitude 0.3mm)

As the load is increased, the probability of asperity contact increases, that is, an increase in the contact area. This could, therefore, result in a slight gradual increase in the coefficient of friction.

4.2.4 Effect of varying temperature

The effect of varying temperature on the coefficient of friction of a ceramic ball sliding on a steel plate under a constant load of 5N (contact pressure 304MNm^{-2}), a frequency of 45Hz and an amplitude of 0.3mm, under lubricated conditions is shown in fig. 4.4. The results show that initially for a temperature range of 30°C to 80°C, the coefficient of friction is in the range of 0.08 to 0.085, however, as the temperature is further increased from 80°C to 100°C, there is a sharp increase in the values from 0.085 to 0.105. On further increase in the temperature from 100°C to 120°C the coefficient of friction remains constant at 0.1. Further increase in temperature from 120°C to 160°C shows a gradual increase in the coefficient of friction from 0.1 to 0.11.

The increase in the coefficient of friction at the higher temperatures could have been due to a decrease in the viscosity of the lubricant, under such conditions, the extent of ceramic-to-steel contact, hence, the asperity-asperity interactions increase resulting in a higher coefficient of friction.

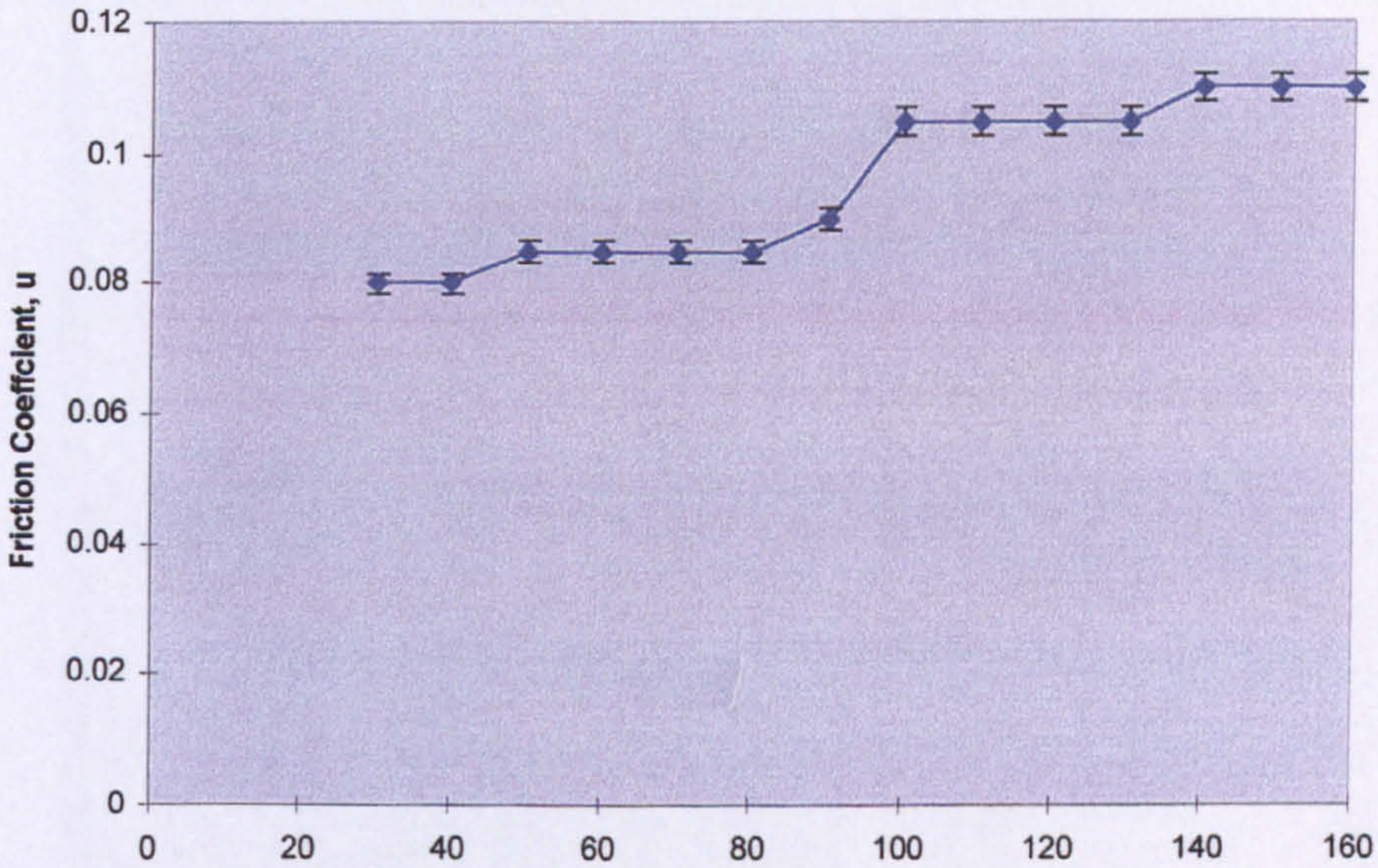

Fig. 4.4 The variation of friction coefficient with temperature for a ceramic ball sliding on a steel plate lubricated with Talpa 20 (Load 5N, frequency 45Hz, amplitude 0.3mm)

4.2.5 Effect of varying the combination of materials in contact

The effect of varying sliding material on the coefficient of friction with temperature under a constant load of 5N, a frequency of 45Hz and an amplitude of 0.3mm under lubricated conditions is shown in fig. 4.5. The results show that initially from a temperature range of 30°C to 70 °C all three sliding contacts give very close values of the coefficient of friction, that is, in the range of 0.08, however, as the temperature is further increased from 70 °C to 100 °C there is a clear difference in the values. The ceramic/ceramic sliding contacts give the highest coefficient of friction of 0.09; the ceramic/steel sliding contacts give a value of 0.085 and the steel/steel contacts give the lowest value of 0.076. On further increase in temperature from 100 °C to 160 °C the ceramic/steel contacts results in a very high coefficient of friction in the range of 0.1 to 0.11 indicating disruption of a boundary film. For the ceramic/ceramic contacts the coefficient of friction ranges from 0.09 to 0.095. The steel/steel contacts give the lowest coefficient of friction in the range of 0.08 to 0.085.

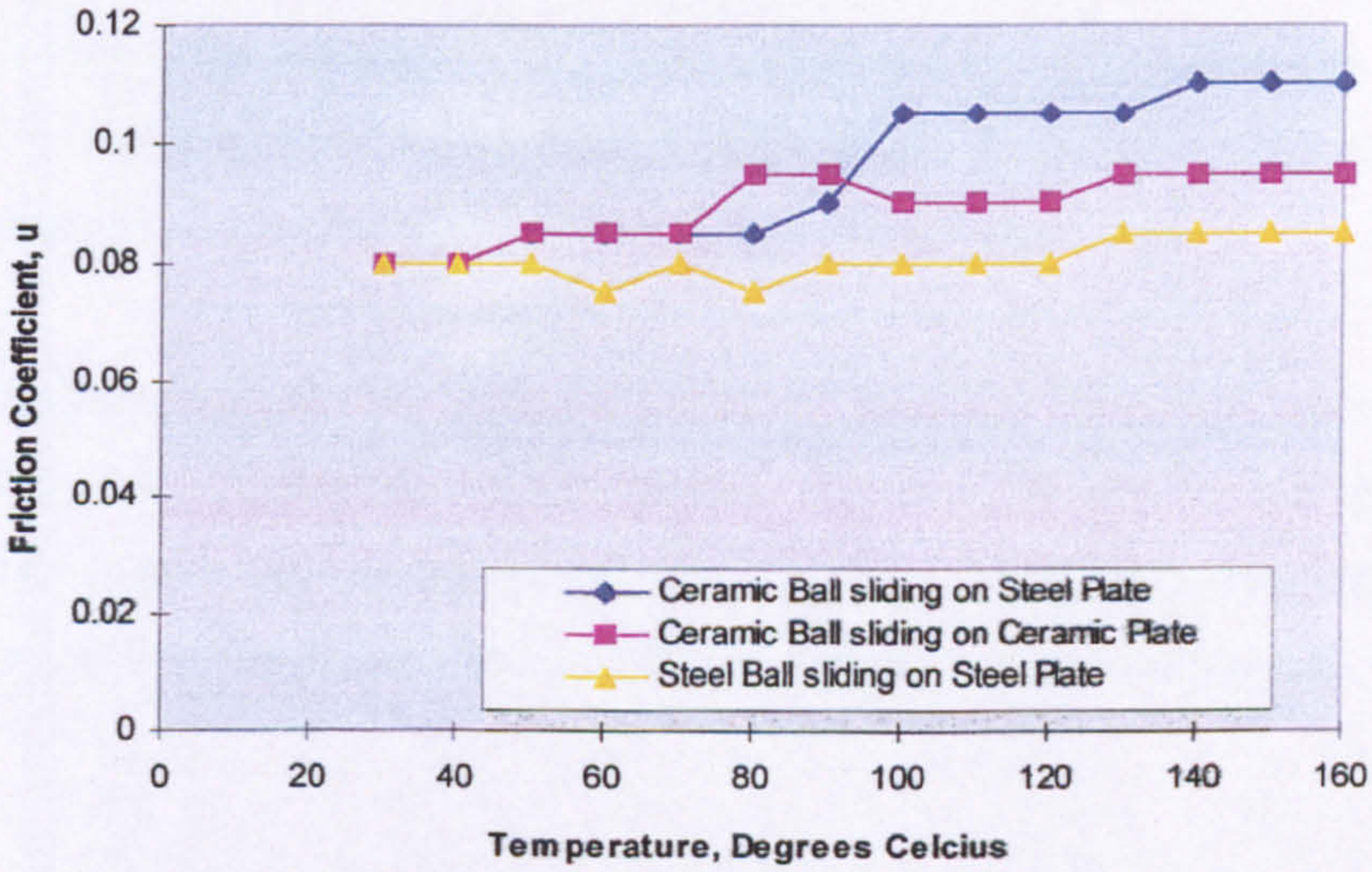

Fig. 4.5 The variation of friction coefficient with temperature for a ceramic ball sliding on a steel plate, ceramic ball on ceramic plate and steel ball on steel plate using the Talpa 20 lubricant

The results show that up to a temperature of 90°C, in the presence of the reference hydrocarbon oil, Talpa 20, the coefficients of friction are in the following order for the different sliding pairs:

ceramic ball/ceramic plate > ceramic ball/ steel plate > steel ball/steel plate

As the temperature is further increased from 90°C - 160°C the coefficients of friction are in the following order:

ceramic ball/steel plate > ceramic ball/ceramic plate > steel ball/steel plate.

Studies done by Mimaroglu and Yilmaz, 1997, also showed similar results. They found ceramic-ceramic pairs gave the highest coefficient of friction values in the range of 0.125. The coefficient of friction values for steel-steel pair and ceramic-steel pair were found to be in the order of 0.1.

The slightly higher friction coefficients of the ceramic-ceramic pairs could be due to their high chemical inertness, i.e., the sliding ceramics not being able to form effective boundary films on their sliding surfaces during lubricated sliding. The lower coefficients of friction observed on the steel-steel or ceramic-steel pairs were most likely due to the formation of an effective boundary film on the sliding surfaces.

Another reason for the high coefficients of friction for the ceramic-ceramic pairs could be due to the much higher elastic modulus of silicon nitride, i.e., 320GPa vs 207GPa for steel. Under high contact pressures, the lubrication regime is expected to shift toward thinner boundary films which could lead to higher friction coefficients.

4.3 Friction measurements using mineral and synthetic oils

Coefficient of friction values in relation to temperature for a ceramic ball sliding on a steel plate under constant contact conditions using various lubricants is shown in fig. 4.6. The results show that over a temperature range of 30 °C to 100 °C, the lowest coefficient of friction of 0.07 is obtained using the ester base fluid T80884; the highest value of 0.185 is obtained using the polyglycol T81499 and the reference base oil Talpa 20 gives a value of 0.01. On further increasing the temperature from 100 °C to 170 °C the lowest coefficient of friction of 0.08 is obtained with ester base fluid T80884; the highest value of 0.23 is obtained using the polyalphaolefin T80856 and the reference oil Talpa 20 gives a value of 0.11.

Further testing was carried out for a ceramic ball sliding on a steel plate under lubricated conditions with the reference oil Talpa 20, the ester base fluid T80884 which gave the lowest value in coefficient of friction and the polyglycol T81499 which gave the highest value. Additives phosphate ester, triethanol amine and amine phosphate were mixed with the lubricants at 0.1%, 0.2% and 0.3% by weight concentration. The results are presented in the following sections.

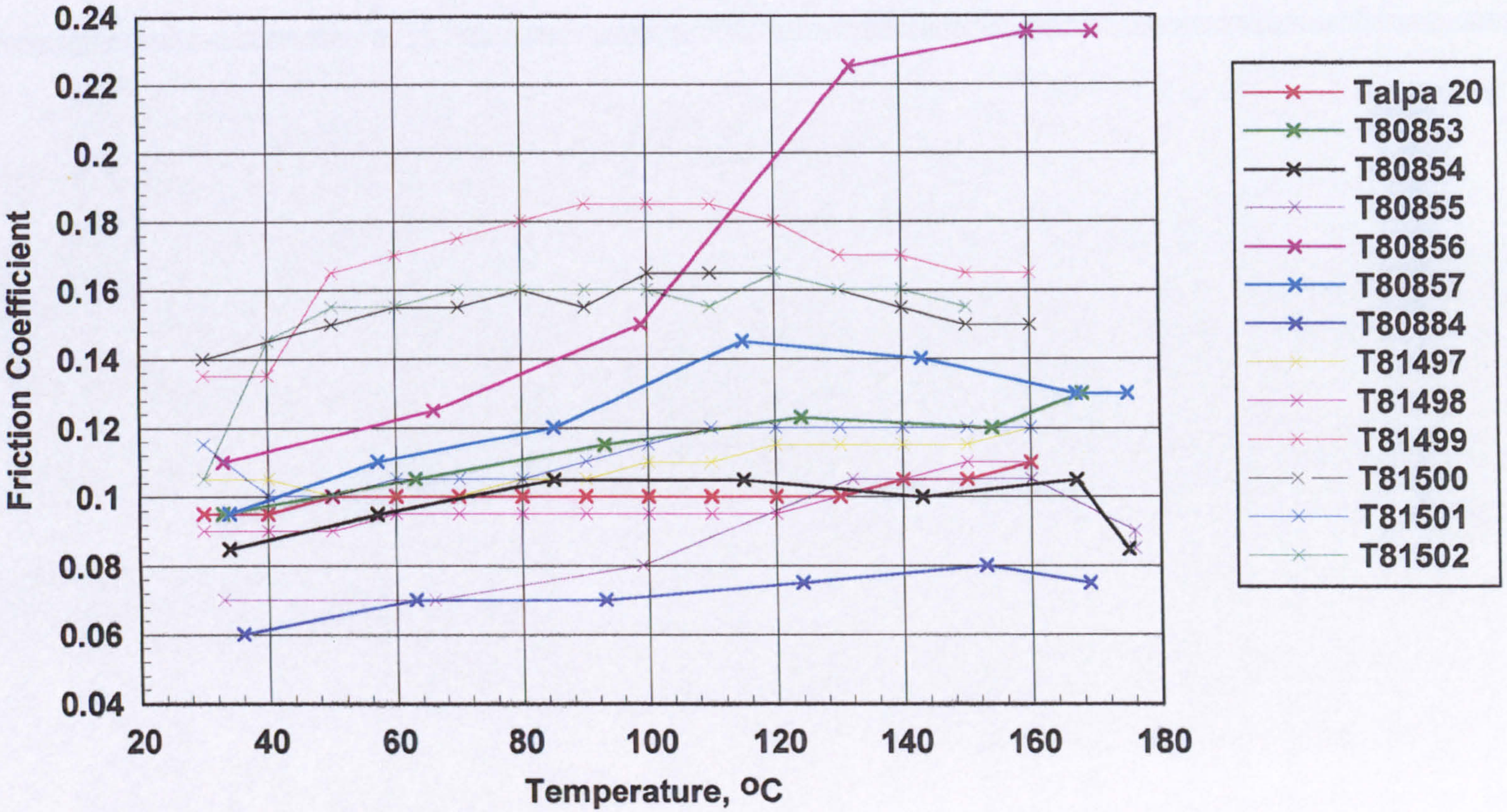

Fig. 4.6 The variation of friction coefficient with temperature for a ceramic ball sliding on a steel plate using various lubricants (Load 5N, frequency 45Hz, amplitude 0.3mm)

4.4 Friction Measurements using the additive Phosphate Ester

Figure 4.7 shows that there is a slight increase in the coefficient of friction of the ceramic ball sliding on the steel plate when using various concentrations of phosphate ester in Talpa 20. At 0.1% and 0.2% concentrations of the additive in Talpa 20 there is a gradual increase in coefficient of friction from 0.1 to 0.14 as the temperature is increased from 30°C to 70°C. When using 0.3% of additive the coefficient of friction at all temperature ranges is similar to that obtained when using only Talpa 20. As the temperature is further increased from 70°C to 160°C all the lubricants with additive and with only Talpa 20 gradually give a constant coefficient of friction in the range of 0.12-0.13.

Figure 4.8 shows that there is an increase in the coefficient of friction of ceramic ball sliding on steel plate when ester base fluid T80884 is mixed with phosphate ester at the various concentrations. When using only the ester base fluid T80884 the coefficient of friction gradually increases from 0.08 to 0.1 as the temperature is increased from 30°C to 160°C. When using 0.1% and 0.2% phosphate ester with ester base fluid T80884 the coefficient of friction shows a slight increase from 0.11 to 0.13 as the temperature is increased from 30°C to 70°C. On further increasing the temperature from 70°C to 160°C there is a gradual decrease in the coefficient of friction from 0.13 to 0.1. When using 0.3% phosphate ester the coefficient of friction is fairly constant at 0.1 for all temperature ranges.

Figure 4.9 shows that there is a slight decrease in coefficient of friction of ceramic ball sliding on steel plate when using polyglycol T81499 with phosphate ester at various concentrations. All the lubricants tested, that is, with and without additive show a very similar trend in the coefficient of friction. As the temperature is increased from 30°C to 80°C there is a gradual increase in coefficient of friction, on further increase from 80°C to 120°C there is a plateau of constant values, and on further increase from 120°C to 160°C there is a gradual decrease in the coefficient of friction. When using 0.1% and 0.3% additive the results for coefficient of friction are very similar, that is, a gradual increase in coefficient of friction from 0.13 to 0.15 as the temperature is increased from 30°C to 80°C. On further increase in temperature from 80°C to 120°C the coefficient of friction of 0.16 is constant, and on further temperature increase from 120°C to 180°C there is a gradual decrease from 0.17 to 0.14. When using 0.2% additive the coefficient

of friction showed a gradual increase from 0.13 to 0.15 as the temperature increased from 30°C to 80°C. On further increase from 80°C to 120°C the coefficient of friction is constant at 0.15 and on further increasing from 120°C to 160°C there is a gradual decrease in the coefficient of friction from 0.15 to 0.13.

When comparing the effects of using only Talpa 20 and Talpa 20 with the additive, there is a slight increase in the overall coefficient of friction, however, when using the additive with ester base fluid T80884 there is a more significant increase in the coefficient of friction than without additive. Polyglycol T81499 with the additive gives a significant decrease in coefficient of friction as compared to without additive. Overall, ester base fluid T80884 gives the lowest overall coefficient of friction range with and without the additive phosphate ester. Justification of these results is provided in section 4.4.1 which deals with results of the surface studies and also in the summary of the results in section 4.7.

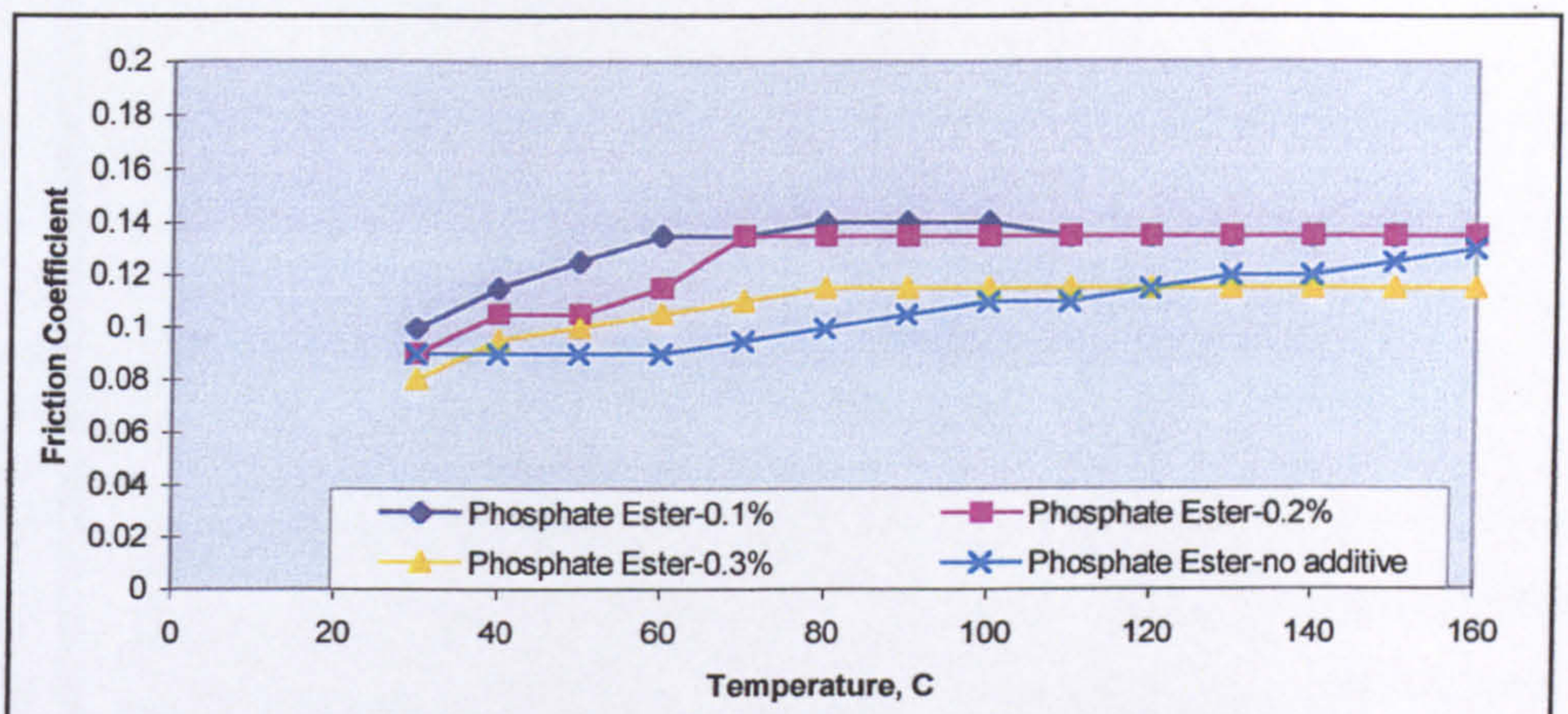

Fig. 4.7 The variation of friction coefficient with temperature for a ceramic ball sliding on a steel plate lubricated with a mixture of Talpa 20 and Phosphate Ester at various concentrations (load 5N, amplitude 0.3mm, frequency 45Hz)

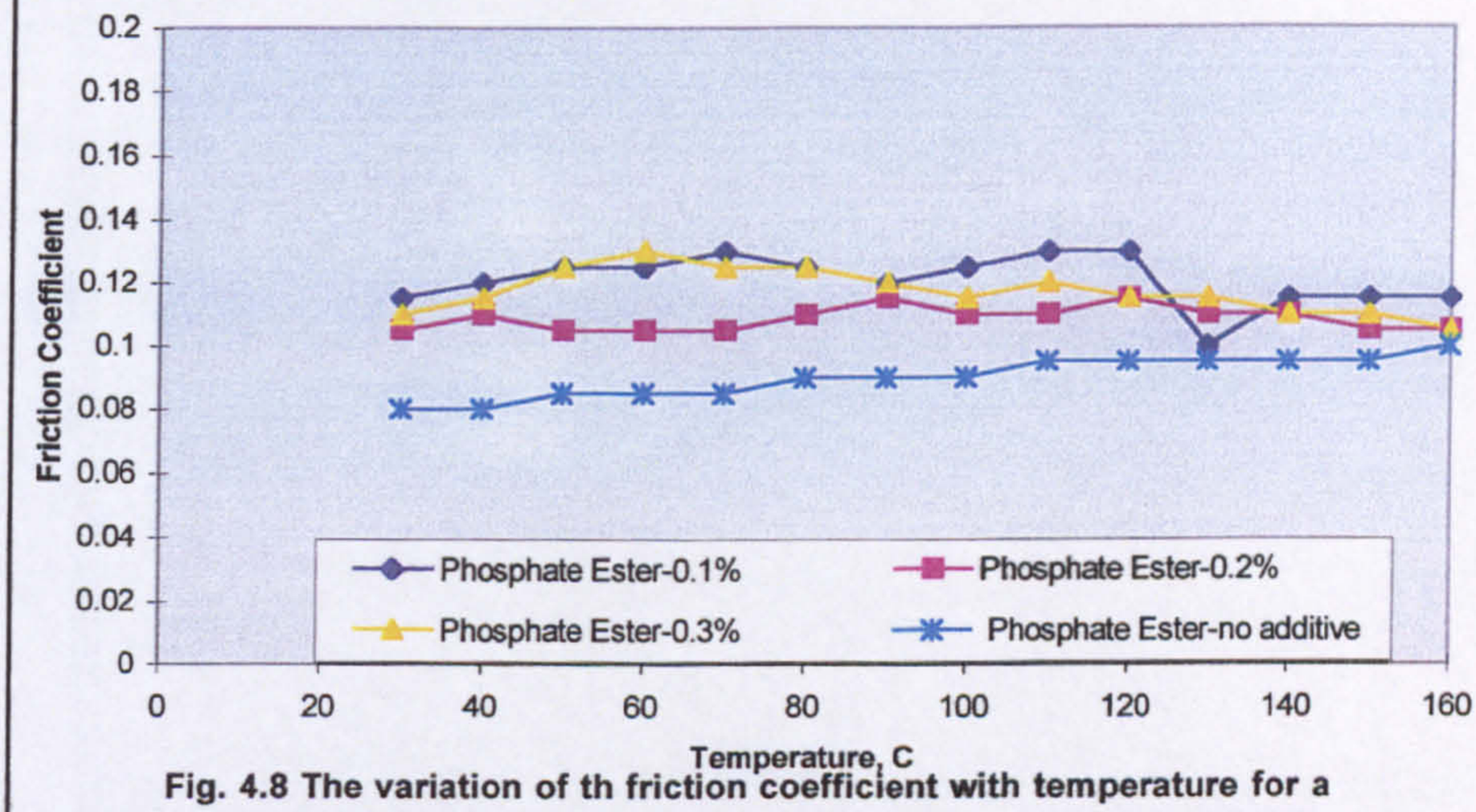

Fig. 4.8 The variation of th friction coefficient with temperature for a ceramic ball sliding against a steel plate lubricated with Ester T80884 with Phosphate ester at various concentrations (load 5N, amplitude 0.3mm, frequency 45Hz)

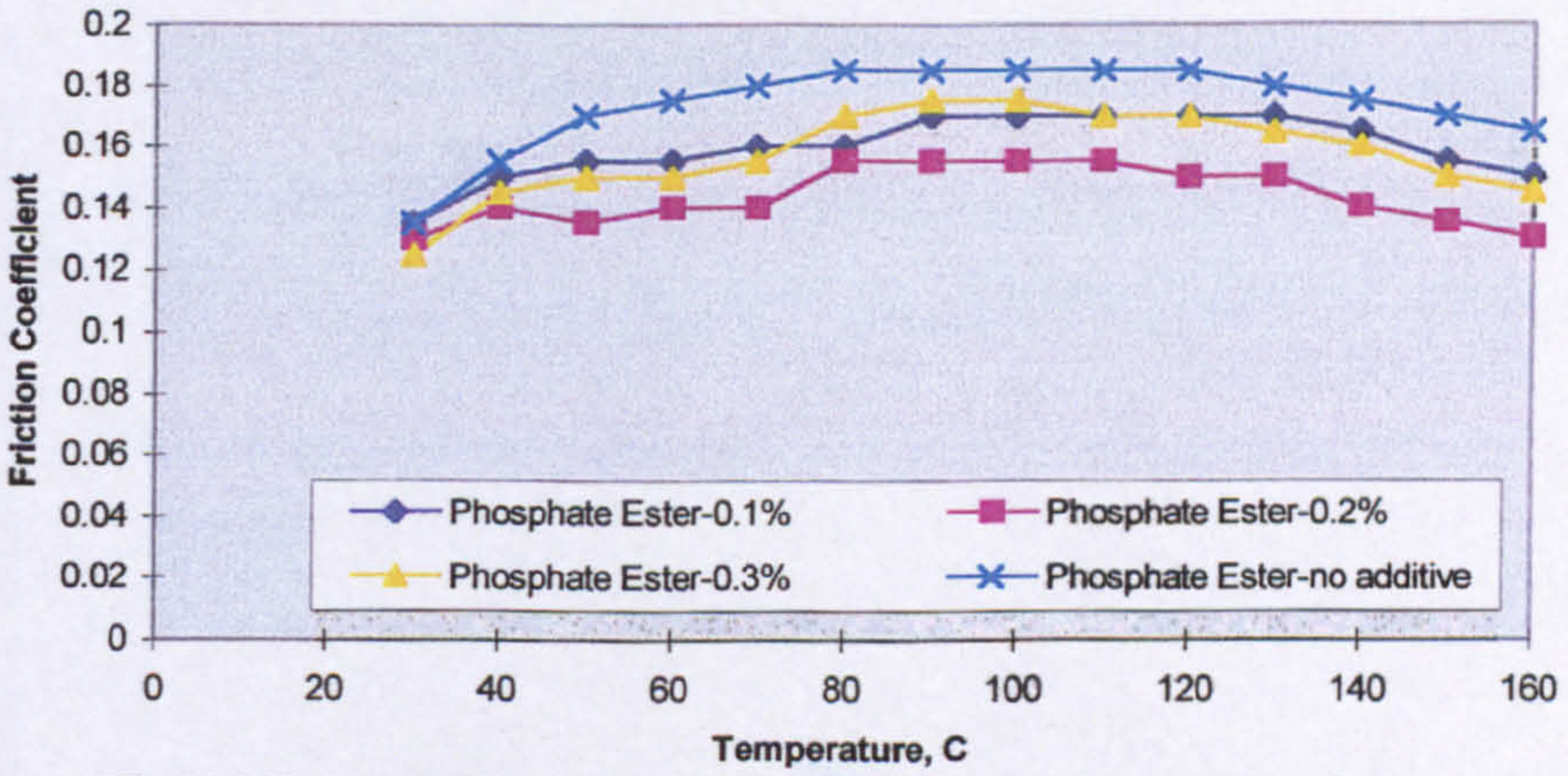

Fig. 4.9 The variation of friction coefficient with temperature for a ceramic ball sliding against a steel plate lubricated with a mixture of Polyglycol T81499 and Phosphate ester at various concentrations (load 5N, amplitude 0.3mm, frequency 45Hz)

4.4.1 Surface Observations

Figures 4.10- 4.12 show the SEM images of the contact area of the silicon nitride ball after friction testing in the presence of the additive phosphate ester in reference oil Talpa 20, the ester base fluid T80884 and the polyglycol T81499. Figures 4.13-4.15 show the corresponding SEM images of the contact area of steel plate after the friction tests.

The silicon nitride ball shows no clear wear scar feature after testing with Talpa 20 + 0.3% phosphate ester, fig.4.10. Although the samples were thoroughly cleaned with acetone after testing there appears to be a deposit on the surface which is more visible under higher magnification. Figure 4.13 shows the presence of a film deposited over the contact area of the steel plate after the friction test with this lubricant. Under high magnification the film appears very smooth and thick.

Figure 4.11 shows a very clear wear scar on the silicon nitride ball after friction testing with ester base fluid T80884 + 0.3% phosphate ester. There appears to be a film on the surface of the wear scar which is more visible under high magnification. This film has abrasion grooves on it which could correspond to the machining marks on the steel plate. Figure 4.14 shows the wear scar area on the steel plate after the friction test with this lubricant. Under high magnification there appears to be a severe plastic deformation taking place at the contact interface.

Figure 4.12 shows a very large wear scar on the contact area of the silicon nitride ball after friction testing with polyglycol T81499 + 0.3% phosphate ester. A film deposited on the wear surface can be seen. There are also abrasion grooves which correspond to the machining marks on the steel plate. Under high magnification there is a lot of fine debris at the contact area. The circulation of wear particles in the sliding interface is reflected by the high coefficient of friction result, which increases when particles are accumulated and decreases when particles are removed from the sliding interface. Figure 4.15 shows the wear scar area on the steel plate after friction testing with this lubricant. There is a lot of wear debris both inside and outside the contact interface. Under high magnification there appears to be plastic deformation at the interface, as well as the presence of a lot of fine debris both inside and outside the interface area. The wear debris has a dual action, it interacts with the sliding surfaces by abrasion, which increases the coefficient of friction and reflects the evolution of the quantity of debris in the sliding interface.

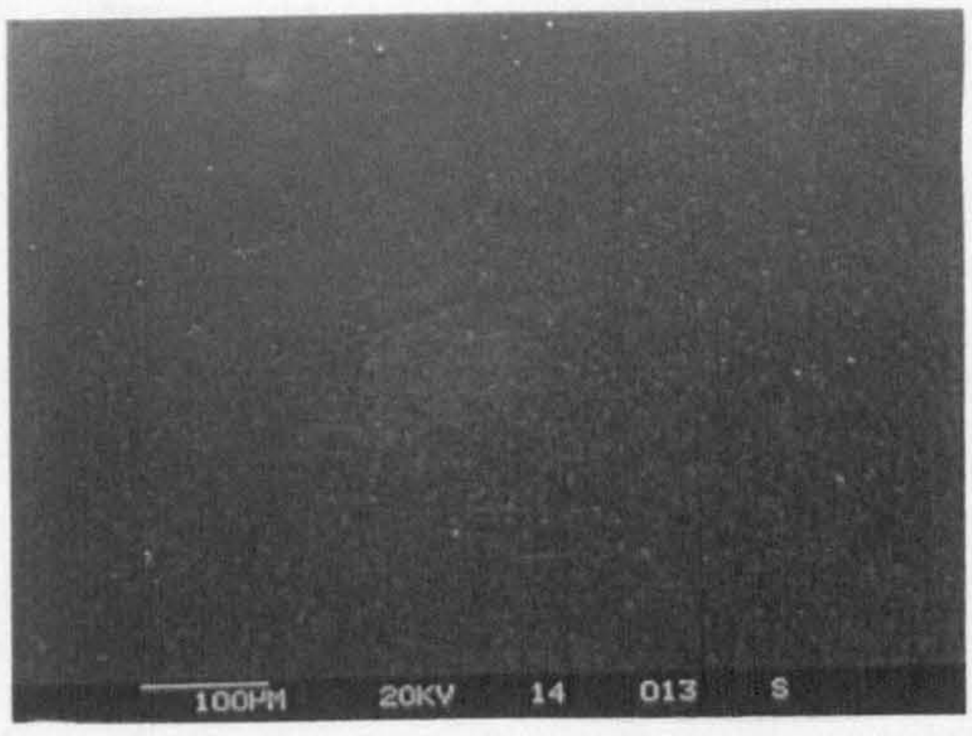

(a) Overall view

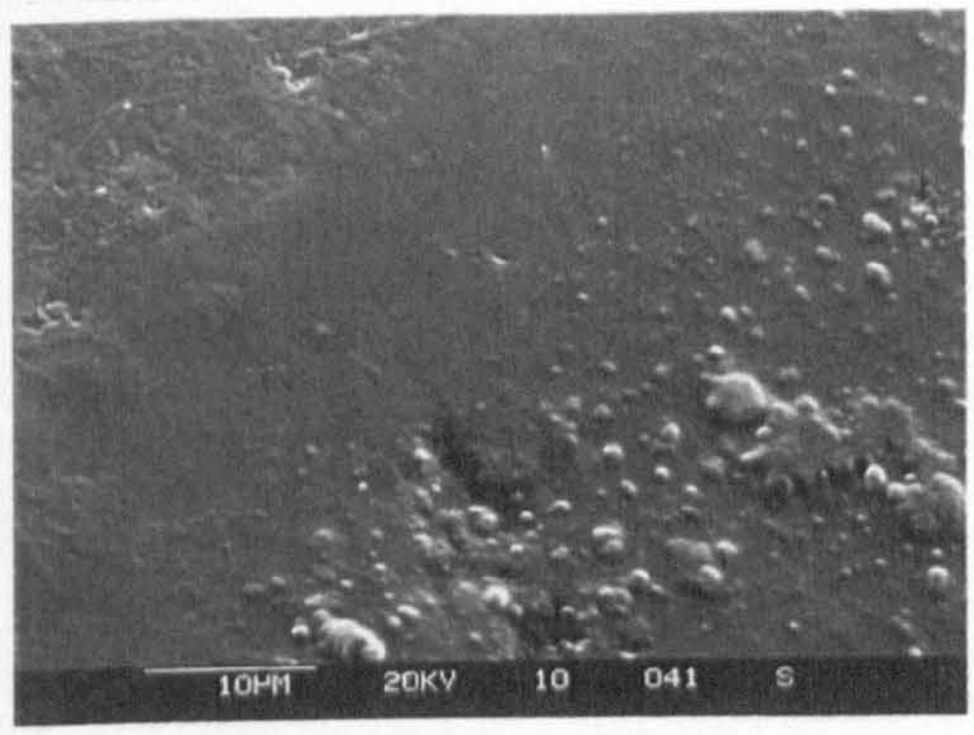

(b) Higher magnification

Fig. 4.10 SEM observations of ceramic ball after friction testing with Talpa 20 + 0.3% Phosphate Ester

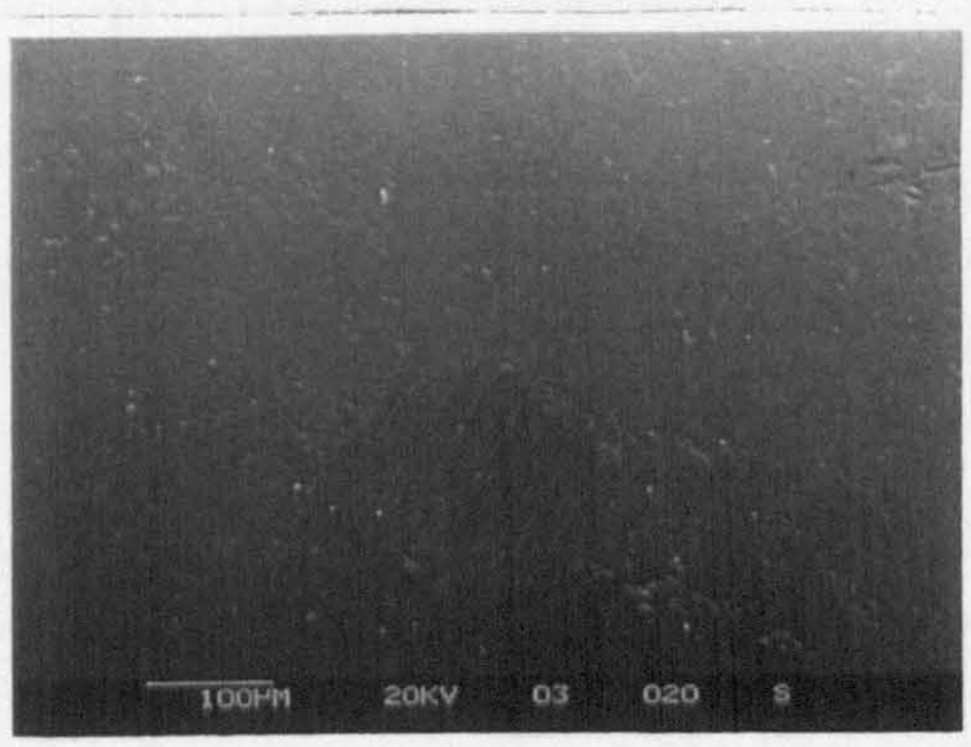

(a) Overall view

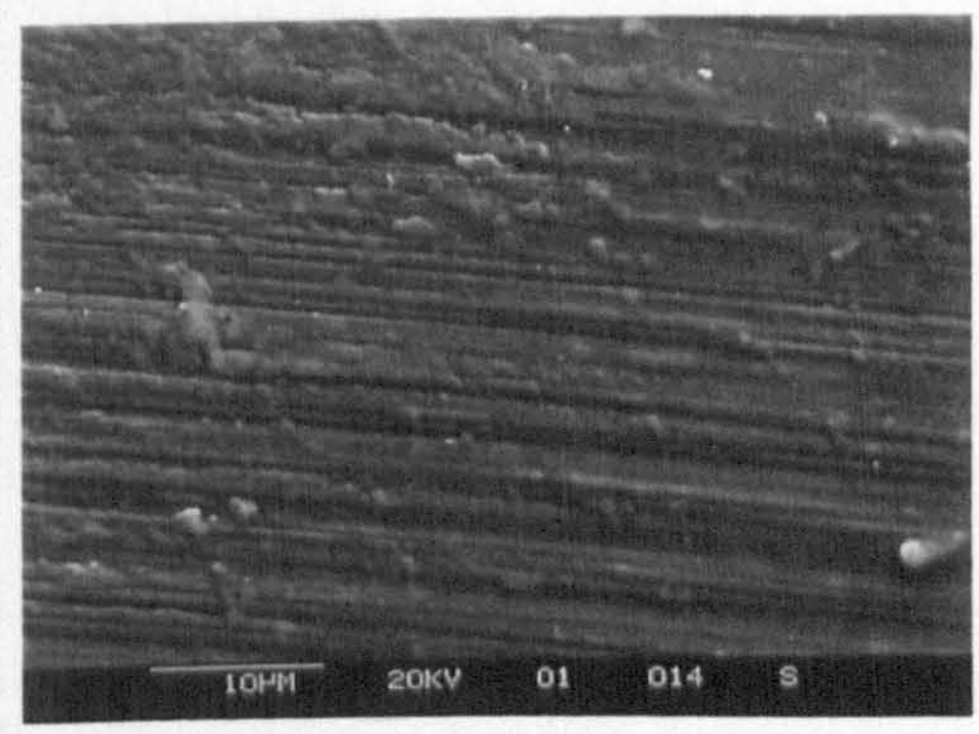

(b) Higher magnification

Fig. 4.11 SEM observations of ceramic ball after friction testing with ester T80884 + 0.3% Phosphate Ester

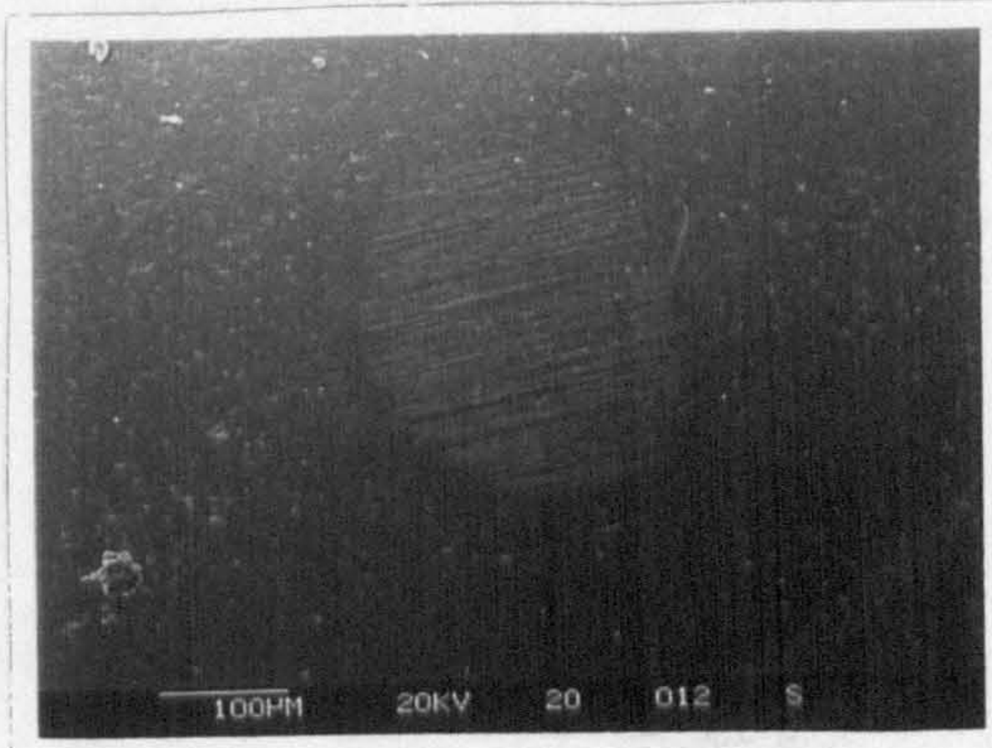

(a) Overall view

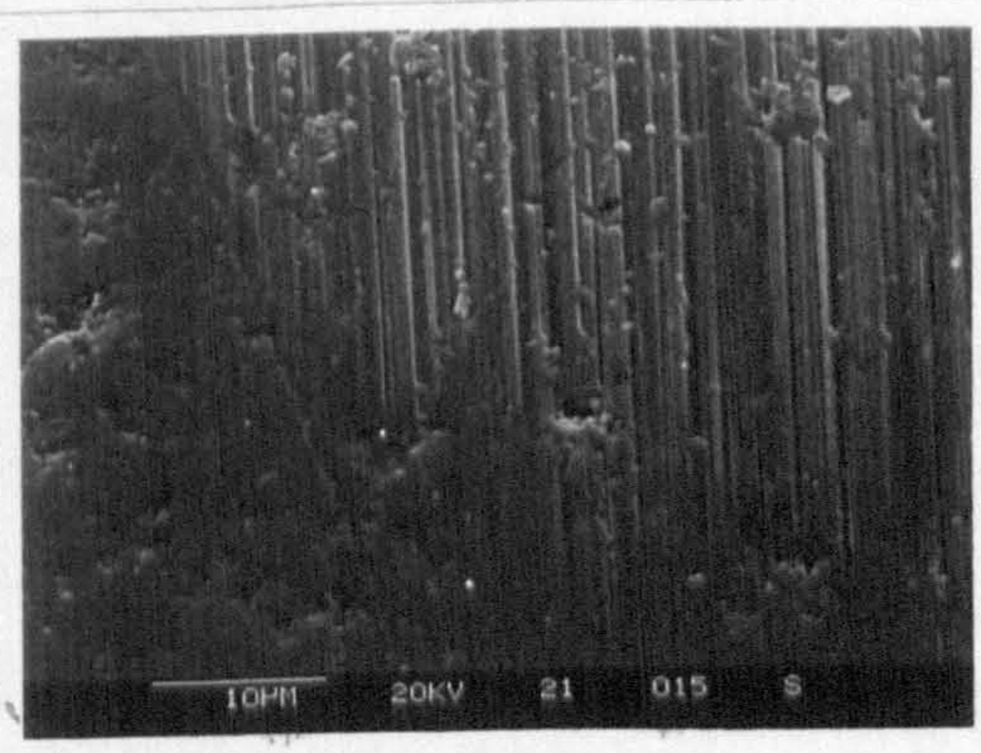

(b) Higher magnification

Fig. 4.12 SEM observations of ceramic ball after friction testing with polyglycol T81499 + 0.3% Phosphate Ester

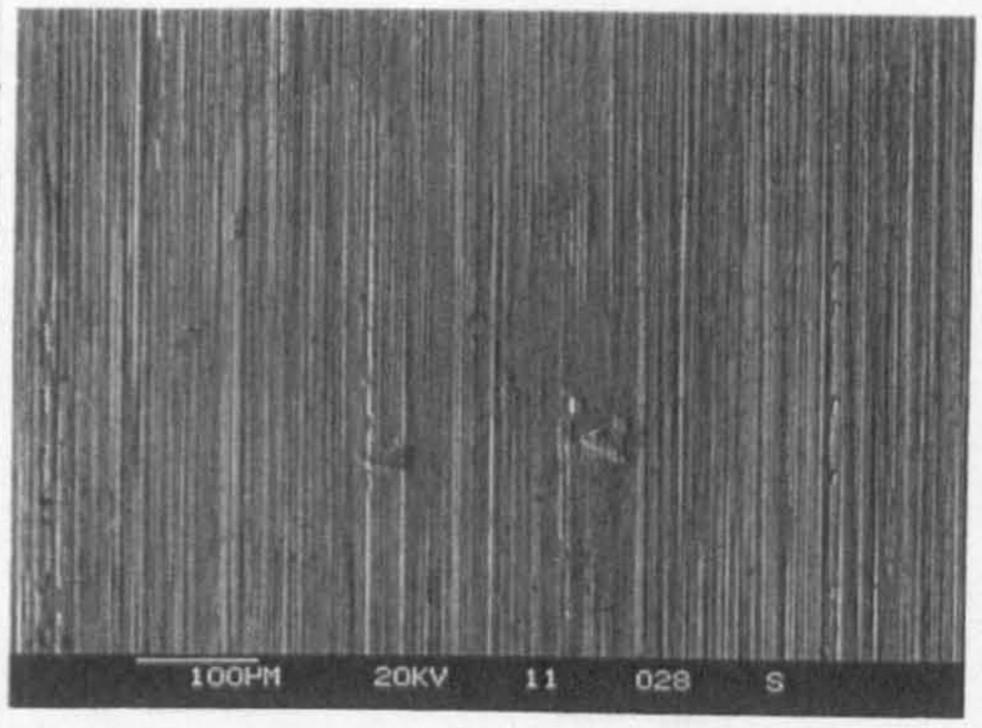

(a) Overall view

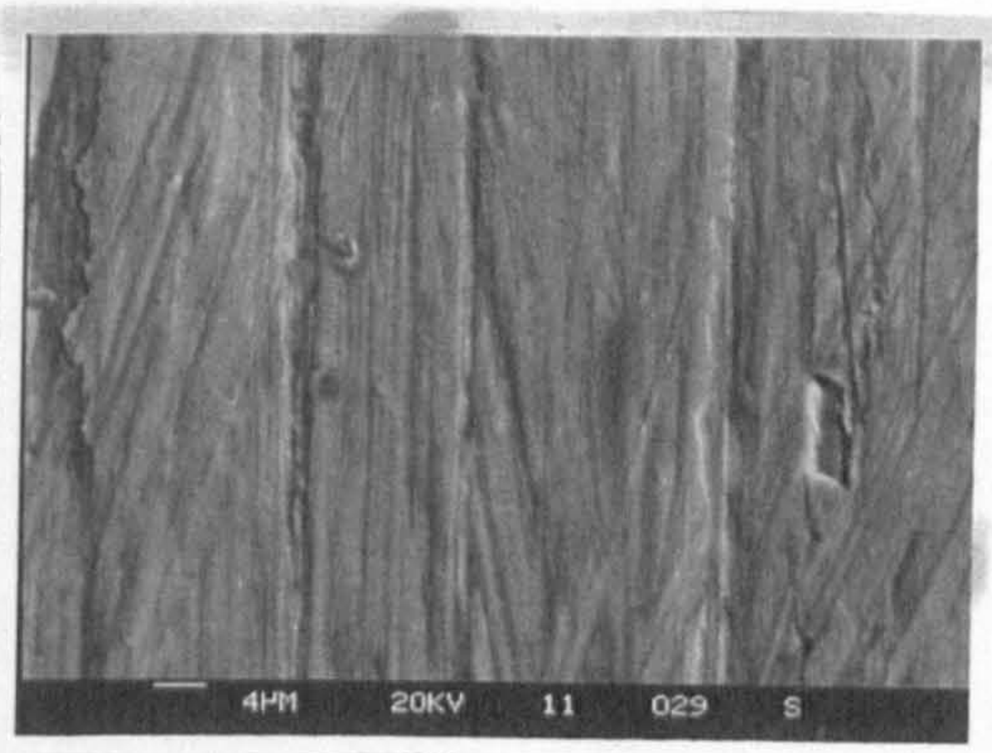

(b) Higher magnification

Fig. 4.13 SEM observations of steel plate after friction testing with Talpa 20 + 0.3% Phosphate Ester

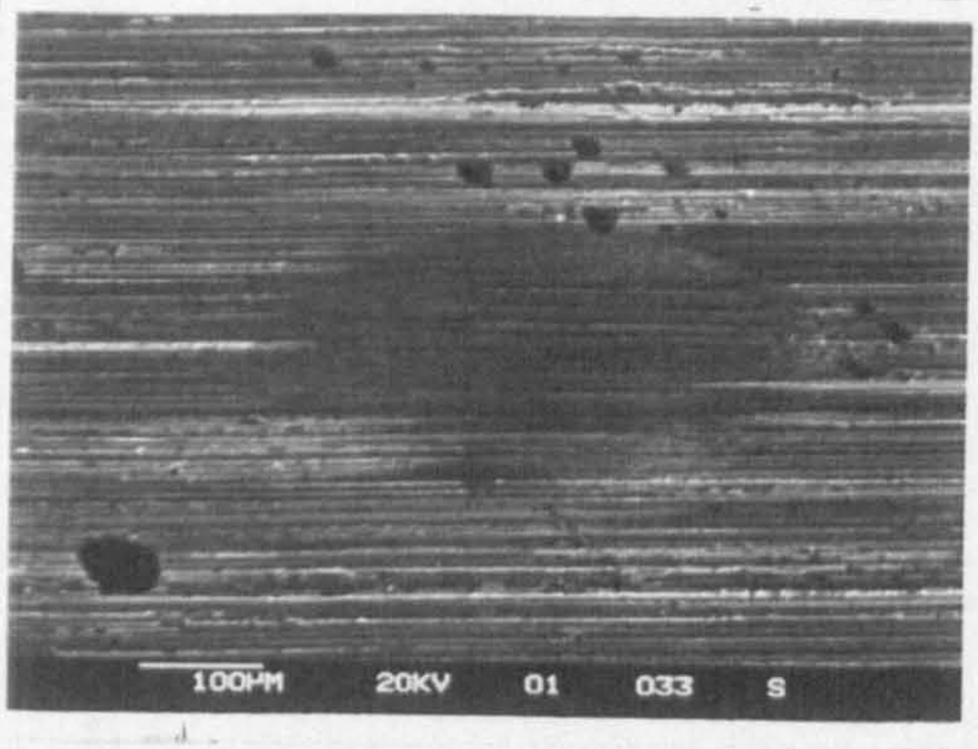

(a) Overall view

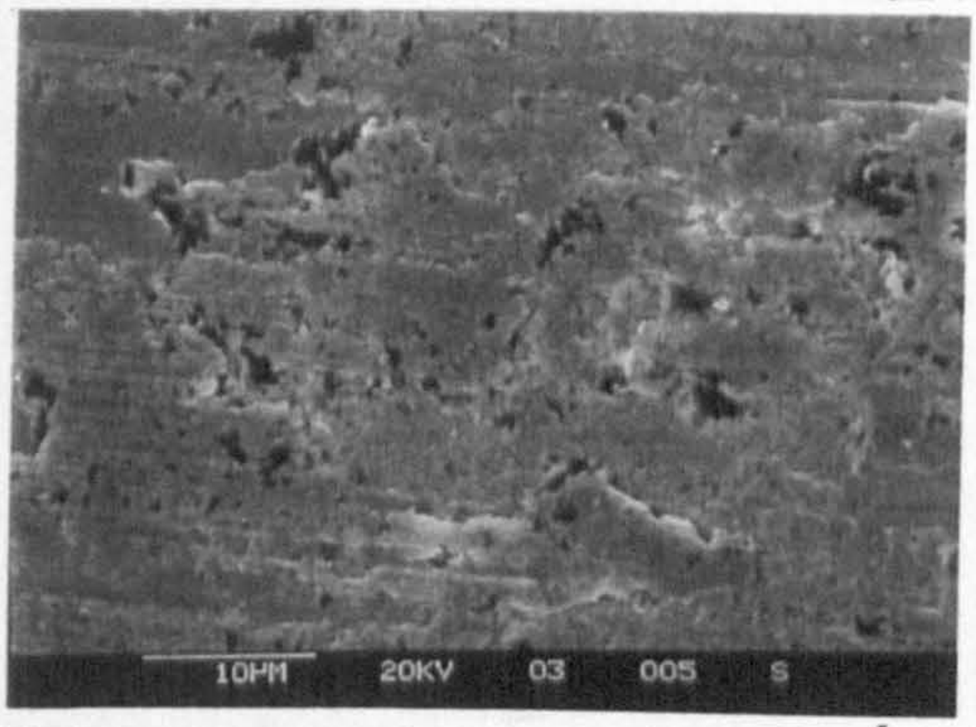

(b) Higher magnification

Fig. 4.14 SEM observations of steel plate after friction testing with ester T80884 + 0.3% Phosphate Ester

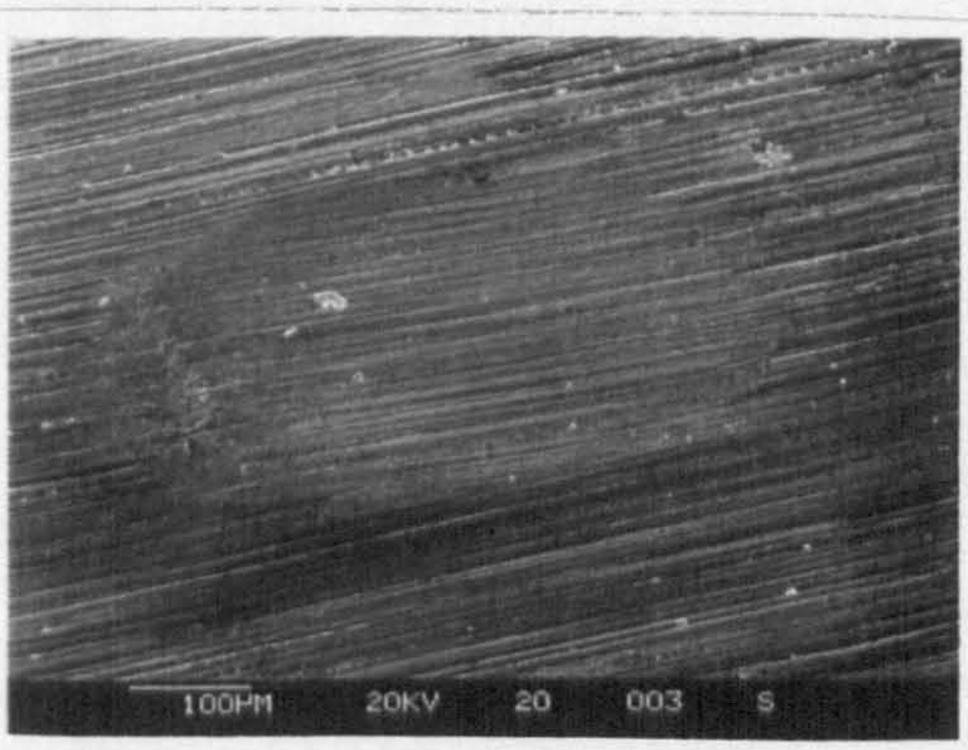

(a) Overall view

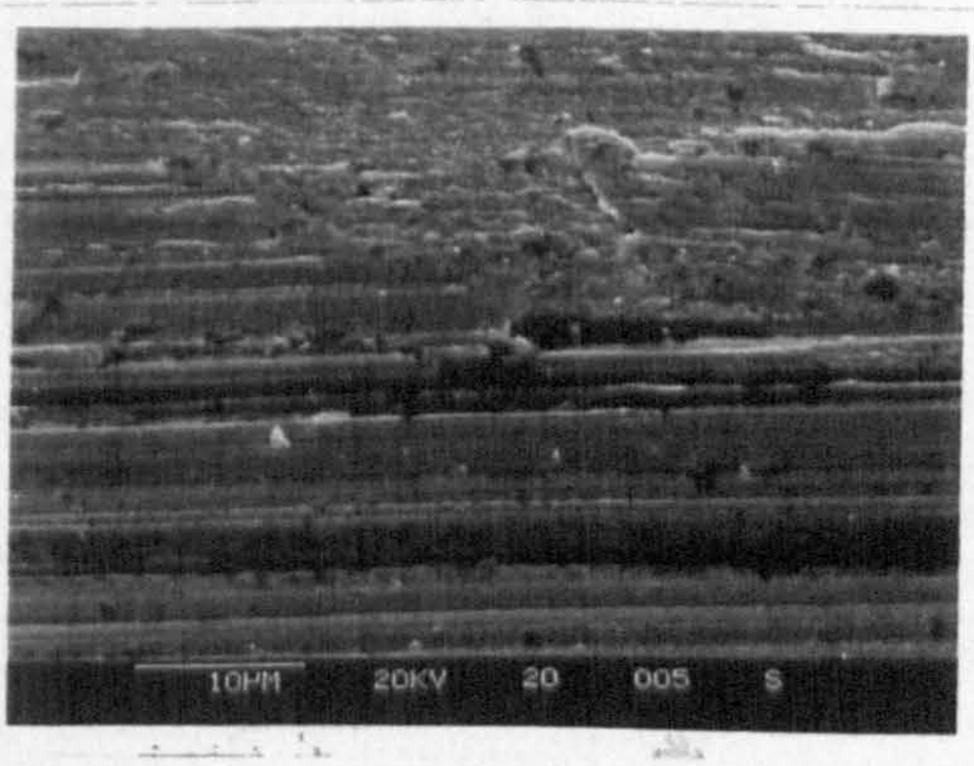

(b) Higher magnification

Fig. 4.15 SEM observations of steel plate after friction testing with polyglycol T81499 + 0.3% Phosphate Ester

4.5 Friction measurements using the additive Triethanol Amine

Figure 4.16 shows that there is no significant effect on the coefficient of friction of the ceramic ball sliding on the steel plate when using the additive triethanol amine with Talpa 20. Only when using Talpa 20 does the coefficient of friction increases very gradually from 0.09 to 0.13 as the temperature is increased from 30°C to 160°C. When using 0.1% triethanol amine with Talpa 20 there is an initial increase in the coefficient of friction from 0.09 to 0.115 as the temperature is increased from 30°C to 60°C. However, as the temperature is further increased from 60°C to 160°C the coefficient of friction is constant at 0.115. For 0.1% and 0.2% triethanol amine with Talpa 20 the coefficient of friction is constant at about 0.1 for all temperature ranges.

Figure 4.17 shows the significant effect on the coefficient of friction for the ceramic ball sliding on the steel plate when using the additive triethanol amine. When using 0.1%, 0.2% and 0.3% triethanol amine with ester base fluid T80884 the coefficient of friction is in the range of 0.155 to 0.16 as the temperature is increased from 30°C to 80°C, whereas without additive it is 0.08. As the temperature is further increased from 80°C to 140°C, the coefficient of friction increases significantly from 0.16 to 0.215 when using 0.2% and 0.3% triethanol amine with ester base fluid T80884, however, for 0.1% triethanol amine with ester base fluid T80884 there is a gradual decrease from 0.16 to 0.125.

Figure 4.18 shows a slight decrease in the coefficient of friction of the ceramic ball sliding on the steel plate when using the additive triethanol amine with polyglycol T81499. As in the case of phosphate ester with polyglycol T81499, triethanol amine with polyglycol T81499 also shows a similar trend in the results, that is, an initial increase in coefficient of friction from 30°C to 80°C then constant values in the range of 80°C to 120°C and on further increase in temperature to 160°C a gradual decrease in coefficient of friction. The coefficient of friction for 0.1%, 0.2% and 0.3% triethanol amine with polyglycol T81499 are very similar, and range from 0.11 to 0.16 as the temperature is increased from 30°C to 80°C. On further increase from 80°C to 120°C the coefficient of friction is constant at about 0.16 and on further increase in temperature to 160°C the coefficient of friction gradually decreases from 0.16 to 0.135. The results for polyglycol T81499 without additive show an initial increase in the coefficient of friction from 0.135 to 0.18 as the temperature is further increased from 80°C to 120°C the

coefficient of friction remains constant at 0.185, and as the temperature is further increased to 160°C the coefficient of friction gradually decreases from 0.185 to 0.165.

In general the addition of the additive triethanol amine to Talpa 20 had no significant effect on the coefficient of friction, whereas when using with ester base fluid T80884 the coefficient of friction is typically doubled; when using with polyglycol T81499 it gave a slight decrease in the coefficient of friction. Overall, Talpa 20 gave the lowest values for the coefficient of friction when mixed with triethanol amine. Justification of these results is provided in section 4.5.1 which deals with results of the surface studies and also in the summary of the results in section 4.7.

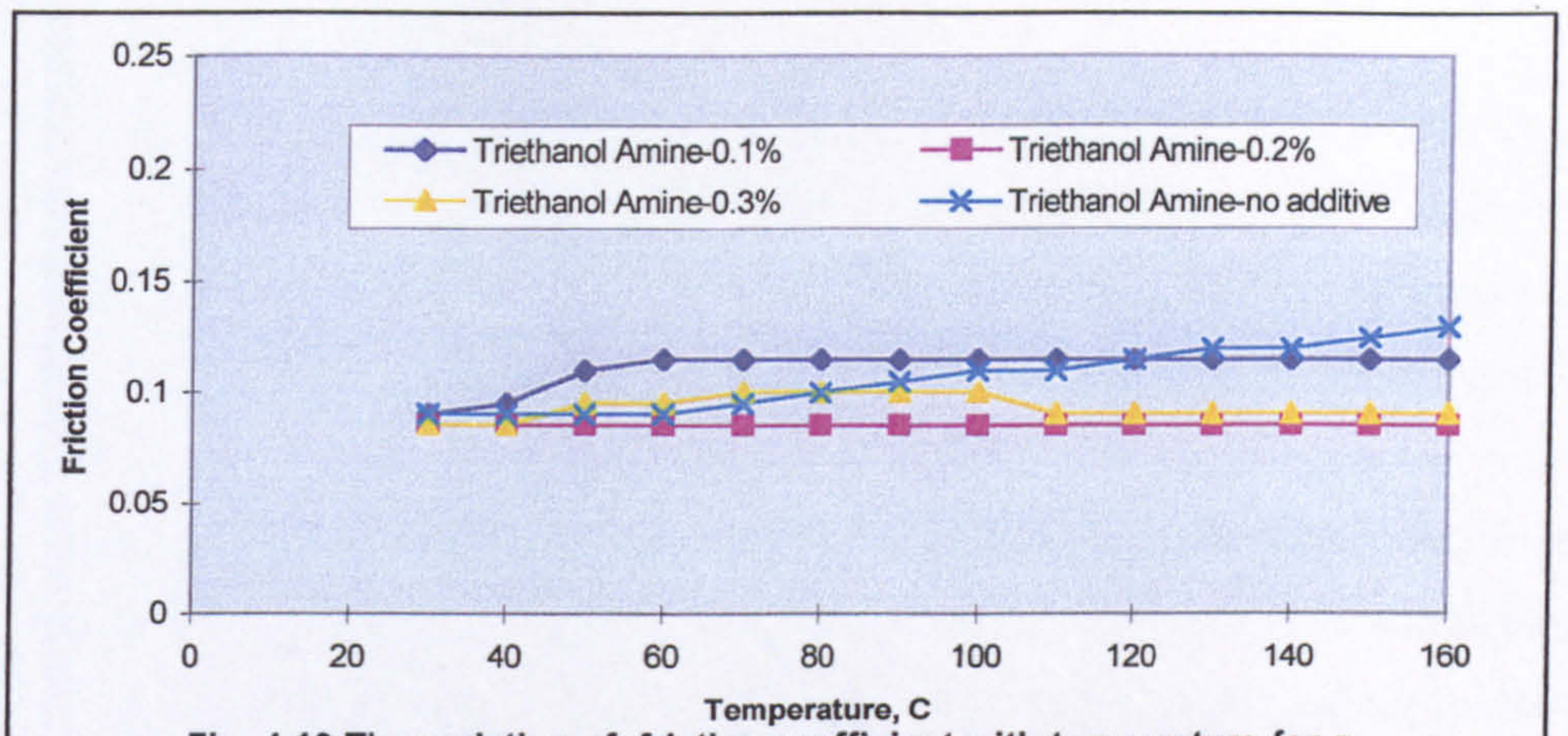

Fig. 4.16 The variation of friction coefficient with temperature for a ceramic ball sliding against a steel plate lubricated with a mixture of Talpa 20 and Triethanol Amine at various concentrations (load 5N, amplitude 0.3mm, frequency 45Hz)

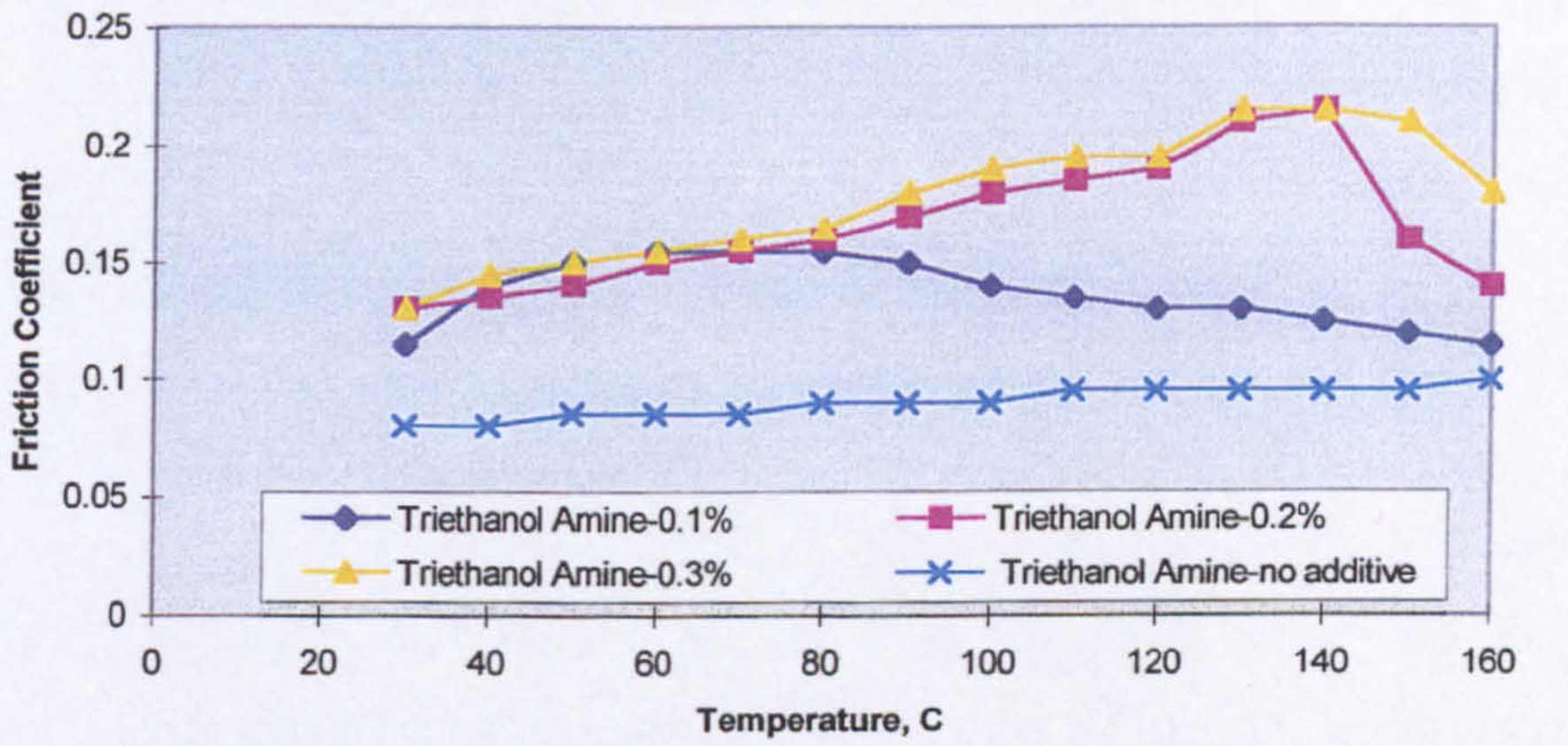

Fig 4.17 The variation of friction coefficient with temperature for a ceramic ball sliding against a steel plate lubricated with a mixture of Ester T80884 and Triethanol Amine at various concentrations (load 5N, amplitude 0.3mm, frequency 45Hz)

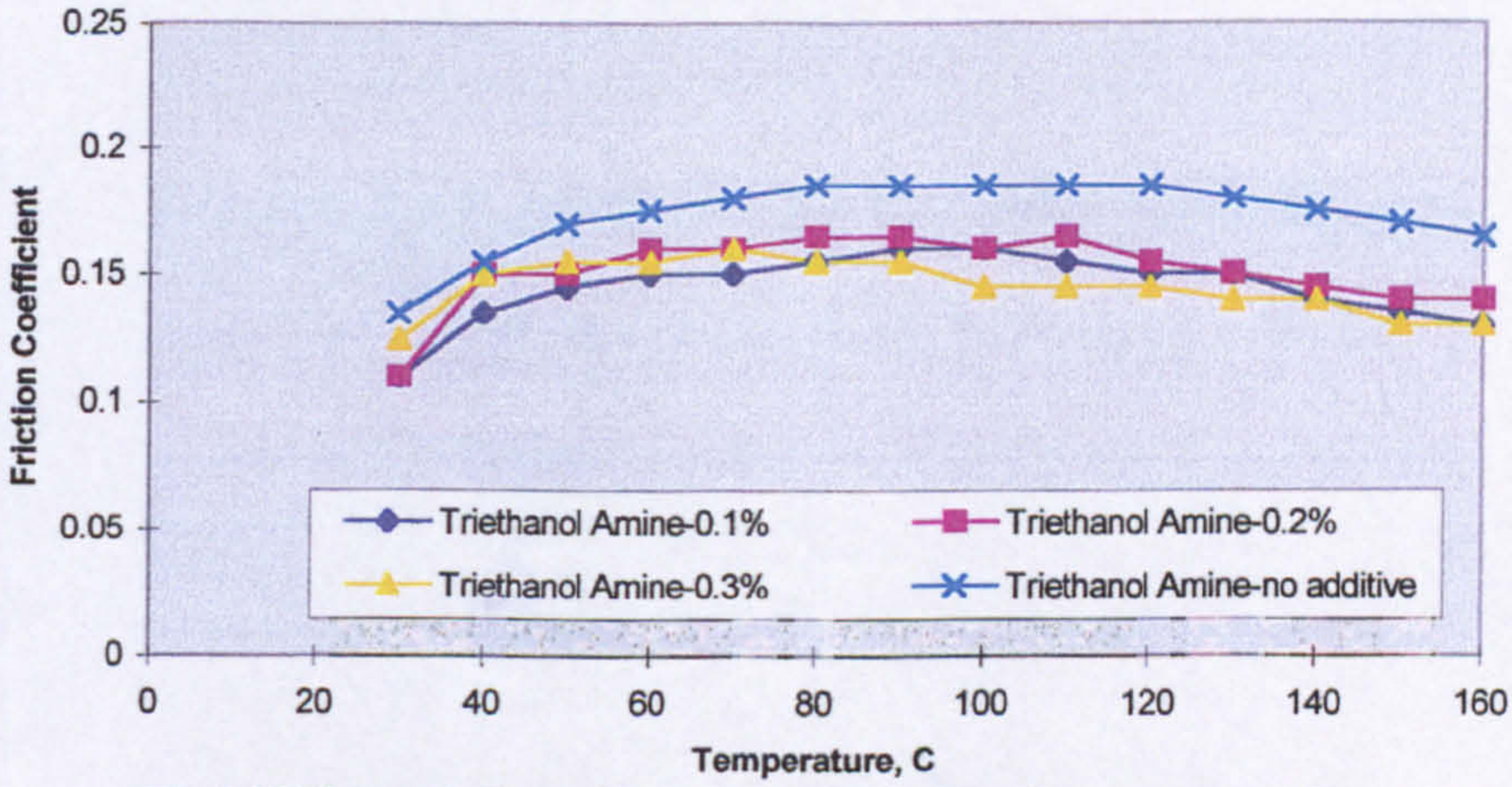

Fig.4.18 The variation of friction coefficient with temperature for a ceramic ball sliding against a steel plate lubricated with a mixture of Polyglycol T81499 and Triethanol Amine at various concentrations (load 5N, amplitude 0.3mm, frequency 45Hz)

4.5.1 Surface Observations

Figures 4.19-4.21 show the SEM images of the contact area of the silicon nitride balls after friction testing with the additive triethanol amine mixed with the reference slurry Talpa 20, the ester base fluid T80884 and the polyglycol T81499. Figures 4.22-4.24 show the SEM images of the contact area of the steel plate after the friction tests.

Figure 4.19 shows no clear wear scar on the surface of the silicon nitride ball after friction testing with Talpa 20 +0.3% triethanol amine. Although the ball was thoroughly cleaned in acetone after the friction test there still appears to be a deposit on the surface which is clearer under high magnification. The contact area of the steel plate after friction testing with this lubricant, fig.4.22, shows a film being present over the contact area. Under high magnification the film appears very smooth. These SEM observations correlate very well with the low coefficient of friction results with this additive, since under SEM observations there appears to be a protective film being deposited on both the ball and plate at the contact interface.

Figure 4.20 shows a very clear wear scar on the contact area of the ceramic ball after friction testing with ester base fluid T80884 +0.3% triethanol amine. There appear to be grooves present on the wear scar with debris embedded into them. The shape of the grooves on the ball surface correspond to the machining marks on the steel plate. These observations together with the high coefficient of friction results could be due to the fact that the debris generated during sliding is trapped at the contact interface, resulting in a rise in friction and damage to the surface. The contact area of the steel plate after friction testing with this lubricant, fig. 4.23, shows very clearly a wear scar with abrasion grooves and signs of plastic deformation.

Figure 4.21 shows a film in the contact area of the silicon nitride ball after friction testing with polyglycol T81499 + 0.3% triethanol amine. Under high magnification there appears to be a film on the surface and abrasion grooves with a lot of fine debris. The wear scar on the steel plate after friction testing with this lubricant shows signs of intense plastic deformation, fig.4.24.

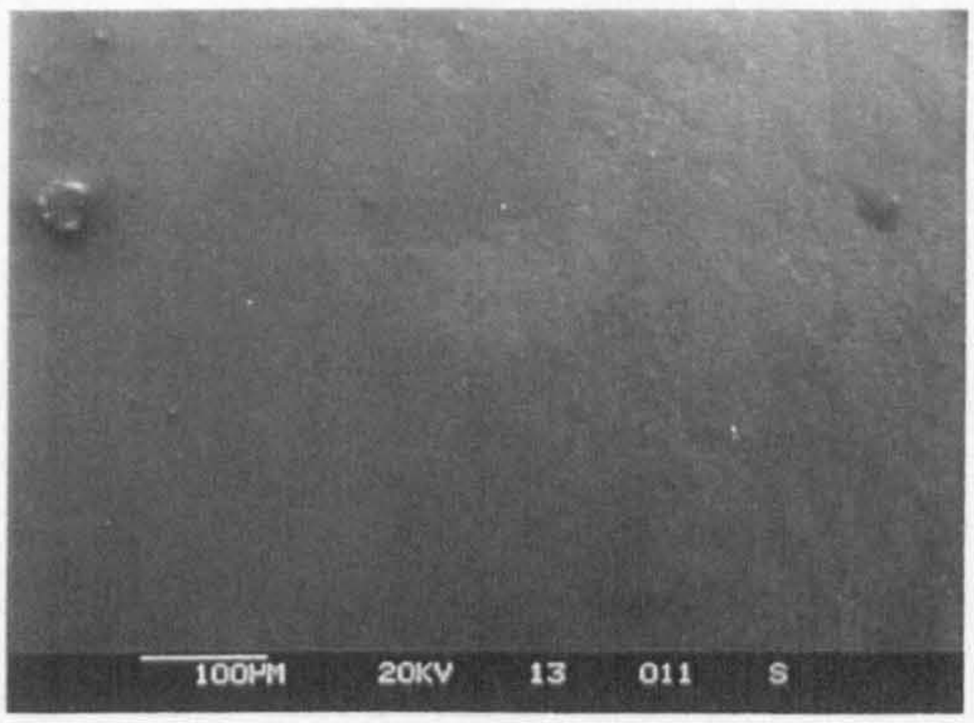

(a) Overall view

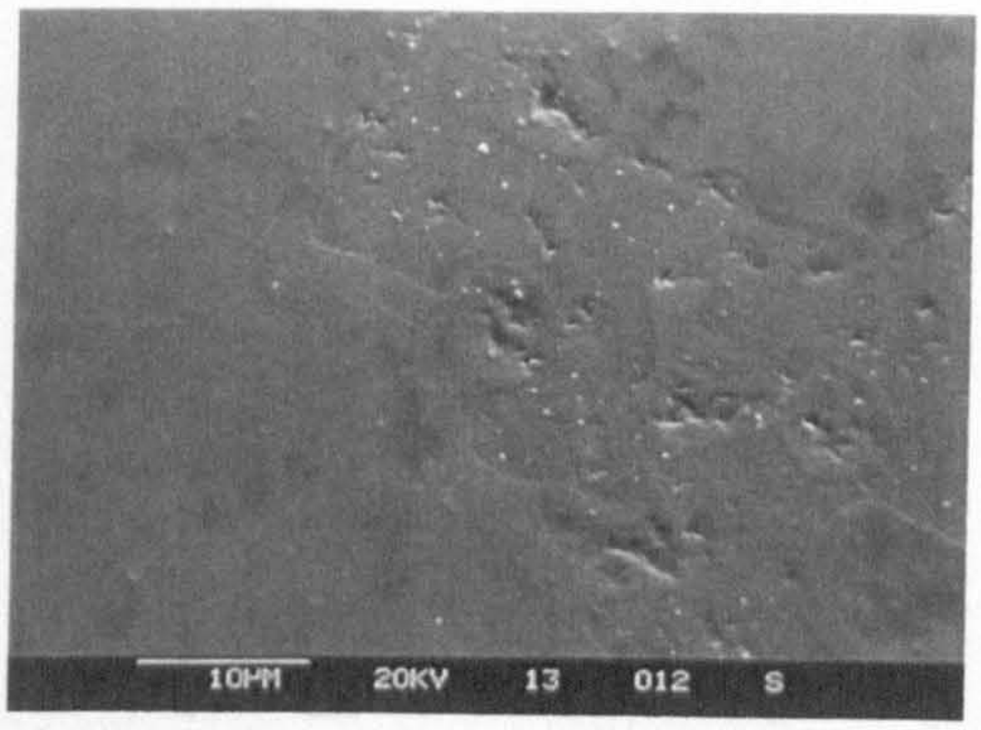

(b) Higher magnification

Fig. 4.19 SEM observations of ceramic ball after friction testing with Talpa 20 + 0.3% Triethanol Amine

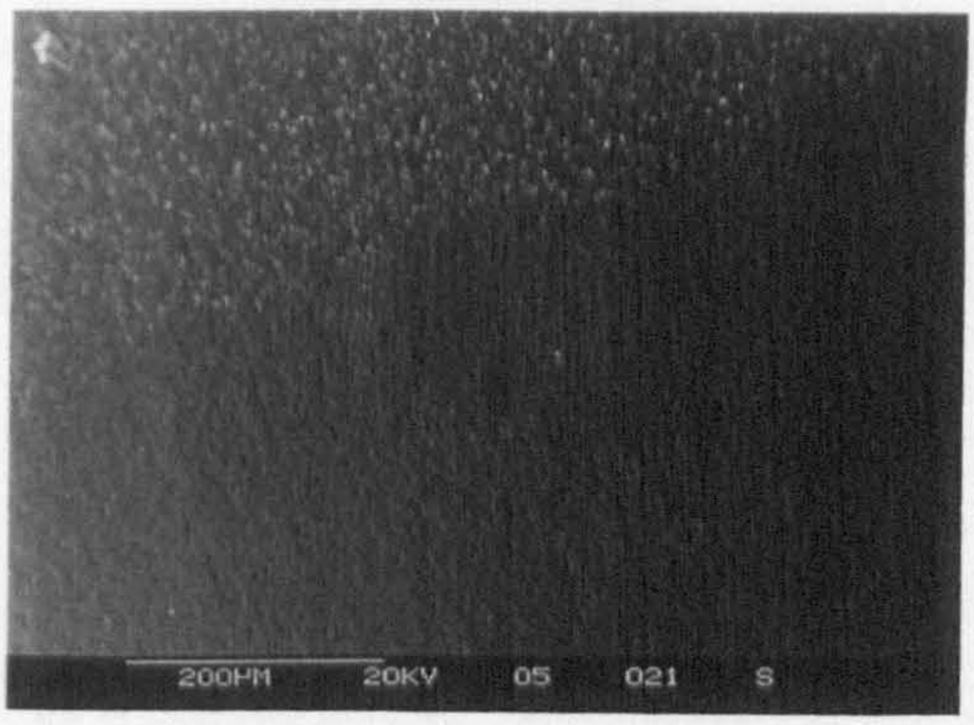

(a) Overall view

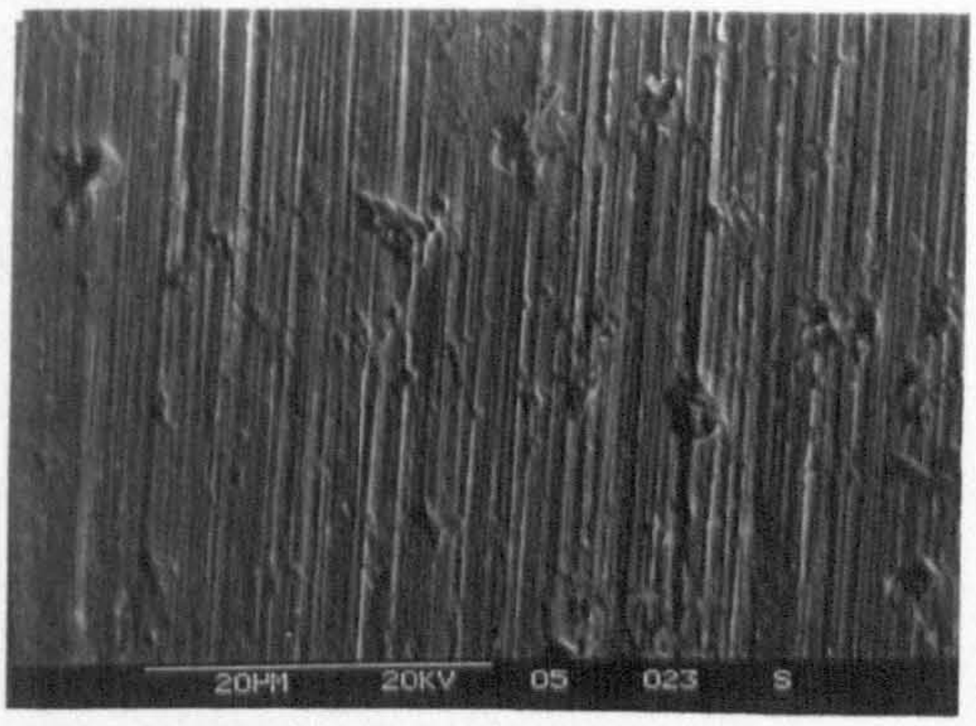

(b) Higher magnification

Fig. 4.20 SEM observations of ceramic ball after friction testing with ester T80884 + 0.3% Triethanol Amine

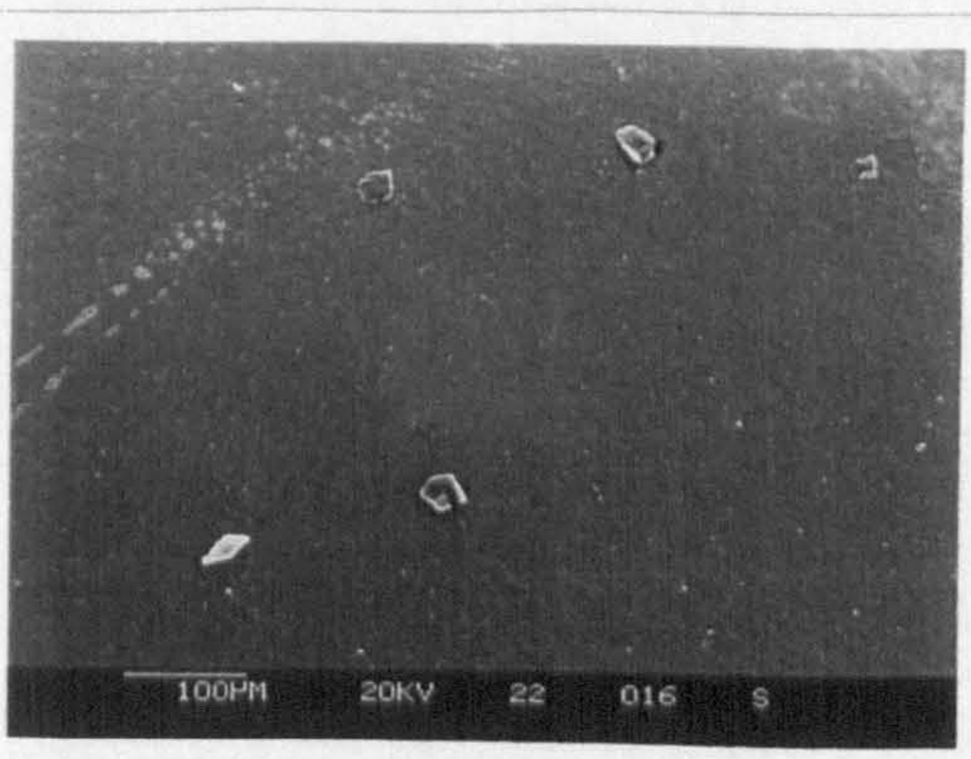

(a) Overall view

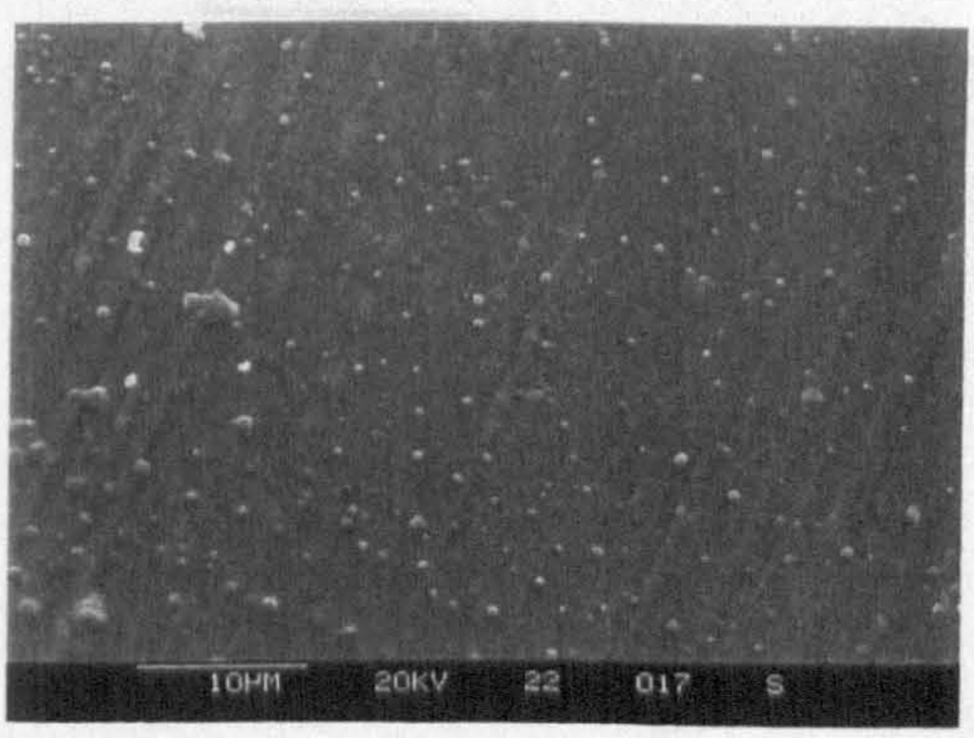

(b) Higher magnification

Fig. 4.21 SEM observations of ceramic ball after friction testing with polyglycol T81499 + 0.3% Triethanol Amine

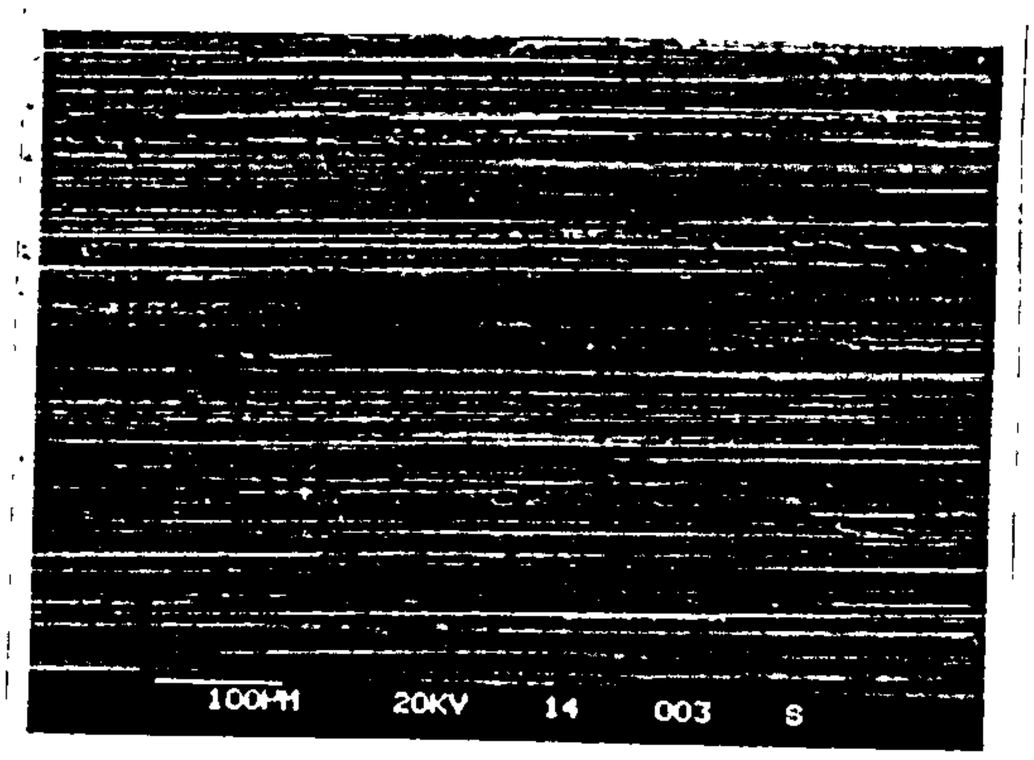

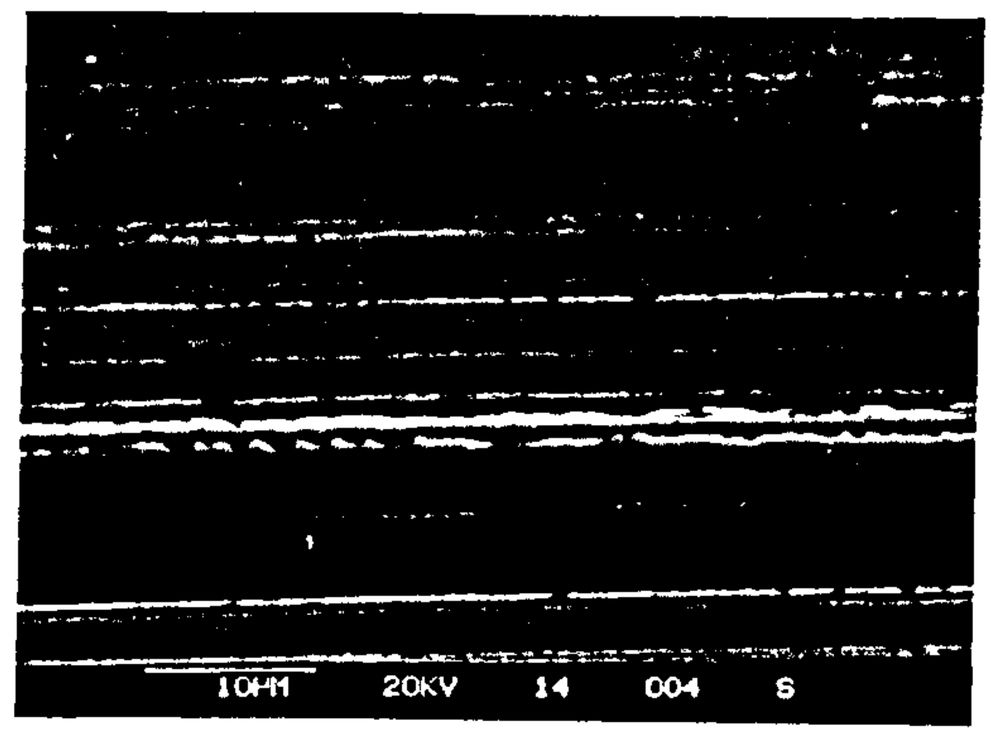

(a) Overall view **(b) Higher magnification**

Fig. 4.22 SEM observations of steel plate after friction testing with Talpa 20 + 0.3% Triethanol Amine

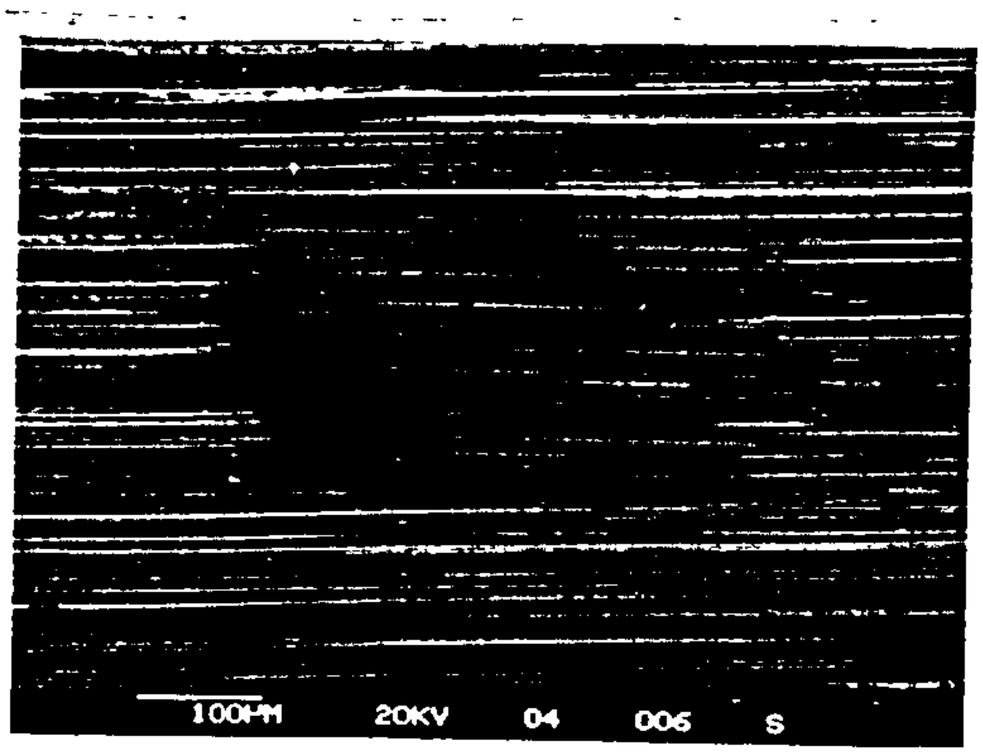

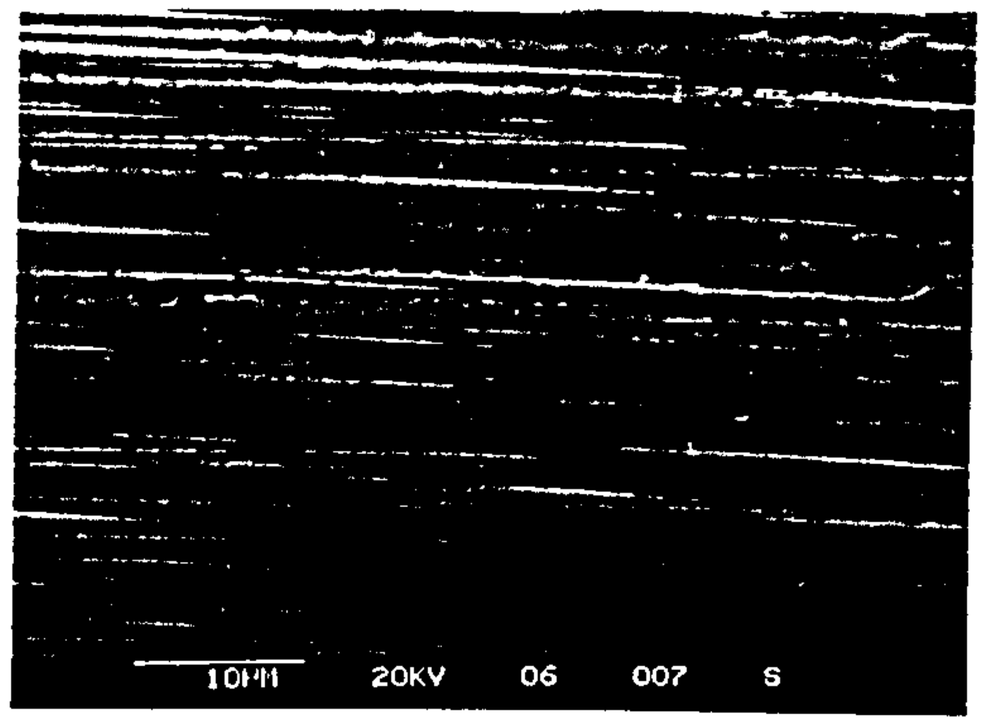

(a) Overall view **(b) Higher magnification**

Fig. 4.23 SEM observations of steel plate after friction testing with ester T80884 + 0.3% Triethanol Amine

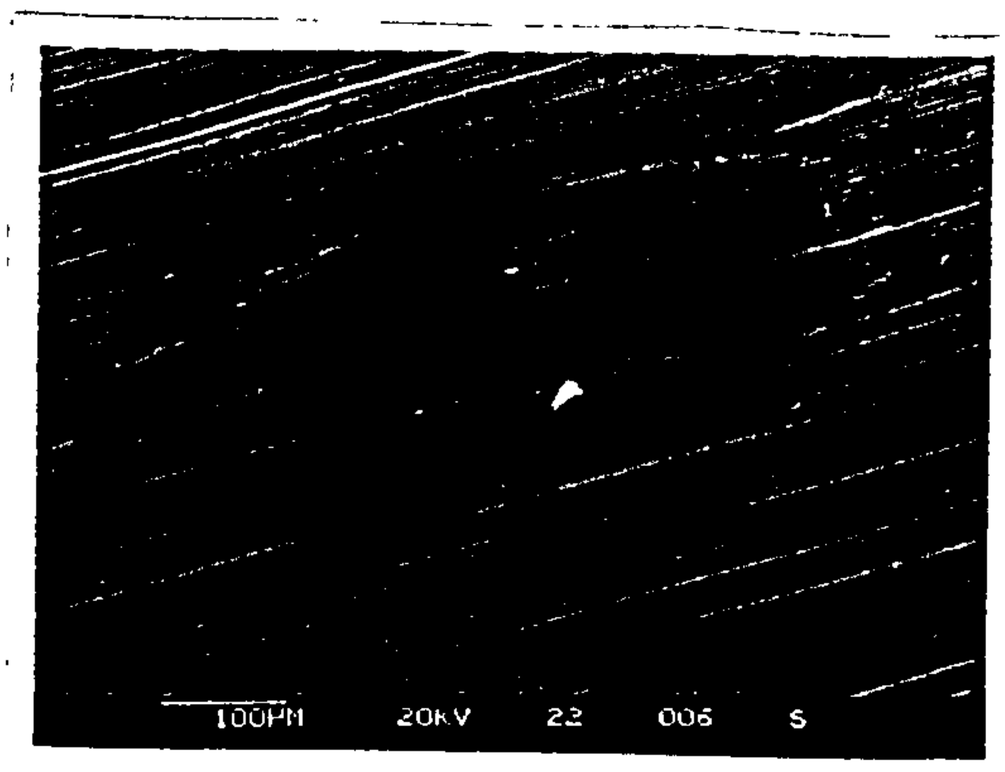

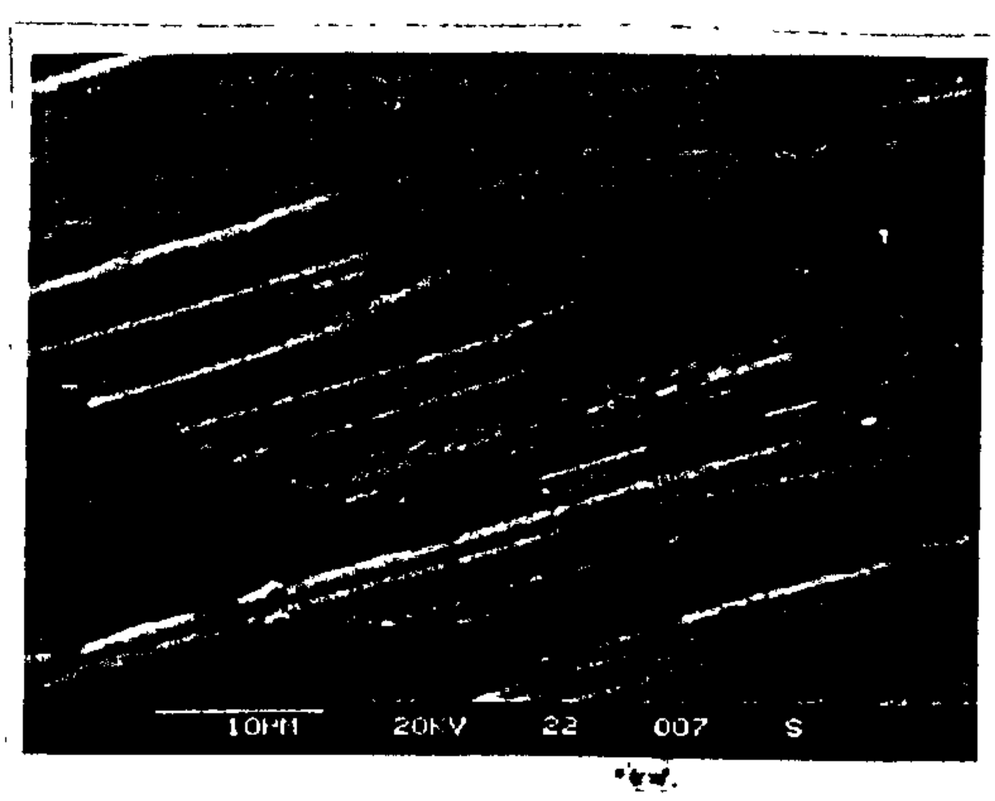

(a) Overall view **(b) Higher magnification**

Fig. 4.24 SEM observations of steel plate after friction testing with polyglycol T81499 + 0.3% Triethanol Amine

4.6 Friction measurements using the Amine Phosphate

Figure 4.25 shows no significant effect on the coefficient of friction of the ceramic ball sliding on the steel plate when using the additive amine phosphate with Talpa 20. For Talpa 20 without additive and with the additive amine phosphate at 0.1% and 0.2% concentration the coefficient of friction remains constant in the range of 0.09 to 0.095 as the temperature is increased from 30°C to 80°C, whereas when using 0.3% there is a slight increase in the coefficient of friction to 0.11 in this temperature range. On further increase in temperature from 80°C to 160°C, 0.1%,0.2% and 0.3% triethanol amine with Talpa 20 all show similar constant values for the coefficient of friction ranges from 0.095 to 0.1, however, for Talpa 20 without any additive there is a gradual increase in coefficient of friction from 0.095 to 0.13 as the temperature is increased from 80°C to 160°C.

Figure 4.26 shows no significant effect on the coefficient of friction of the ceramic ball sliding on the steel plate when using the additive amine phosphate with ester base fluid T80884. As the temperature is increased from 30°C to 90°C the coefficient of friction range remains constant at 0.085 to 0.09 for ester base fluid T80884 without the additive and with the additive amine phosphate at 0.1%, 0.2% and 0.3% concentrations. On further increase in temperature from 90°C to 160°C the coefficient of friction for ester base fluid T80884 without additive and with additive at 0.1% and 0.2% show a gradual increase from 0.09 to 0.115, however, the coefficient of friction for ester base fluid T80884 with 0.3% amine phosphate shows a greater increase in the coefficient of friction range from 0.09 to 0.13.

Figure 4.27 shows no significant effect on the coefficient of friction of the ceramic ball sliding on the steel plate when using the additive amine phosphate with polyglycol T81499. Initially as the temperature is increased from 30°C to 70°C the coefficient of friction for polyglycol T81499 without additive and with the additive amine phosphate at 0.1%, 0.2% and 0.3% concentration shows a gradual increase from 0.135 to 0.175. On further increase from 70°C to 120°C the coefficient of friction for T81499 with 0.1%, 0.2% and 0.3% amine phosphate shows a gradual decrease from 0.175 to 0.165, however, for polyglycol T81499 without additive the coefficient of friction remains constant at 0.185. As the temperature is further increased from 120°C to 160°C the coefficient of friction for polygylcol T81499 at 0.1%, 0.2% and 0.3% remains constant

at 0.165, however, the coefficient of friction for polyglycol T81499 without additive decreases from 0.185 to 0.16

In general the addition of the additive amine phosphate to Talpa 20, ester basè fluid T80884 and polyglycol T81499 had no significant effect on the friction coefficient. Overall, the ester base fluid T80884 gave the lowest coefficient of friction when mixed with amine phosphate. Justification of these results is provided in section 4.6.1 which deals with results of the surface studies and also in the summary of the results in section 4.7.

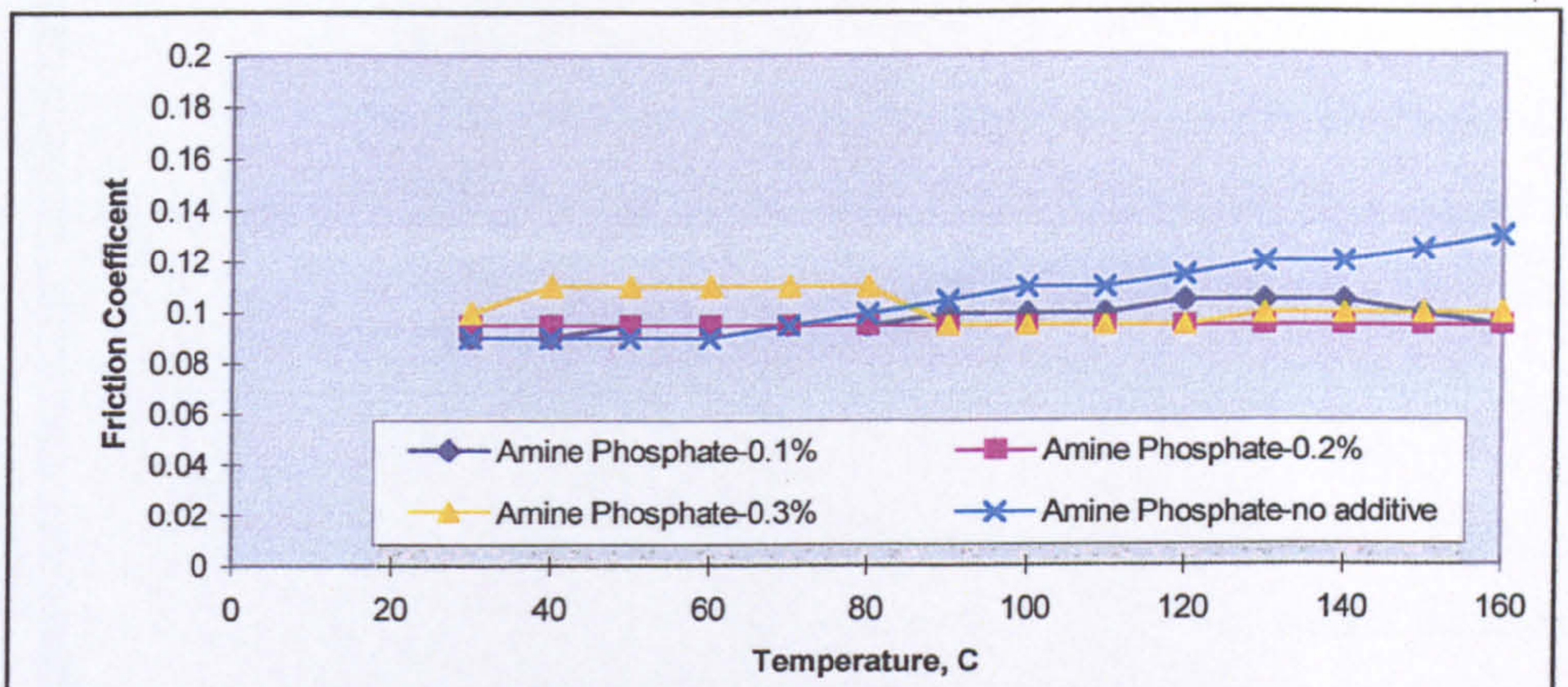

Fig. 4.25 The variation of friction coefficient with temperature for a ceramic ball sliding against a steel plate lubricated with a mixture of Talpa 20 and Amine Phosphate at various concentrations (load 5N, amplitude 0.3mm, frequency 45Hz)

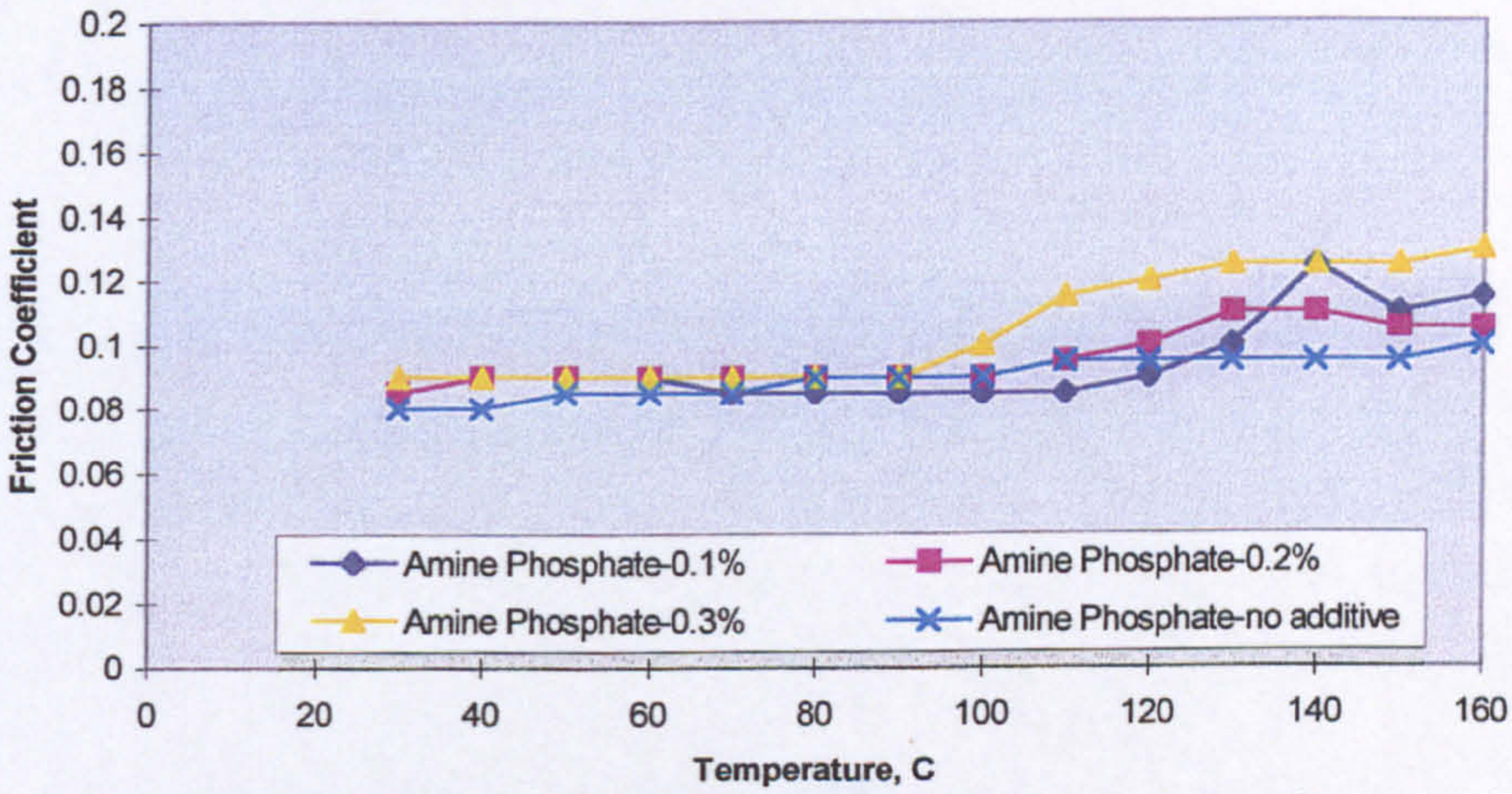

Fig. 4.26 The variation of friction coefficient with temperature for a ceramic ball sliding against a steel plate lubricated with a mixture of ester T80884 and Amine Phosphate at various concentrations (load 5N, amplitude 0.3mm, frequency 45Hz)

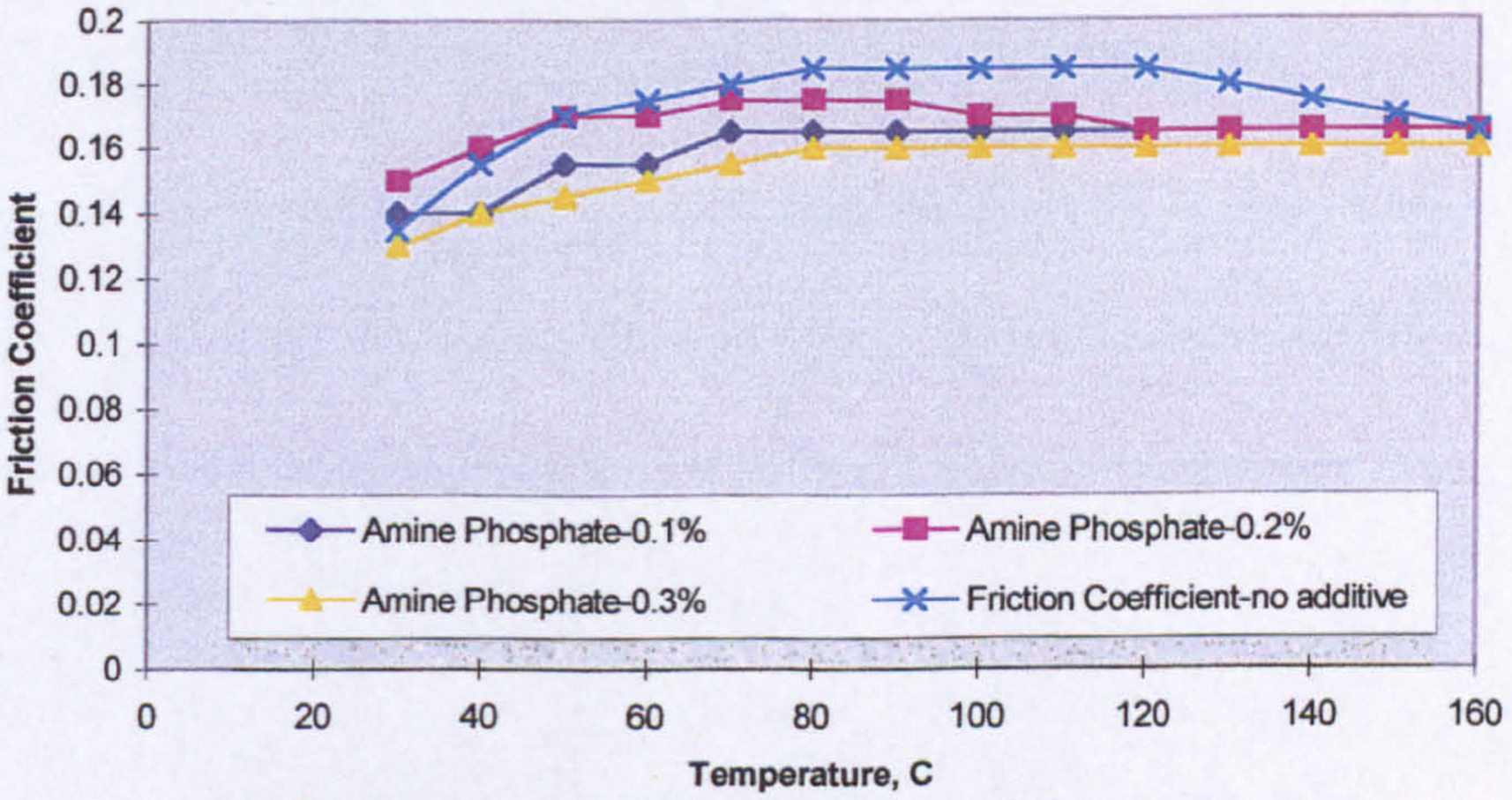

Fig. 4.27 The variation of friction coefficient with temperature for a ceramic ball sliding against a steel plate lubricated with a mixture of polyglycol T81499 and Amine Phosphate at various concentrations (load 5N, amplitude 0.3mm, frequency 45Hz)

4.6.1 Surface Observations

Figure 4.28-4.30 shows the SEM images of the contact area of the silicon nitride balls after friction testing with the additive amine phosphate mixed with the reference Talpa 20, the ester base fluid T80884 and the polyglycol T81499. Figures 4.31-4.33 show the SEM images of the steel plates after the friction tests with these lubricants.

The silicon nitride ball shows a small wear scar after friction testing with Talpa 20 +0.3% amine phosphate, fig.4.28. There appears to be a lot of fine debris surrounding the contact area. The contact area of the steel plate after friction testing with this lubricant, fig. 4.31, is very small and is covered by a film, which is more visible under high magnification. Although the steel plate was thoroughly cleaned with acetone there were black charging spots visible on the contact area which could imply that the film is composed of an oily residue.

Figure 4.29 shows a very clear wear scar in the contact area of the silicon nitride ball after friction testing with ester base fluid T80884 +0.3% amine phosphate. There are grooves on the contact area which correspond to the machining marks on the steel plate. The contact area of the steel plate after friction testing with this lubricant, fig. 4.32 shows a very clear plastically deformed wear scar with abrasion grooves, but there does not appear to be much debris on the surface.

Figure 4.30 shows a film on the contact area of the silicon nitride ball after friction testing with polyglycol T81499 +0.3% amine phosphate. Under high magnification there appears to be abrasion grooves on the film with a lot of fine debris. The wear scar on the steel plate after friction testing with this lubricant shows that intense plastic deformation occurred with lots of debris and scratches, fig.4.33.

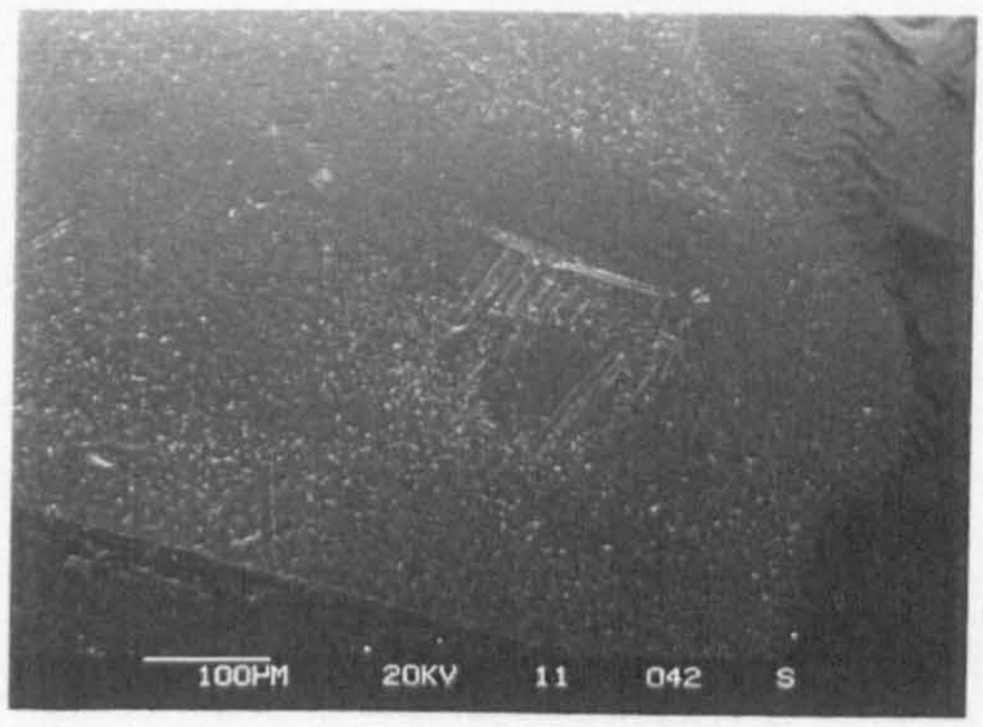

(a) Overall view

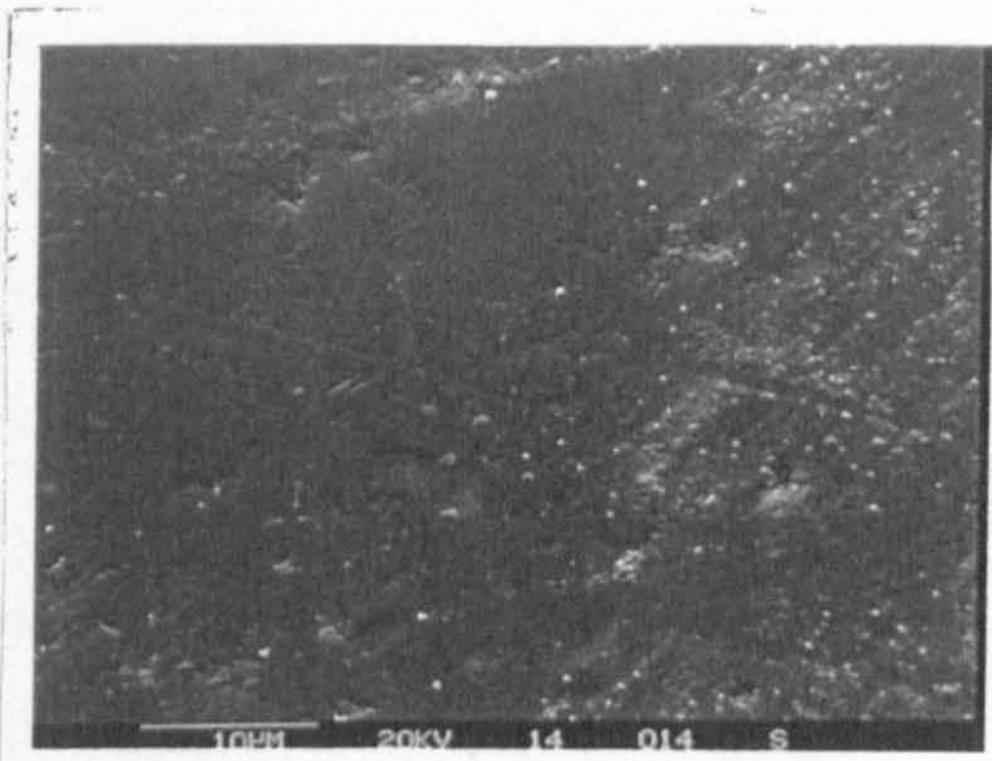

(b) Higher magnification

Fig. 4.28 SEM observations of ceramic ball after friction testing with Talpa 20 + 0.3% Amine Phosphate

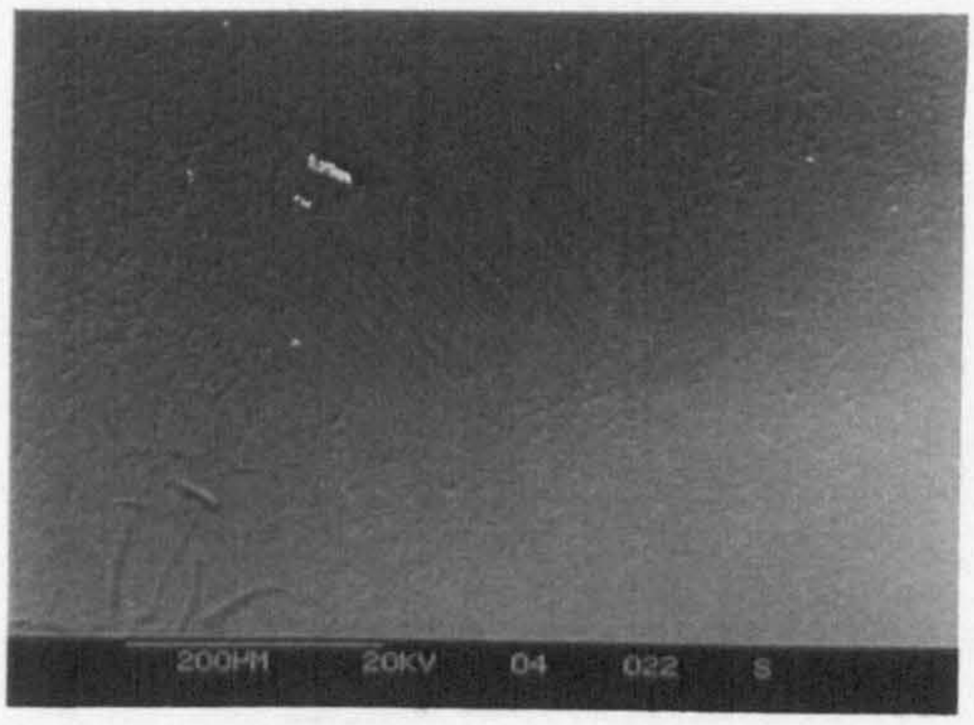

(a) Overall view

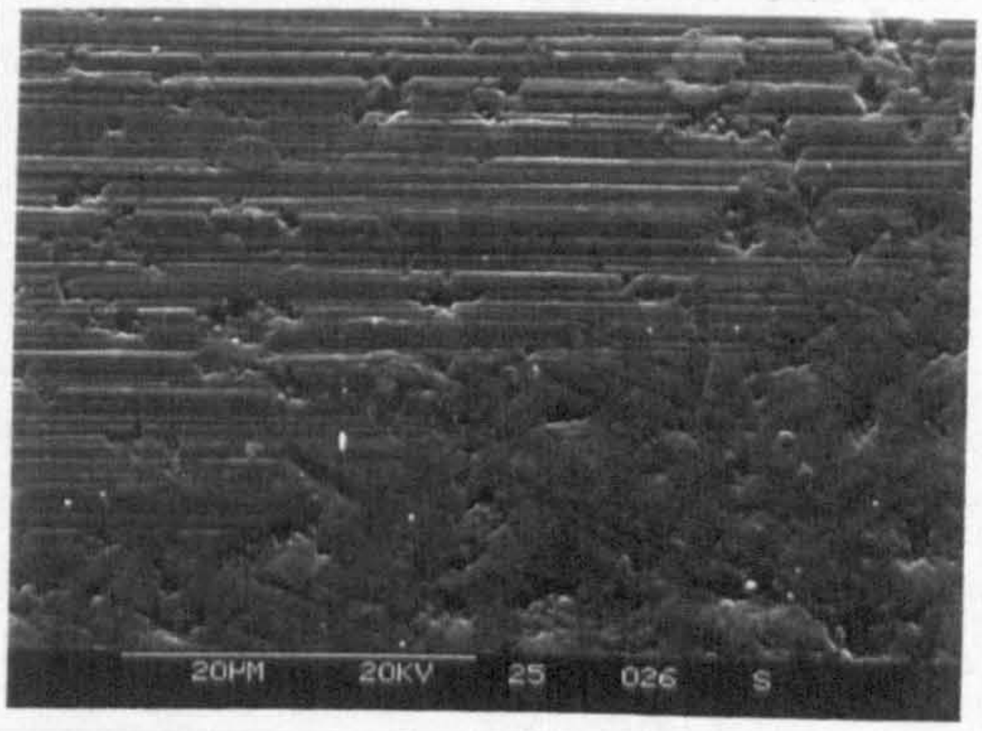

(b) Higher magnification

Fig. 4.29 SEM observations of ceramic ball after friction testing with ester T80884 + 0.3% Amine Phosphate

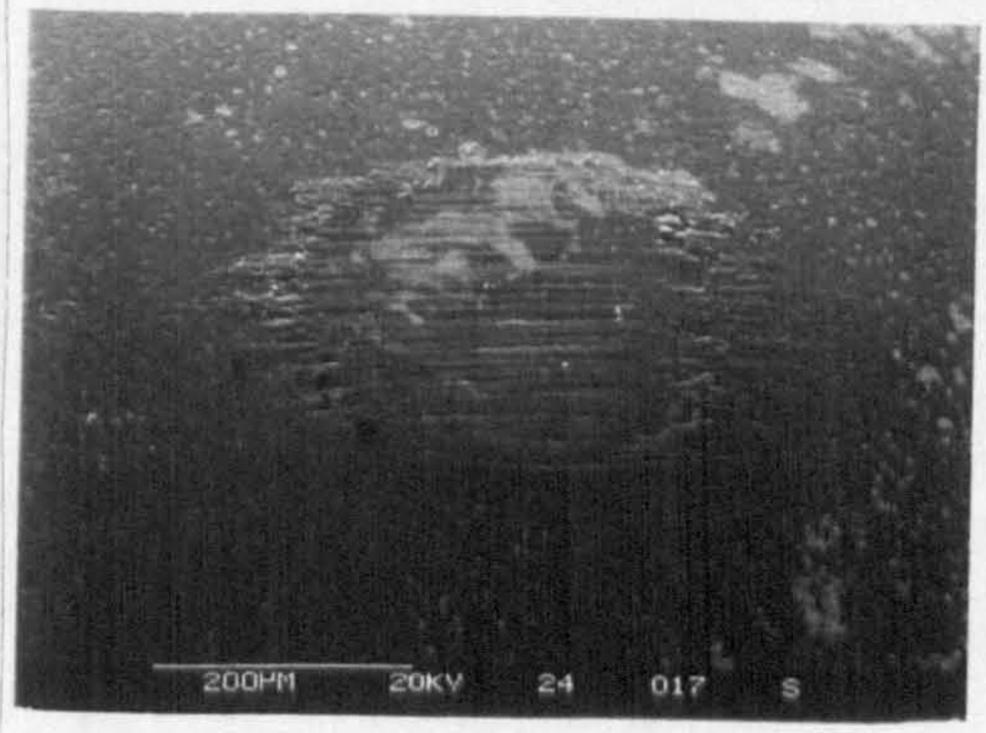

(a) Overall view

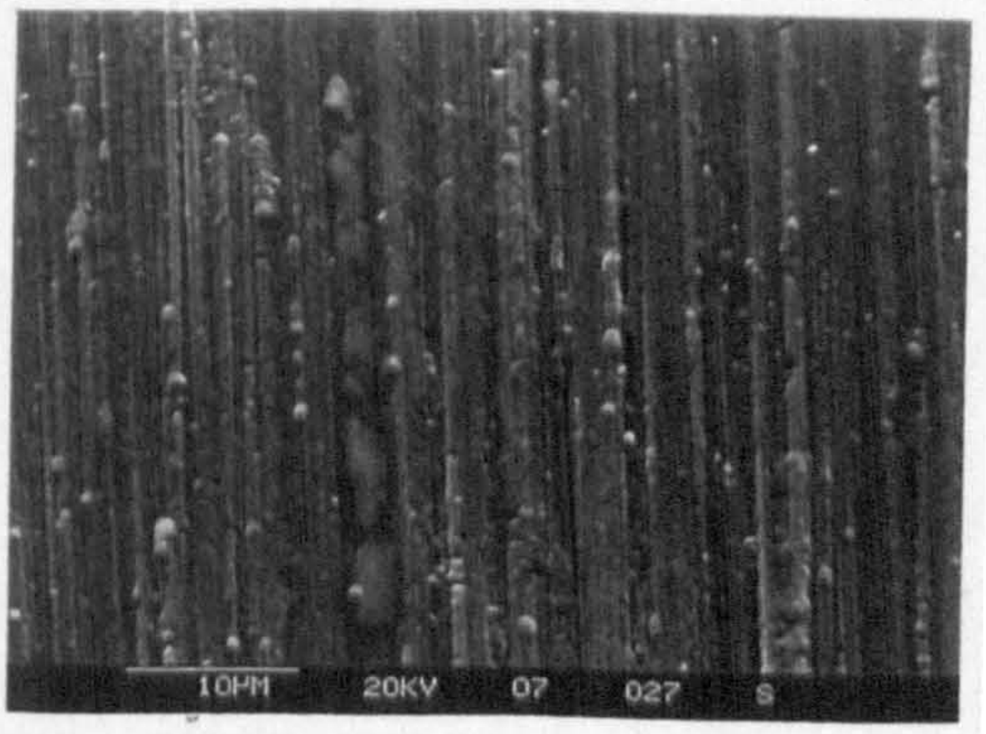

(b) Higher magnification

Fig. 4.30 SEM observations of ceramic ball after friction testing with polyglycol T81499 + 0.3% Amine Phosphate

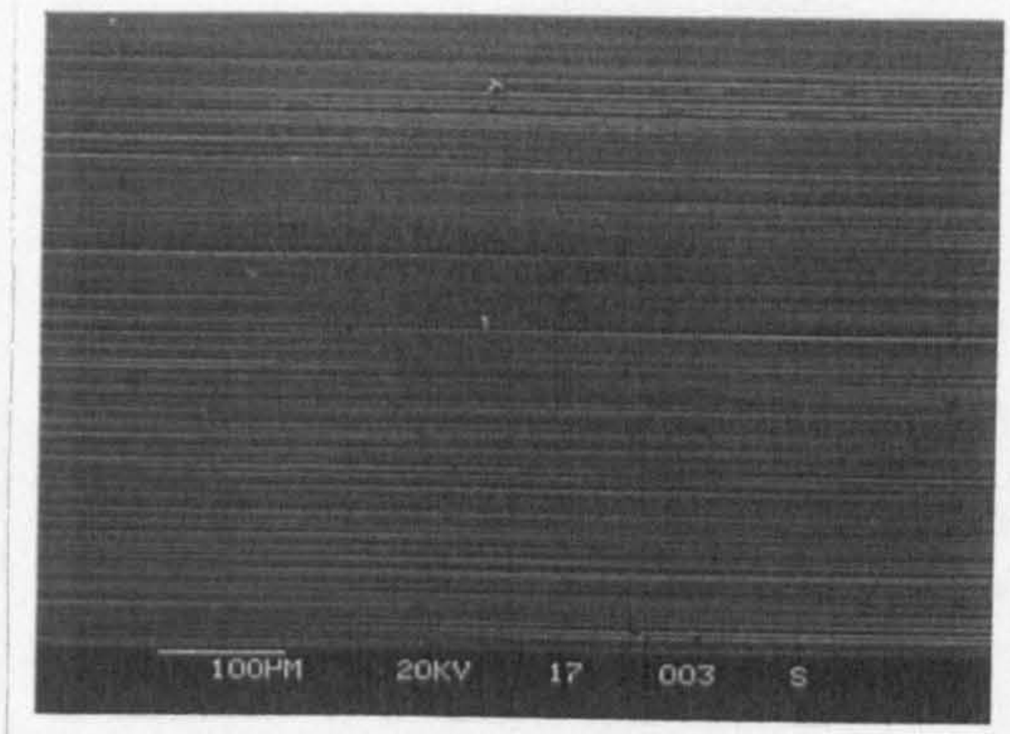

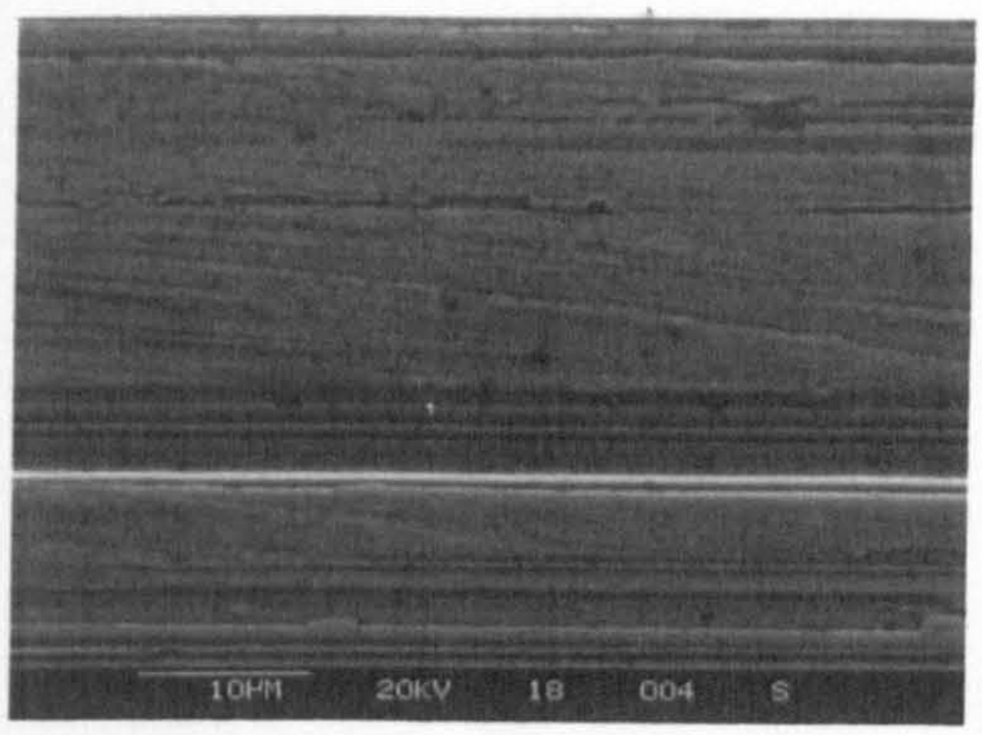

(a) Overall view **(b) Higher magnification**

Fig. 4.31 SEM observations of steel plate after friction testing with Talpa 20 + 0.3% Amine Phosphate

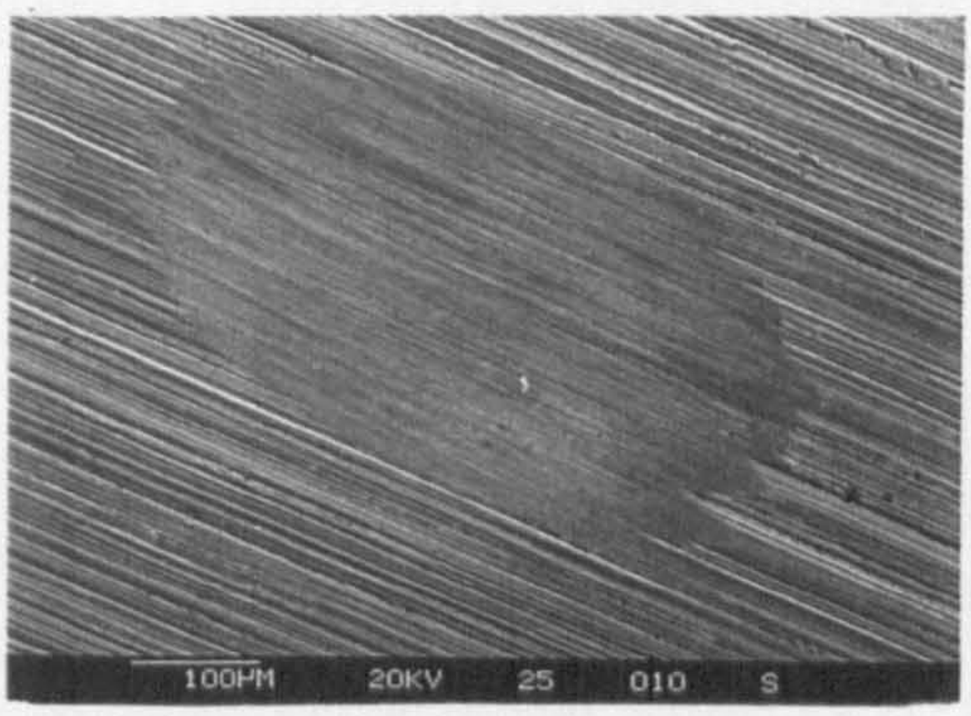

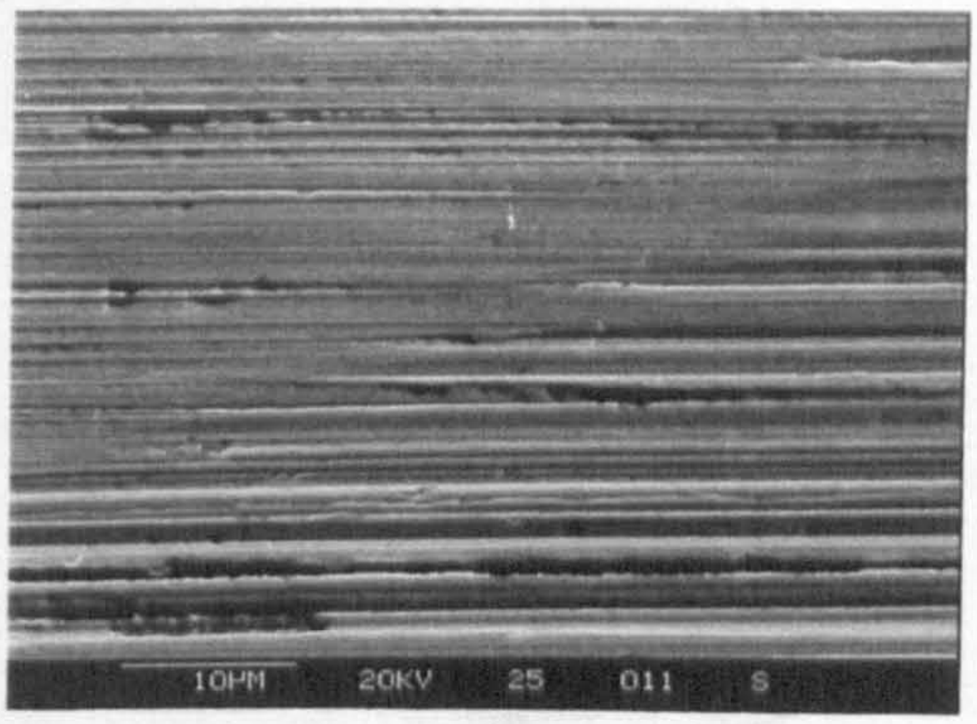

(a) Overall view **(b) Higher magnification**

Fig. 4.32 SEM observations of steel plate after friction testing with ester T80884 + 0.3% Amine Phosphate

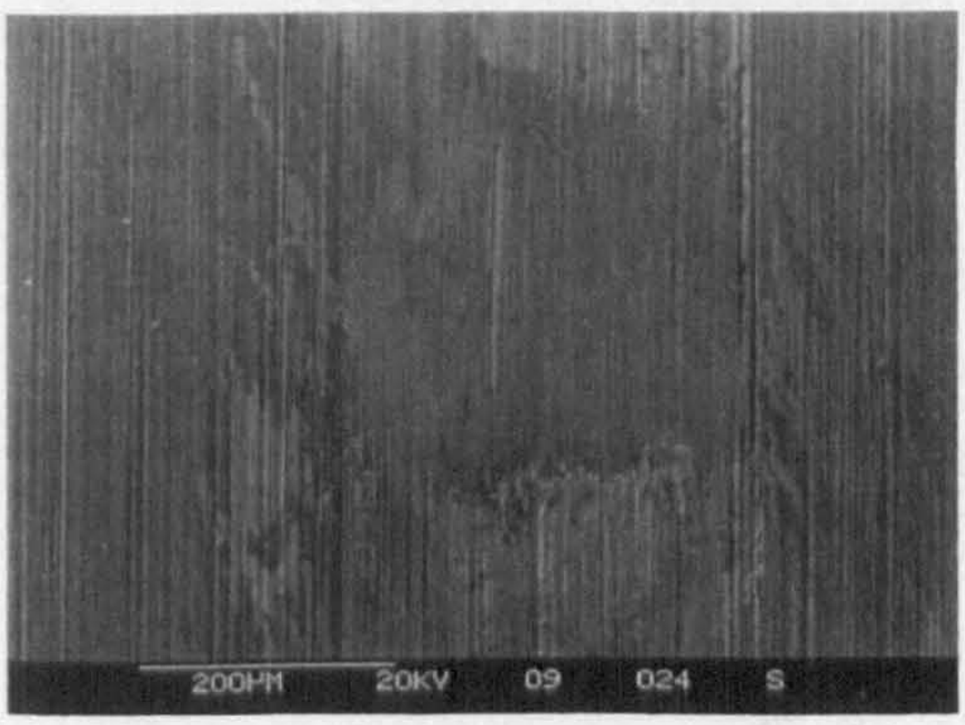

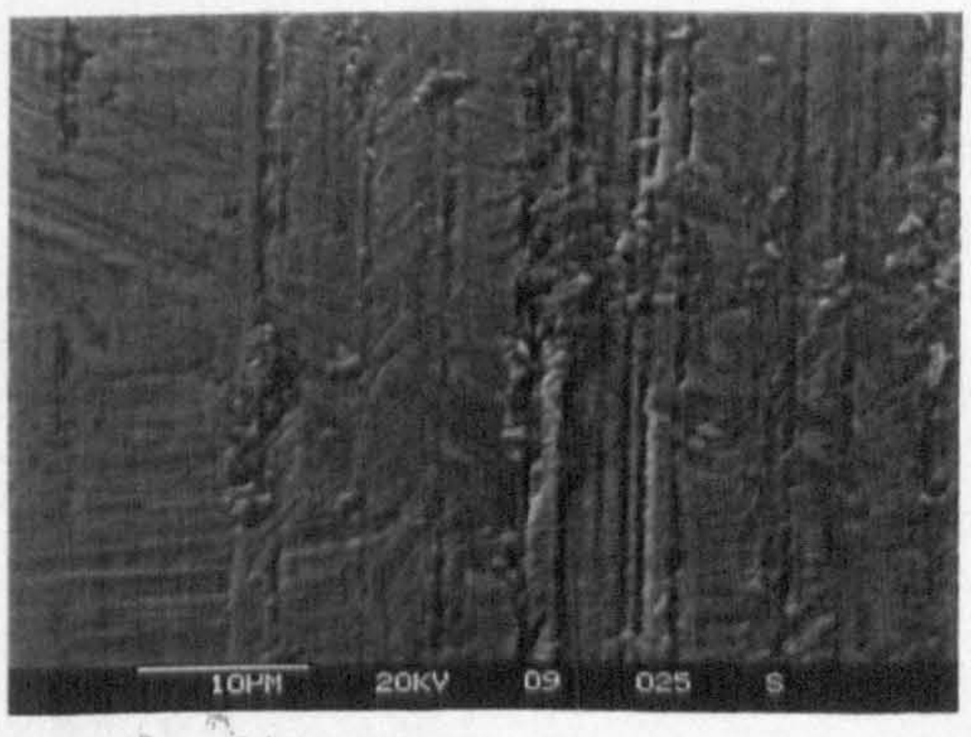

(a) Overall view **(b) Higher magnification**

Fig. 4.33 SEM observations of steel plate after friction testing with polyglycol T81499 + 0.3% Amine Phosphate

4.7 Summary of Results

The coefficient of friction is a measure of the instantaneous mechanical interactions between the contacting surfaces in relative motion. The different friction coefficient values observed in this study reflect the change in the severity of interaction between contacting surfaces. The following conclusions can be formulated on the basis of results presented in this chapter:

- the effects of temperature, load, frequency and amplitude of sliding affect the friction of silicon nitride ceramics lubricated with various liquids.

- under lubricated conditions and the temperature of up to 80°C the coefficients of friction for different combinations of contacting materials are as follows:

  ceramic ball/ceramic plate > ceramic ball/ steel plate > steel ball/steel plate

  As the temperature is further increased to 160°C the coefficients of friction are in the following order:

  ceramic ball/steel plate > ceramic ball/ceramic plate > steel ball/steel plate.

- The results show that the ester base fluid T80884 gave the lowest coefficient of friction of about 0.07 and the polyglycol T81499 gave the highest coefficient of friction of about 0.185.

- The effectiveness of the additive phosphate ester in the lubrication of silicon nitride ball sliding on the steel plate at temperatures ranging from 20°C - 160°C is summarised in the table below:

	Friction Behaviour		**Damage to Specimens after Test**	
Lubricant	**Temperature Increase °C**	**Coeff. Friction**	**Ball**	**Plate**
Talpa 20 + phosphate ester	30°C - 70°C 70°C - 160°C	0.1 - 0.14 .12 - 0.13	Build up of lubricant. No apparent damage or wear.	Smooth built up film on wear track surface.
Ester T80884 + phosphate ester	30°C - 70°C 70°C - 160°C	0.11 - 0.136 decreasing from 0.13 - 0.1	Wear scar covered with film, with abrasion grooves on it.	Severe plastic deformation on wear track.
Polyglycol T81499 + phosphate ester	30°C - 80°C 80°C - 120°C 120°C - 160°C	0.13 - 0.15 0.16 decreasing from 0.17 - 0.14	Wear scar covered with film, which has abrasion grooves on it and a lot of fine debris.	Severe plastic deformation on wear track and a lot of fine debris present both inside and outside of wear track.

When using the phosphate ester triethanol amine in the reference lubricant Talpa 20, the ester base fluid T80884 and the polyglycol T81499, it was found that the additive increased the coefficient of friction for Talpa 20 and ester base fluid T80884 and decreased it slightly with polyglycol T81499. However, the ester base fluid T80884 still gave the lowest coefficient of friction.

- The effectiveness of triethanol amine in the lubrication of silicon nitride ball sliding on the steel plate at temperatures ranging from 20°C - 160°C is show in the table below:

	Friction Behaviour		**Damage to Specimens after Test**	
Lubricant	**Temperature Increase °C**	**Coeff. Friction**	**Ball**	**Plate**
Talpa 20 + Triethanol amine	30°C - 60°C 60°C - 160°C	0.09 - 0.115 0.115	Build up of lubricant. No apparent damage or wear.	Smooth built up film on wear track surface.
Ester T80884+ Triethanol amine	30°C - 80°C 80°C - 140°C	0.155 - 0.16 0.16 - 0.215	Wear scar has abrasion grooves with large wear debris embedded into grooves. Shape of abrasion grooves correspond to machining marks on plate.	Plastic deformation on wear track and abrasion grooves present.
Polyglycol T81499 + triethanol amine	30°C - 80°C 80°C - 120°C 120°C - 160°C	0.11 - 0.16 0.16 0.16 - 0.135	Wear scar covered with film with a lot of fine debris.	Large wear track with very smooth surface due to intense plastic deformation.

When using the additive triethanol amine in the reference lubricant Talpa 20, the ester base fluid T80884 and the polyglycol T81499, it was found that the additive had no effect on the coefficient of friction for Talpa 20, it increased the coefficient of friction with ester base fluid T80884 and decreased it slightly with polyglycol T81499. Overall, Talpa 20 gave the lowest values for the coefficient of friction and this could have been due to a protective film being formed at the contact interface.

- The effectiveness of the amine phosphate in the lubrication of silicon nitride ball sliding on the steel plate at temperatures ranging from 20°C - 160°C are show in the table below:

	Friction Behaviour		**Damage to Specimens after Test**	
Lubricant	**Temperature Increase °C**	**Coeff. Friction**	**Ball**	**Plate**
Talpa 20 + Amine phosphate	30°C - 80 °C 80 °C - 160 °C	0.09 - 0.095 0.095 - 0.1	No distinct wear scar - a lot of fine debris present.	Oily film on wear track surface.
Ester T80884+ Amine phosphate	30 °C - 90 °C 90 °C - 160 °C	0.085 - 0.09 0.09 - 0.115	Well defined abrasion grooves on wear scar which correspond to machining marks on steel plate.	Plastic deformation on wear track with abrasion grooves present.
Polyglycol T81499 + Amine phosphate	30 °C - 70 °C 70 °C - 120 °C 120 °C - 160 °C	0.135-0.175 0.175-0.165 0.165	Compacted lubricant film on surface with abrasion grooves on it and a lot of fine debris.	Severe plastic deformation on wear track with lots of debris and scratches.

When using the amine phosphate in the reference lubricant Talpa 20, the ester base fluid T80884 and the polyglycol T81499, there was no significant effect on the coefficient of friction. Overall, ester base fluid T80884 gave the lowest values in coefficient of friction. Similar investigations have been done by Morimoto, 1993, on the effect of a mineral oil with the addition of tricresyl phosphate (TCP) on the wear of silicon nitride sliding against steel. He found that the addition of TCP reduced the wear of silicon nitride and decreased the coefficient of friction slightly. A film composed of a phosphorus compound, probably iron phosphate, was produced on the wear track formed on the steel rod, indicating that the phosphorus reacted tribochemically with the iron and the reaction product formed a film on the surface of the silicon nitride-steel pair.

REFERENCES

Morimoto, T., 1993, **"Effect of tricresyl phosphate on wear of silicon nitride sliding against bearing steel"**, Wear, Vol. 169, pp.127-134.

Mimaroglu, A. & Yilmaz, F., 1997, **"Influence of Carbide Size, Hardness and Temperature on the Sliding Friction and Wear of a Boundary Lubricated High-Speed Steel and Si_3N_4 Ceramics"**, Tribology Transactions, Vol. 40, pp.173-177.

Chapter 5

RESULTS AND DISCUSSION OF MODEL GRINDING TESTS

5.1 Introduction

In this chapter the influence of lubricants on the material removal of silicon nitride balls is investigated using the four ball machine. Preliminary testing was carried out in order to select the size of abrasive particles, the load, the counterface material, the velocity and the different types of lubricating liquids.

Further investigations were carried out on the surface features generated during the grinding experiments using a scanning electron microscope and a surface roughness profilometer. These were used to determine the effects of the lubricants and to elucidate the possible material removal mechanism.

5.2 Preliminary Grinding Experiments

5.2.1 Effect of varying load and abrasive particle size

Grinding fluids consisting of oil based diamond slurries of particle size ranging from 1 to 45 μm were used. The synthetic diamond particles in these slurries were homogeneously mixed and suspended in Kerosene type oil based solution. The load on the set of nine balls was varied from 200 to 4000N. The run-in balls were placed in the cup of the four ball test machine and 3ml of the diamond slurry of known particle size and percentage weight concentration was added to it. The experiment was then started at a known load, constant rotational speed of 3000rpm and run for 60 minutes. Further details regarding testing procedure can be found in a paper by Stolarski et al., 1995.

Figure 5.1 shows the material removal rate plotted against applied load as a function of the particle sizes. For the 1μm particle size diamond slurry, only a small quantity of the material is removed (removal rate 0.15μm/min) at 200N load, and further increase in the load from 200N to 4000N results in a small gradual increase in the material removal rate (0.5μm/min). Increasing the particle size from 1μm to 6μm alters the material removal significantly. For the 6μm particle size the material removal rate changes only slightly from 0.66μm/min to 0.74μm/min when the load is further increased 200N to 1200N. However, further increase in the load to 2000N for this particle size results in the five

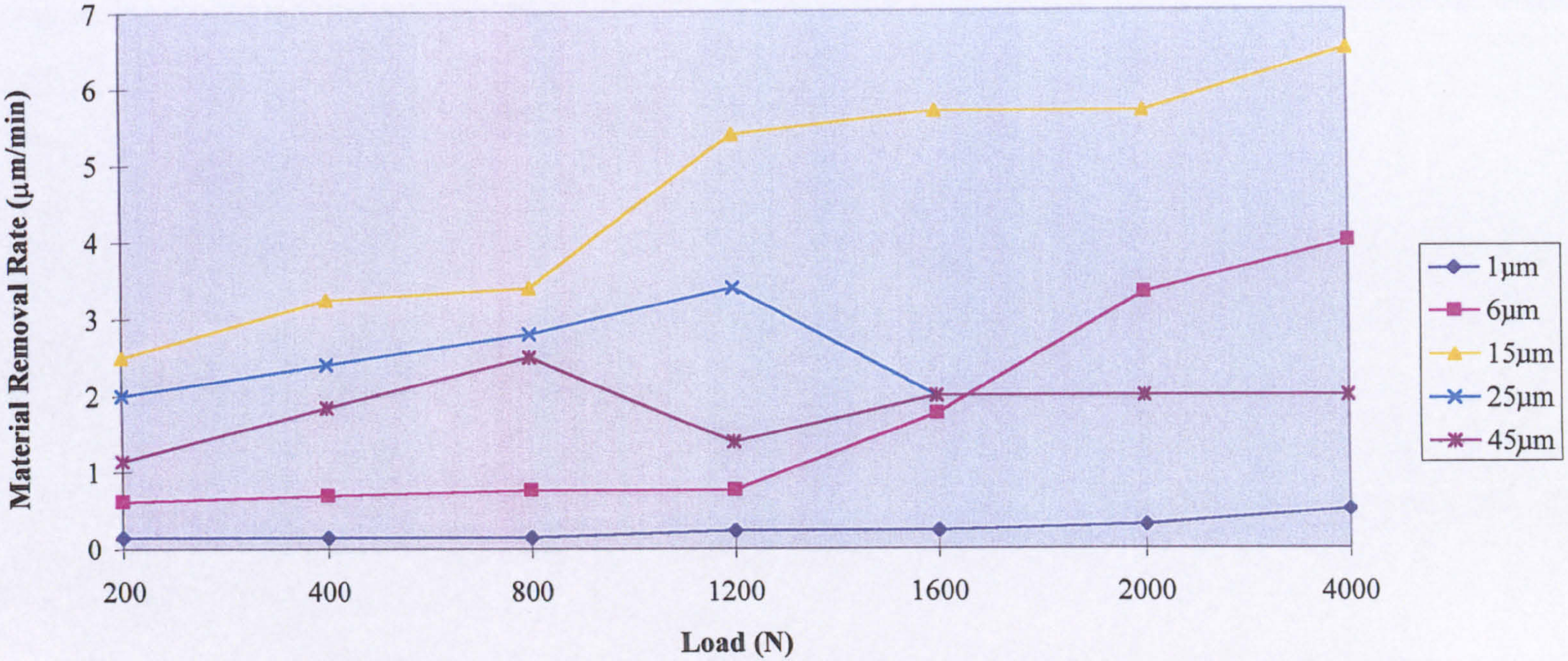

Fig. 5.1 Material removal rate as a function of load for different abrasive particle sizes (Rotational velocity-3000rpm, test duration-1hour, grinding fluid-3ml oil based diamond slurry)

fold increase in the removal rate to 3.34μm/min. A further rise in the load to 4000N only produces a slight increase in the material removal rate.

Increasing the particle size from 6μm to 15μm results in a four fold increase in the material removal rate at higher loads (200N to 1200N) and the increase in the removal rate of 1.5 times is achieved at heavier loads (1600N-4000N). Further increase in the particle size to 25μm reduces the material removal rate by 20% at lighter loads (200N to 800N) and by 70% at heavier loads (1200N to 4000N). Further increase in the particle size from 25μm to 45μm results in a similar material removal trend.

In general, the material removal rate with respect to the load shows two clear trends. Firstly, the initial increase in the load does not change the material removal rate significantly until a critical load is reached. When, the transition is reached the material removal rate then increases two- or three-fold. Once the transition has occurred, the material removal rate is again independent of the load. Secondly, the material removal rate is affected by the particle size of the diamond slurry. The material removal rate increases as the particle size is increased from 1μm to 15μm. Further increase in the particle size from 25μm to 45μm results in reversal of the trend. Thus it can be concluded that the optimum material removal rate is reached at a 15μm particle size.

5.2.2 Effect of varying counterface material

Four counterface materials were tested, namely, mild steel, stainless steel, aluminium alloy and brass under the same test conditions as outlined in section 5.2.1. It was found that aluminium alloy proved to be the most effective counterface material in increasing the removal rate. Both brass and mild steel turned out to be far less effective. The difference between the highest material removal rate recorded for the aluminium counterface and that observed for mild steel and brass counterfaces is about three times. The disadvantage of using aluminium alloy is that it is much softer than the other materials and has to be replaced after each test run, therefore stainless steel was used for the testing.

5.2.3 Effect of velocity and viscosity effects of lubricating liquids

Grinding experiments were carried out at five rotational velocities of the spindle, that is, 1500, 5000, 7000 and 10 000rpm, Stolarski, 1992. Three normal loads on a set of nine balls were used, that is, 100, 200 and 400N. To explore the effect of lubricating fluid on the rate of material removal, the following fluids were used: brake fluid, brake fluid with distilled water in a 1:1 volume ratio, very viscous silicon oil and lithium based grease. Diamond abrasive particles of 25μm were added to all the fluids and each test run lasted 45 minutes.

It was observed that at very high rotational velocities there was a tendency to ejecting lubricating fluid together with abrasive particles from the contact zone. Therefore, it was thought that a fluid with a very high viscosity might help to retain the abrasive particles within the contact zone. From the results of this study it was found that silicon oil, which had a higher viscosity than the other lubricating liquids gave a much higher material removal rate for various rotational velocities. Lithium based grease which was chosen on the same rationale as in the case of high viscosity silicon oil, gave the lowest rate of material removal and this was due to the formation of a film by the grease which completely screened the contact zone from the abrasive particles.

The rotational velocity has a substantial influence on the rate of material removal. The increase in material removal is not proportional to the increase in speed, as at the highest speeds used the increase in grinding rate is not as rapid as at lower speeds. No clear correlation between viscosity of lubricating liquids and the material removal rate was found, however, grinding in high viscosity liquids produced balls with a substantial deviation from an ideal sphere. This was mainly due to the inability of a ball to spin freely during grinding in a viscous slurry.

5.2.4. Effect of contact configuration

Two different contact configurations were tested under the same test conditions as outlined in section 5.2.3. Figure 5.2 shows three-point-contact configuration and figure 5.3 shows four-point-contact configuration. It was found that four point contact configuration is more effective in material removal than three point contact. However, the four-point contact configuration proved to be more sensitive to any mass imbalance or lack of alignment which was indicated by excessive vibration during test runs at high speeds.

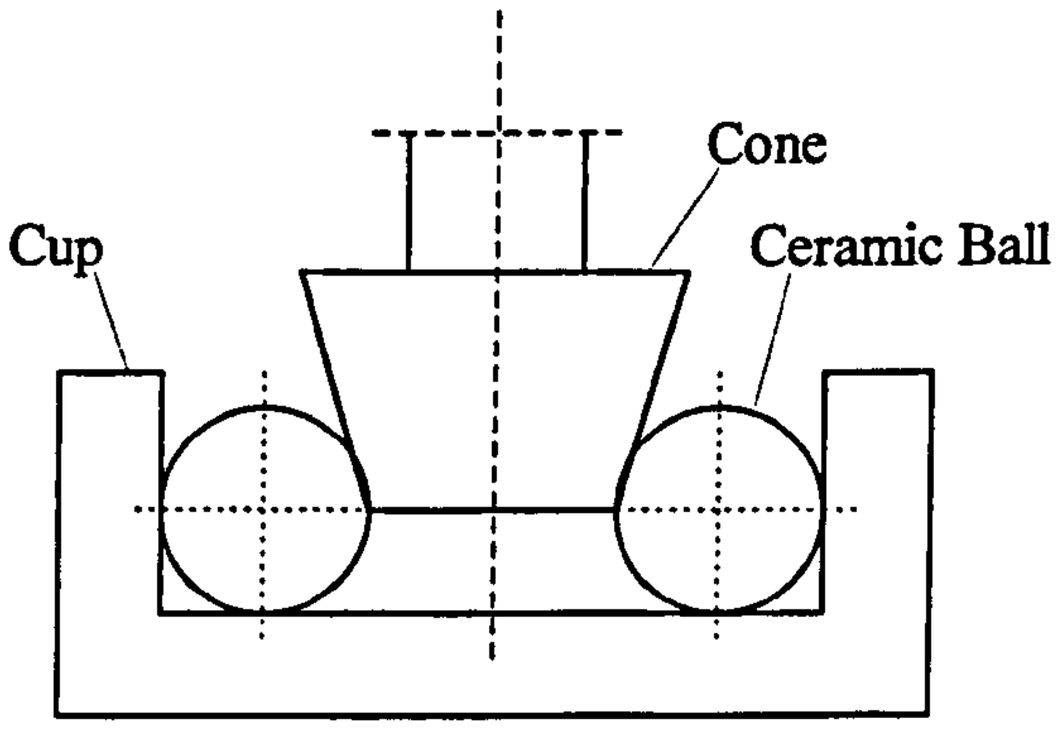

Fig. 5.2 Three-point-contact configuration

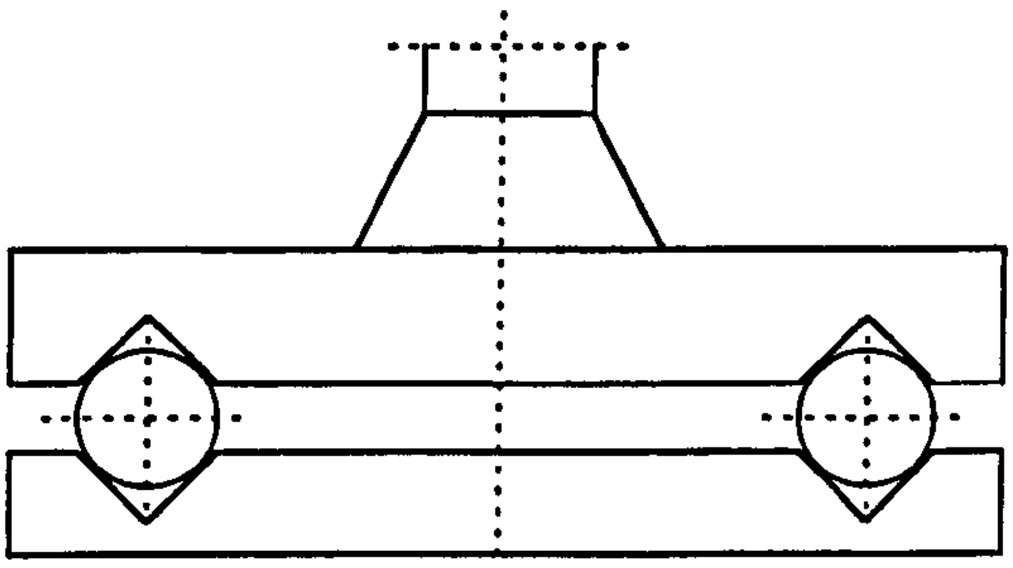

Fig. 5.3 Four-point-contact configuration

5.2.5 Effect of water

To test the hypothesis, Y. Tsunai, 1988, that water might react with silicon nitride to produce surface films of silicon oxide which could be removed during grinding, an emulsion of brake fluid and distilled water (in 1:1 volume ratio) was used. The results of this study showed there was no significant increase in material removal rate as compared with that obtained when brake fluid alone was used.

5.3 Grinding Effectiveness in the presence of Mineral and Synthetic Oils

Figure 5.4 shows the results of material removal rates of silicon nitride balls after the grinding tests using the four ball machine at a load of 400N, rotational velocity 3000rpm and test duration 1hour. The test lubricants containing 15μm diamond particles at 2% by weight concentration were:

- reference-Kemet (used in industry)
- mineral oils -T80853, T80854
- ester base fluid - T80855, T80884
- polyalphaolefin - T80855, T80856
- polyglycols - T81497, T81498, T81499, T81500, T81501 and T81502

The highest material removal rate of 1.8μm/min is obtained when using the polygylcol T81499, this gives an increase by two fold when compared to the reference slurry Kemet which gives a value of 0.6μm/min. Among the mineral oils, polyesters and polyalphaolefins, the ester base fluid T80884 gives the highest material removal rate of 1.2μm/min; this is an increase by one fold. Further testing was conducted with Kemet and the two most effective lubricants, that is , ester base fluid T80884 and polyglycol T81499 using various concentrations of the additive phosphate ester, triethanol amine and amine phosphate.

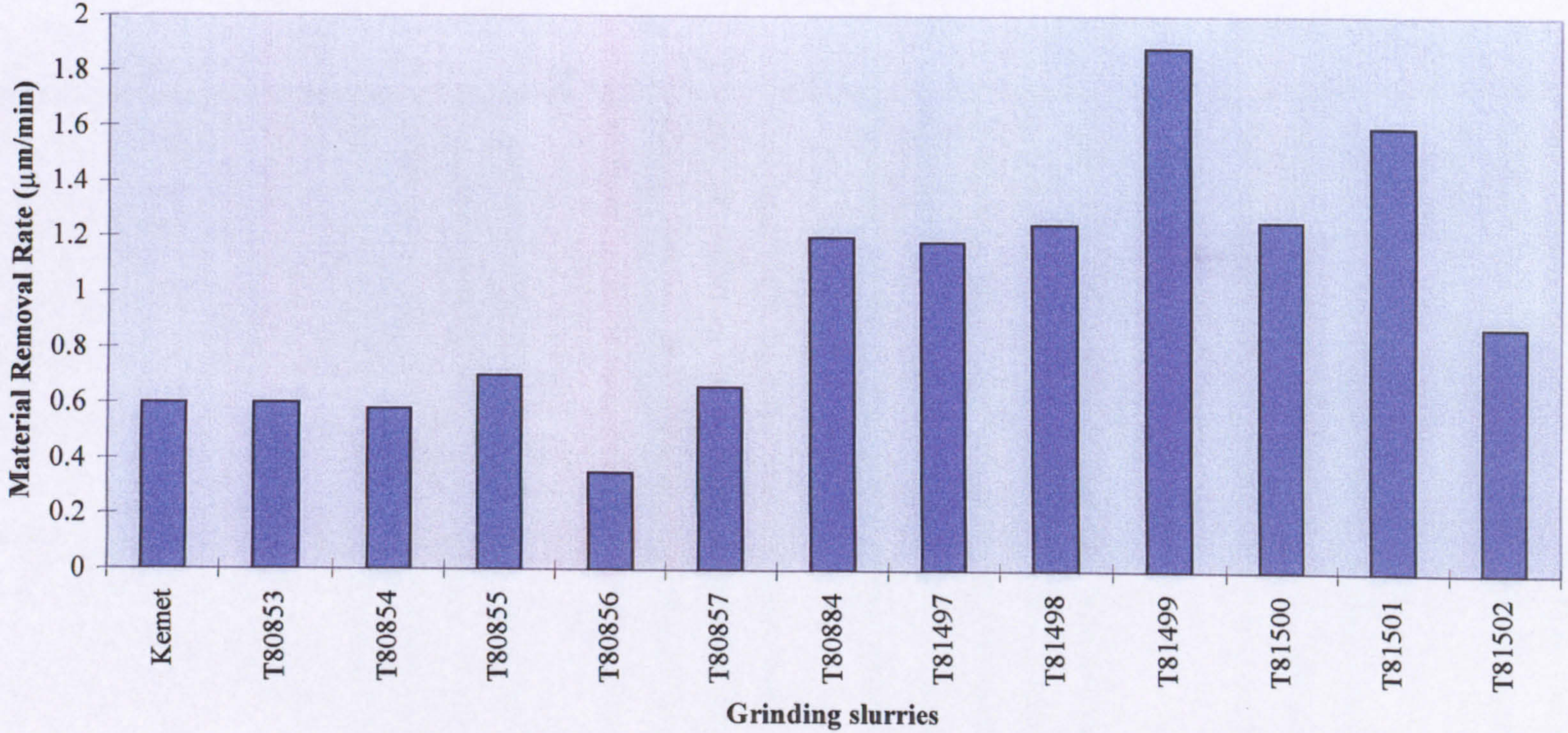

Fig. 5.4 The material removal rate of silicon nitride balls using various grinding slurries

5.4 Grinding measurements using Phosphate Ester

Figure 5.5 shows the material removal rate of silicon nitride balls using Kemet, ester base fluid T80884 and polyglycol T81499 with various concentrations of the additive phosphate ester. All the results show a comparison of with and without additive for each of the three test lubricants.

When using 0.1% phosphate ester with Kemet there is an increase in material removal rate from 0.6μm/min (without additive) to 1μm/min, however, when using 0.2% and 0.3% phosphate ester the material removal rate is 1.6μm/min, that is an increase greater than one fold.

When using 0.1% phosphate ester with ester base fluid T80884 there is a reduction in material removal rate to 0.95μm/min from 1.2μm/min when using ester base fluid T80884 only. When using 0.2% phosphate ester with ester base fluid T80884 there is a slight increase in material removal rate to 1.4μm/min, however, when using 0.3% phosphate ester there is a decrease in material removal rate to 0.7μm/min.

When using 0.1%, 0.2% and 0.3% phosphate ester with polyglycol T81499 there is no significant effect on the material removal rate when comparing polyglycol T81499 without additive. The material removal rate ranges between 1.7-2.0μm/min for polyglycol T81499 with and without additive.

In general the additive phosphate ester has a significant effect only on the material removal rate with the reference slurry Kemet. It has a reducing effect on ester base fluid T80884 and no significant effect on polyglycol T81499. Overall, the highest material removal rate is obtained when using polyglycol T81499.

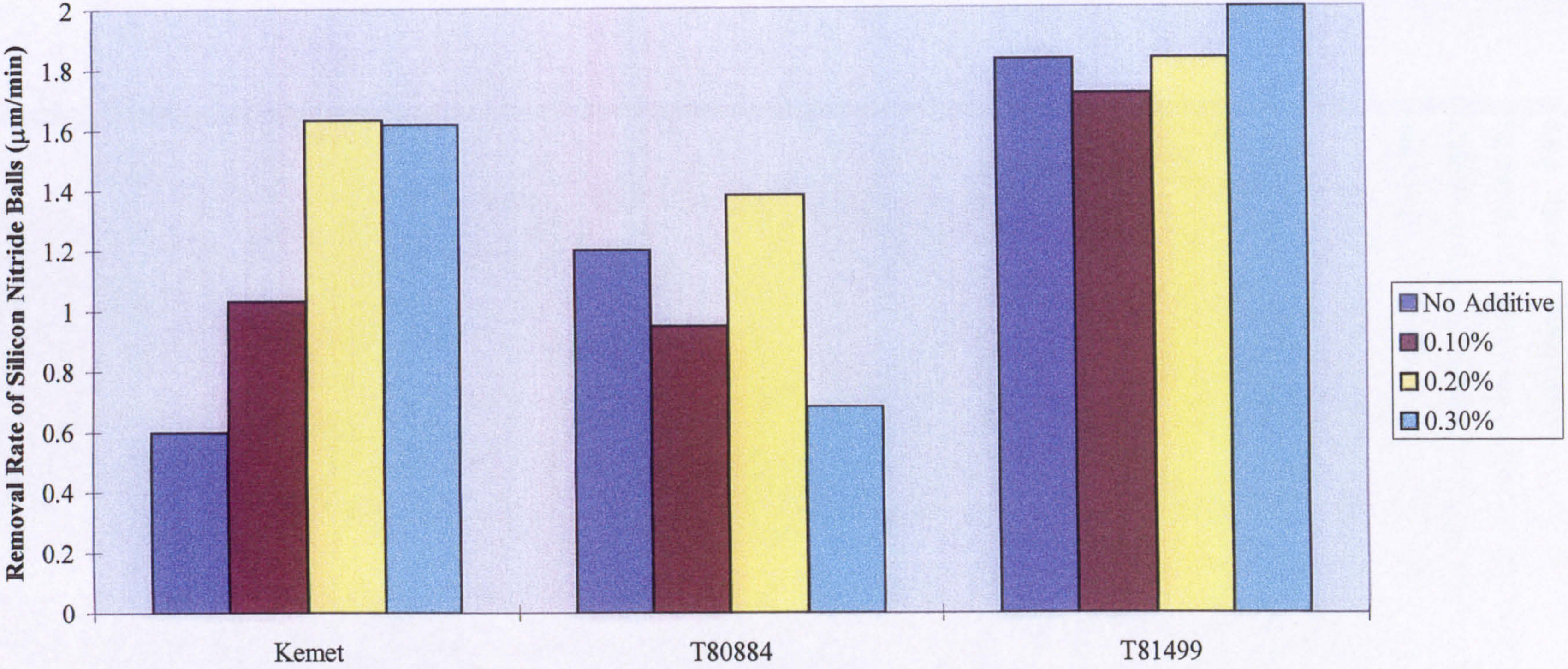

Fig. 5.5 Removal Rate of Silicon Nitride Balls in Kemet , ester base fluid T80884 and polyglycol T81499 with various concentrations of the additive Phosphate Ester

5.4.1 Surface Observations

Figures 5.6-5.8 show the surface of the ceramic balls after grinding tests with the additive phosphate ester mixed with the reference slurry Kemet, ester base fluid T80884 and polyglycol T81499.

Figure 5.6 shows a severely damaged surface after testing with Kemet + 0.3% phosphate ester. It seems, that the major mechanism of grinding was brittle fracture resulting in high removal of relatively large fragments of material.

Figure 5.7 and 5.8 shows a very pitted surface after testing with the ester base fluid T80884 +0.2% phosphate ester and polyglycol T81499 + 0.3% phosphate ester, which could be due to brittle fracture. At a high magnification both surfaces show scratches on a micrometer scale, which indicates a ploughing action during grinding.

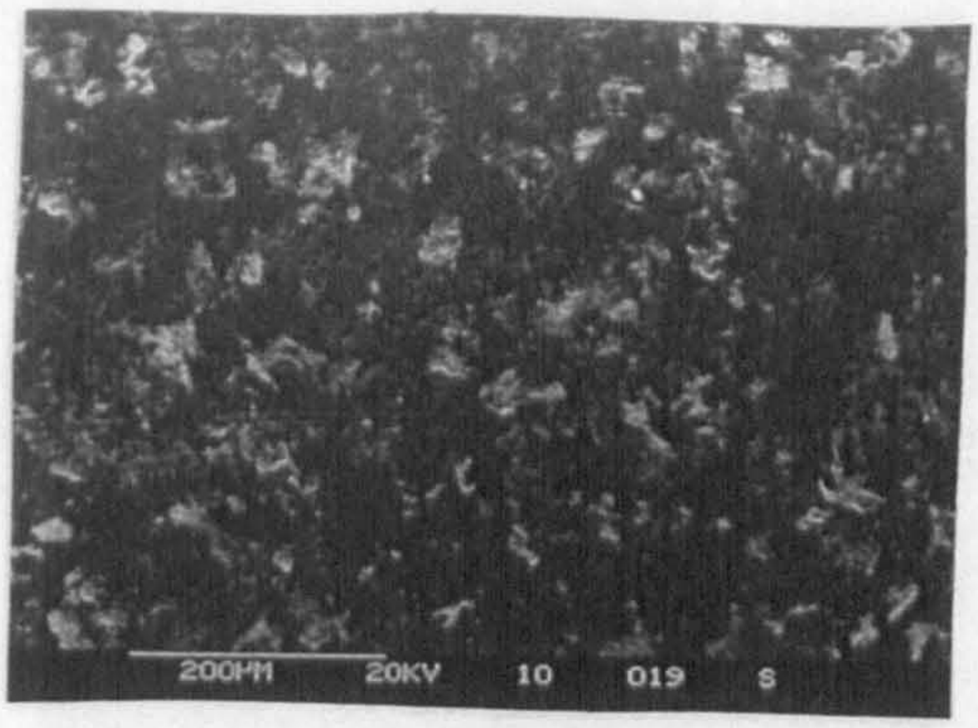

(a) Overall view

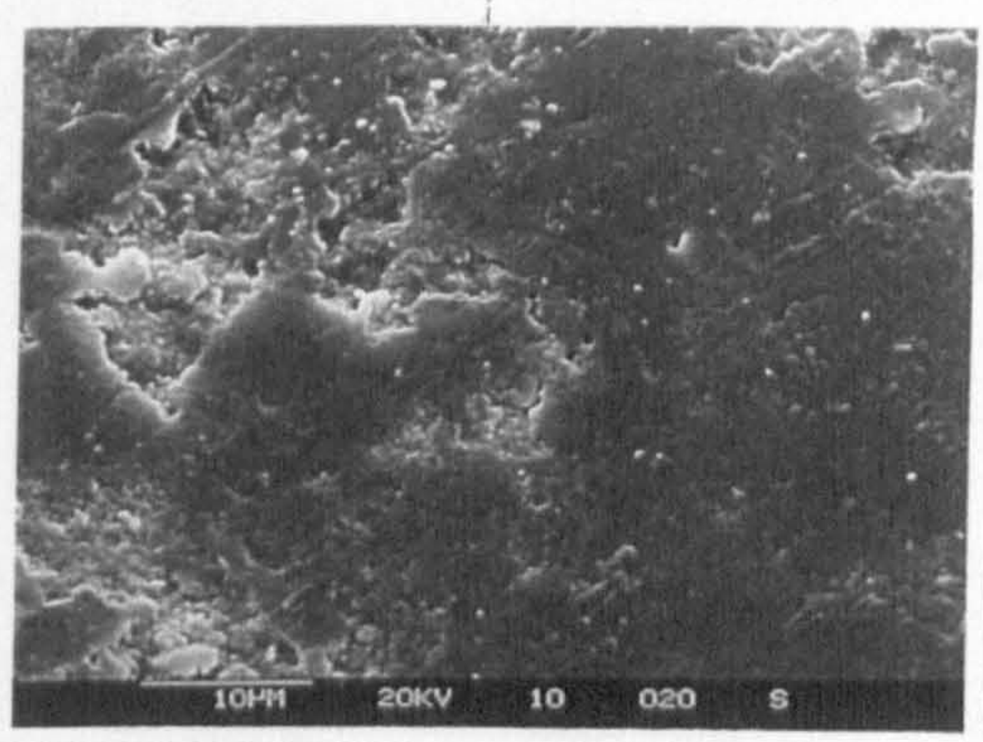

(b) Higher magnification

Fig. 5.6 SEM observations of ceramic ball after grinding with Kemet + 0.3% Phosphate Ester

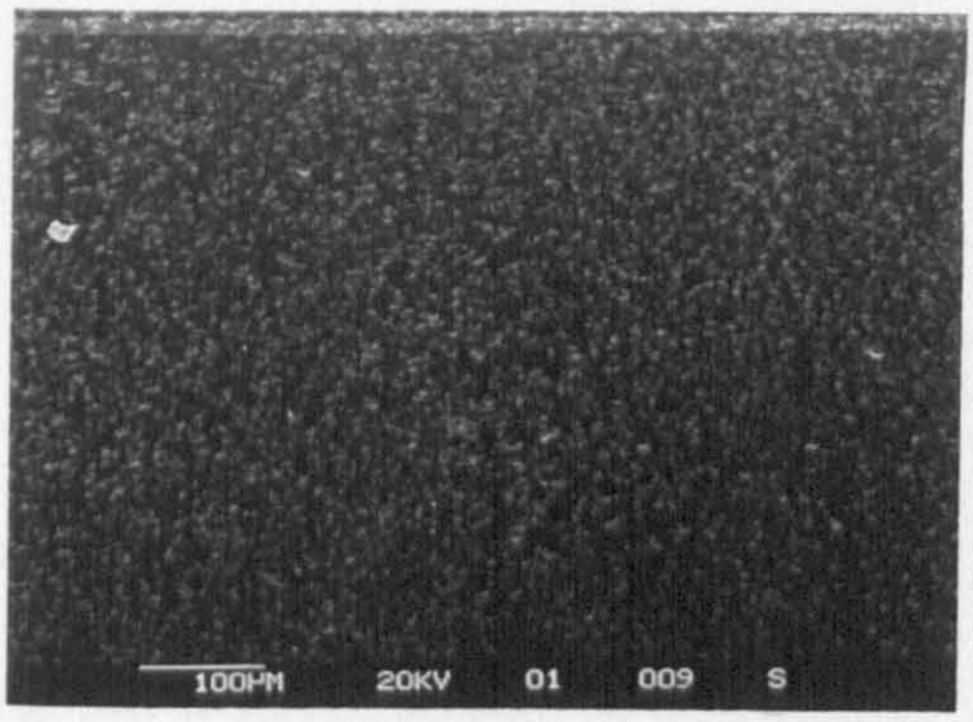

(a) Overall view

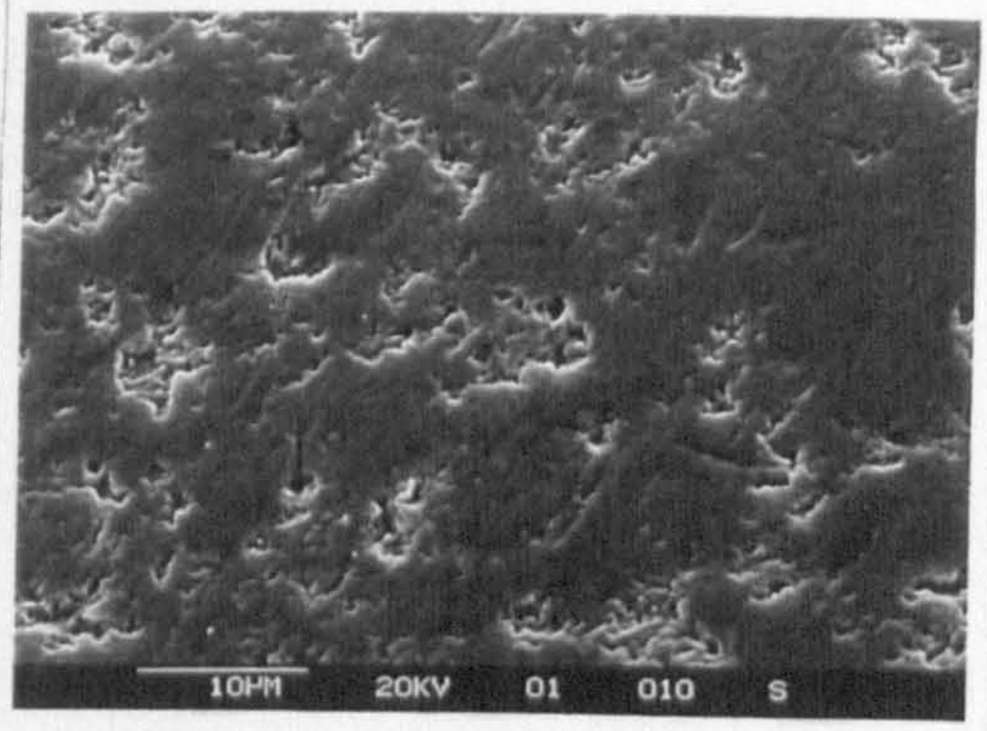

(b) Higher magnification

Fig. 5.7 SEM observations of ceramic ball after grinding with ester T80884 + 0.2% Phosphate Ester

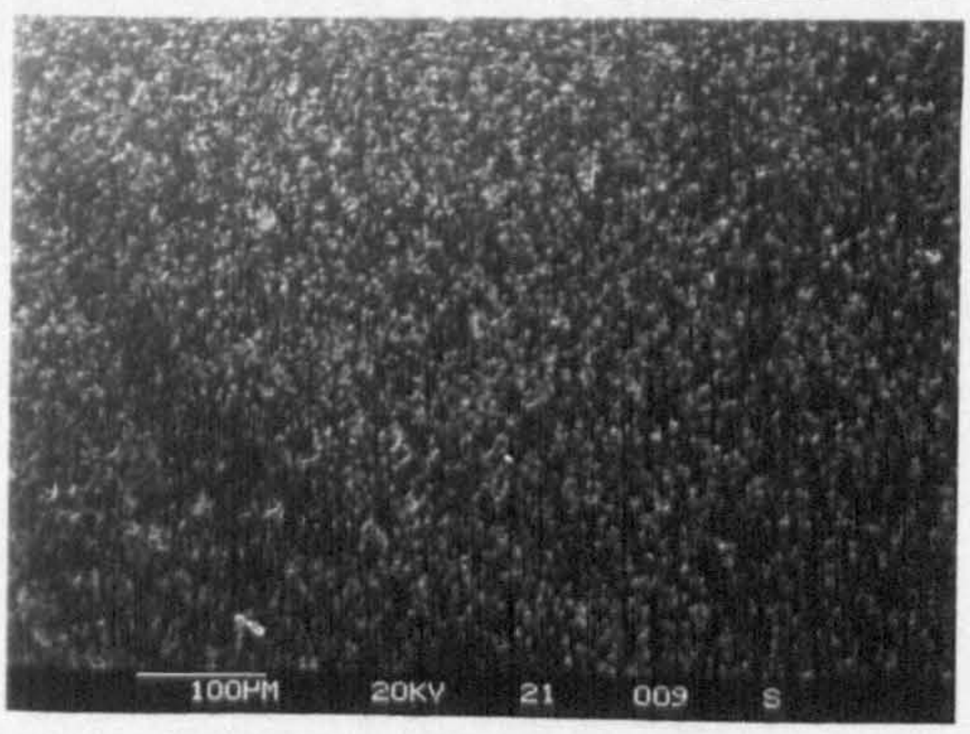

(a) Overall view

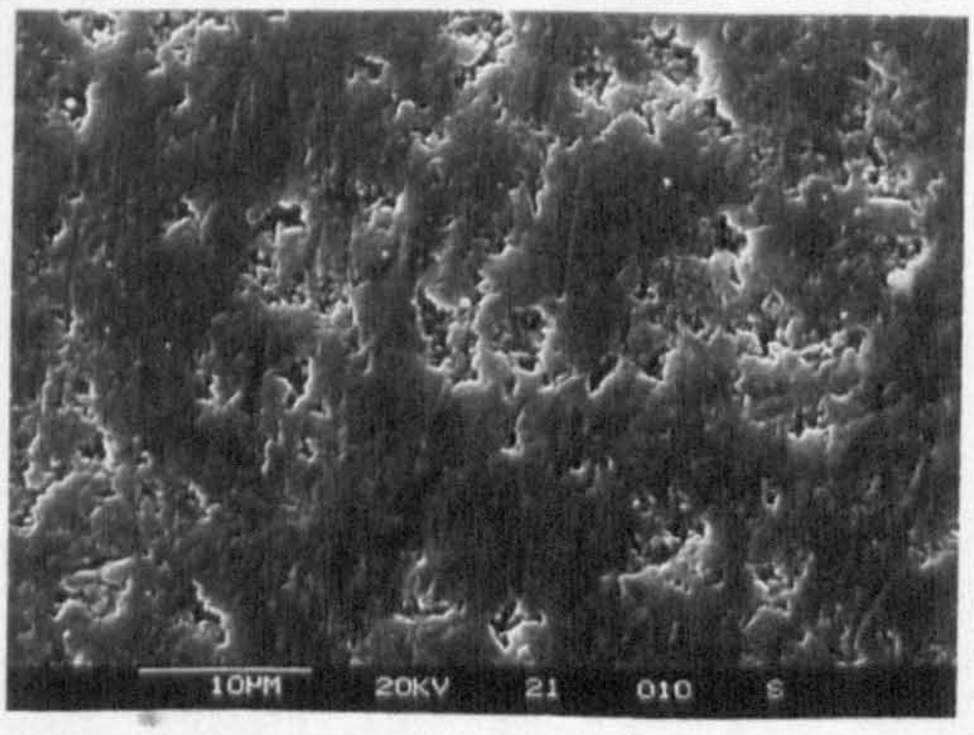

(b) Higher magnification

Fig. 5.8 SEM observations of ceramic ball after grinding with polyglycol T81499 + 0.3% Phosphate Ester

5.4.2 Surface Roughness Measurements

The initial surface roughness, R_a, for the ball blanks before testing is in the range of 0.0832 ± 0.02μm. Figure 5.9 shows the surface profiles of the silicon nitride balls after the grinding test with the reference lubricant Kemet, the ester base fluid T80884 and the polyglycol T81499 with the additive phosphate ester. The surface profile of the silicon nitride ball after testing with Kemet and phosphate esters shows a significant increase in the peak heights and depths and a very high R_a value of 0.1746μm. For ester base fluid T80884 and polyglycol T81499 with phosphate ester the surface profiles appear to have a very even and consistent peak height and depth distribution, similar to the surface profile of the ball blank before testing.

Fig. 5.9 Surface profiles of silicon nitride balls before and after grinding tests

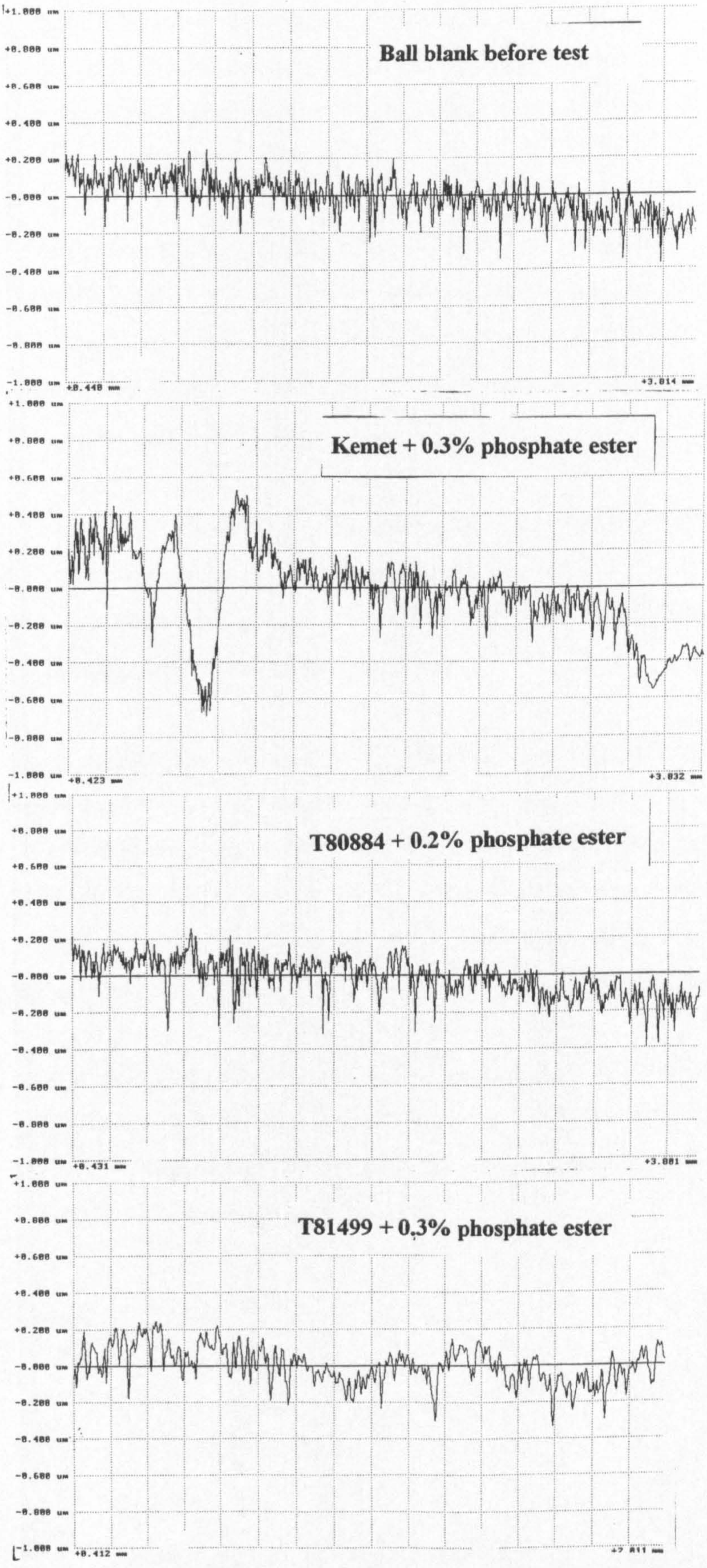

Surface Roughness, R_a (μm)
0.0832 ± 0.02

Surface Roughness, R_a (μm)
0.1746

Surface Roughness, R_a (μm)
0.0876

Surface Roughness, R_a (μm/min)
0.09

5.5 Grinding measurements using Triethanol Amine

Figure 5.10 shows the material removal rate of silicon nitride balls with Kemet, ester base fluid T80884 and polyglycol T81499 with the additive triethanol amine. All the results show a comparison of using additive with each of the three lubricants with the results of without using any additive.

When using 0.1% triethanol amine with Kemet the material removal rate increases slightly to 0.75μm/min from 0.6μm/min without any additive. When using 0.2% triethanol amine with Kemet the material removal rate increases to 1.3μm/min, that is by one fold, however, when using 0.3% triethanol amine the material removal rate results in an even greater increase to 1.7μm/min.

When using 0.1% and 0.2% triethanol amine with ester base fluid T80884 the material removal rate increases to 2.0μm/min and 2.1μm/min from 1.2μm/min without any additive. When using 0.3% triethanol amine the material removal rate increases to 2.5μm/min, that is, an increase by one fold.

When using 0.1%, 0.2% and 0.3% triethanol amine with polyglycol T81499 there is no significant effect on the material removal rate when compared to the results without any additive. The material removal rate ranges very closely for polyglycol T81499 without additive and with 0.1% and 0.2% triethanol amine at 1.8μm/min, 1.86μm/min and 1.76μm/min. The material removal rate for 0.3% triethanol amine shows a slight increase to 2μm/min.

In general the additive triethanol amine has a significant effect on increasing the material removal rate with Kemet and the ester base fluid T80884, however it has no significant effect on polyglycol T81499. Overall the ester base fluid T80884 with triethanol amine gives the highest material removal rate.

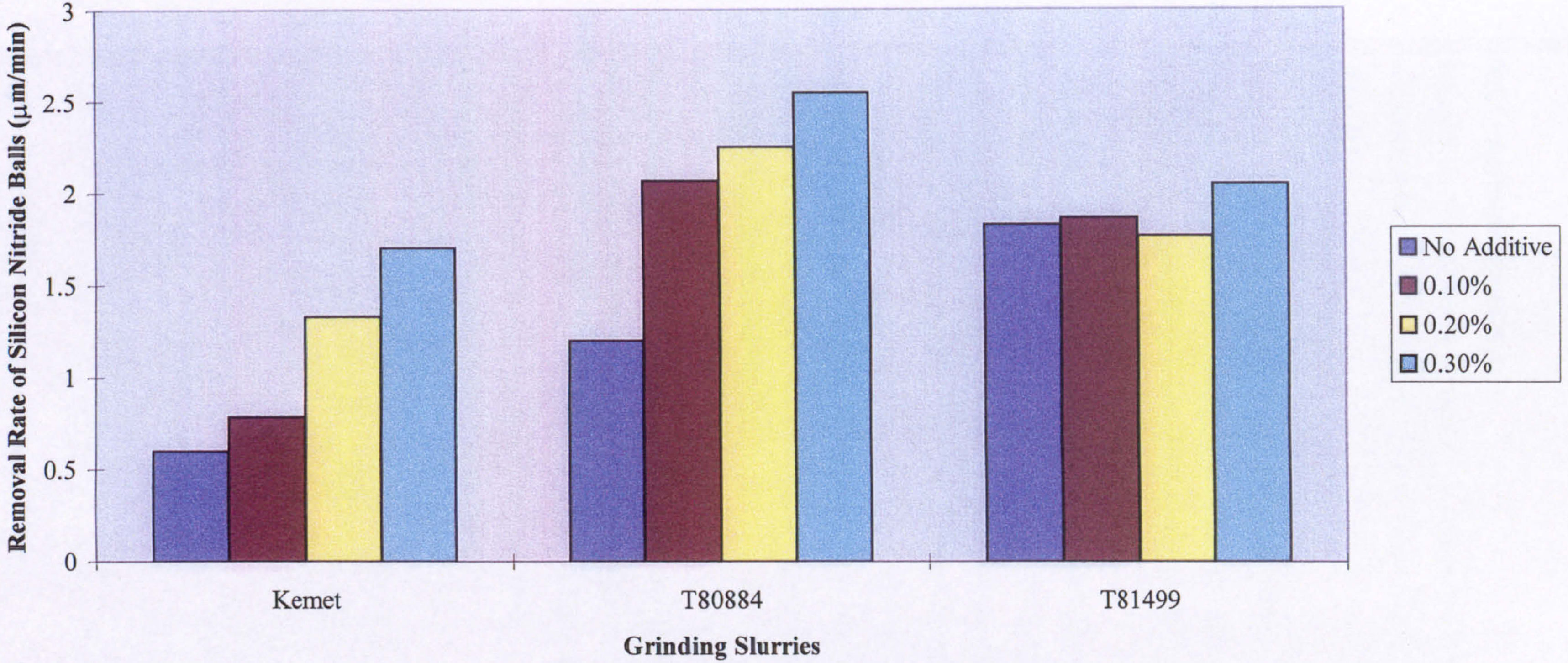

Fig. 5.10 Removal Rate of Silicon Nitride Balls in Kemet, ester base fluid T80884 and polyglycol T81499 with various concentrations of the additive Triethanol Amine

5.5.1 Surface Observations

Figure 5.11-5.13 shows the surface of the silicon nitride balls after grinding tests with the additive triethanol amine and the reference slurry Kemet, the ester base fluid T80884 and the polyglycol T81499.

Figure 5.11 shows the pitted surface after testing with Kemet + 0.3% amine phosphate. Under high magnification there are only a few scratches present, therefore, the possible mechanism for material removal could be brittle fracture.

Figure 5.12 shows a much less pitted surface than fig. 5.11 or 5.13, after testing with ester base fluid T80884 + 0.3% triethanol amine. Under high magnification the surface appears very smooth with no distinct scratch marks, which could imply that the surface has been plastically deformed. From these surface observations, the reason for the high rate of material removal could be due to a tribochemical reaction occurring at the interface which creates a much softer film on the surface, which is then removed very rapidly by the abrasive particles. This not only gives a very good material removal rate but also a very good surface finish.

Figure 5.13 shows a very pitted surface after testing with polyglycol T81499 + 0.3% triethanol amine. Under high magnification there also appears to be a film being deposited on the surface. This could imply that initially the material removal rate is high by brittle fracture, but as the grinding test proceeds a film is being deposited on the surface which reduces the material removal rate.

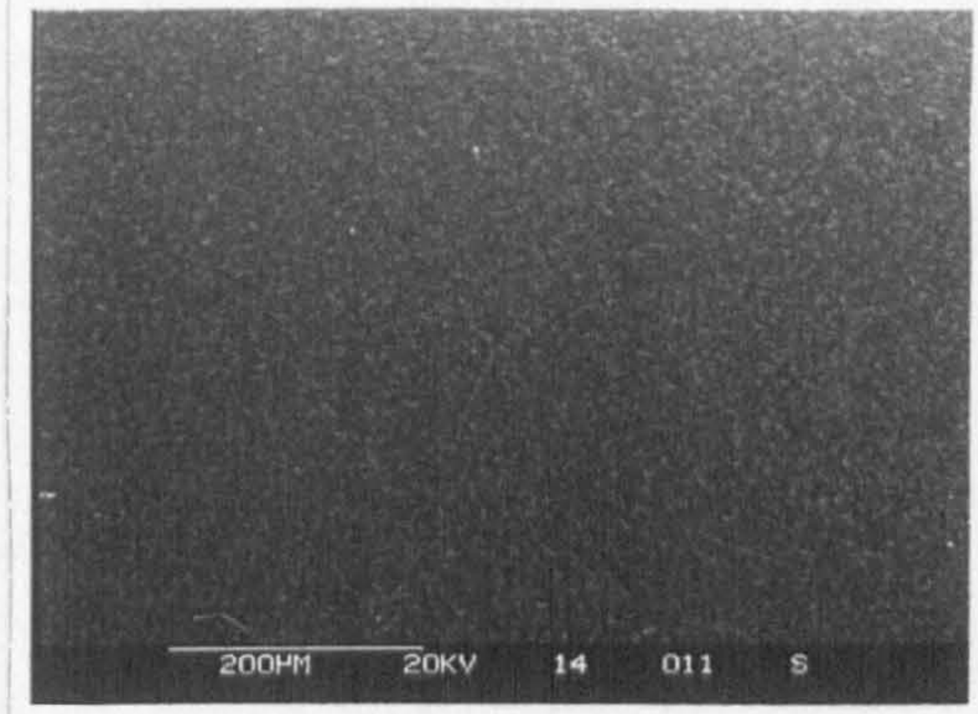

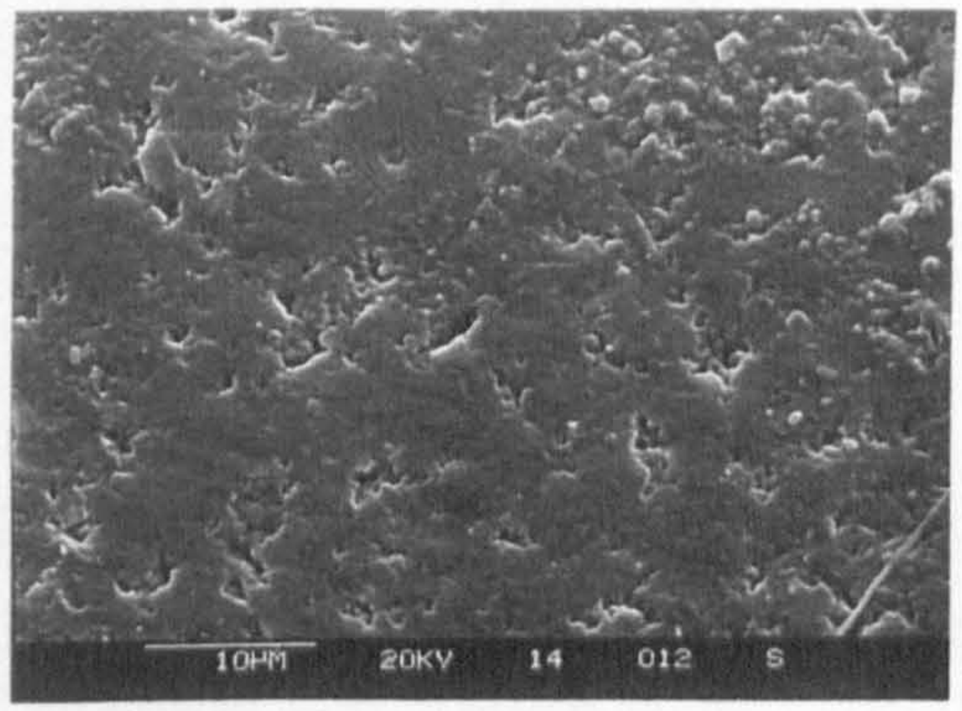

(a) Overall view **(b) Higher magnification**

Fig. 5.11 SEM observations of ceramic ball after grinding with Kemet + 0.3% Triethanol Amine

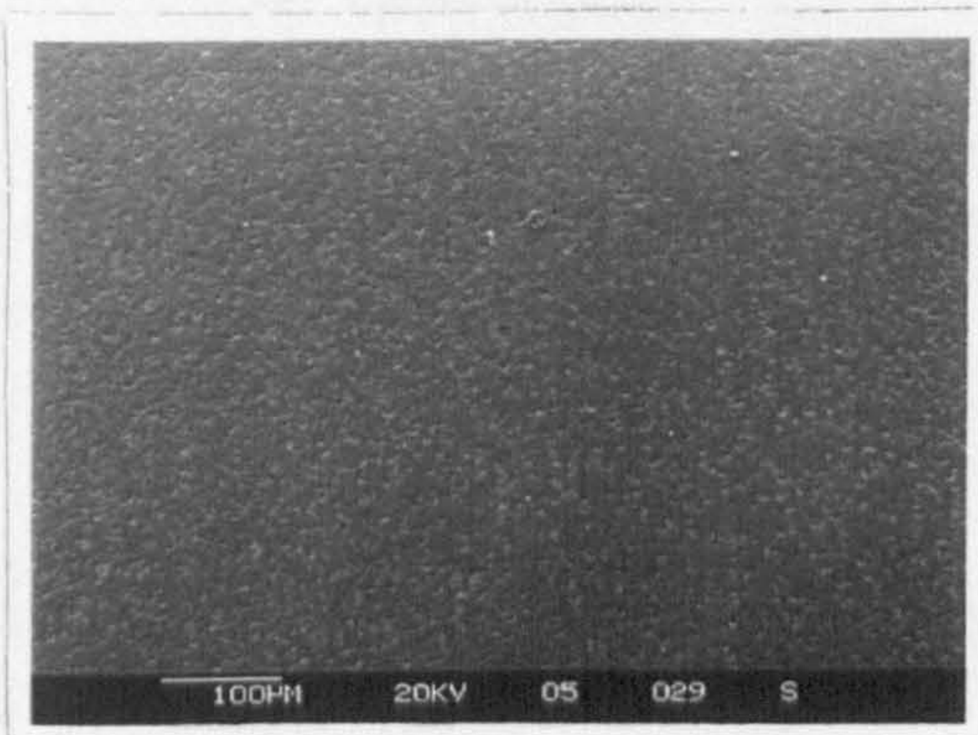

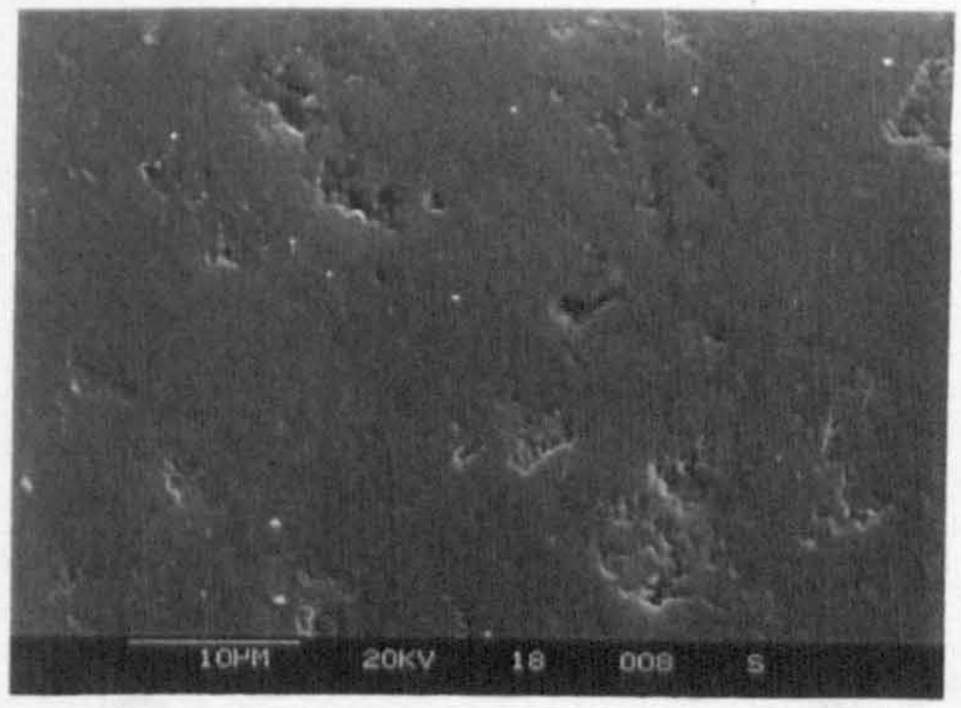

(a) Overall view **(b) Higher magnification**

Fig. 5.12 SEM observations of ceramic ball after grinding with ester T80884 + 0.3% Triethanol Amine

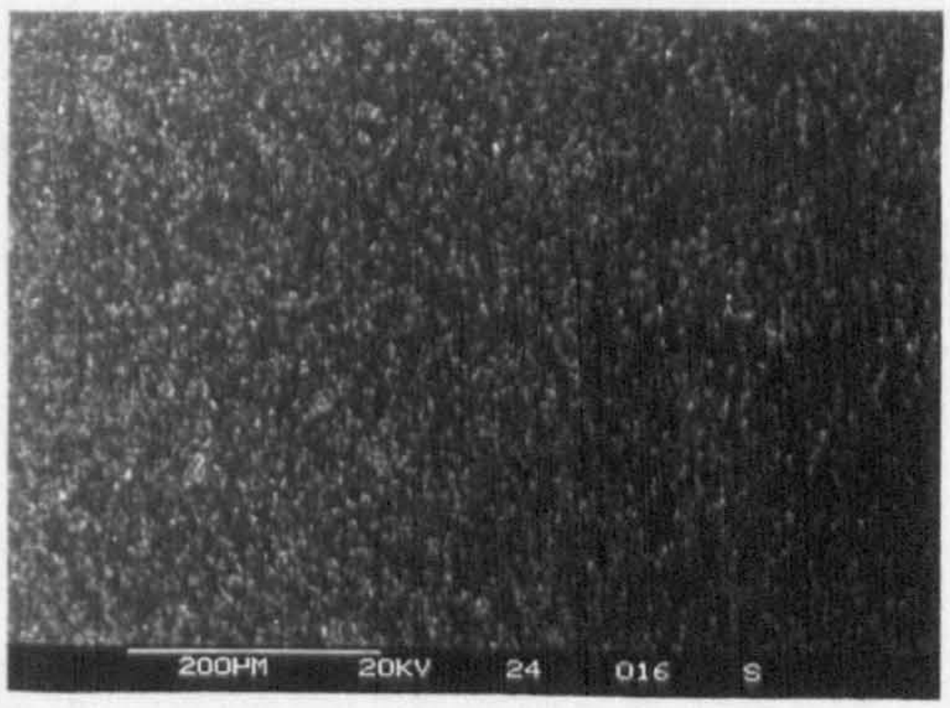

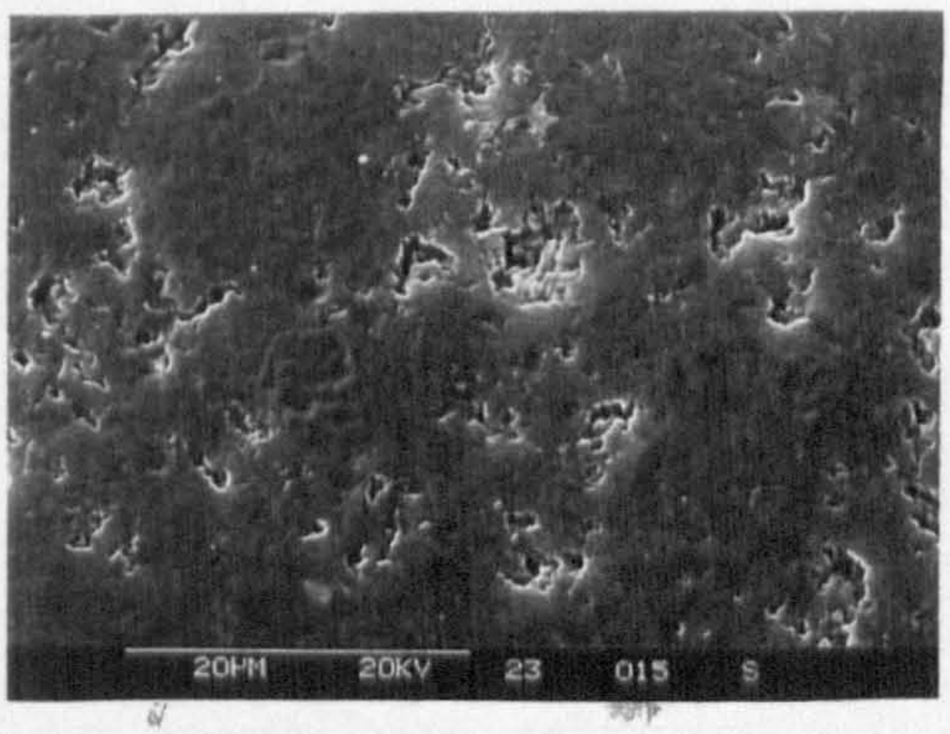

(a) Overall view **(b) Higher magnification**

Fig. 5.13 SEM observations of ceramic ball after grinding with polyglycol T81499 + 0.3% Triethanol amine

5.5.2 Surface Roughness Measurements

The initial surface roughness, R_a, for the ball blanks before testing is in the range of $0.0854 \pm 0.02\mu m$. Figure 5.14 shows the surface profiles of the silicon nitride balls after the grinding test with the reference lubricant Kemet, the ester base fluid T80884 and the polyglycol T81499 with the additive triethanol amine. The surface profile of the silicon nitride ball after testing with Kemet and triethanol amine shows a very inconsistent pattern in the peak heights and depths and the surface roughness, R_a, of $0.1498\mu m$ is very high. The surface profile of the silicon nitride ball after testing with the ester base fluid T80884 and triethanol amine appears very much smoother than the ball blank before testing, there is a significant reduction in the peak heights and depths and the surface roughness value of $0.0562\mu m$ is also very low. The surface profile of the silicon nitride ball after testing with polyglycol T81499 and triethanol amine appears similar to the surface profile of the ball blank before testing.

Fig. 5. 14 Surface profiles of silicon nitride balls before and after grinding tests

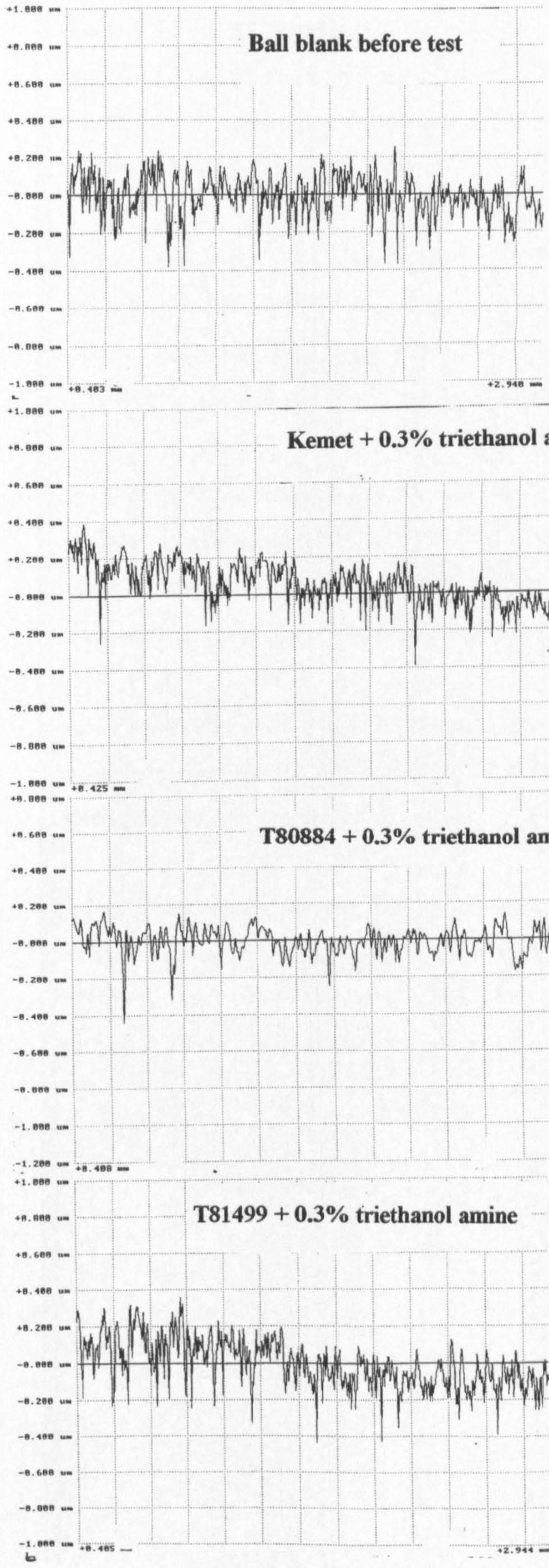

Surface Roughness, R_a (μm)
0.084 ± 0.02

Surface Roughness, R_a (μm)
0.1498

Surface Roughness, R_a (μm)
0.0562

Surface Roughness, R_a (μm)
0.1083

5.6 Grinding measurements using Amine Phosphate

Figure 5.15 shows the material removal rate of silicon nitride balls using Kemet, ester base fluid T80884 and polyglycol T81499 with the additive amine phosphate. All the results show a comparison of using additive with each of the three lubricants with the results of without using any additive.

When using 0.1% and 0.3% amine phosphate with Kemet there is a significant increase in material removal rate to 1.6μm/min and 1.65μm/min from 0.6μm/min without any additive. However, when using 0.2% amine phosphate there is an even greater increase in material removal rate to 1.95μm/min, that is an increase by two fold.

When using 0.1% amine phosphate with ester base fluid T80884 there is a significant decrease in the material removal rate to 0.7μm/min from 1.2μm/min without any additive. When using 0.2% and 0.3% amine phosphate with ester base fluid T80884 again there is a decrease in material removal rate to 0.8μm/min and 0.9μm/min.

When using 0.1%, 0.2% and 0.3% amine phosphate with polyglycol T81499 there is a significant decrease in the material removal rate to 1.1μm/min, 1.25μm/min and 0.9μm/min from 1.8μm/min without any additive.

In general the additive amine phosphate has a significant effect on increasing the material removal rate with Kemet, however, it has a reducing effect with the ester base fluid T80884 and polyglycol T81499. Overall the highest material removal rate is obtained when using Kemet with amine phosphate.

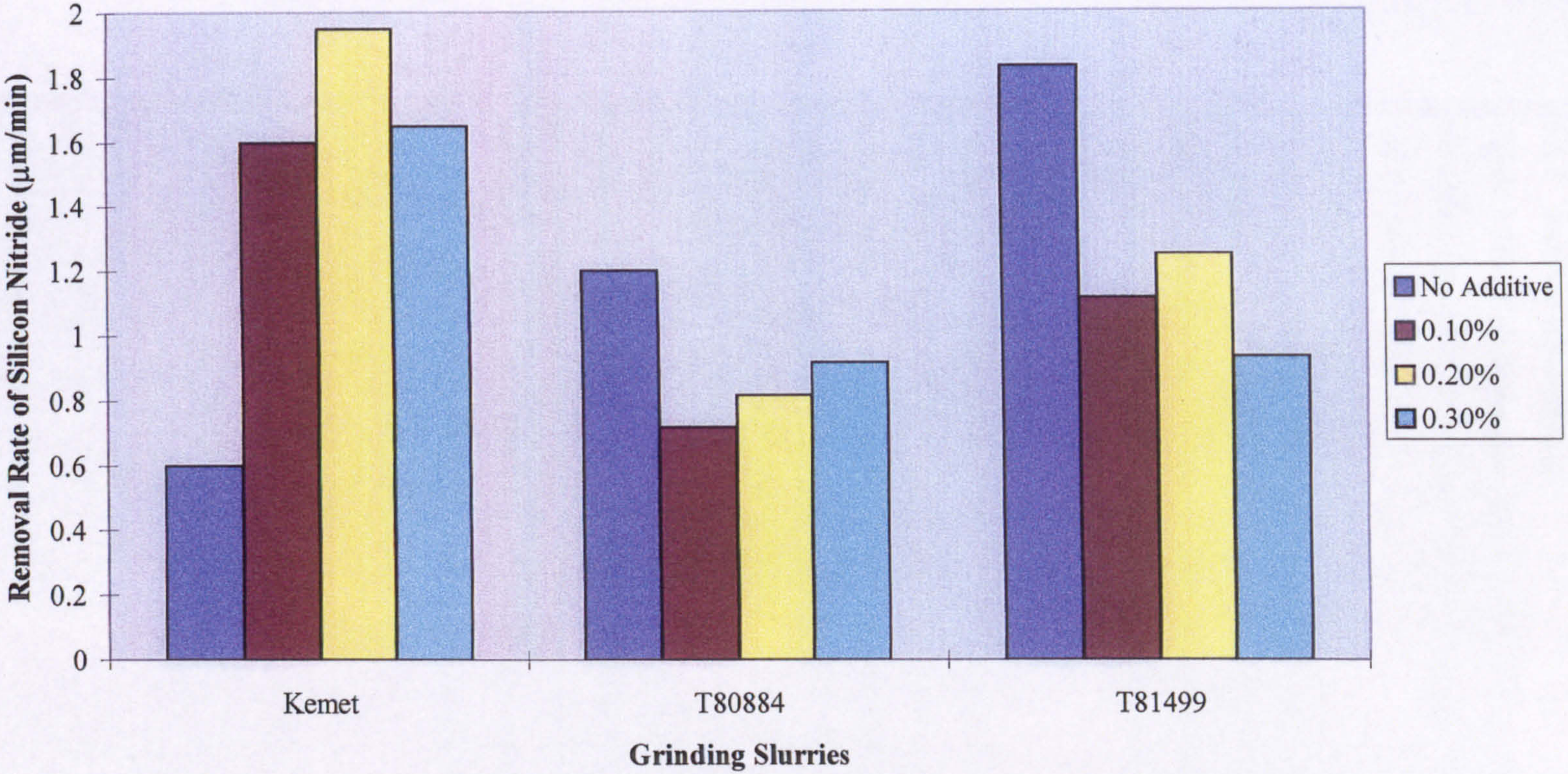

Fig. 5.15 Removal Rate of Silicon Nitride Balls in Kemet, ester base fluid T80884 and polyglycol T81499 with various concentrations of the additive Amine Phosphate

5.6.1 Surface Observations

Figure 5.16 - 5.18 shows the surface of the silicon nitride balls after grinding tests with the additive amine phosphate and the reference slurry Kemet, the ester base fluid T80884 and the polyglycol T81499.

Figure 5.16 shows a severely pitted surface after testing with Kemet + 0.2% amine phosphate. The pit size is in the range of 15-20 microns. Examination of this area under high magnification shows that the area around the pits is very smooth and the pitted region shows a rough surface with an open texture. These pitted regions could be due to brittle fracture or by a tribochemical reaction.

Figure 5.17 shows many small pits between smooth patches of surface after testing with ester base fluid T80884 + 0.3% amine phosphate. Under high magnification there appears to be a lot of fine debris present but no distinct scratch marks. From the material removal results it appears that this additive is having a reducing effect, which could be due to the formation of a protective film.

Figure 5.18 shows a very pitted region in between smooth black patches of surface after testing with polyglycol T81499 + 0.2% amine phosphate. Under high magnification there are many small pits which could be produced by brittle fracture. There is also a film deposited on the surface which could protect the surface and hence be the reason for the reduction in material removal rate when using this additive with polyglycol T81499.

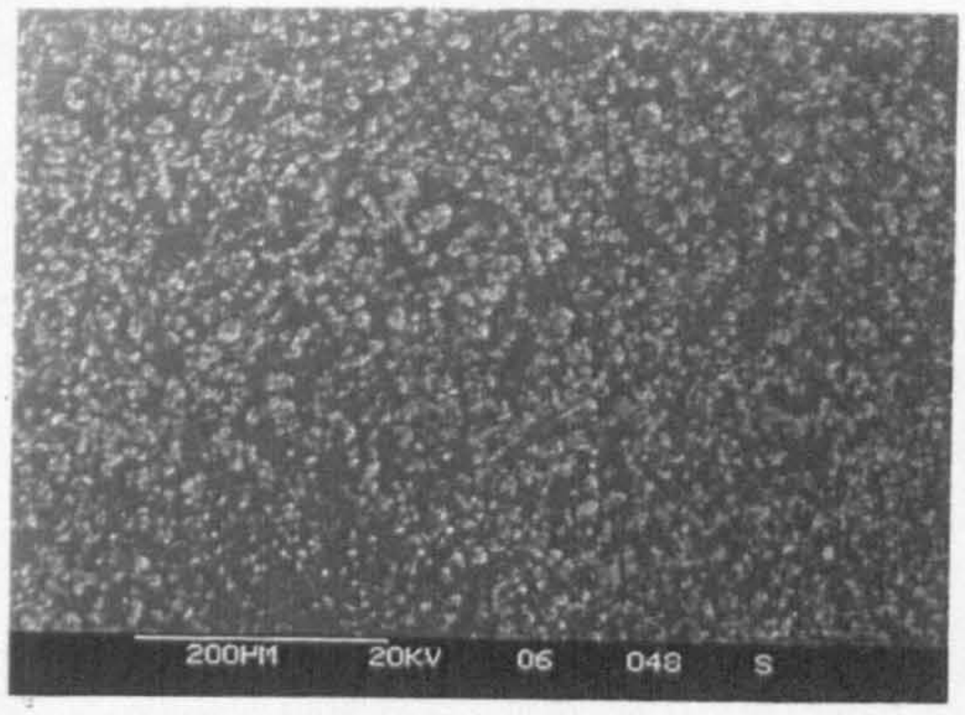

(a) Overall view

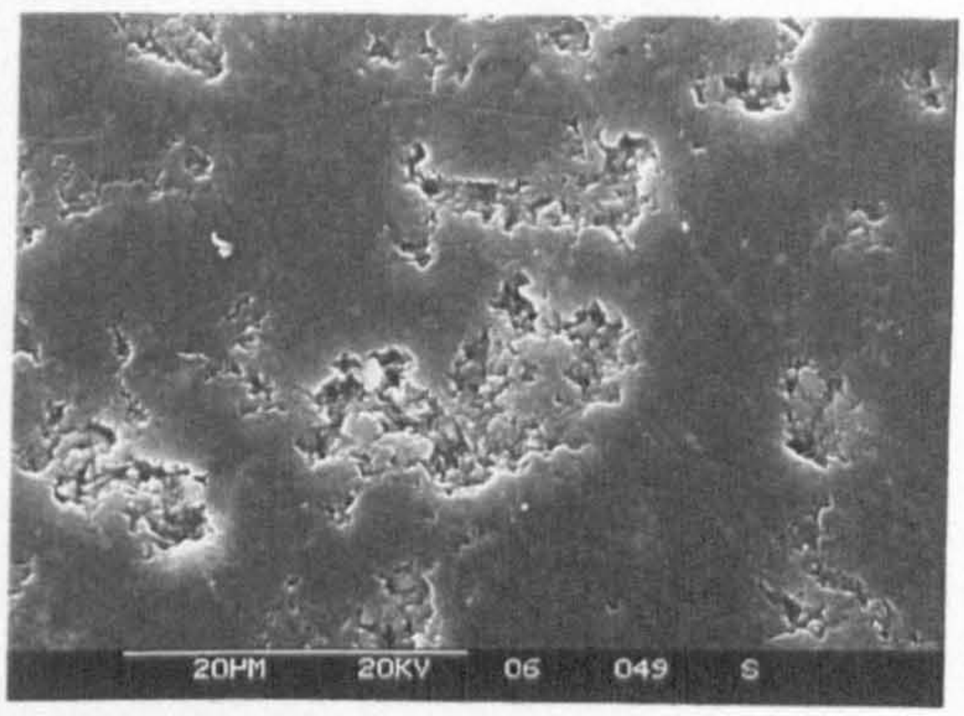

(b) Higher magnification

Fig. 5.16 SEM observations of ceramic ball after grinding with Kemet + 0.2% Amine Phosphate

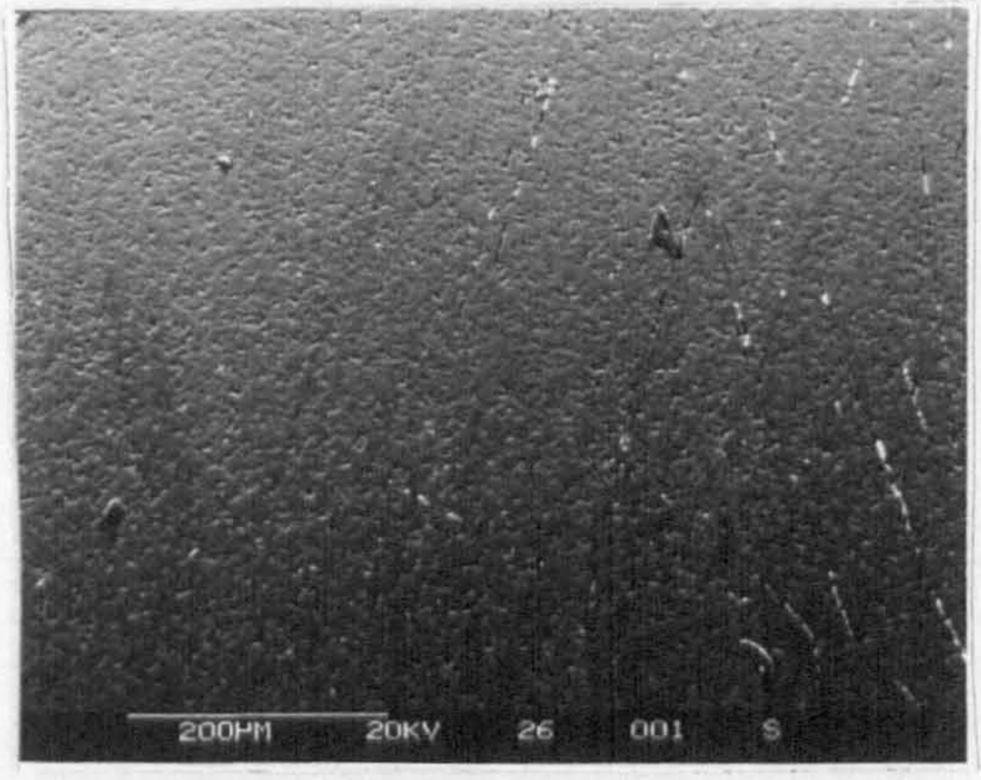

(a) Overall view

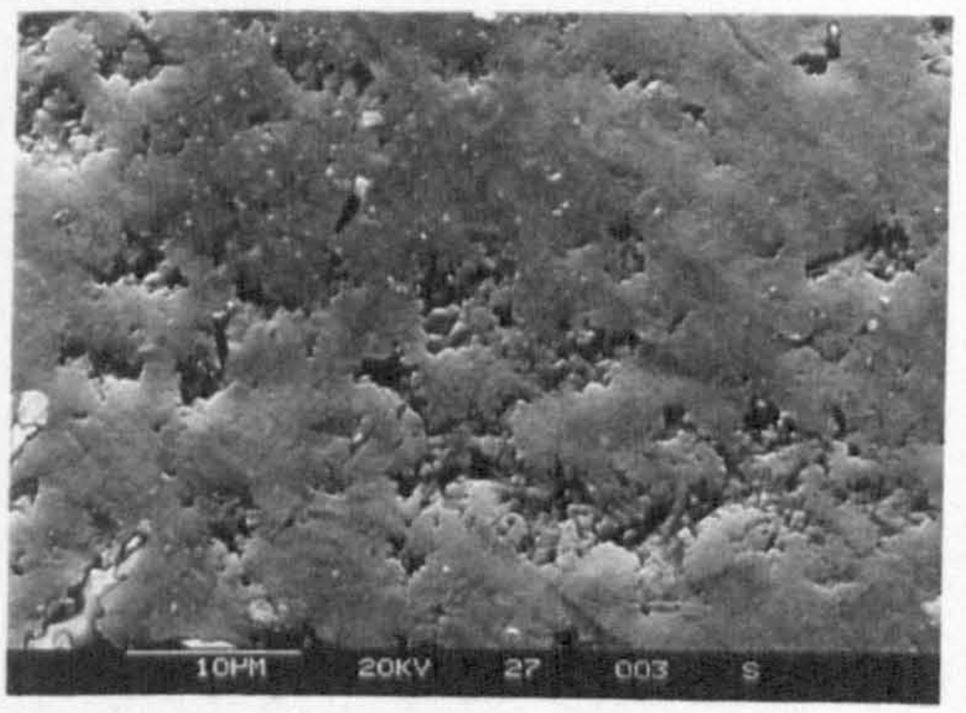

(b) Higher magnification

Fig. 5.17 SEM observations of ceramic ball after grinding with ester T80884 + 0.3% Amine Phosphate

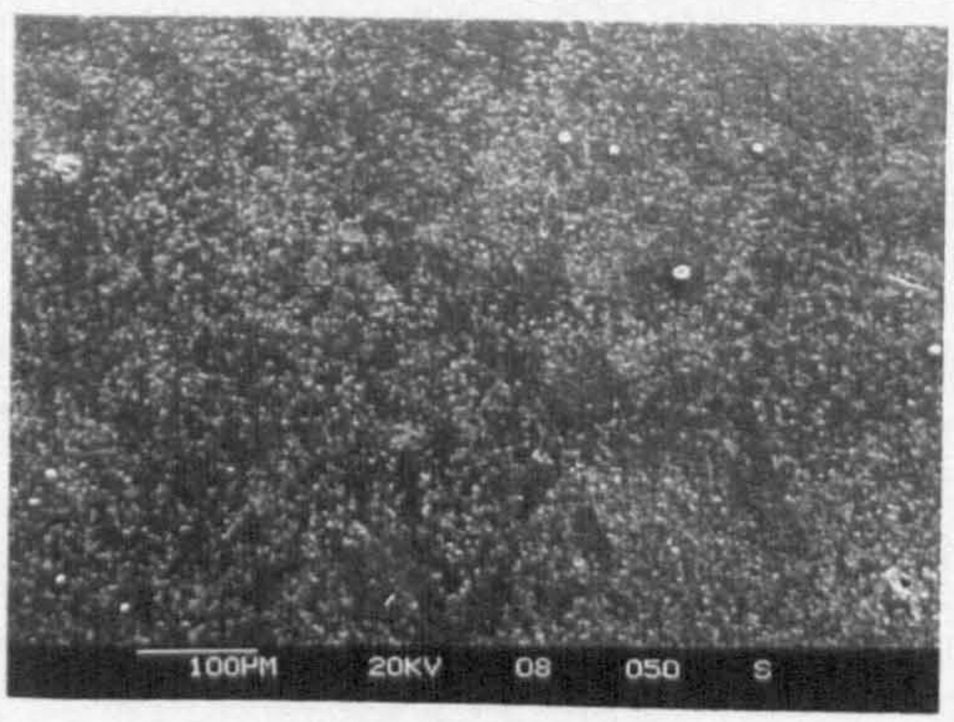

(a) Overall view

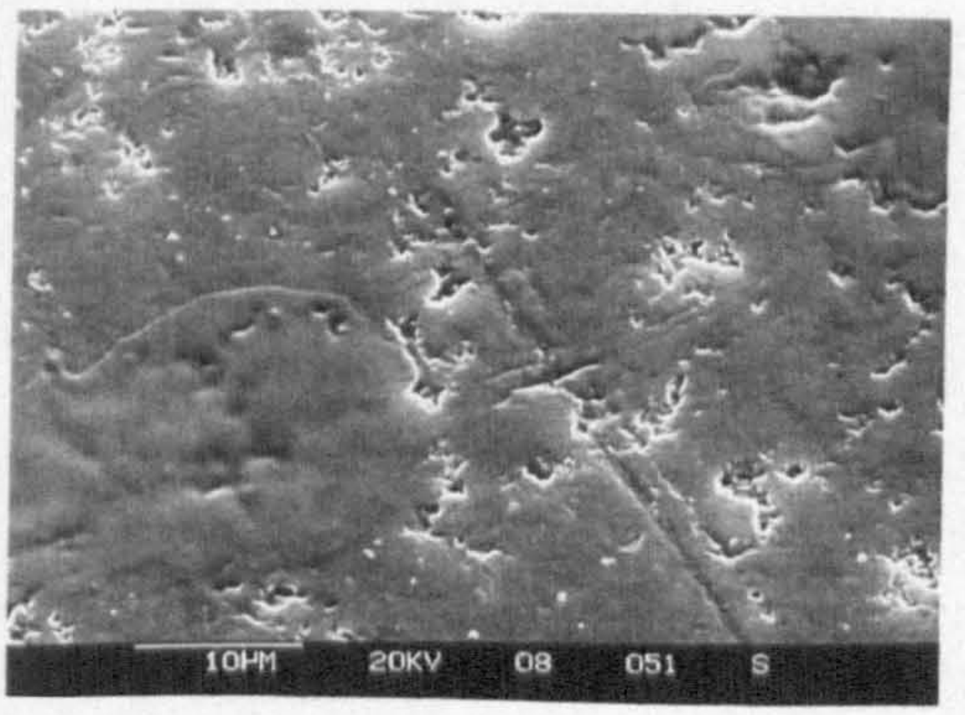

(b) Higher magnification

Fig. 5.18 SEM observations of ceramic ball after grinding with polyglycol T81499 + 0.2% Amine Phosphate

5.6.2 Surface Roughness Measurements

The initial surface roughness, R_a, for the ball blanks before testing was in range of 0.082 ± 0.02μm. Figure 5.19 shows the surface profiles of the silicon nitride balls after the grinding test with the reference lubricant Kemet, the ester base fluid T80884 and the polyglycol T81499 with the additive amine phosphate. The surface profile of the silicon nitride ball after testing with Kemet and amine phosphate shows a significant difference in the peak height area and depths and from the original ball blank; the surface appears very uneven and the surface roughness value of 0.1301μm is high. The surface profiles of the silicon nitride balls after testing with ester base fluid T80884 and polyglycol T81499 with amine phosphate appear similar to the surface profile of the ball blank before testing.

Fig. 5.19 Surface profiles of silicon nitride balls before and after grinding tests

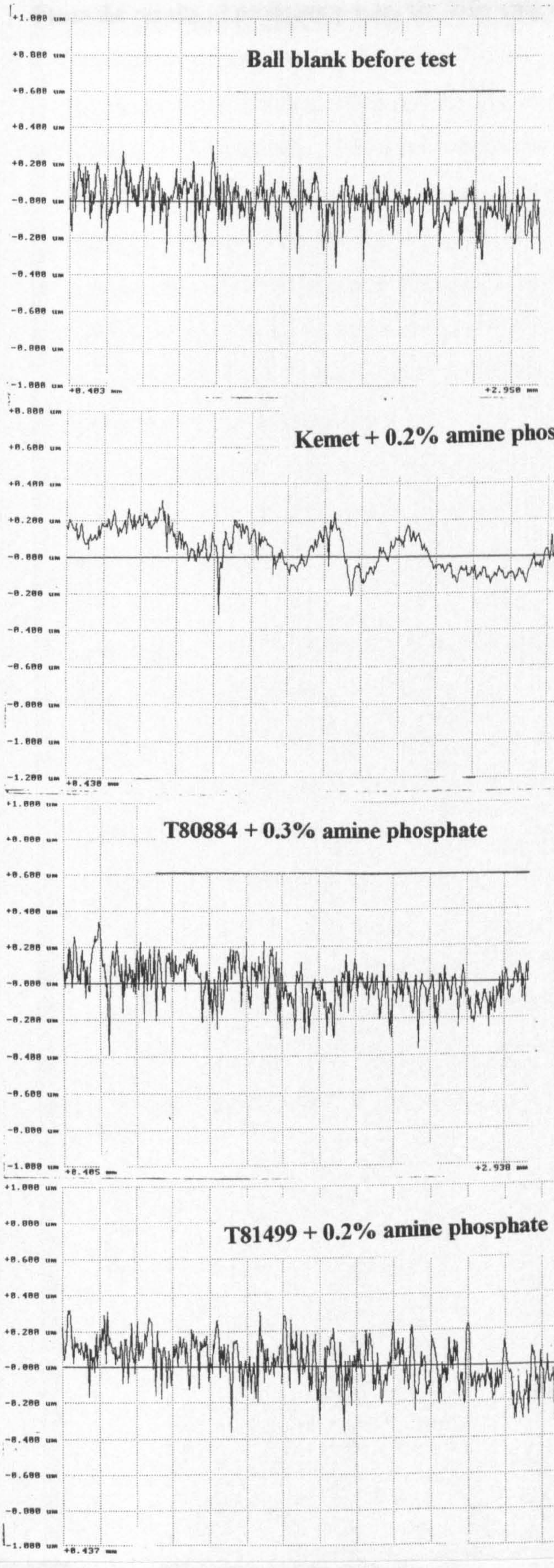

Surface Roughness, R_a (μm)
0.082 ± 0.02

Surface Roughness, R_a (μm)
0.1301

Surface Roughness, R_a (μm)
0.093

Surface Roughness, R_a (μm)
0.1081

5.7 Summary

From the results of preliminary tests the following conclusions can be formulated:

- The highest material removal occurred in the presence of 15 abrasive particles where the predominant mechanism was probably microfracture.
- Rotational velocity has a substantial influence on the rate of material removal. The increase in material removal is not proportional to the increase in speed, as at the highest speeds the increase in grinding rate is not as rapid as at lower speeds.
- A four-point contact configuration gives slightly higher material removal rates than three-point contact configurations. However, the four-point contact configuration was too sensitive to any mass imbalance or lack of alignment causing excessive vibration during test runs at high speeds.
- The topography of a ground surface can serve as an indication of the predominant mechanisms of material removal. With many brittle workpiece materials, material is removed via microfracture, thus leaving an irregular surface with isotropic roughness.

The response of silicon nitride balls to the different grinding slurries after the initial grinding tests concluded that:

- the highest material removal rates were obtained using the polyglycol T81499 which gave a value of 1.8μm/min and the ester base fluid T80884 which gave a value of 1.2μm/min. The reference lubricant, Kemet, which is used in industry gave a material removal rate of 0.6μm/min.

The results from all the tests using polyglycol T81499, ester base fluid T80884 and Kemet with and without the additives phosphate ester, triethanol amine and amine phosphate show that the overall highest material removal rate of 2.5μm/min is obtained using ester base fluid T80884 + 0.3% triethanol amine.

Further testing conducted with the reference lubricant Kemet, the polyglycol T81499 and the ester base fluid T80884 with phosphate ester, triethanol amine and amine phosphate as additives concluded the following:-

The performance of the phosphate ester as an additive to a lubricant used during grinding tests are summarised in the table below:

Lubricant	**Material Removal Rate, µm/min**	**Surface Roughness,R_a, µm** (Initial ball blank 0.0832 ± 0.2)	**Ball Surface after test**	**Possible wear mechanism**
Kemet + 0.3% phosphate ester	1.6µm/min	0.1746µm	Severely damaged surface	Brittle fracture
T80884 + 0.2% phosphate ester	1.4µm/min	0.0876µm	Very pitted surface with scratches on micrometer scale	Brittle fracture and ploughing
T81499 + 0.3% phosphate ester	2.0µm/min	0.09µm	Very pitted surface with scratches on micrometer scale	Brittle fracture and ploughing

The highest material removal rate is obtained using polyglycol T81499.

The performance of the triethanol amine as an additive to a lubricant used during grinding tests is summarised in the table below:

Lubricant	**Material Removal Rate, µm/min**	**Surface Roughness,R_a, µm** (Initial ball blank 0.0854 ± 0.2)	**Ball Surface after test**	**Possible wear mechanism**
Kemet + 0.3% triethanol amine	1.7µm/min	0.1498µm	Pitted surface with only a few scratches	Brittle fracture
T80884 + 0.3% triethanol amine	2.5µm/min	0.0562µm	Plastically deformed smooth surface with no distinct scratch marks	Tribochemical reaction
T81499 + 0.3% triethanol amine	2.0µm/min	0.1083µm	Very pitted surface with a film deposited on surface	Brittle fracture

Ester base fluid T80884 +0.3% triethanol amine gives the highest material removal rate and also a very good surface finish.

- The performance of the amine phosphate as an additive to a lubricant used during the grinding tests is summarised in the table below:

Lubricant	**Material Removal Rate, µm/min**	**Surface Roughness,R_a, µm** (Initial ball blank 0.084 ± 0.2)	**Ball Surface after test**	**Possible wear mechanism**
Kemet + 0.2% amine phosphate	1.95µm/min	0.1301µm	Severely pitted surface. Pitted region shows a rough surface with open texture	Brittle fracture or tribochemical reaction
T80884 + 0.3% amine phosphate	0.9µm/min	0.093µm	Many small pits and a lot of fine debris but no distinct scratch marks	Brittle fracture
T81499 + 0.2% amine phosphate	1.25µm/min	0.1081µm	Many small pits	Brittle fracture

The highest material removal rate is obtained using Kemet + 0.2% amine phosphate.

It can be safely concluded that all three additives improve the material removal rate when used with Kemet, the industrial slurry. Based on these results further work was carried out to observe whether by increasing the concentration of each of the three additives in Kemet a further increase in material removal rate could be obtained. The results are presented in fig.5.20.

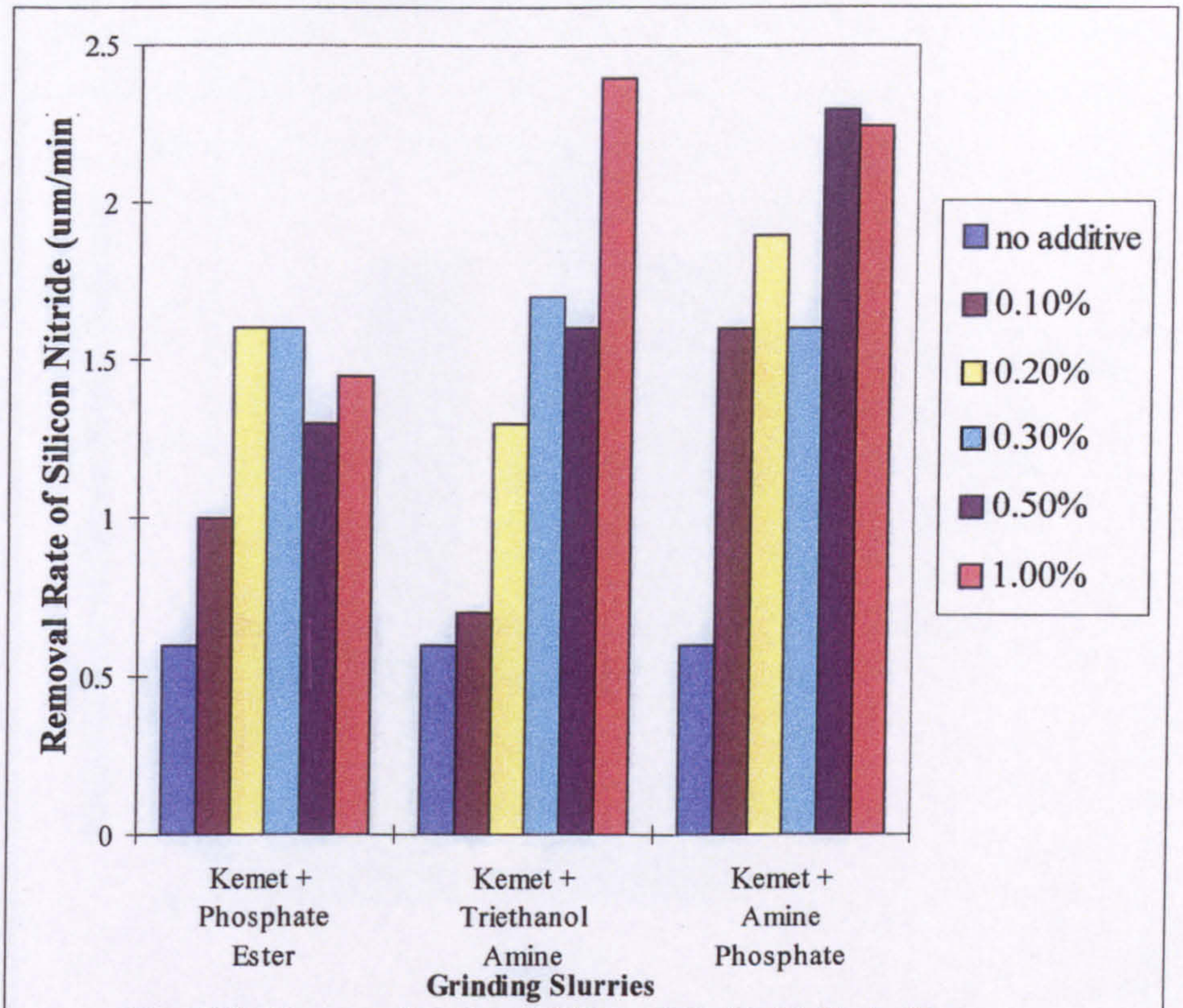

Fig. 5.20 Removal Rate of Silicon Nitride Balls in Kemet with various concentrations of the additives Phosphate Ester, Triethanol Amine and Amine Phosphate

Figure 5.20 shows that the highest material removal rates of 2.4μm/min and 2.25μm/min are obtained by using 1% triethanol amine with Kemet and 0.5% amine phosphate with Kemet. Further increase in additive concentrations showed no significant effect on the material removal rate.

Further work was also done by increasing the concentration of triethanol amine in T80884. The results are presented in figure 5.21.

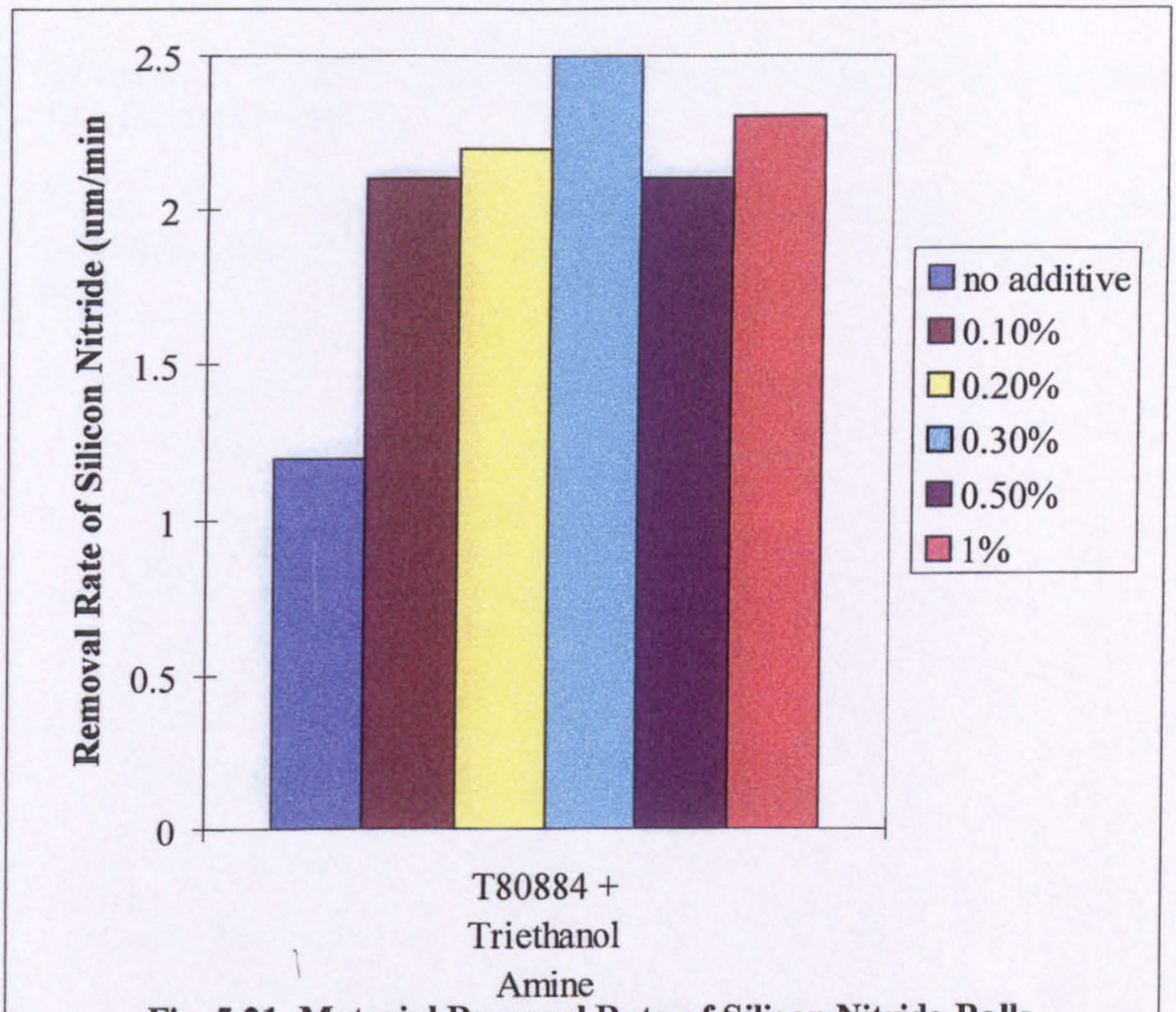

Fig. 5.21 Material Removal Rate of Silicon Nitride Balls with various concentrations of the additive Triethanol Amine with T80884

The results show that the highest material removal rate of 2.5μm/min is obtained when using 0.3% triethanol amine and that a further increase in additive concentration has a reducing effect.

Testing was also done by further mixing the most effective lubricants, that is, Kemet with 10% ester base fluid T80884 and 0.3% triethanol triethanol amine, however, this showed a very low material removal rate of 0.25μm/min. In conclusion the highest material removal rate is obtained using ester base fluid T80884 and 0.3% triethanol amine.

REFERENCES

Stolarski, T. A., Jisheng, E., Gawne, D. T. & Panesar, S., 1995, **"The effect of load and abrasive particles size on the material removal rate of silicon nitride artefacts"**, Ceramics International, Vol. 21, pp.355-366.

Stolarski, T. A., 1992, **"Accelerated wear of ceramic balls"**, Ceramics International, Vol. 18, pp.379-384.

Tsunai, Y. & Enomoto, Y., 1988, **"Tribochemistry of alcohol/silicon-based ceramics"**, Proc. 32nd JSLE Conf., Japanese Society of Lubrication Engineers, pp.29-32.

Chapter 6

DISCUSSION OF SURFACE AND CHEMICAL ANALYSIS RESULTS

6.1 Introduction

From the friction and grinding tests, the lubricants ester base fluid T80884 and ester base fluid T80884 with 0.3% of the additive triethanol amine proved to be the most effective lubricants in producing high material removal rates and a good surface finish for the silicon nitride balls. They also produced a low coefficient of friction as represented in the results in chapters 4 and 5. On the basis of these results further surface and chemical analysis was carried using these lubricants to:

- analyse the surface of the contact area of the ceramic ball and steel plate after the friction test using the scanning electron microscope and the atomic force microscope
- analyse the wear debris after the grinding test using scanning electron microscope and energy dispersive x-ray analysis
- analyse the abrasive slurry after the grinding test using Infra Red Spectroscopy
- analyse the effect of material removal after the grinding test on the residual stresses in the silicon nitride ball

6.2 Friction Test

The contact surface of the silicon nitride ball and steel plate were analysed after friction testing with the lubricant T80884 using the scanning electron microscope and energy-dispersive X-ray analysis. Further surface analysis studies on the contact surfaces after friction testing with the lubricant T80884 + 0.3% triethanol amine were carried out using the atomic force microscope.

6.2.1 Scanning Electron Microscope Studies of Contact Surfaces

Figures 6.1 and 6.2 show the contact area of the silicon nitride ball and steel plate after the friction test with the ester base fluid T80884. The wear scar on the silicon nitride ball in fig. 6.1 clearly shows grooves on the surface, these grooves correspond to the machining marks on the steel plate. There is also a deposit on the wear scar which was further analysed using EDX. The results in figure 6.3 show that before testing the characteristic silicon peak is present (the gold peak(Au), is the coating required in order

to do the analysis). After testing the deposit the results in figure 6.4 show that it is composed of iron (Fe).

The contact area on the steel plate in figure 6.2 shows the presence of a film deposited on the surface. On further analysis using EDX, the results in figure 6.5 show that before testing the characteristic iron (Fe), manganese (Mn) and chromium (Cr) peaks are present, however after testing the film the results in figure 6.6 show a trace of silicon (Si).

The results show that a transfer of matter has occurred in the contact areas during the friction testing with ester base fluid T80884. Iron being deposited on the ball and silicon being deposited on the plate.

The ester base fluid T80884 lubricant used under boundary conditions in the sliding friction test could have served two possible roles to enable this transfer to occur in the contact area:

1. It provided molecules that adsorbed onto, or reacted with the sliding solids, thereby inhibiting the direct contact of the surfaces and thus causing a decrease in the shear strength of the conjunction;
2. It modified the chemical nature of the upper most layers of the solid surfaces.

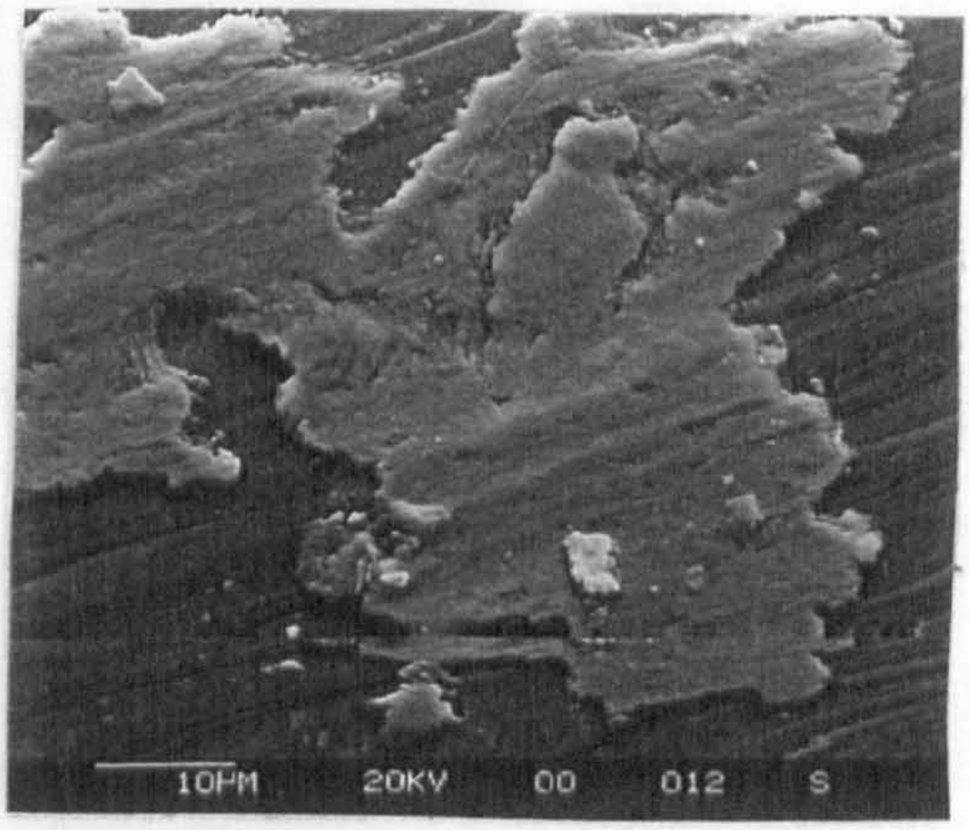

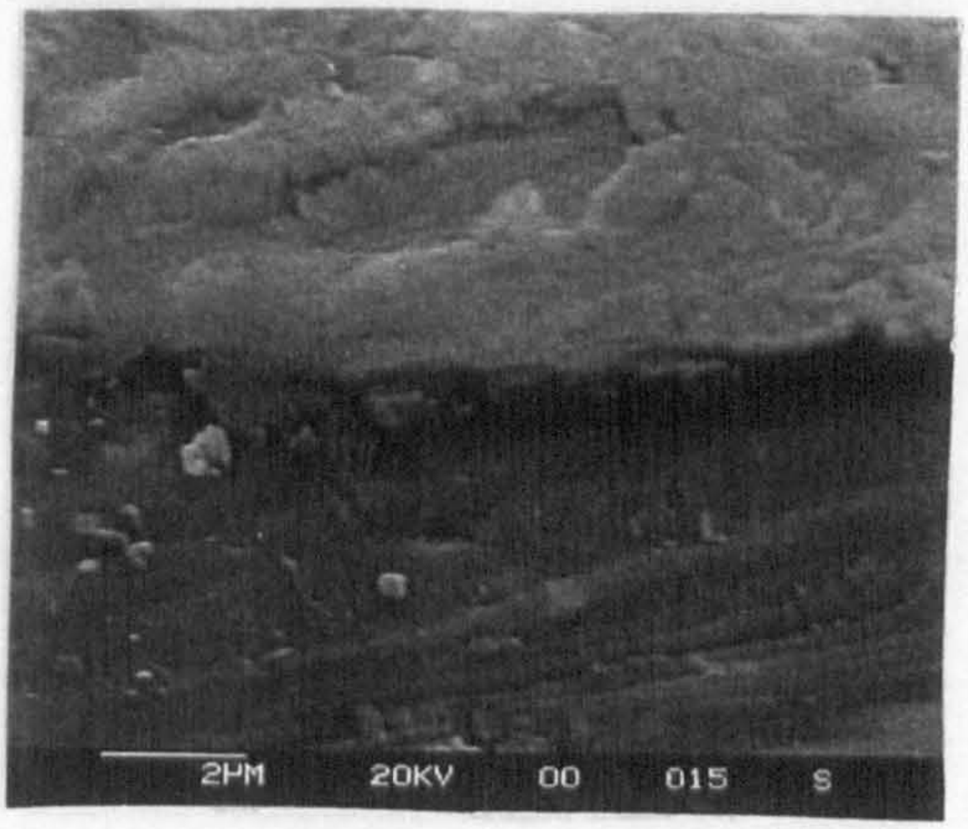

Fig. 6.1 SEM observations of ceramic ball after friction testing with the ester base fluid T80884

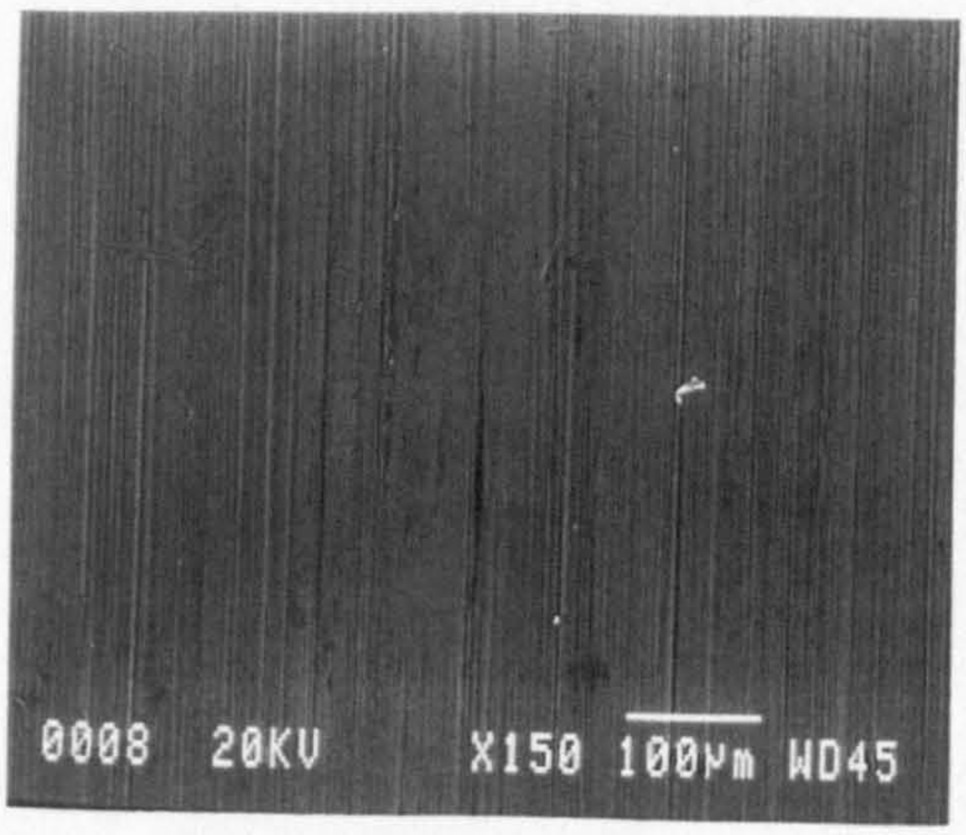

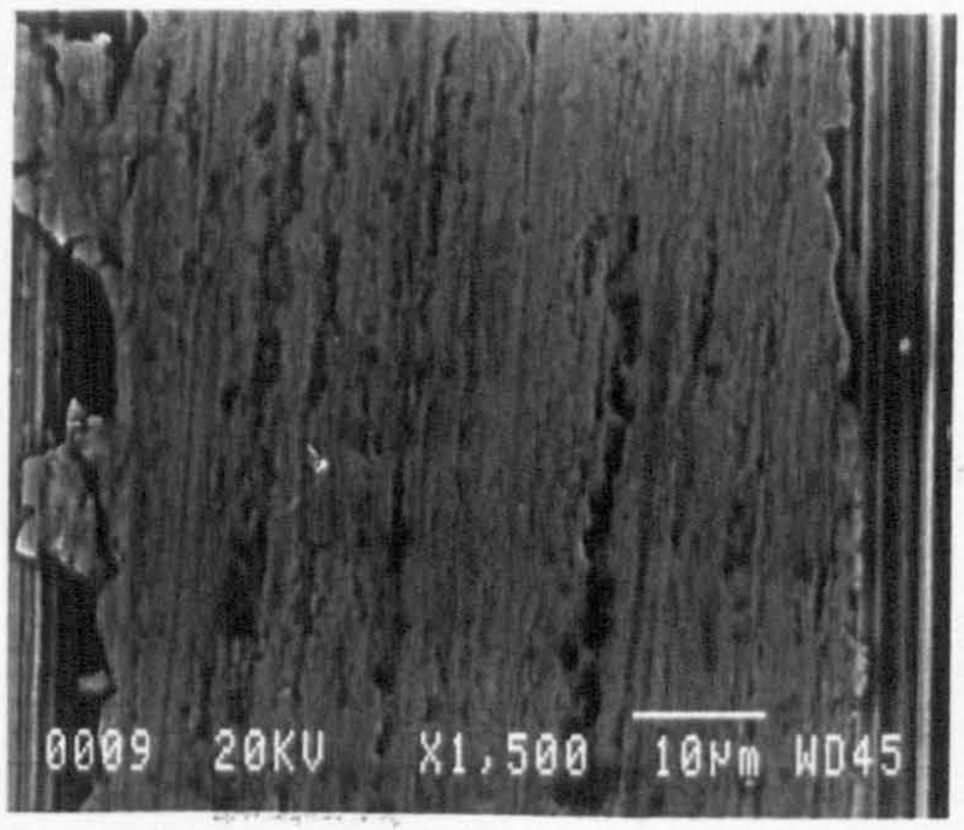

Fig. 6.2 SEM observations of steel plate after friction testing with the ester base fluid T80884

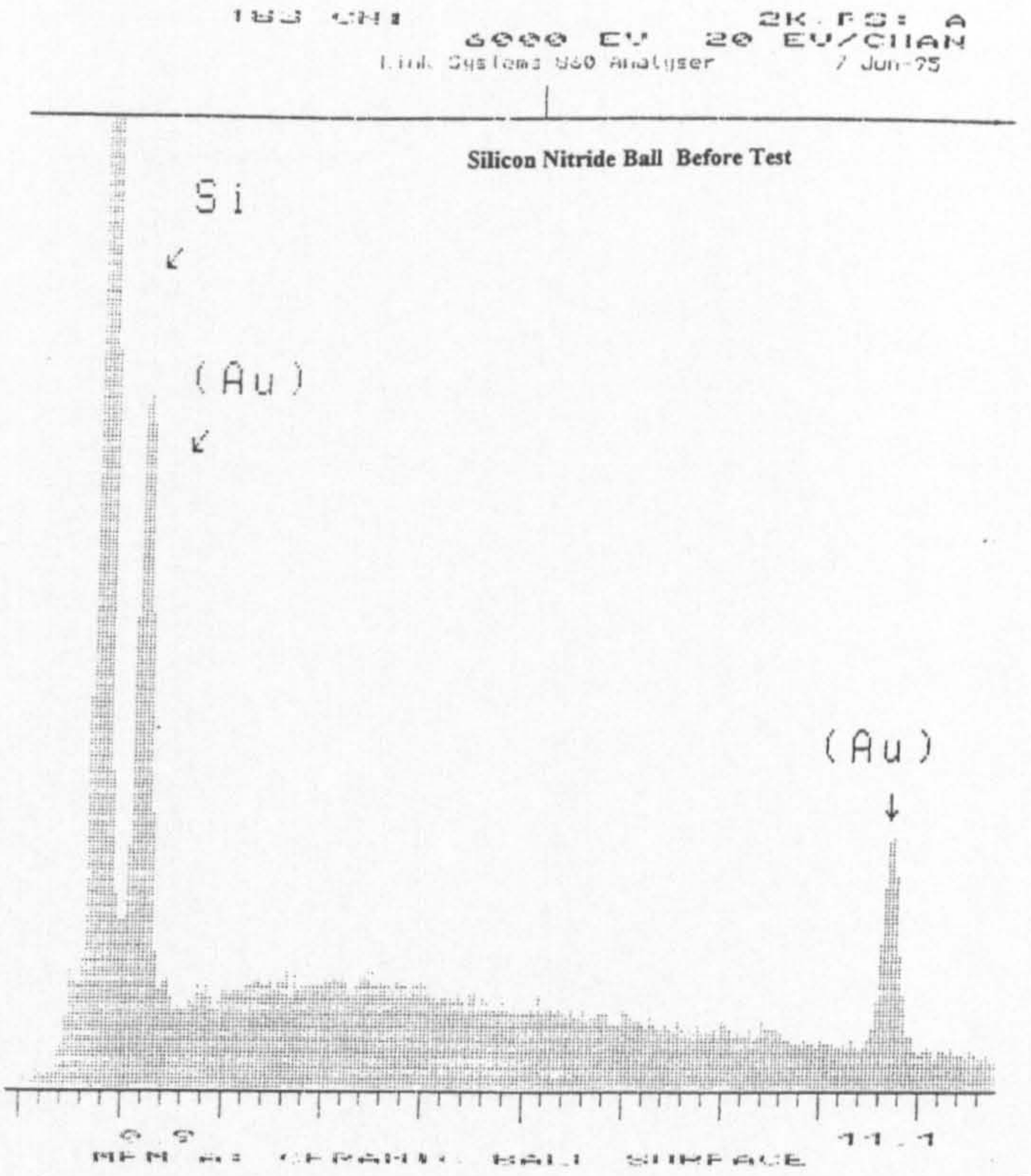

Fig. 6.3 **EDX Analysis of ceramic ball before testing**

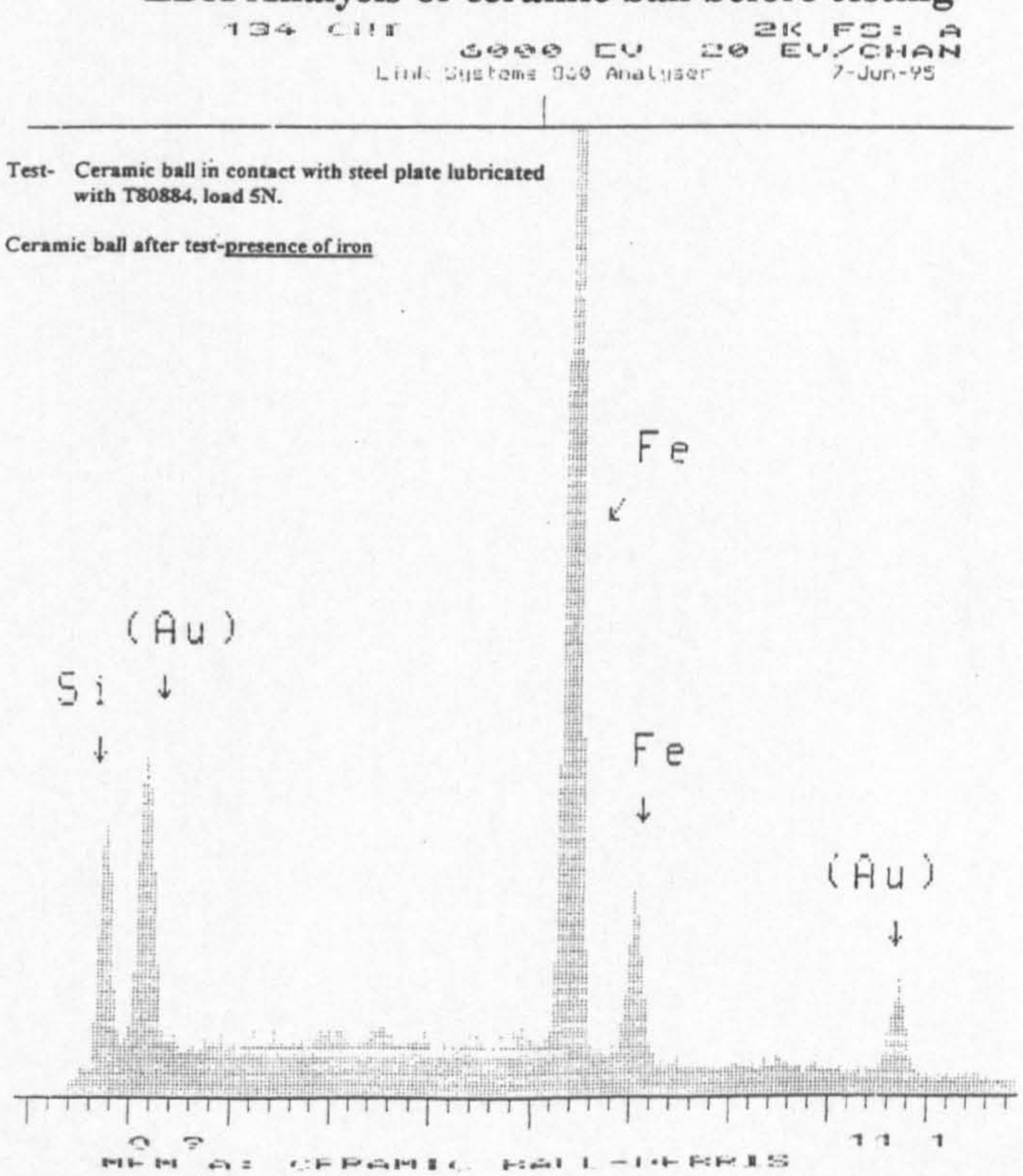

Fig. 6. 4 **EDX Analysis of ceramic ball after friction testing with the ester base fluid T80884**

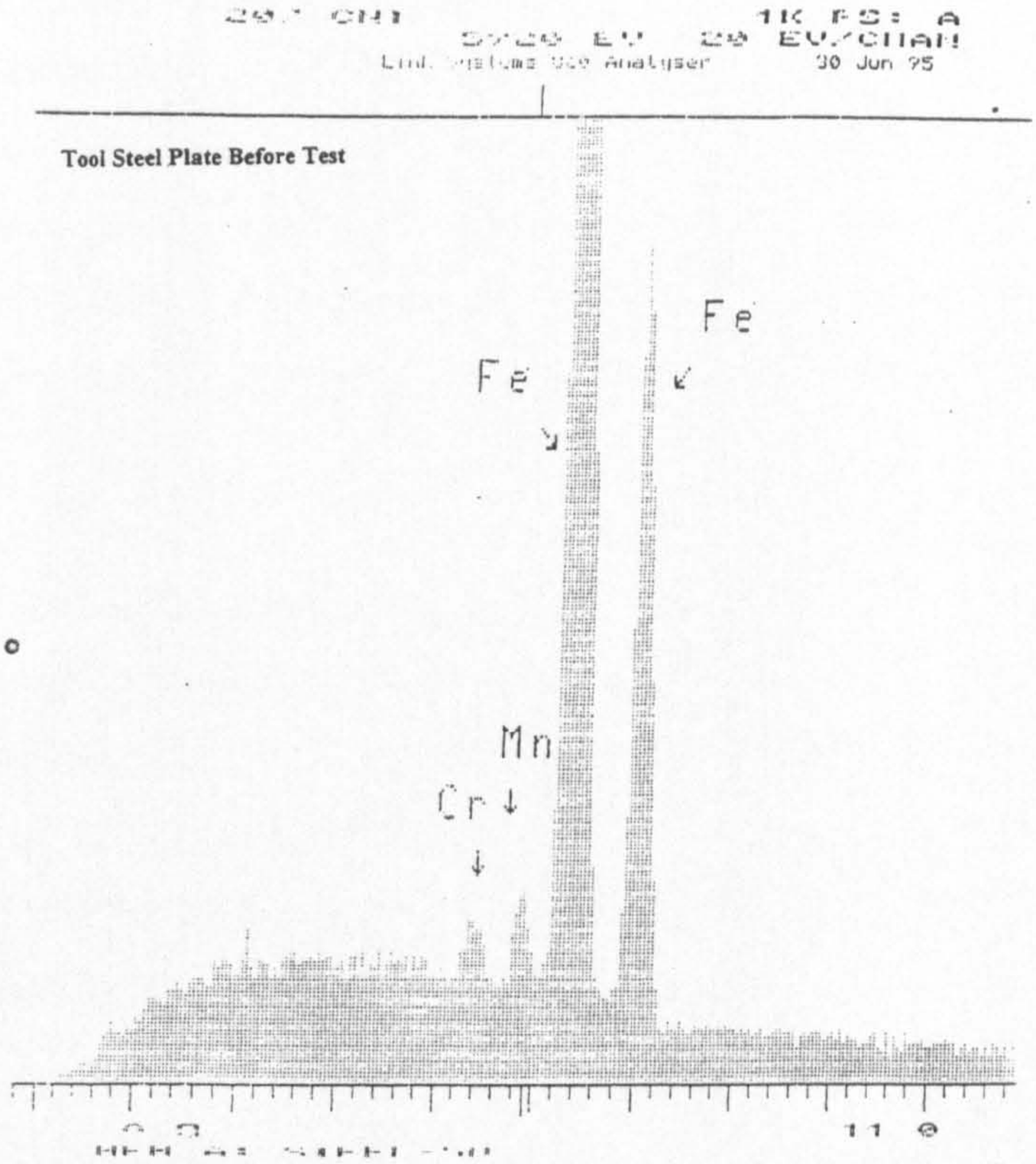

Fig. 6.5 **EDX Analysis of steel plate before testing**

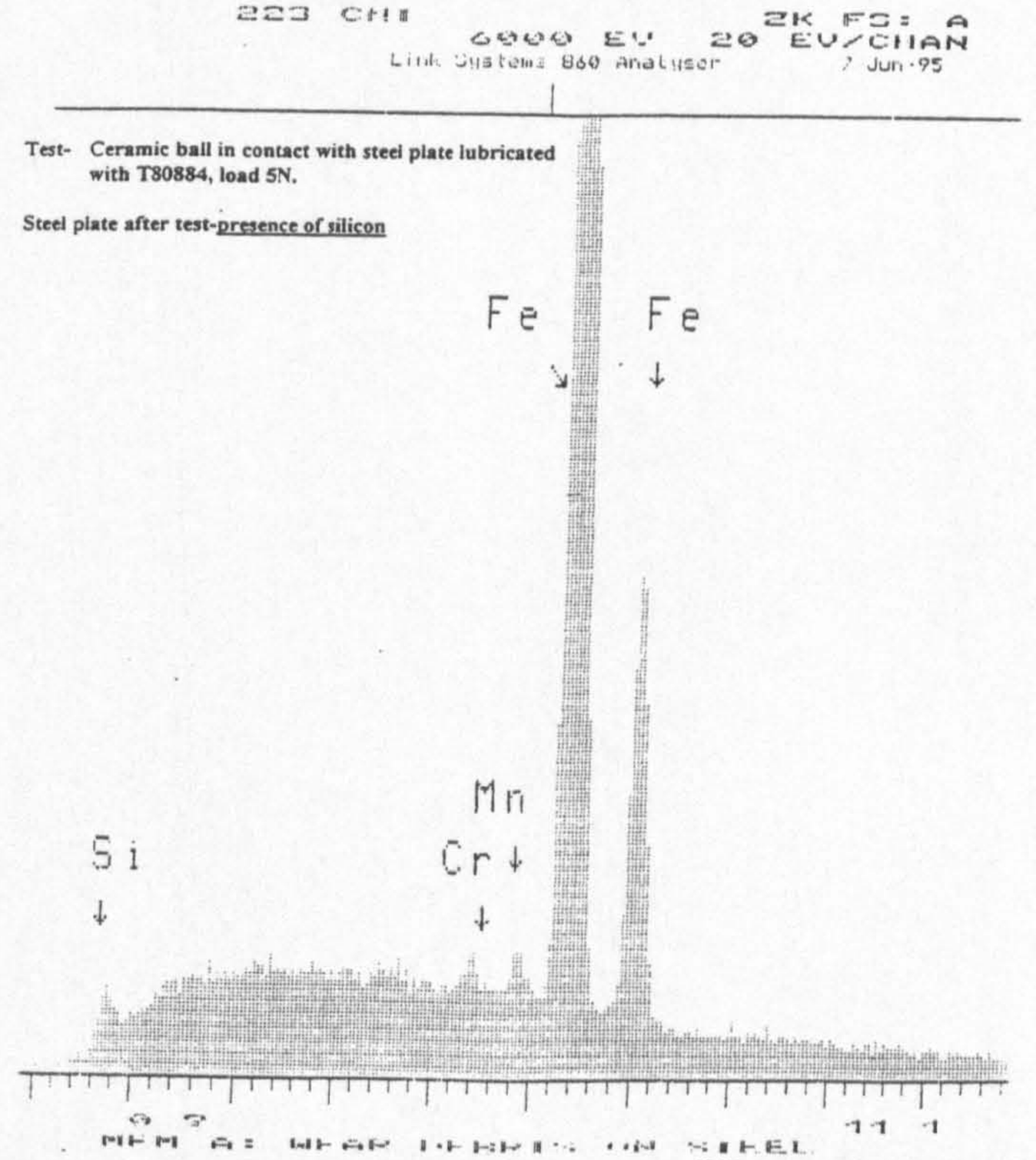

Fig. 6.6 **EDX Analysis of steel plate after friction testing with the ester base fluid T80884**

6.2.2 Atomic Force Microscope Studies

The contact area of the silicon nitride ball and steel plate was analysed after friction testing with the ester base fluid T80884 + 0.3% triethanol amine. Figures 6.7 and 6.8 show the AFM images of the contact area of the silicon nitride ball. The contact area appears to be very smooth, less pitted than the area outside the contact and it also has abrasion grooves on it. The abrasion grooves appear similar to the machining marks on the steel plate.

Figure 6.9 and 6.10 show the AFM images of the contact area of the steel plate. There appears to be a film on the surface with abrasion grooves on it. There is no evidence of any transfer occurring, but what is very clear is that the softer material, that is, the steel plate aided by the ester base fluid T80884 with 0.3% triethanol amine is modifying the silicon nitride ball surface which is a much harder material. This could be due to a tribochemical reaction occurring at the contact interface.

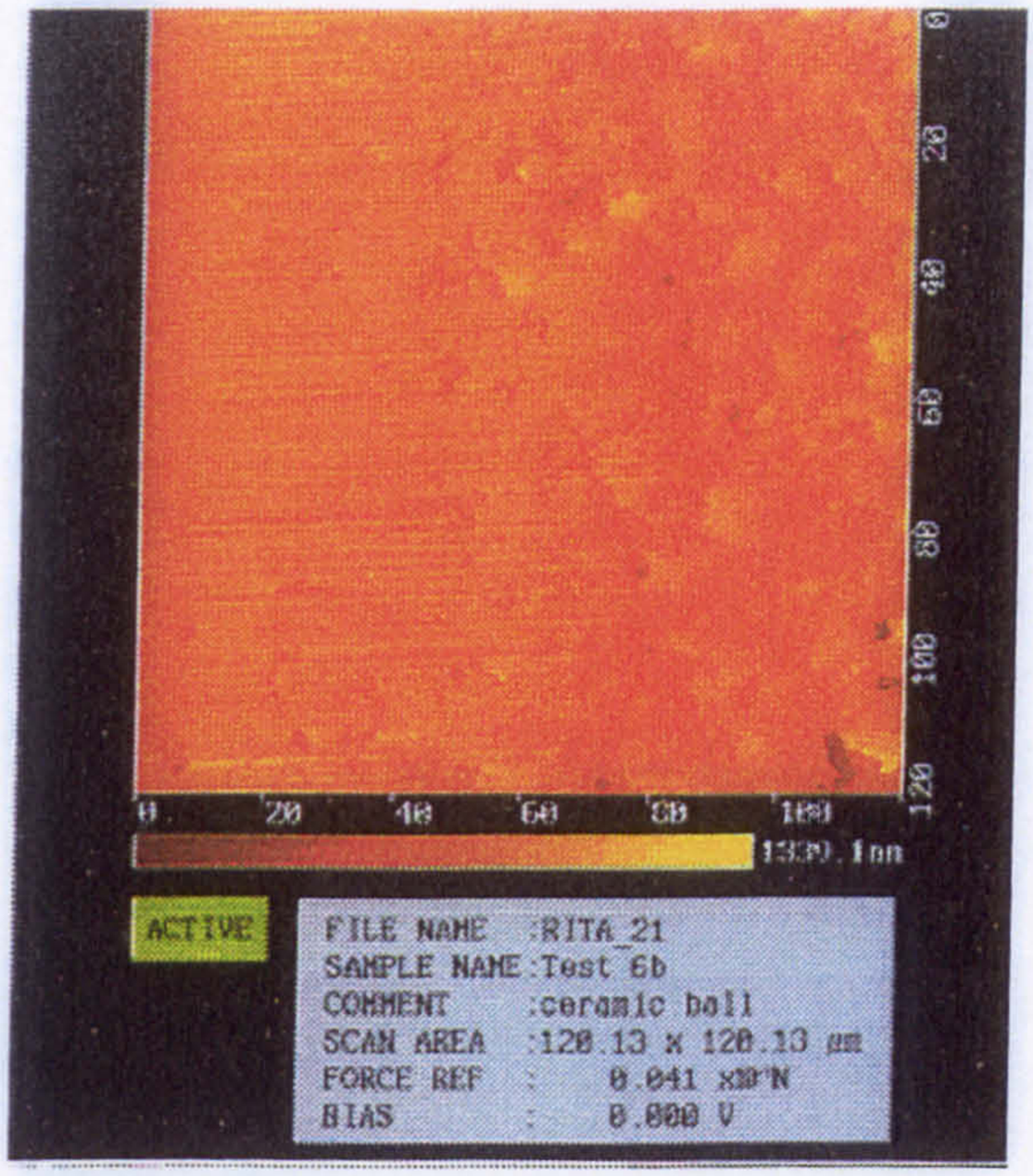

Fig. 6.7 **Two dimensional AFM image of contact area of ceramic ball after friction testing with ester T80884 + 0.3% triethanol amine**

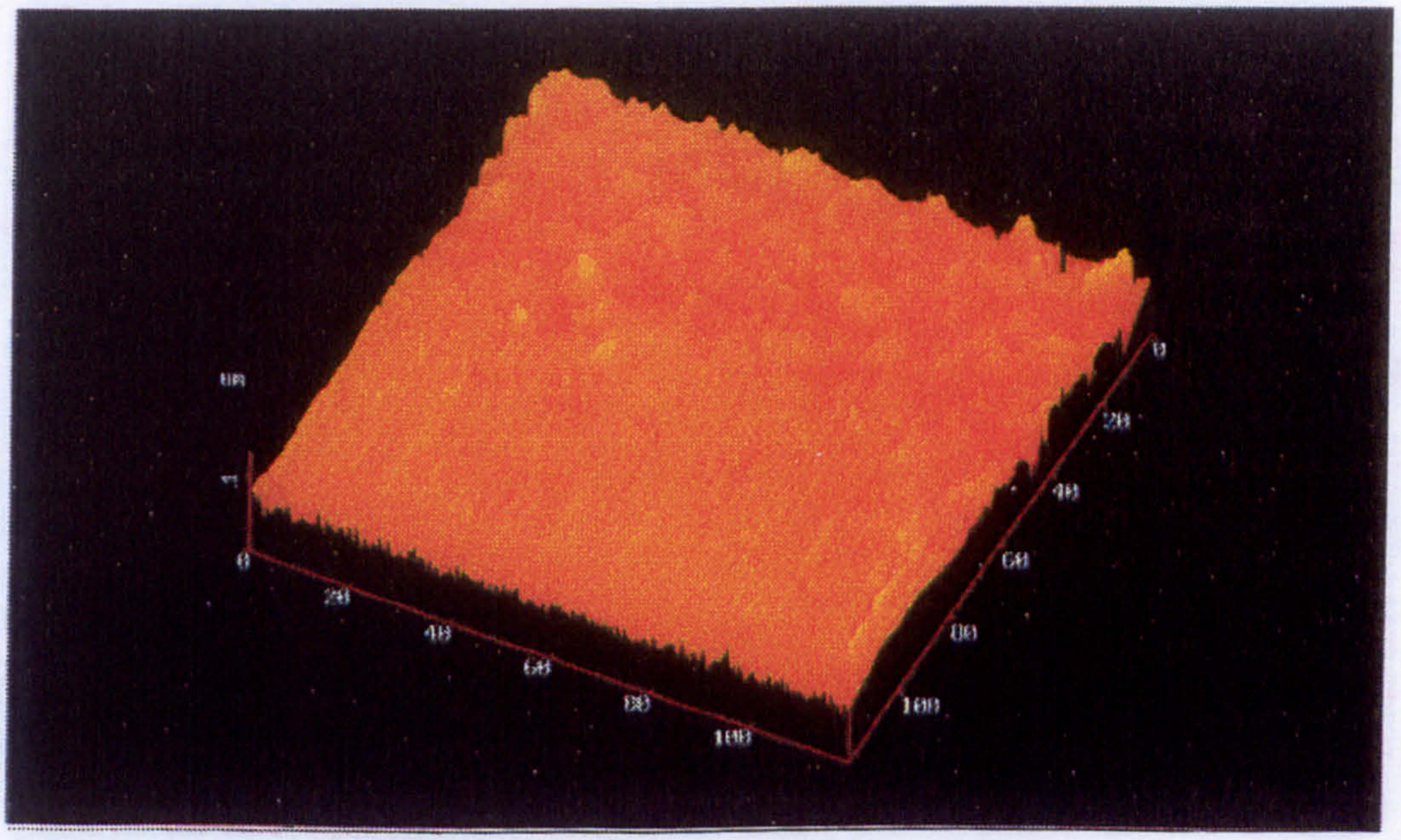

Fig. 6. 8 **Three dimensional AFM image of contact area of ceramic ball after friction testing with ester T80884 + 0.3% triethanol amine**

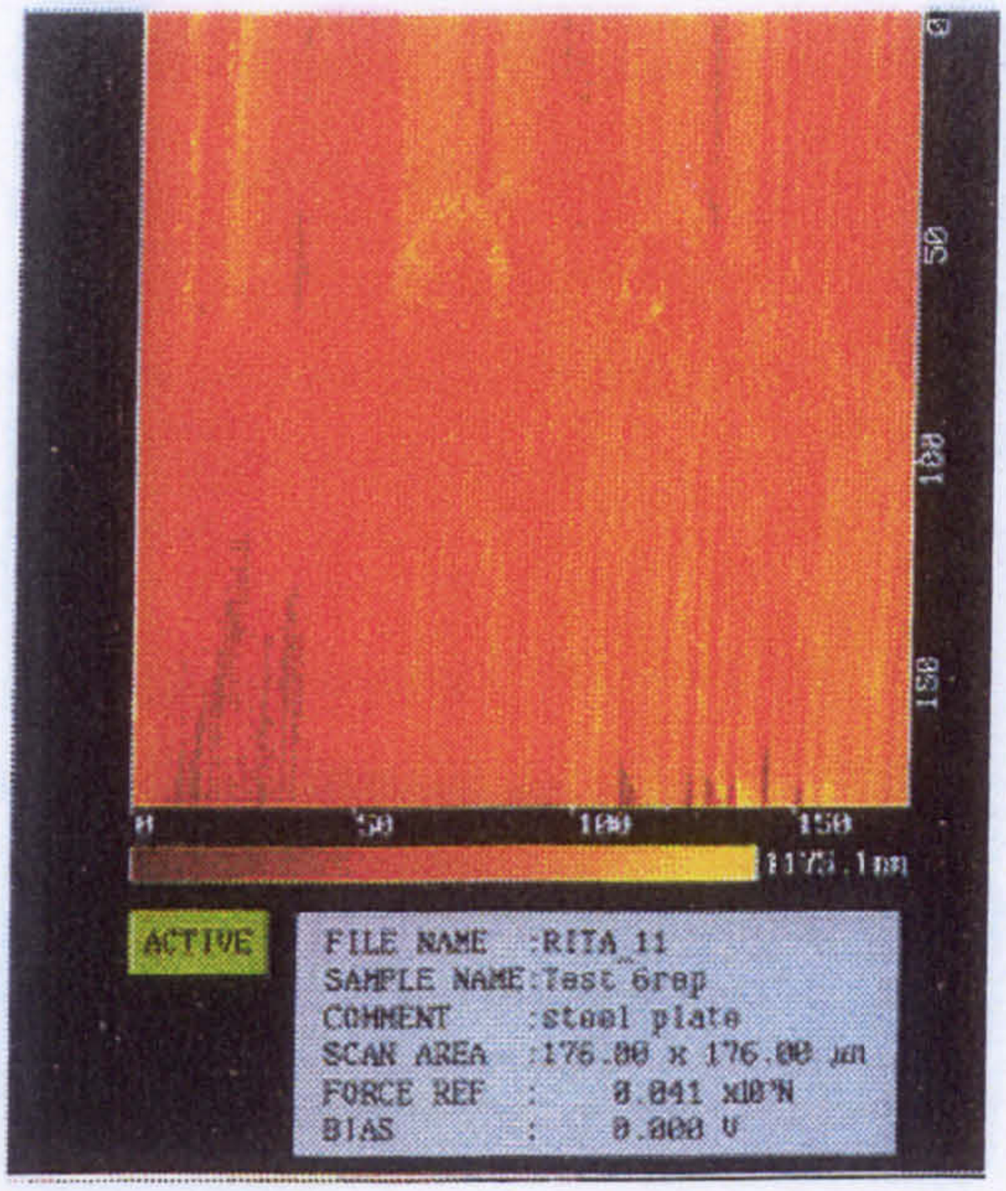

Fig. 6.9 **Two dimensional AFM image of contact area of steel plate after friction testing with ester T80884 + 0.3% triethanol amine**

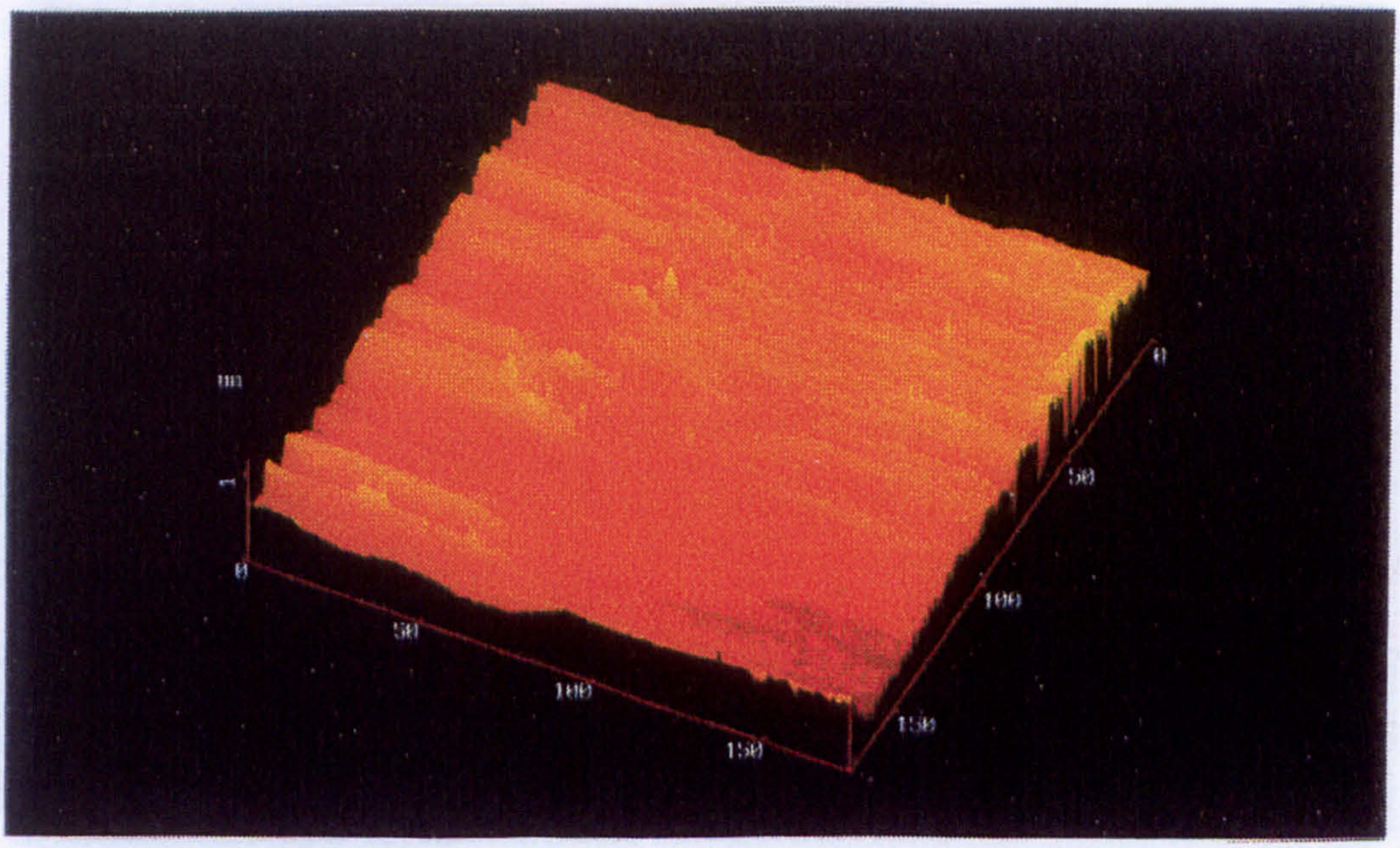

Fig. 6. 10 **Three dimensional AFM image of contact area of steel plate after friction testing with ester T80884 + 0.3% triethanol amine**

6.3 Grinding Test

A more in-depth analysis was carried out after the grinding test on the silicon nitride balls using the ester base fluid T80884 + 0.3% triethanol amine. Surface and chemical analyses were done on the wear debris using SEM and EDX techniques. Microhardness and residual stress measurements were also carried out after each 1 hour grinding run, in order to identify whether grinding tests using ester base fluid T80884 + 0.3% triethanol amine had any effect on these parameters.

6.3.1 Wear Debris Analysis using SEM and EDX

Wear debris produced during grinding tests were collected by filtering the abrasive slurry and analysed using SEM and EDX techniques. Figures 6.11a,b,c show the SEM images of debris collected after the grinding test with the reference lubricant Kemet. The debris appears in the form of thin sheets typical of the delamination type of wear, approximately 1 micron in thickness and with a length of 10 to 40 microns. Numerous cracks can be seen on the debris particle as shown in figure 6.11a, which could be due to a delamination process. However, there is also a possibility that the debris became rolled in the cup assembly and became agglomerated to form a cluster of debris as shown in figure 6.11c. Further EDX analysis was done on the Kemet debris and the results in figure 6.13 show that both the iron and silicon peaks are strong.

Figure 6.12 show the SEM images of the debris collected after the grinding test with the ester base fluid T80884 + 0.3% triethanol amine. The size of the debris is 2 to 5 microns in diameter, this is much smaller than the debris collected after testing with Kemet. These debris are also more spherical in shape and could have been caused by a tribochemical type of wear. Further EDX analysis was done on the debris and results in figure 6.14 show both silicon and iron peaks, however, the silicon peak appears much stronger.

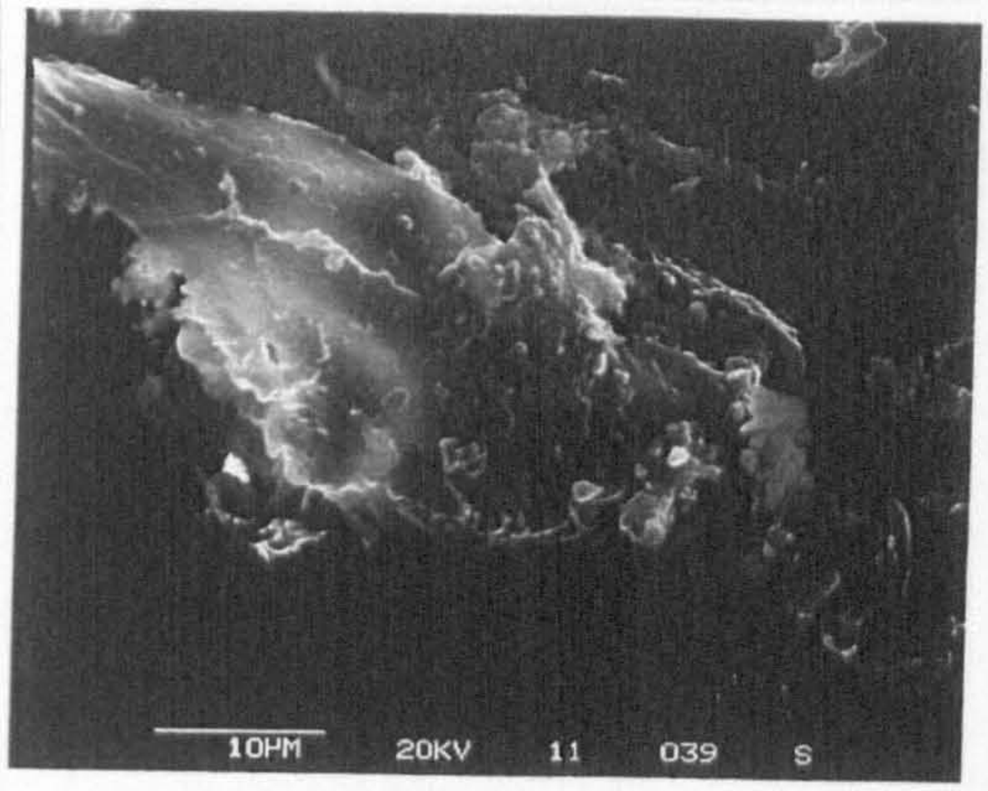

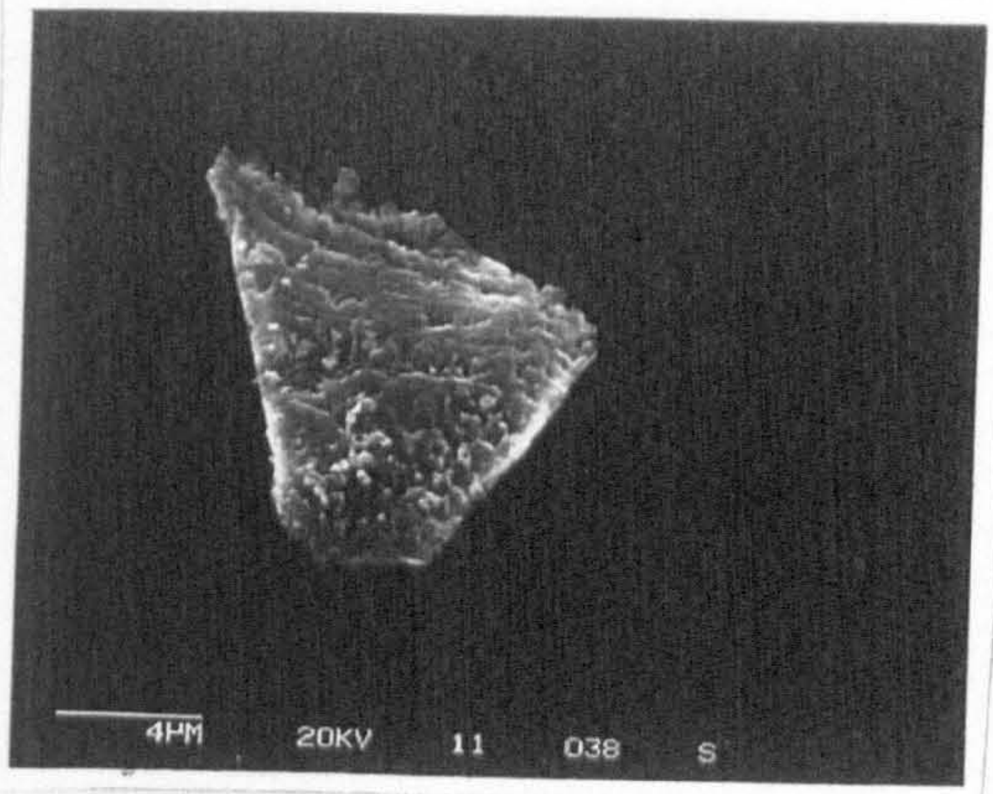

a)

b)

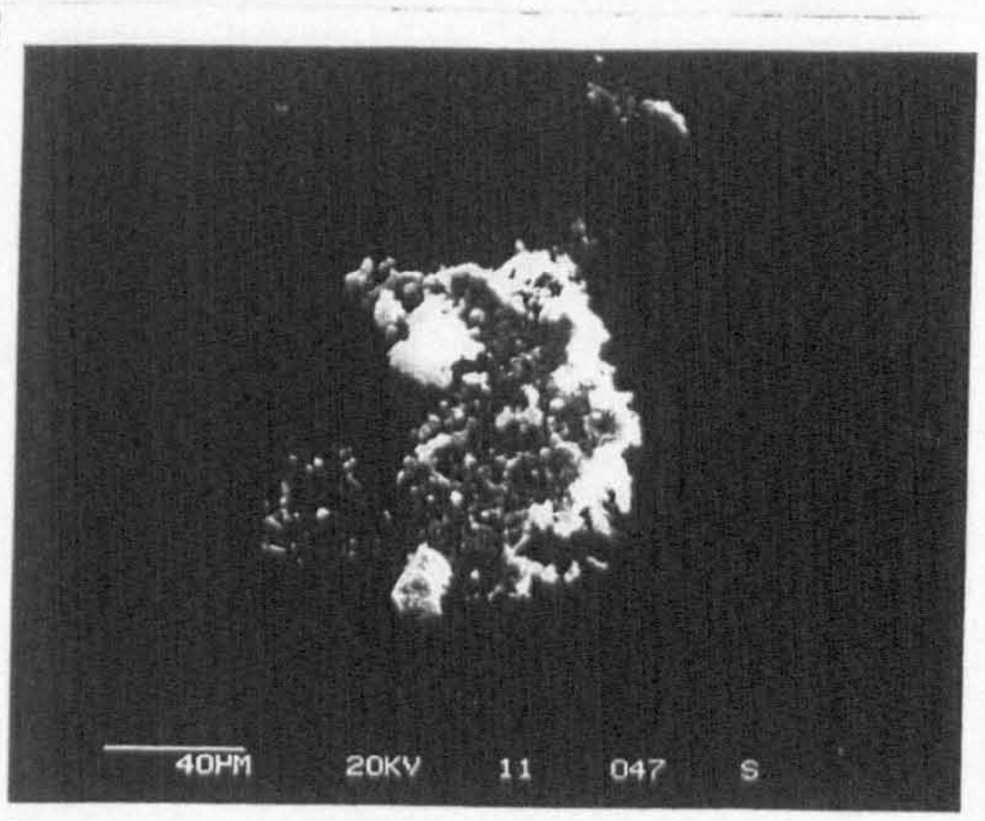

c)

Fig. 6.11 SEM observations of debris produced during grinding test with reference lubricant Kemet

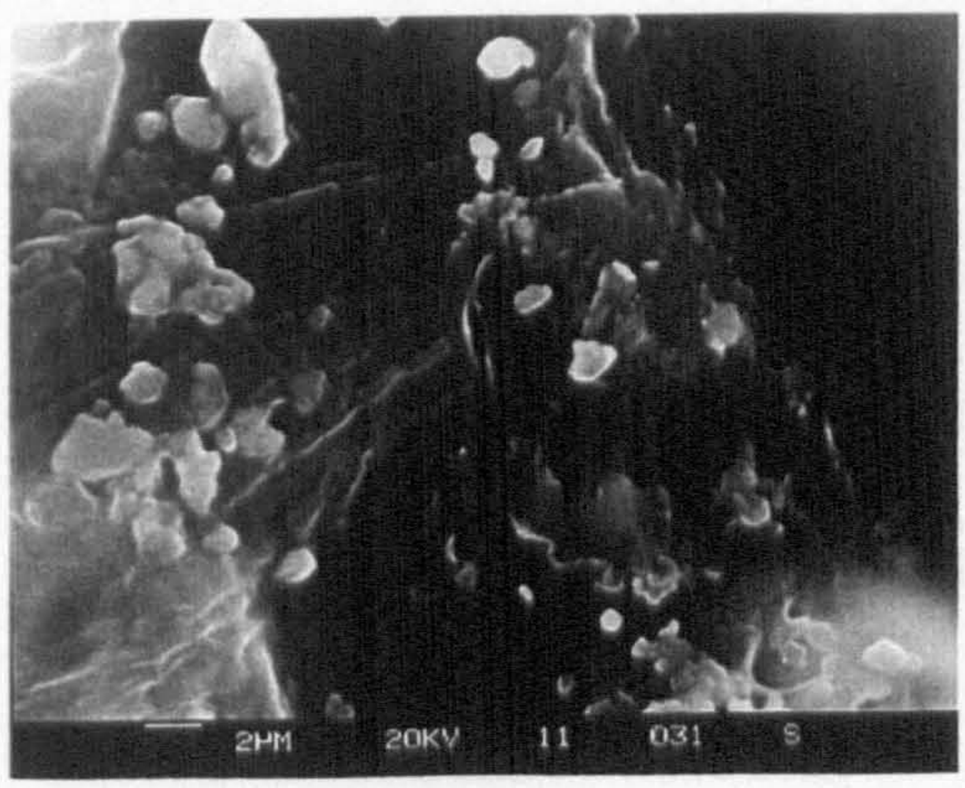

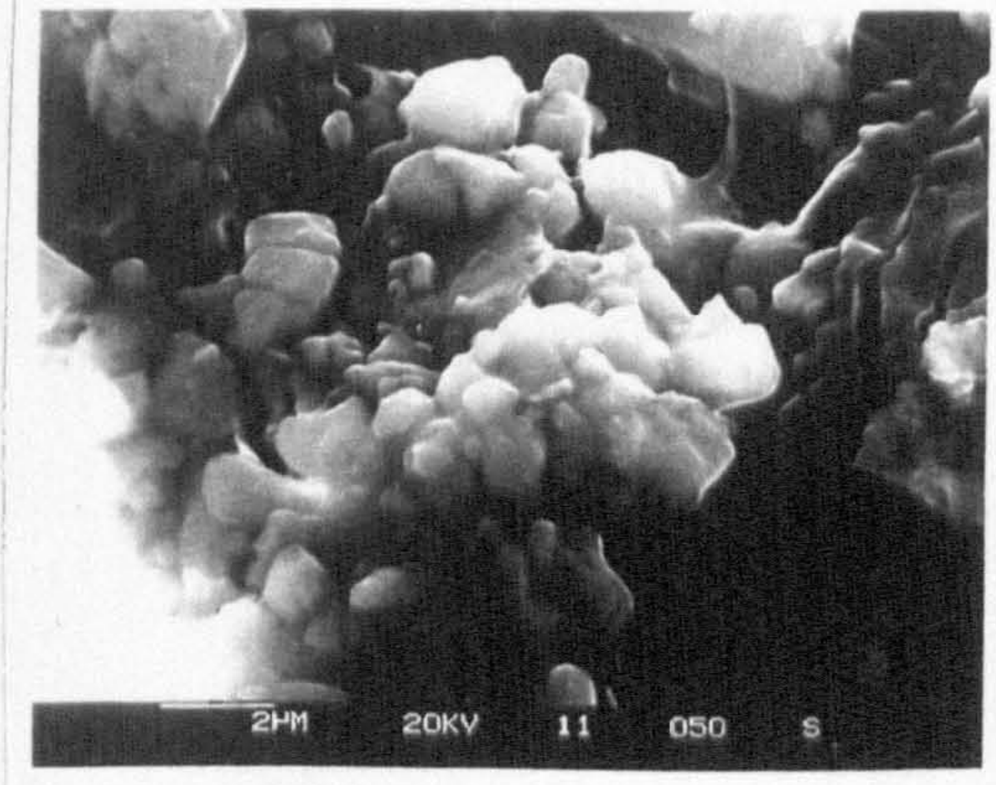

Fig. 6.12 SEM observations of debris produced during grinding test with ester base fluid T80884 + 0.3% triethanol amine

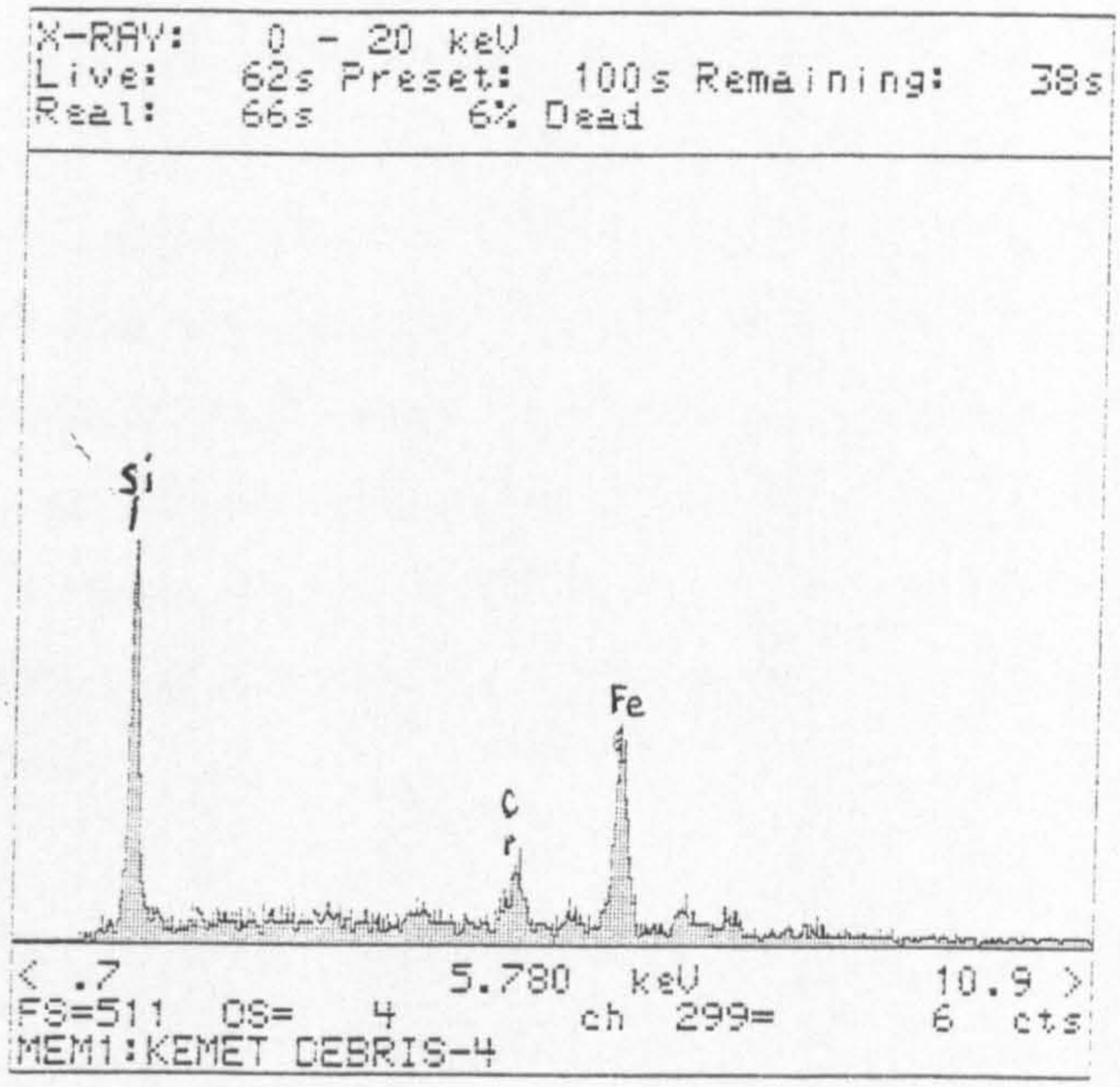

Fig. 6.13 EDX analysis of debris produced during grinding test with reference lubricant Kemet

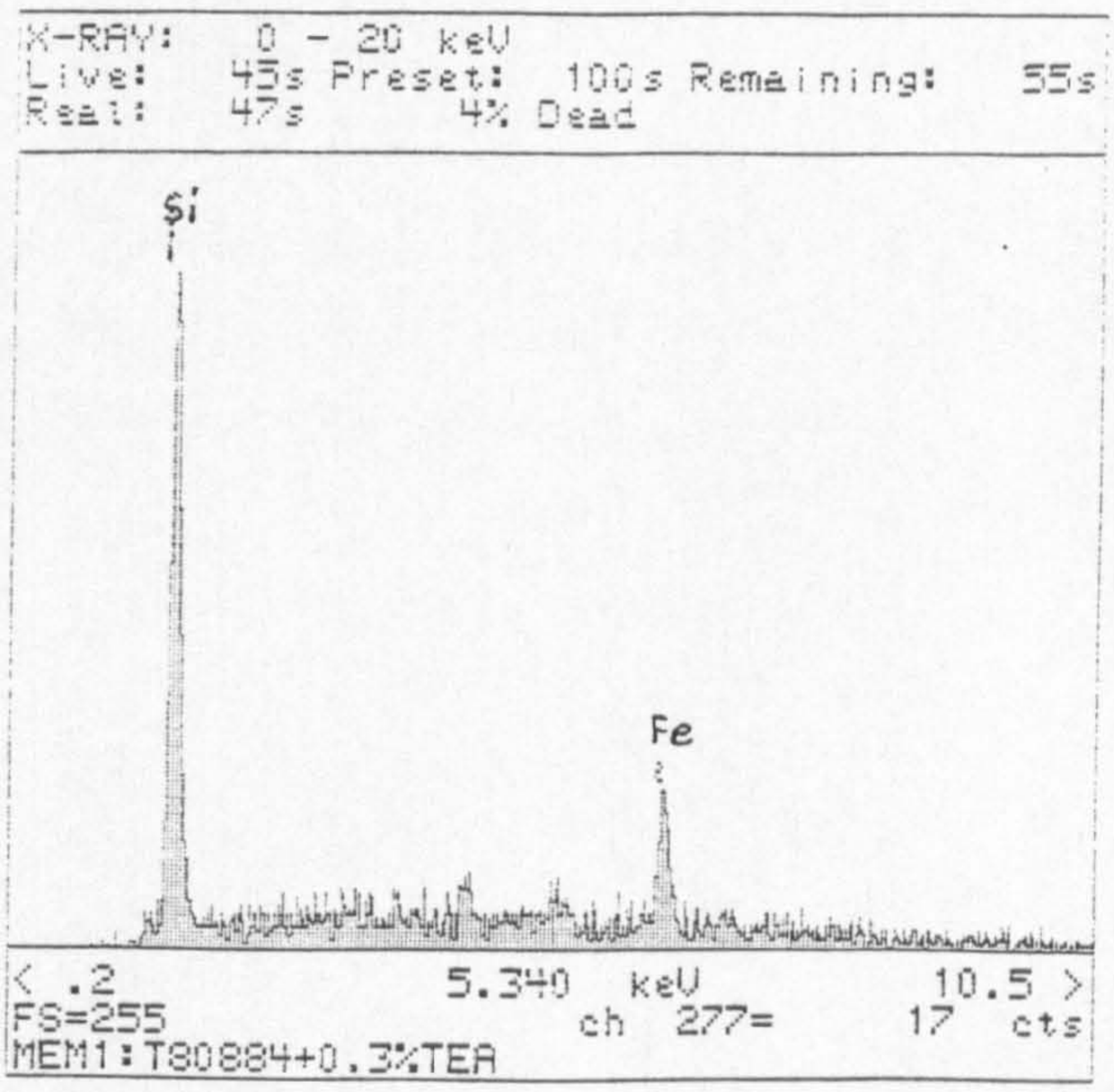

Fig. 6.14 EDX analysis of debris produced during grinding test with ester base fluid T80884 + 0.3% triethanol amine

6.3.2 Micro-hardness Measurements

Hardness is considered to be an important factor in wear, where in general, wear loss is inversely proportional to the hardness or its fractional power (Evans, 1981).

A Leitz Miniload 2, Vickers hardness tester was used to measure the hardness of the silicon nitride balls after several grinding runs with the ester base fluid T80884 + 0.3% of the additive triethanol amine. Preliminary measurements on the microhardness of the test pieces using a variety of loads ranging from 50p to 400p, revealed that a load of 300p provide consistent values. A measurement was done on the initial ball blank then after each 1 hour grinding runs. The results presented in table 6.1 are an average value after several repeated tests.

Table 6.1 Microhardness Measurements

Sample	Vickers Hardness
Initial Ball blank	1924HV
1 grinding run	1717HV
2 grinding runs	1880HV
3 grinding runs	1900HV
4 grinding runs	1840HV
5 grinding runs	1780HV

The major objective of this analysis was to investigate the variation in hardness after several grinding runs. The results show that there is no significant effect on the hardness of the silicon nitride balls after the repeated grinding runs.

6.3.3 Residual Stress Measurements

Residual stresses induced during grinding of the silicon nitride ceramics may have an important influence on the mechanical properties of the ceramic, therefore, residual stress measurements were done after each 1 hour grinding run with the ester base fluid T80884 + 0.3% triethanol amine and the results are shown in fig. 6.15.

A relatively high initial level of residual stress of 1200MPa quickly falls to 880MPa as a result of the running-in of the as sintered ball. It is seen that after the first running-in a very substantial decrease in residual stress level occurs from 880MPa to 190MPa. The second round of tests produce a much smaller decrease in residual stress to 59MPa and then to 40.23MPa in comparison to the first round of tests. The material removed for each grinding run remained constant at about 2.5μm/min even though there was a significant difference in the initial residual stresses.

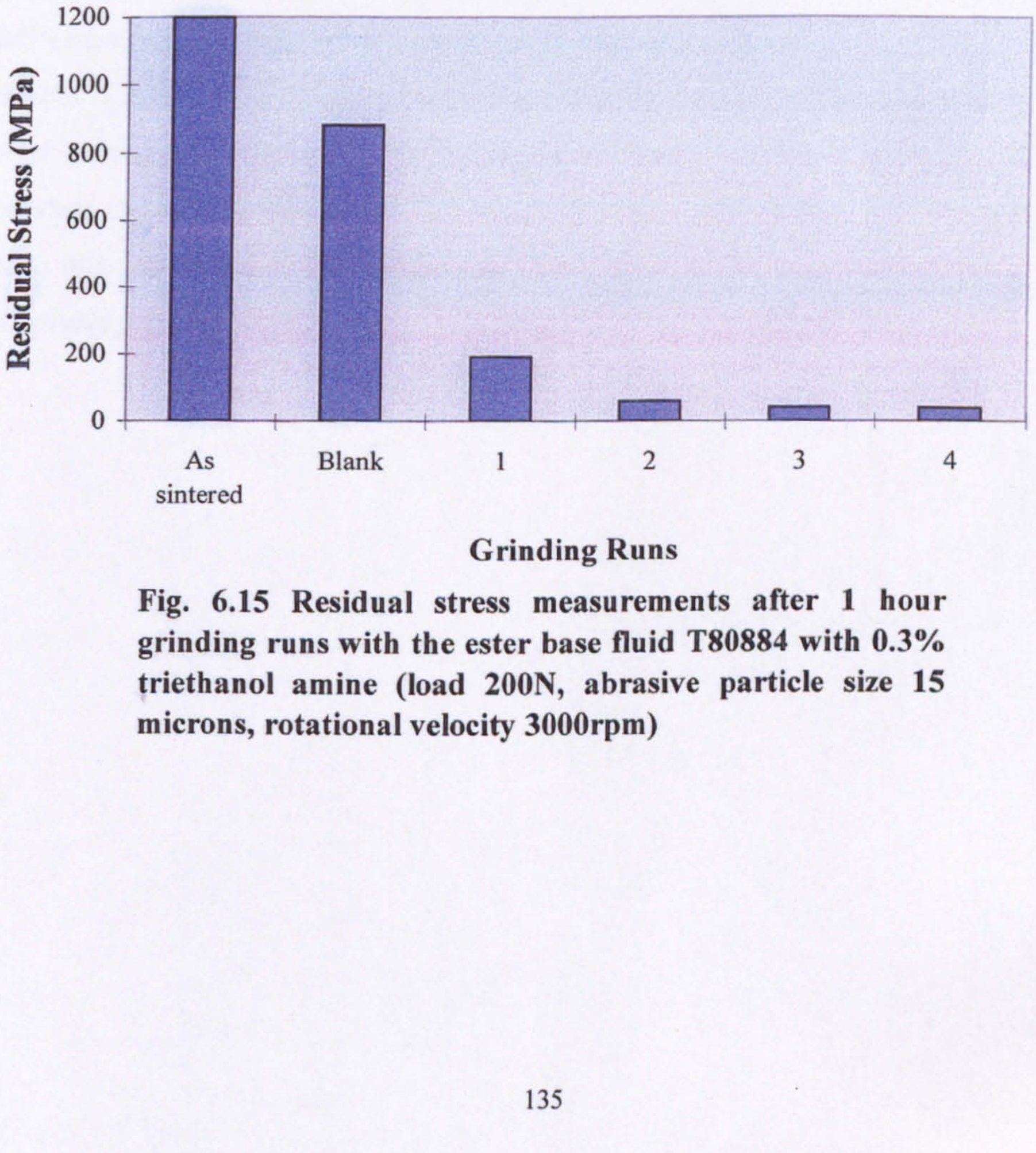

Fig. 6.15 Residual stress measurements after 1 hour grinding runs with the ester base fluid T80884 with 0.3% triethanol amine (load 200N, abrasive particle size 15 microns, rotational velocity 3000rpm)

6.4 Chemical Analysis Using Infrared Spectroscopy

The Nicolet Fourier Transform Infrared laser spectrometer was used to analyse the ceramic balls tested in the presence of the most effective grinding lubricants under various conditions, in order, to evaluate the possible chemical reactions which might occur. The most effective grinding lubricants used for all the IR analysis were:-

- reference lubricant Kemet
- polyglycol - T81499
- ester base fluid - T80884
- ester base fluid T80884 + 0.3% triethanol amine additive

A fixed path length cell was used for the analysis which meant that the results would be both qualitative and quantitative.

6.4.1 Infrared Analysis of the Abrasive Slurries after the Grinding Tests

Before doing the Infrared spectroscopy analysis the abrasive slurries were filtered after testing to remove the abrasive particles and debris particles. Figure 6.16 shows the infrared spectra results before and after the grinding tests with the reference lubricant Kemet. The results show that there is no significant change in the characteristics peaks after testing. Therefore, there is no evidence for any occurrence of a chemical reaction between the reference lubricant Kemet and the silicon nitride balls. Although Kemet is a base mineral oil the C-CO-C bond at 1097cm^{-1} could be due to an additive used for suspending the diamond slurry.

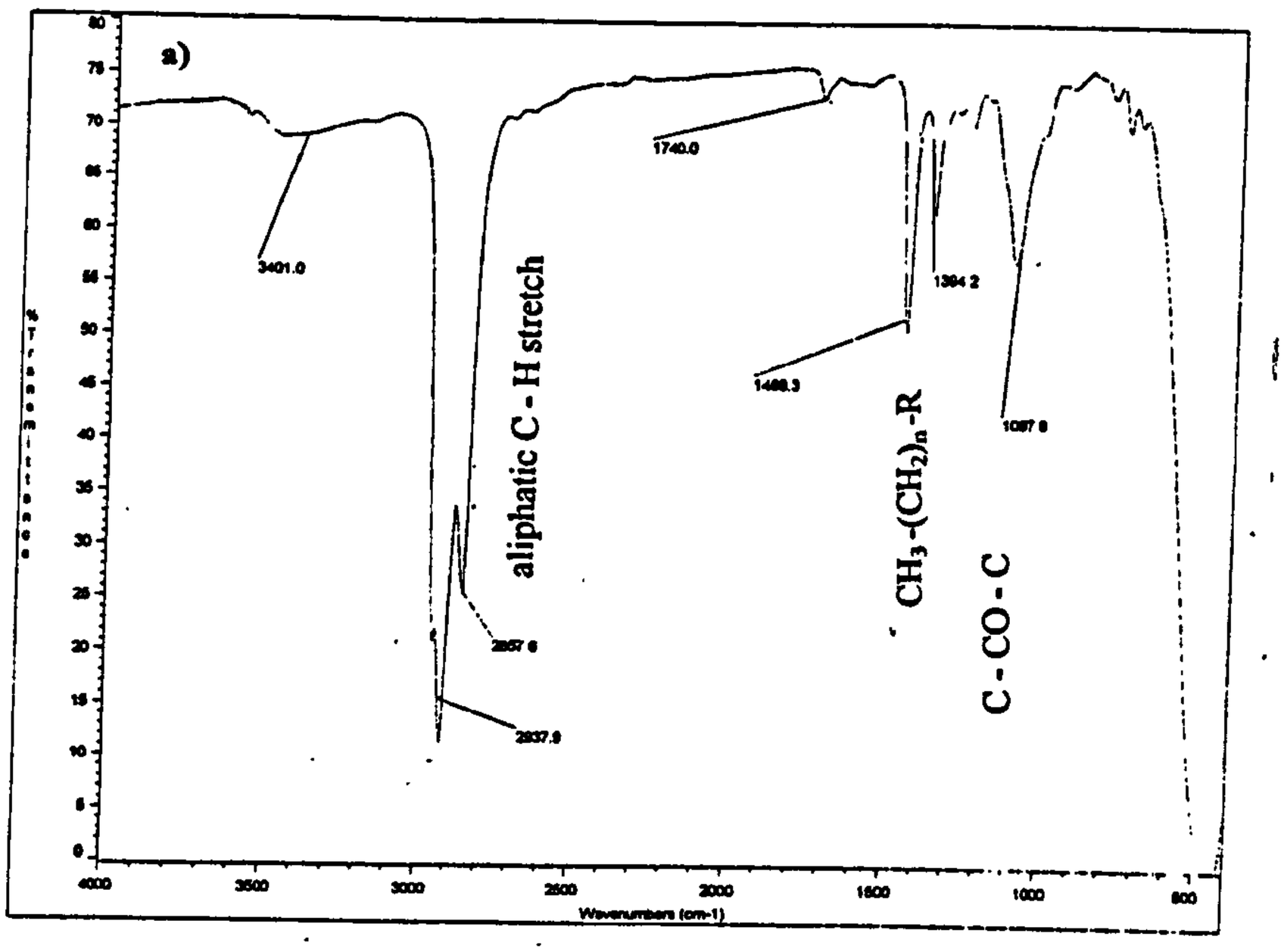

Fig. 6.16 **Infrared Spectra of the reference lubricant Kemet a)before and b)after grinding test**

Figure 6.17 shows the infrared spectra results before and after the grinding tests with the polyglycol T81499. The results show that after testing there is no change in the characteristics peaks. This implies that there is no structural change in the T81499 slurry after the grinding test, therefore, there is no indication of a chemical reaction between the polyglycol T81499 and the silicon nitride balls.

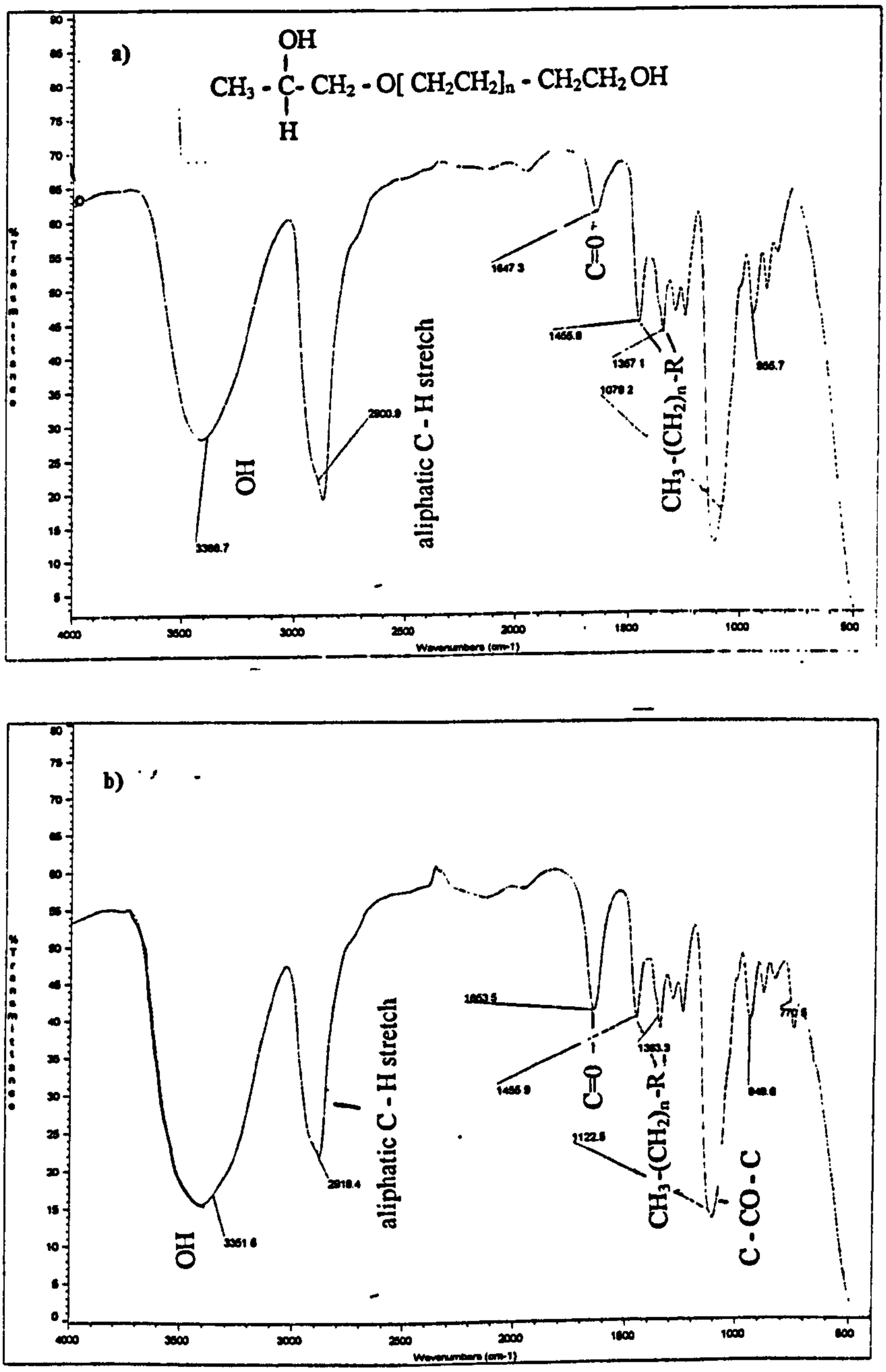

Fig. 6.17 **Infrared Spectra of the polyglycol T81499 a) before and b) after grinding test**

Figure 6.18. shows the infrared spectra results before and after the grinding tests with the ester base fluid T80884. The results show a significant reduction in the peak intensities and there is also no peak at 739.6cm^{-1} after testing. This implies that there is some significant change occurring in the ester base fluid T80884 slurry during the grinding test.

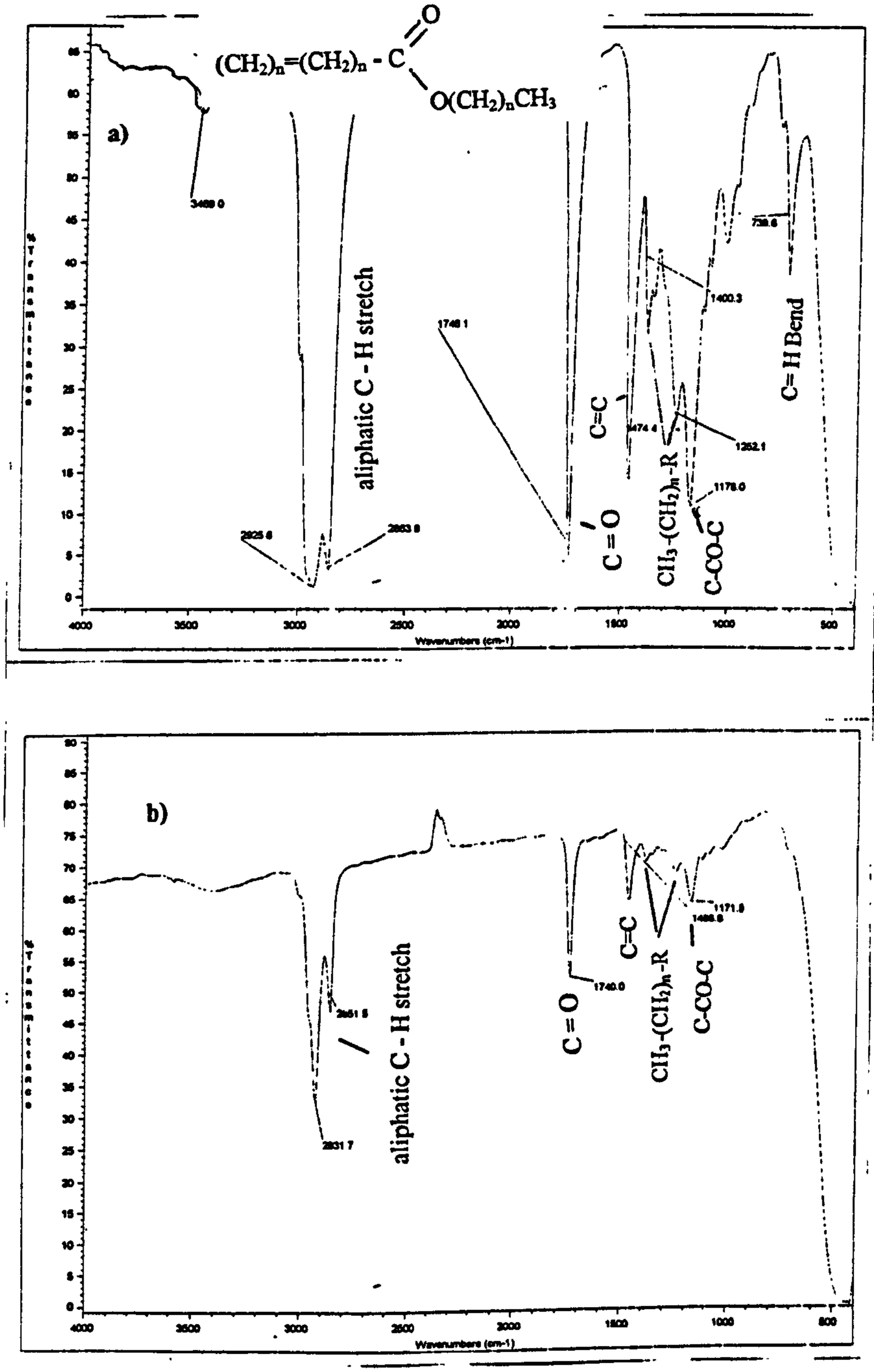

Fig. 6.18 **Infrared Spectra of the ester base fluid T80884 a)before and b)after grinding test**

Figure 6.19 shows the infrared spectra results before and after the grinding tests with the ester base fluid T80884 mixed with 0.3% of the additive triethanol amine. The results show a significant reduction of the intensity of the characteristic peaks, as obtained in the infrared results for ester base fluid T80884. This implies that there is some significant change occurring in the ester base fluid T80884 + 0.3% triethanol amine slurry during the grinding test.

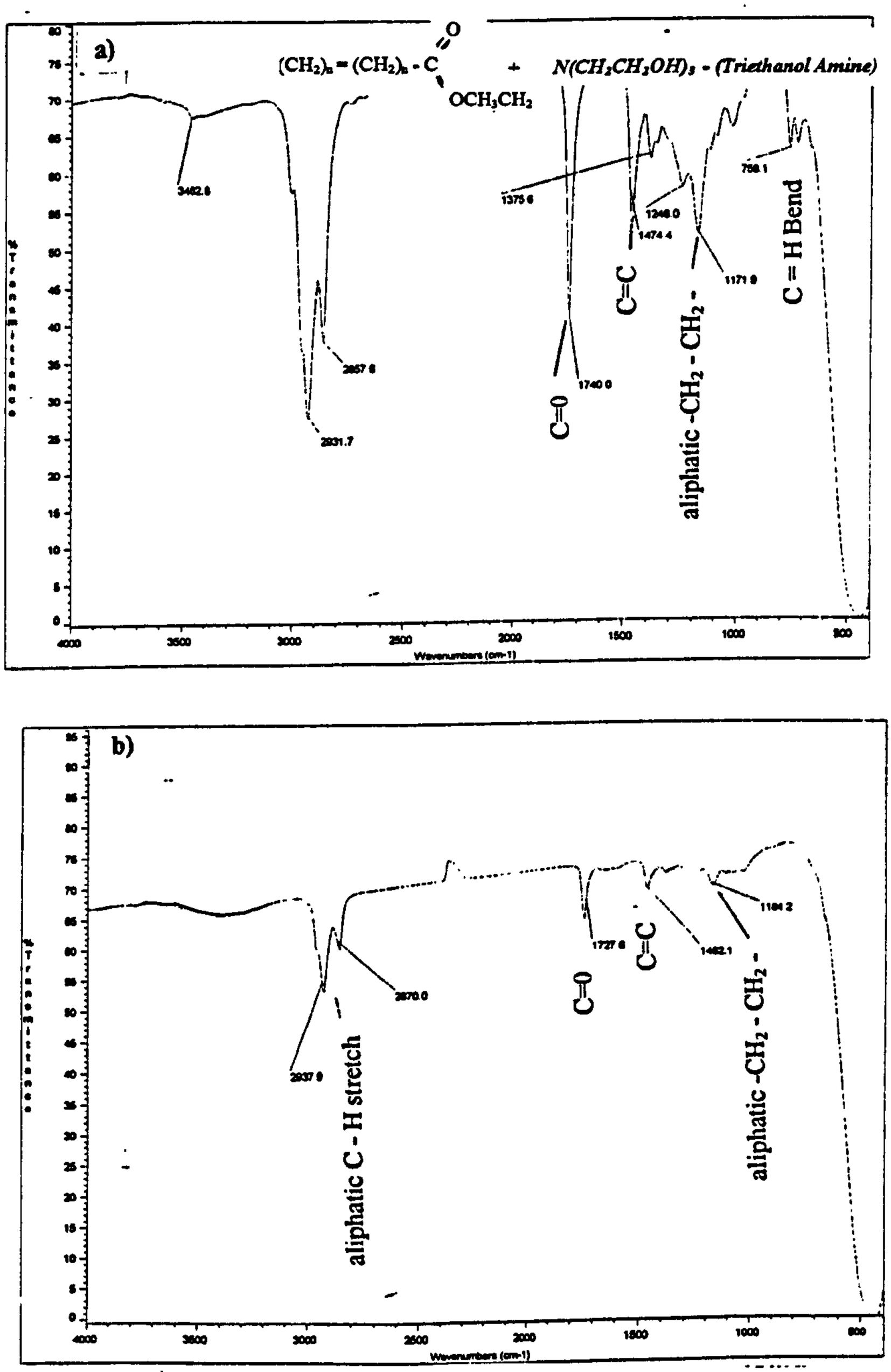

Fig. 6.19 **Infrared Spectra of the ester base fluid T80884 with 0.3% of the additive triethanol amine a)before and b)after grinding test**

6.4.2 Infrared Analysis of lubricants after Immersing Silicon Nitride Balls

A silicon nitride ball was completely immersed in each of the test lubricants for 24 hours in order to evaluate any significant structural changes in each of these lubricants after this test procedure. Figure 6.20 shows the infrared results before and after testing with reference lubricant Kemet. The results show all the characteristics peaks in the spectrum before and after testing. It is apparent that there is no difference between them, hence there is no indication of any chemical reaction between Kemet and the silicon nitride ball.

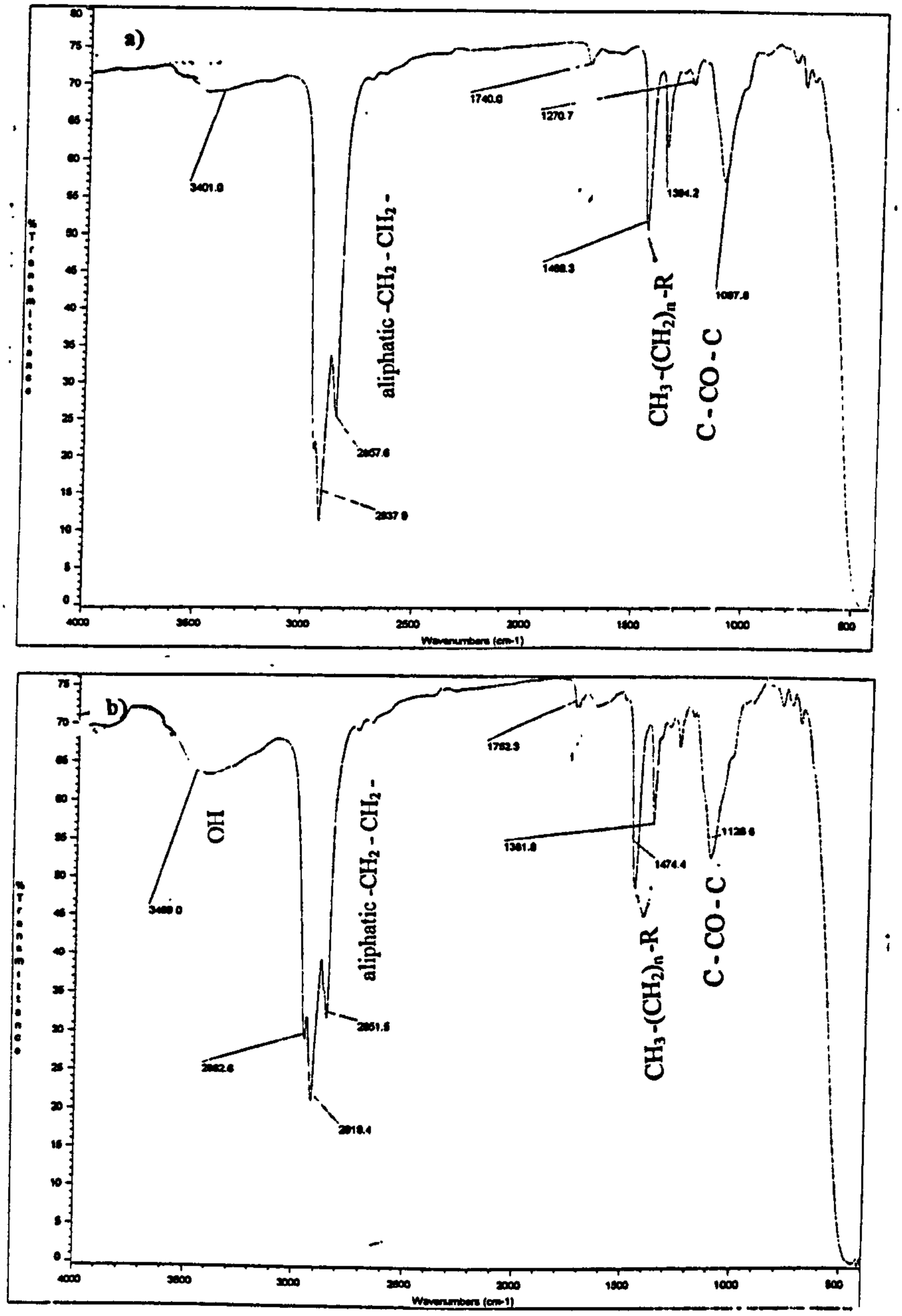

Fig. 6.20 Infrared Spectra of the reference lubricant Kemet a)before and b) after ball immersing test

Figure 6.21 shows the infrared results before and after testing with polyglycol T81499. The results show all the characteristic peaks in the spectrum before and after testing. It is seen that they are the same, hence, there is no indication of any chemical reaction between polyglycol T81499 and the silicon nitride ball.

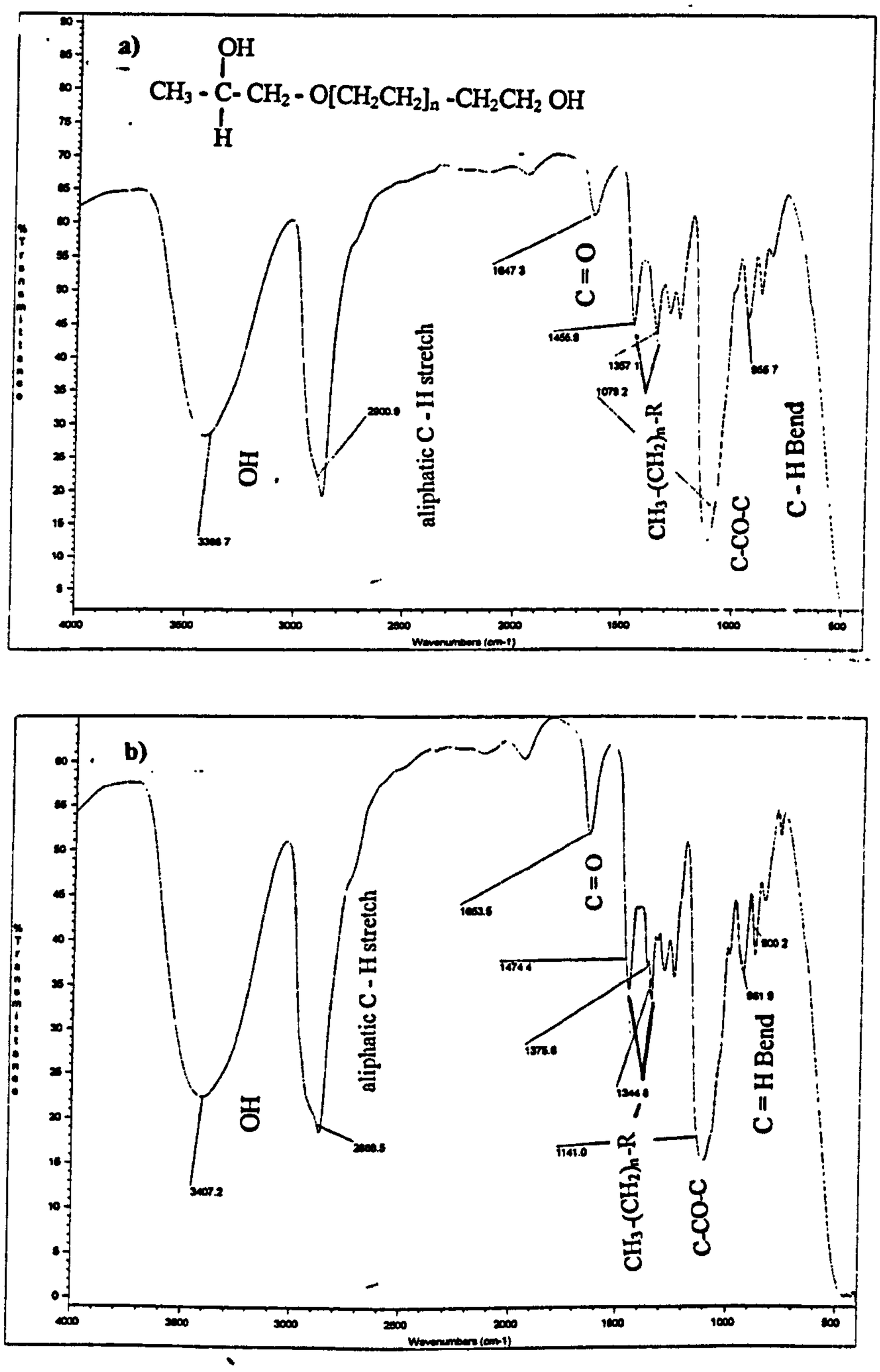

Fig. 6.21 Infrared Spectra of the polyglycol T81499 a)before and b) after the ball immersing test

Figure 6.22 shows the infrared analysis results before and after testing with the ester base fluid T80884. The results show that after testing there is slight broad peak OH peak forming at 3420cm^{-1} and also the peak intensity is very much reduced. This shows that there is some change occurring in the ester base fluid T80884 lubricant during the ball immersing test.

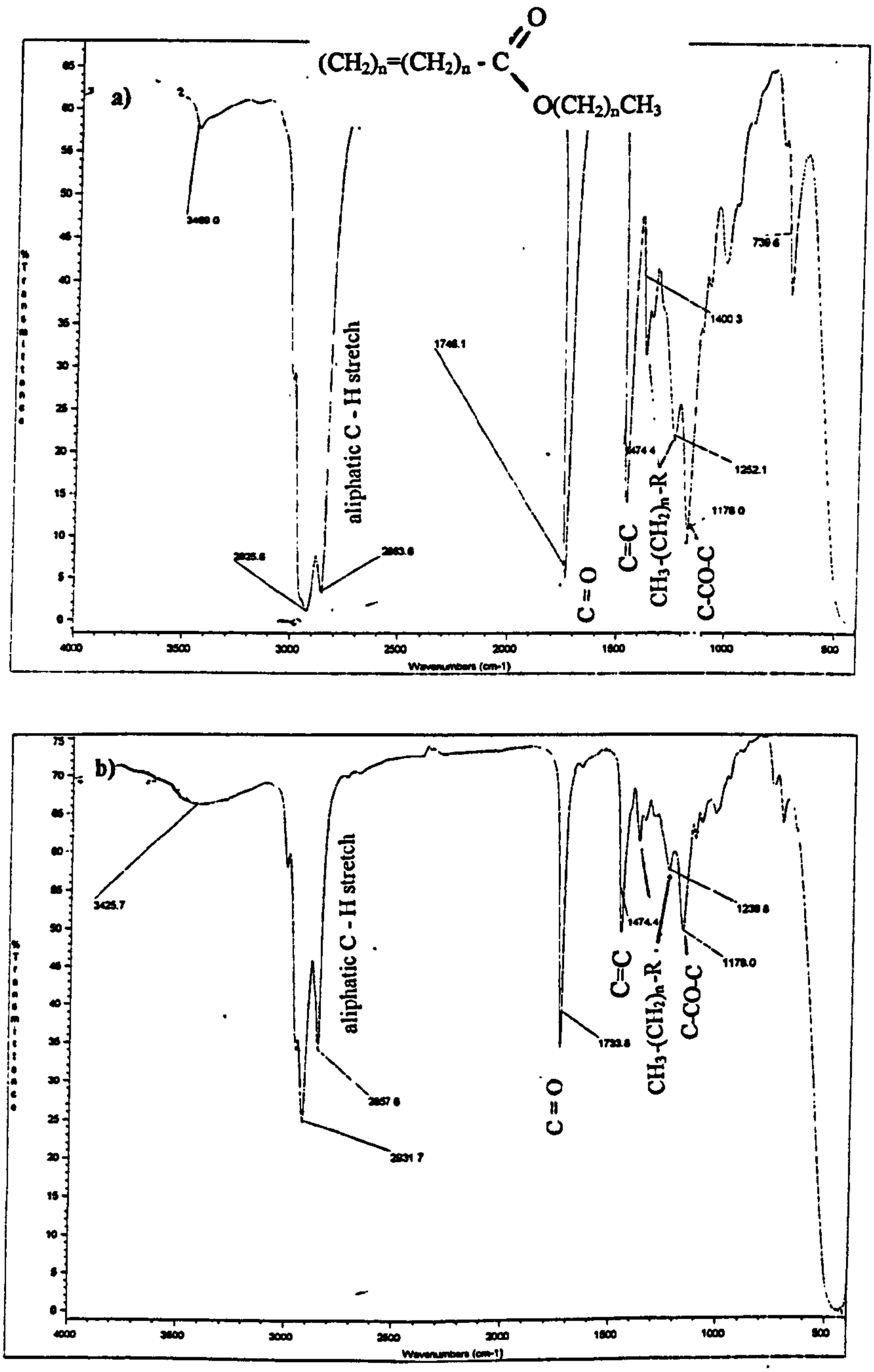

Fig. 6.22 Infrared Spectra of the ester base fluid T80884 a)before and b) after the ball immersing test

Figure 6.23 shows the infrared results before and after testing with the ester base fluid T80884 with 0.3% of the additive triethanol amine. The results show that after testing there is a very broad peak appearing at 3456 cm^{-1}. This peak is a characteristic hydroxyl peak (OH) peak. There are also changes occurring in the aliphatic part of the spectra, where a broad peak is forming at 1100 cm^{-1}, this could be a Si-O peak. These results clearly show a very significant structural change occurring in the T80884 + 0.3% lubricant during the ball immersing test. It is evident from these results that there is some chemical interaction occurring between the ester base fluid T80884 with 0.3% of the additive triethanol amine with the silicon nitride ball.

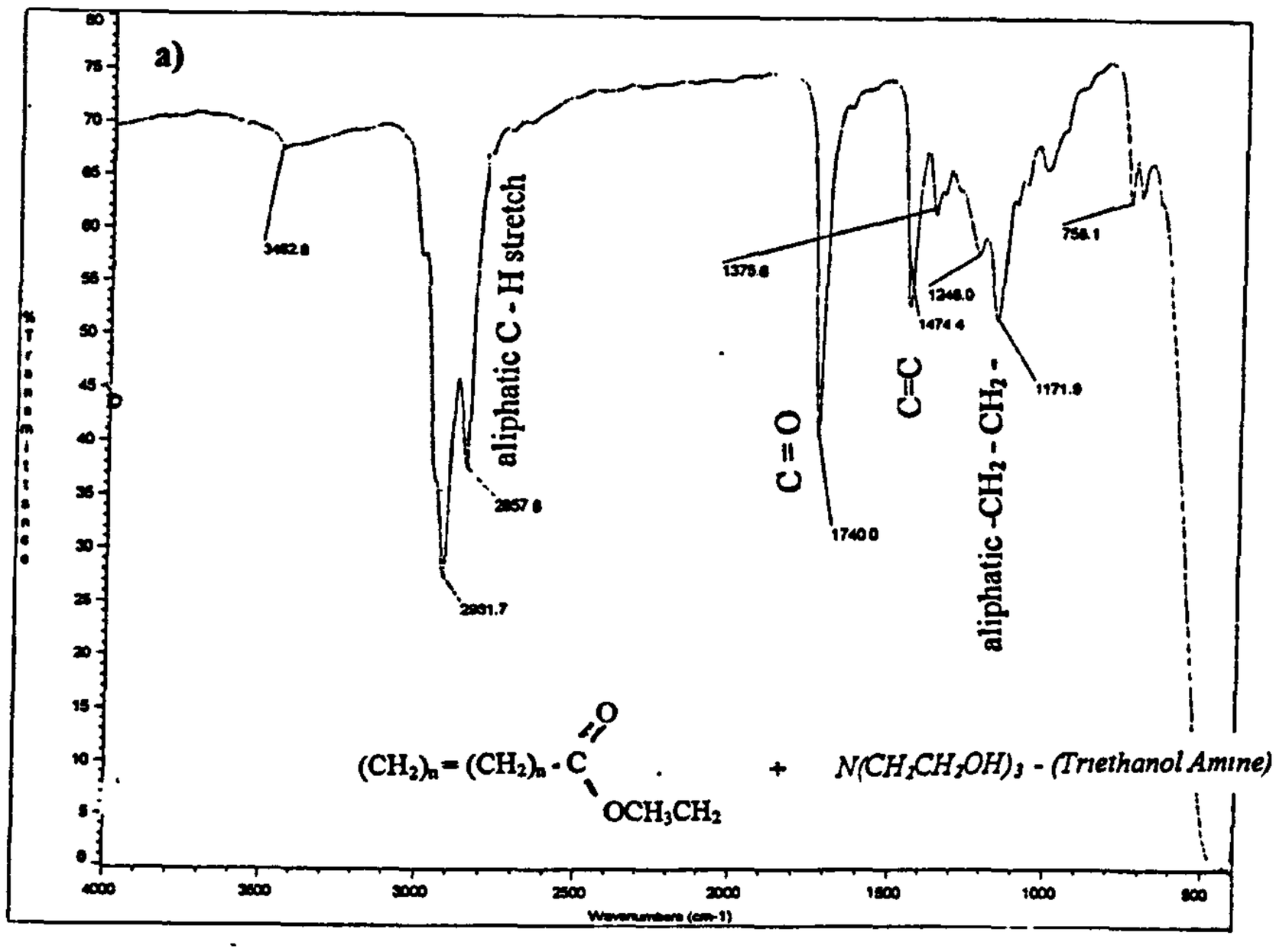

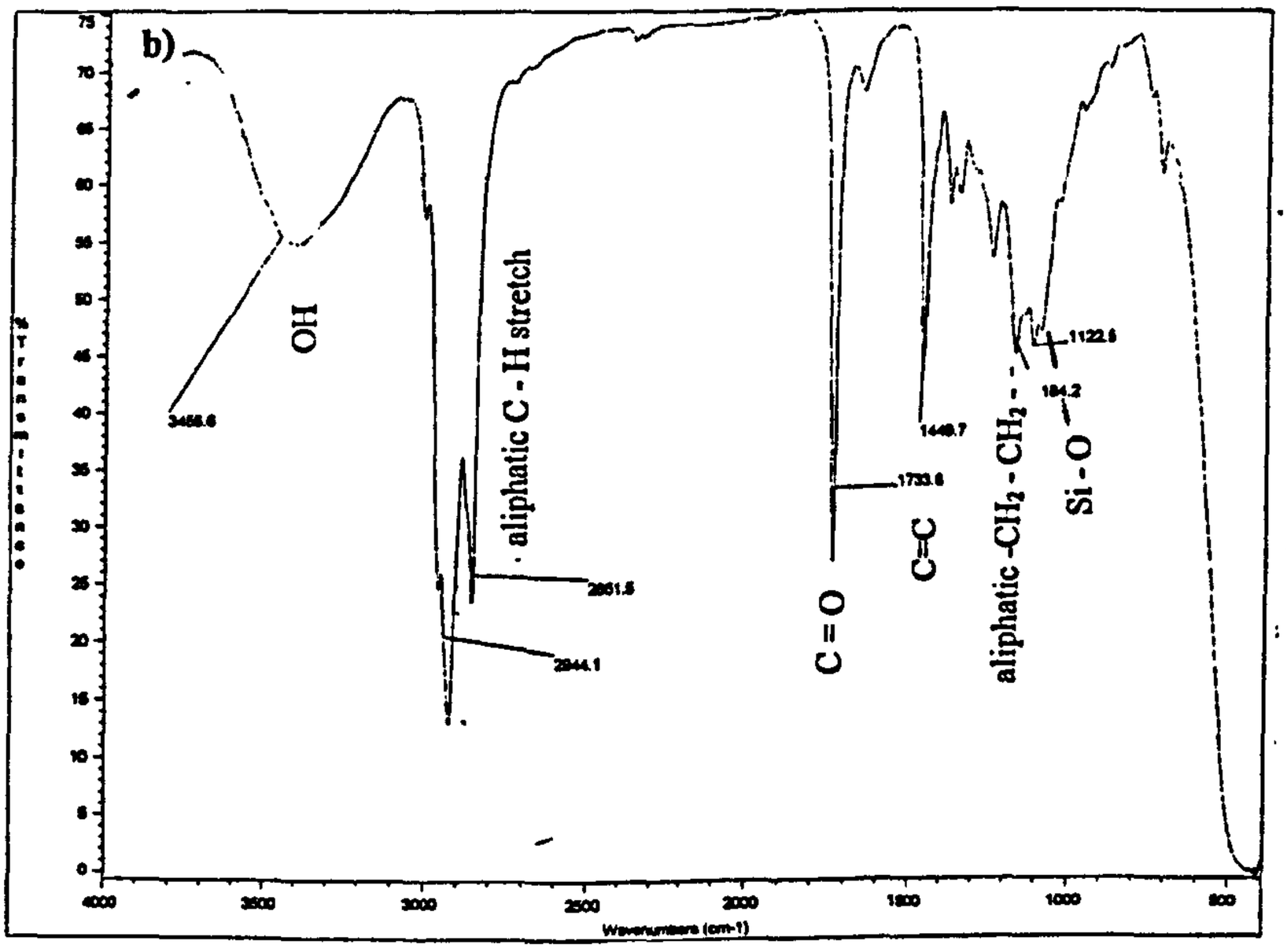

Fig. 6.23 **Infrared Spectra of the ester base fluid T80884 with 0.3% of the additive triethanol amine a)before and b)after the ball immersing test**

6.4.3 Infrared Analysis of Lubricants mixed with Silicon Nitride Powder

A small quantity of silicon nitride powder was mixed thoroughly with each of the four test lubricants. The mixture was then filtered to remove the large powder particles and the remaining lubricant was analysed using infrared spectroscopy.

Figure 6.24 shows the infrared analysis results before and after testing with the reference lubricant Kemet. It is clear that there are no changes in the characteristic peaks after testing, therefore, it can be concluded that no chemical reaction took place.

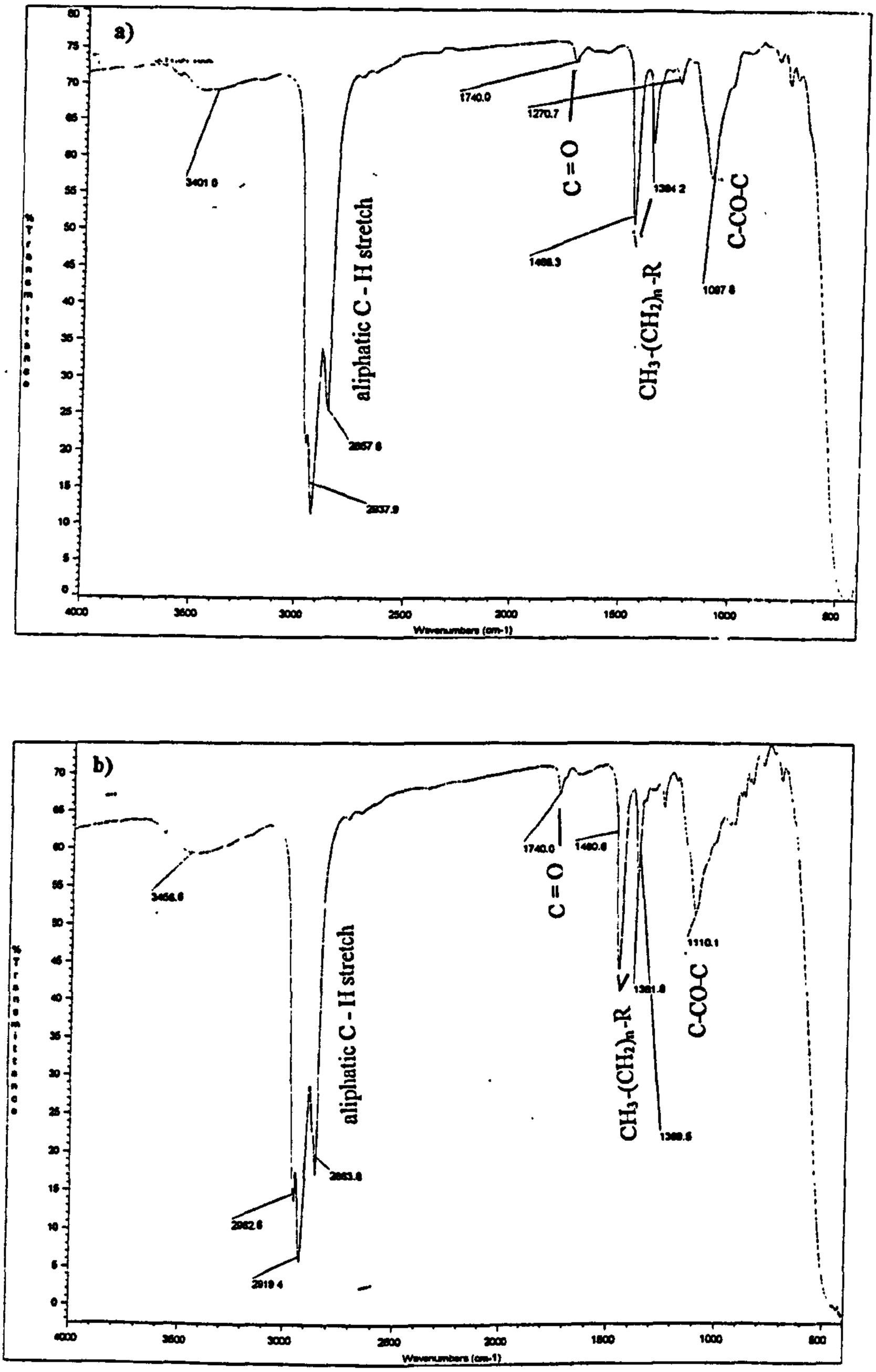

Fig. 6.24 **Infrared Spectra of the reference lubricant Kemet a)before and b) after mixing with silicon nitride powder**

Figure 6.25 shows the infrared analysis results before and after testing with the polyglycol T81499. The results show no changes in the characteristic peaks after testing. Therefore, the conclusion is that there was no chemical interaction between the polglycol T81499 and the silicon nitride powder.

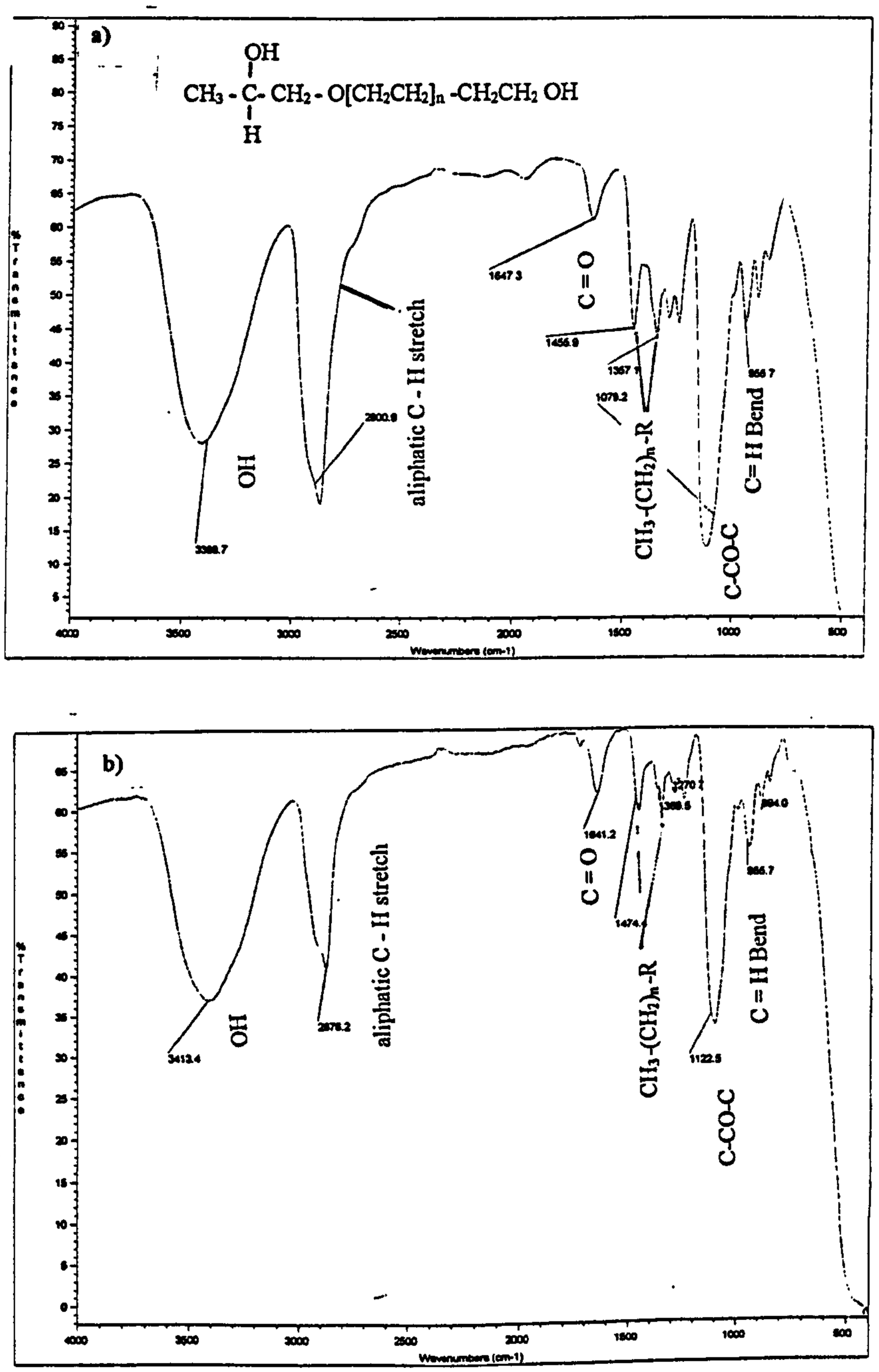

Fig. 6.25 **Infrared Spectra of the polyglycol T81499 a)before and b)after mixing with silicon nitride powder**

Figure 6.26 shows the infrared analysis results before and after testing with the ester base fluid T80884. The results show no changes in the characteristic peaks after testing, Therefore, the conclusion is that there was no chemical interaction between the ester base fluid T80884 and the silicon nitride powder.

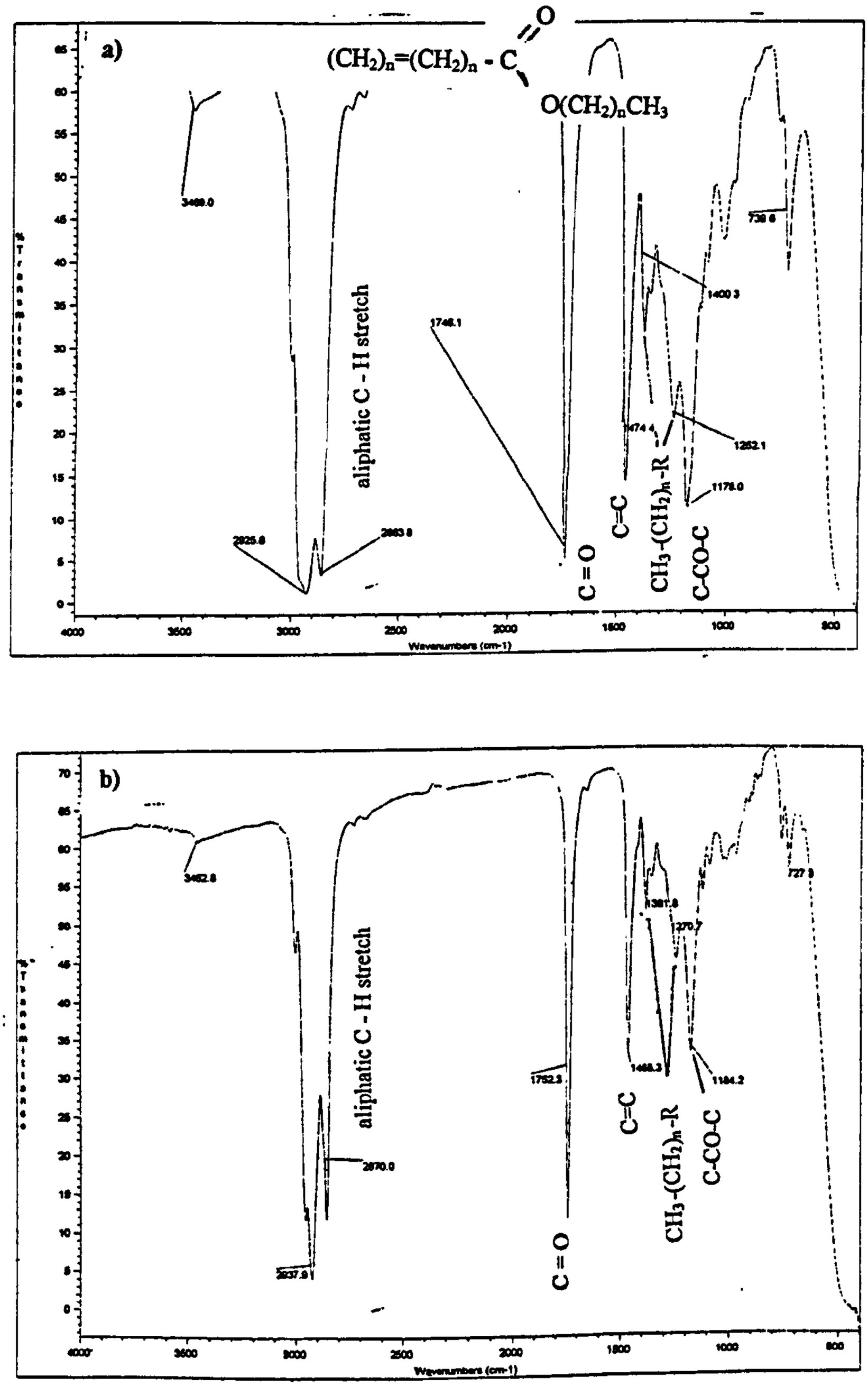

Fig. 6.26 **Infrared Spectra of the ester base fluid T80884 a)before and b)after mixing with silicon nitride powder**

Figure 6.27 shows the infrared spectra analysis before and after testing with the ester base fluid T80884 with 0.3% of the additive triethanol amine. The results show no changes in the characteristic peaks after testing. Therefore, the conclusion is that there was no chemical interaction between the ester base fluid T80884 with 0.3% of the additive triethanol amine and the silicon nitride powder.

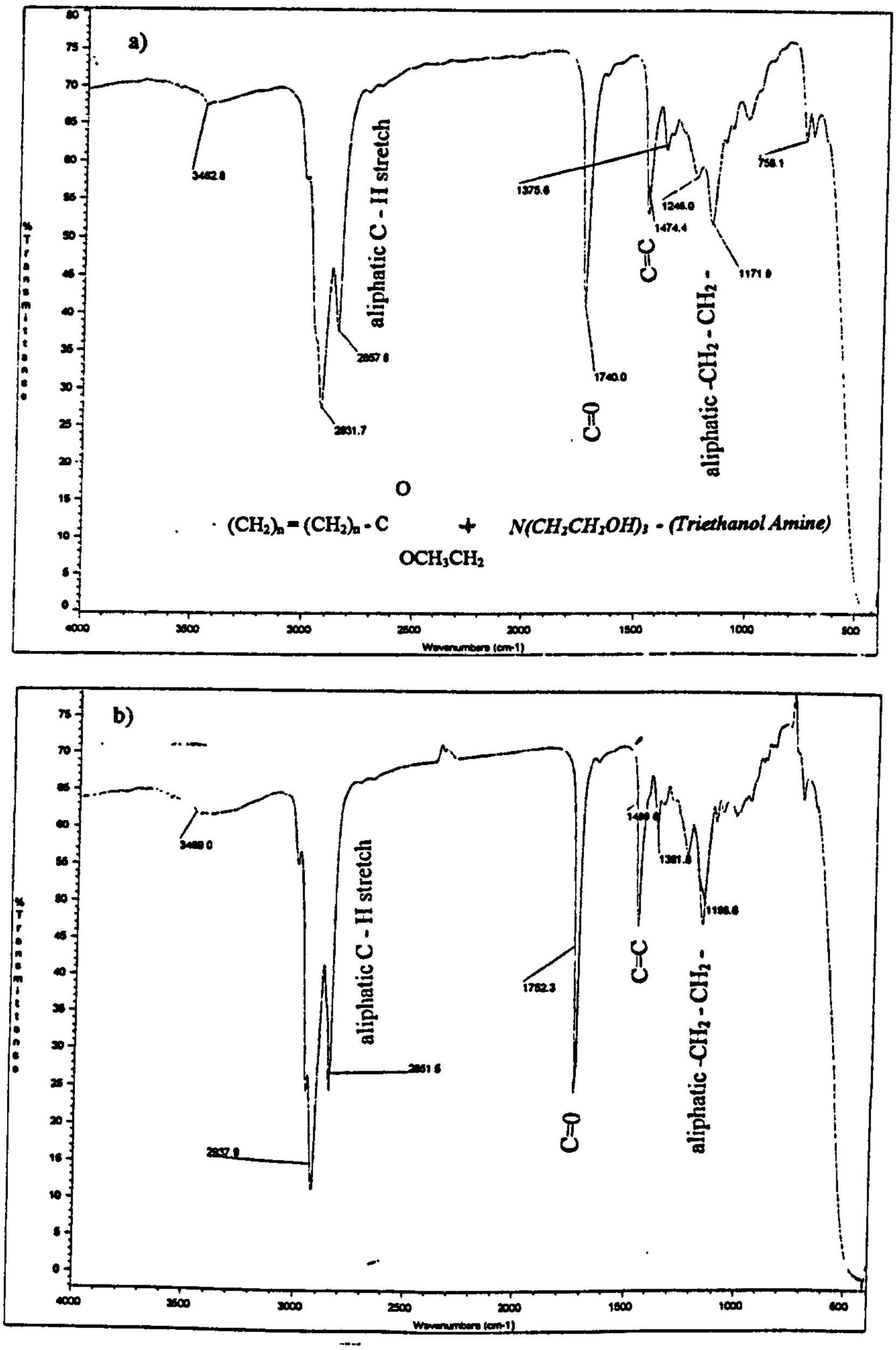

Fig. 6.27 **Infrared Spectra of the ester base fluid T80884 with 0.3% of the additive triethanol amine a)before and b)after mixing with silicon nitride powder**

Summary of Results

From the results of the surface and chemical analysis after the friction tests the following conclusions can be drawn:

Lubricant	Test Sample	Surface Analysis	Chemical analysis-EDX
T80884	Silicon nitride ball	Abrasion grooves and deposit on wear scar	Transfer mechanism occurring -
	Steel plate	Film deposited on wear Track	Silicon found on plate and iron on ball
T80884 + 0.3% Triethanol amine	Silicon nitride ball	Abrasion grooves on wear scar	No transfer mechanism
	Steel plate	Film deposited on wear track with abrasion grooves	

With the presence of the esterbasefluid T80884 some chemical interaction is occurring at the contact interface of the ball and plate, which is causing the much harder silicon nitride ball to be modified by the softer surface of the steel plate, this is evident from the abrasion grooves on the ball surface which correspond to the machining marks on steel plate. With the addition of the additive triethanol amine this ball modification mechanism is more pronounced.

While esters have superior oxidational stability compared with mineral oils at relatively low temperatures of about 100°C, Barnes et al., 1989, both fluids experience severe oxidation at temperatures in excess of 250°C (mineral oil) and 350°C (esters). Lockwood et al., 1982, demonstrated that ester oxidation products can react with iron at temperatures considerably lower than those encountered in boundary and even elastohydrodynamic conjunctions. Furthermore, the oxidation of ester based lubricants results in the formation of acids and hydroperoxides which are not formed in appreciable quantities with the mild oxidation of conventional mineral oil base stocks, Willermet et al., 1981. After investigating the friction and wear characteristics of silicon nitride and steel couples Winn and co-workers, 1995, found that the acids formed in the contact zone of the ester based lubricant lead to increased wear in the silicon nitride pins, compared with that of mineral oils.

From the results of the surface and chemical analysis of silicon nitride balls after the grinding tests the following conclusions can be drawn:

A summary comparing the wear debris analysis after testing with the reference slurry Kemet and T80884 + 0.3% triethanol amine is presented in the table below:

Lubricant	**SEM Features of Debris**	**EDX Analysis of Debris Cluster**	**Possible Wear Mechanism**
Reference slurry - Kemet	Thin sheets - 1 micron in thickness	Characteristic Silicon and Iron peaks	Brittle fracture (delamination type debris)
T80884 + 0.3% triethanol amine	Small spherical debris - 2-5 microns in diameter	Characteristic silicon and iron peak, but silicon peak very strong	Tribochemical reaction

There is no significant effect on the hardness of the silicon nitride balls after repeated grinding tests with T80884 + 0.3% triethanol amine.

The residual compressive stresses in the silicon nitride balls decrease as a result of material removal from the ball surface using the lubricant T80884 + 0.3% triethanol amine. The relationship between the decrease in rate of residual stress and the amount of material removed is not a linear function. The highest rate od decrease in residual stress is achieved when the first layer of material is removed. Subsequent tests on the same ball result in a much reduced rate of decrease of residual stress.

The table below shows a comparison of the IR analysis results for the test lubricants before and after the grinding test, the ball immersion test and powder mix test.

Lubricant	**IR analysis of lubricant after grinding test**	**IR analysis of lubricant after ball immersing test**	**IR analysis of lubricant after powder mix test**
Kemet	No change in characteristic peaks, therefore no structural change occurring in slurry during test	No change in characteristic peaks, therefore no structural change in lubricant during test	No change in characteristic peaks, therefore no structural change in lubricant during test
T81499	No change in characteristic peaks, therefore no structural change occurring in slurry during test	No change in characteristic peaks, therefore no structural change occurring in lubricant during test	No change in characteristic peaks, therefore no structural change in lubricant during test
T80884	Significant reduction in peak intensities, therefore, it is possible some structural change is occurring in slurry during test	Slightly broad OH peak forming at 3420cm^{-1} and significant reduction in peak intensities, therefore, it is possible some structural change is occurring in slurry during test	No change in characteristic peaks, therefore no structural change occurring in lubricant during test
T80884 + 0.3% triethanol amine	Significant reduction in peak intensities, therefore, it is possible some structural change is occurring in slurry during test	Very broad OH peak forming at 3400cm^{-1} and also a broad peak forming at 1100cm^{-1}, therefor there is evidence of structural change occurring during test. This could be due to a chemical reaction with the silicon nitride ball.	No change in characteristic peaks, therefore no structural change in lubricant during test

The IR results show certain changes when using the ester base fluid T80884 in the grinding test and the ball immersing test, however, no such change occurred in the powder form test. This behaviour could be due to the fact that for the powder mix pure silicon nitride was used, rather than a ground sintered silicon nitride which contains oxides of silicon nitride, also the powder form contains α-Si_3N_4 whereas most of the grains in the hot pressed ball are β grains surrounded by glass at the grain boundaries due to the sintering process. The powder mix also contains different amounts of surface silica and other trace impurities from the initial powder used for the manufacture of the hot

isostatically pressed silicon nitride ball. A hypothetical explanation for the change in IR results during the ball immersion test is that it is possible that a very slow reaction is occurring during this test due to the very reactive functional carbonyl group of the ester base fluid T80884, however this reaction could be greatly enhanced by the tribological conditions of the grinding tests. Some possible reaction mechanisms of silicon nitride with the ester base fluid can be speculated as follows:

It has already been demonstrated by Cranmer (1987), and Gates (1994) that the surface of silicon nitride (Si_3N_4) contains silicon oxide(s). It is understood that silicon nitride is decomposed by oxygen, Imada et al., 1992, as:

$$Si_3N_4 + 3O_2 \rightarrow 3SiO_2 + 2N_2$$

(through oxynitride intermediates this forms silica)

$$3SiO_2 + 6H_2O \rightarrow 3Si(OH)_4$$

Further reaction of the silica with the ester base fluid T80884 + 0.3% triethanol amine can be speculated as a nucleophilic substitution reaction with the triethanol amine acting as a catalyst, that is, increasing the rate of reaction. The reaction mechanism could be as follows:

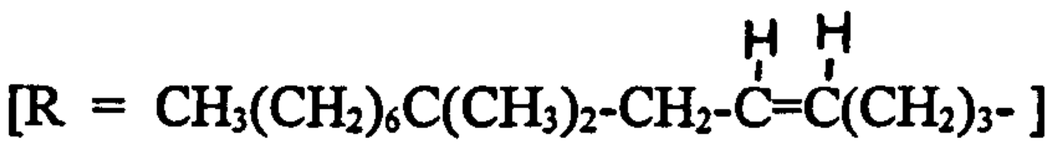

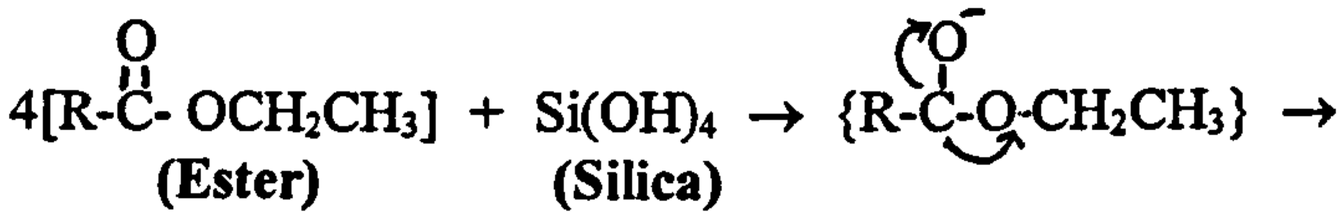

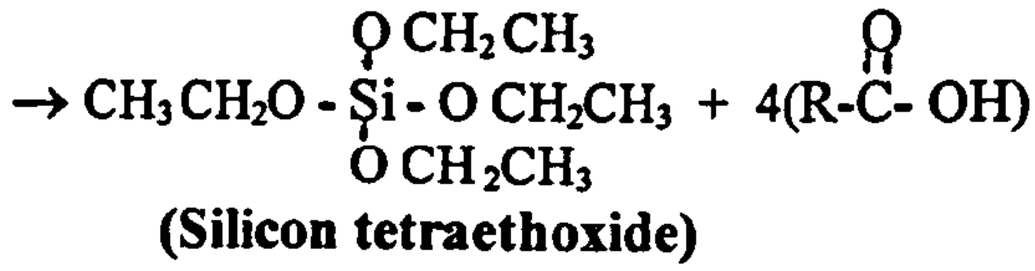

The IR results for the ester base fluid T80884 in the ball immersing test show absorption bands at 1100cm^{-1}, these are, consistent with the expected adsorption of Si - O - C bands, and also the very broad OH peak at 3400cm^{-1} which could be due to the reaction products of the above mechanism.

Another possible reaction mechanism could be between the triethanol amine with the ester T80884 and the silica to form a complex structure as follows:

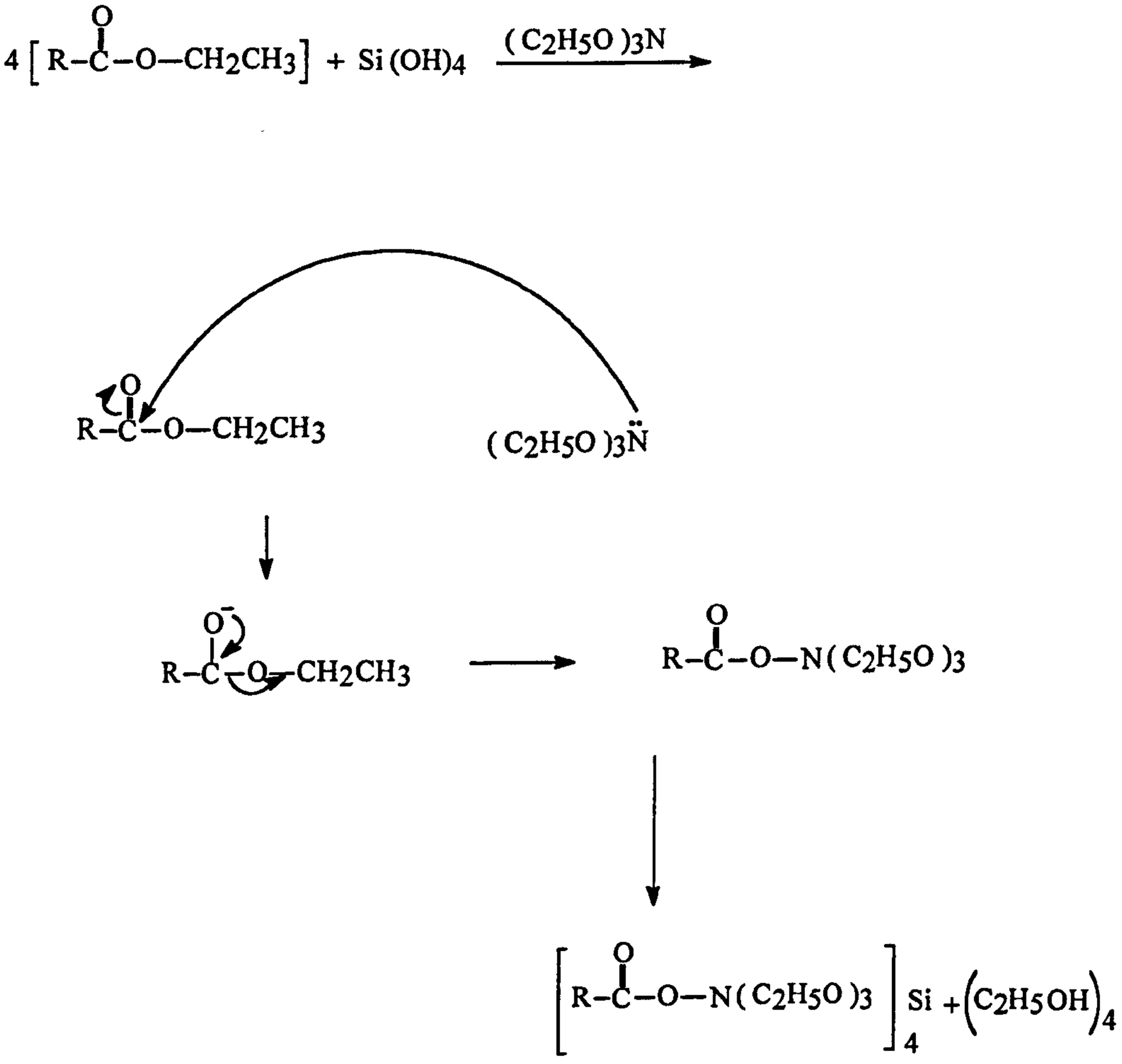

Complex Structure

REFERENCES

Barnes, J. R. & Bell, J. C., 1989, **"Laboratory screening of engine lubricants for high temperature performance"**, Lubr. Eng. Trans. S.T.L.E., Vol. 45 (9), pp.549-555.

Cranmer, D. C., 1987, **"Wear surface analysis of silicon nitride"**, Lubr. Eng., Vol.44 (12), pp.975-980.

Evans, A.G. & Marshall, D. B., 1981, **"Wear mechanisms in Ceramics"**, Fundamentals of Friction and Wear of Materials, Metals Park, OH, pp.439-452.

Gates, R.S. & Hsu, S. M., 1994, **"Silicon Nitride Boundary Lubrication: Effect of Oxygenates"**, ASME/STLE Tribology Conference STLE, Preprint No.94-CC-4C-3.

Imada, Y. Kamamura, K., Honda, F. & Nakajima, 1992, **"The tribological reaction accompanying friction and wear of silicon nitride containing titanium nitride"**, Transactions of the ASME, Vol. 114,pp.230-235.

Lockwood, F. and Klaus, E. E., 1982, **"Ester oxidation- the effect of an iron surface"**, Trans. A.S.L.E., Vol. 25 (2), pp.236-244.

Winn, A. J., Dowson, D and Bell, J. C., 1995, **"The lubricated wear of ceramics"**, Tribology International, Vol.28, No.6, pp.395-402.

Chapter 7

CONCLUSIONS AND FURTHER WORK

7.1 Conclusions

Chemical interactions with the lubricants have been found to influence the coefficient of friction and material removal rates of silicon nitride ceramics and also to determine the mechanisms by which these materials wear. However, the chemical stability of ceramics is much better than that of metals. At room temperature and without sliding, the surfaces of silicon nitride ceramics will not react with most chemical substances. However, the fresh surface on silicon nitride ceramics produced by the grinding process possesses a very high surface energy and the bonds of the surface atoms are imperfect which makes the surface very active. It is quite possible for the surface atoms (silicon and nitrogen) to react with the elements in the lubricants used during grinding. On the basis of the friction and grinding studies the following conclusions can be made:

- The ester base fluid T80884 gave the lowest coefficient of friction of about 0.7 for a ceramic ball sliding on steel plate.The polyglycol gave the highest coefficient of friction of 0.185 under the same conditions.

- From the surface analysis results a transfer of matter occurred at the contact area of the ceramic ball and steel plate during friction testing with the ester base fluid T80884.

- The highest material removal rate of 2.5μm/min for the grinding of silicon nitride was obtained when the ester base fluid T80884 + 0.3% of the triethanol amine was used. This is an increase by four fold when compared to the material removal rate obtained with the industrial reference slurry Kemet.

- The topography of the silicon nitride ball after grinding test with ester base fluid T80884 + 0.3% triethanol amine was found to be very smooth indicating that the predominant mechanism of material removal was due a tribochemical reaction as a soft outer surface was formed by this reaction and could be rapidly removed by the action of the abrasive particles.

- The hardness of the silicon nitride balls does not change significantly as a result of repeated grinding tests with the most effective lubricant (ester base fluid T80884 +0.3% triethanol amine).

- The residual compressive stresses in the silicon nitride balls decrease as a result of material removal from the ball surface in the presence of the ester base fluid T80884 + 0.3% triethanol amine.

- The hypothetical reaction of the silicon nitride ceramics with the ester base fluid T80884 + 0.3% triethanol amine can be as follows:

$$Si_3N_4 + 3O_2 \rightarrow 3SiO_2 + 2N_2$$

(through oxynitride intermediates this forms silica)

$$3SiO_2 + 6H_2O \rightarrow 3Si(OH)_4$$

Further reaction of the silica with the ester base fluid T80884 + 0.3% triethanol amine can be speculated as a nucleophilic substitution reaction with the triethanol amine behaving as a catalyst.

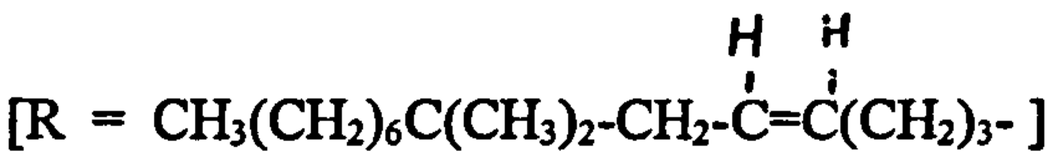

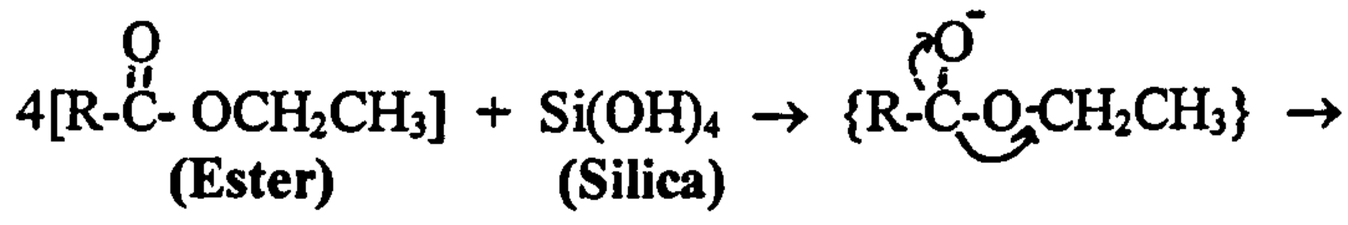

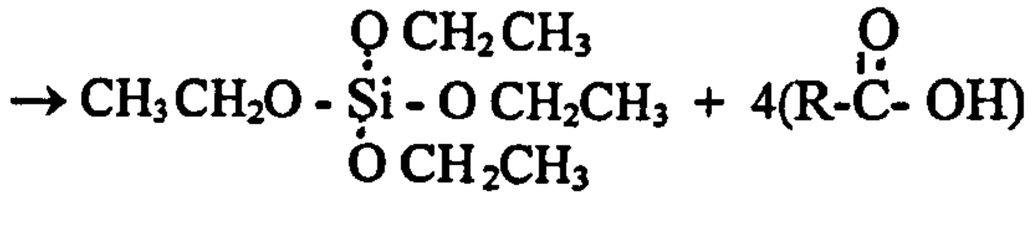

- Another possible reaction mechanism could be between the triethanol amine with the ester T80884 and the silica:

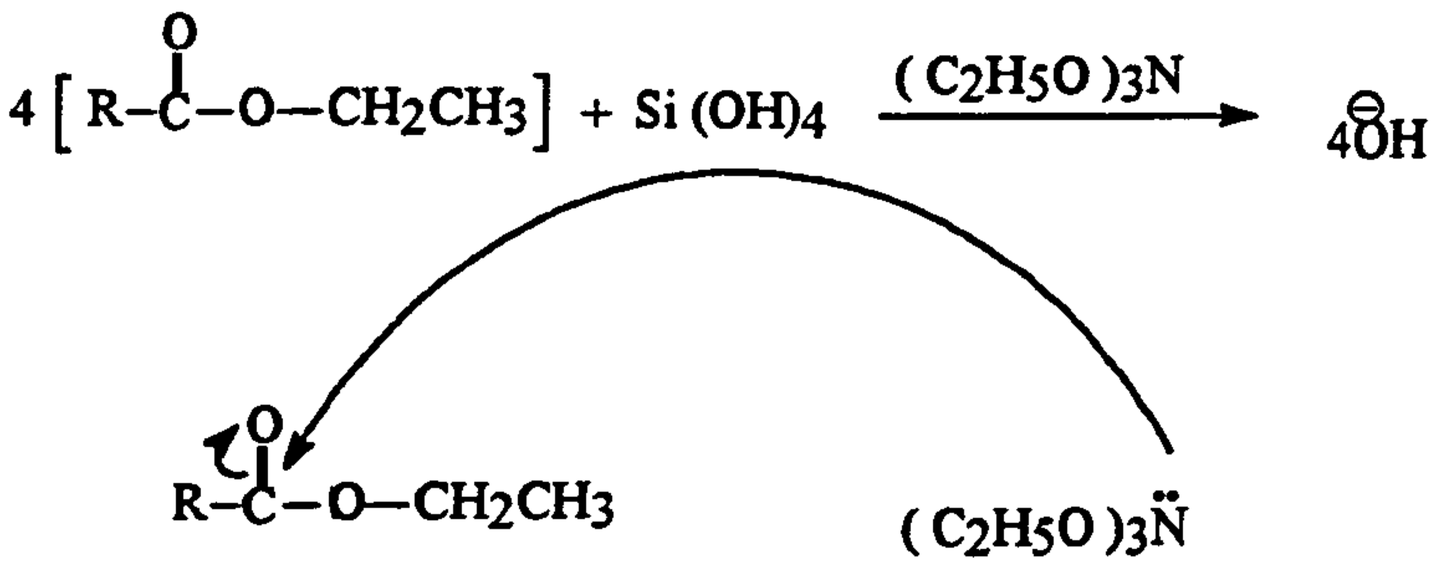

The nitrogen from triethanol amine is a nucleophile due to having a lone pair of electrons attacks to the electropositive carbon of carbonyl group from the ester and makes it electron deficient and therefore a new bond will be formed between the nitrogen and carbon and the final product can be considered to be an amide. This amide complex can be assumed as an X which is an cationic (+) and silicon is a tetravalent elen and the cationic X attaches itself to the silicon and the ethoxy group whi was displaced from the ester remains in the environment in an anioinic fc along with the hydroxyl group which is also anionic

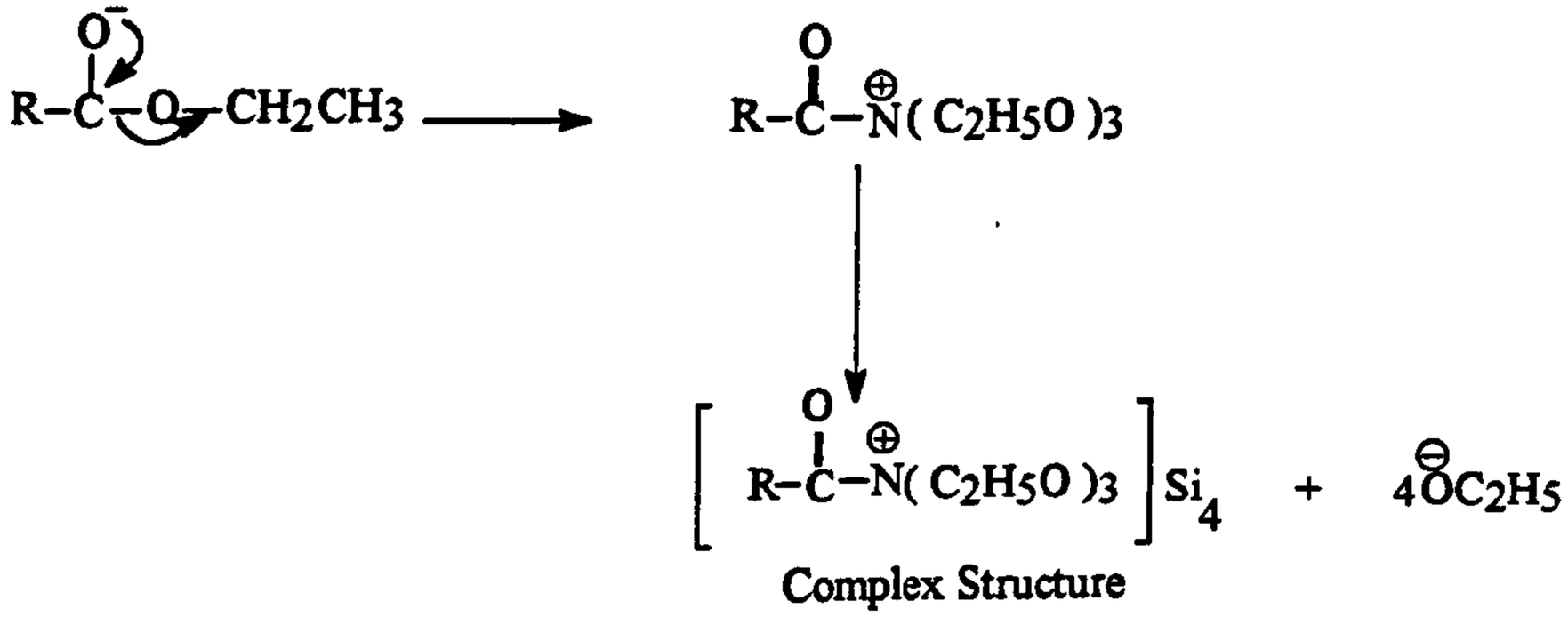

Complex Structure

7.2 Further Work

Further work could be done in order to:

- Study the film formation mechanism and its morphology.
- Study the relationship between the initial microstructure of the ceramic (pores structure and grain boundaries) also the pattern of pits and surface features observed after testing with the most effective lubricant ester base fluid T80884 + 0.3% triethanol amine.
- Examine the effectiveness of the ester base fluid T80884 + 0.3% triethanol amine with other ceramics.